
Electronic Thesis and Dissertation Repository

7-18-2016 12:00 AM

Hyperpolarized ^3He Magnetic Resonance Imaging Phenotypes of Chronic Obstructive Pulmonary Disease

Damien Pike
The University of Western Ontario

Supervisor
Dr. Grace Parraga
The University of Western Ontario

Graduate Program in Medical Biophysics
A thesis submitted in partial fulfillment of the requirements for the degree in Doctor of Philosophy
© Damien Pike 2016

Follow this and additional works at: <https://ir.lib.uwo.ca/etd>

 Part of the [Atomic, Molecular and Optical Physics Commons](#), [Medicine and Health Sciences Commons](#), and the [Nuclear Commons](#)

Recommended Citation

Pike, Damien, "Hyperpolarized ^3He Magnetic Resonance Imaging Phenotypes of Chronic Obstructive Pulmonary Disease" (2016). *Electronic Thesis and Dissertation Repository*. 3975.
<https://ir.lib.uwo.ca/etd/3975>

This Dissertation/Thesis is brought to you for free and open access by Scholarship@Western. It has been accepted for inclusion in Electronic Thesis and Dissertation Repository by an authorized administrator of Scholarship@Western. For more information, please contact wlsadmin@uwo.ca.

Hyperpolarized ^3He Magnetic Resonance Imaging Phenotypes of Chronic Obstructive Pulmonary Disease

Damien Pike

Supervisor

Dr. Grace Parraga

The University of Western Ontario

Graduate Program in Medical Biophysics

A thesis submitted in partial fulfillment of the requirements for the degree in Doctor of Philosophy

© Damien Pike 2016

Follow this and additional works at: <http://ir.lib.uwo.ca/etd>

 Part of the [Atomic, Molecular and Optical Physics Commons](#), [Medicine and Health Sciences Commons](#), and the [Nuclear Commons](#)

Abstract

Chronic obstructive pulmonary disease (COPD) is the third leading cause of death in the world. Identifying clinically relevant COPD phenotypes has the potential to reduce the global burden of COPD by helping to alleviate symptoms, slow disease progression and prevent exacerbation by stratifying patient cohorts and forming targeted treatment plans. In this regard, quantitative pulmonary imaging with hyperpolarized ^3He magnetic resonance imaging (MRI) and thoracic computed tomography (CT) have emerged as ways to identify and measure biomarkers of lung structure and function. ^3He MRI may be used as a tool to probe both functional and structural properties of the lung whereby static-ventilation maps allow the direct visualization of ventilated lung regions and ^3He apparent diffusion coefficient maps show the lung microstructure at alveolar scales. At the same time, thoracic CT provides quantitative measurements of lung density and airway wall and lumen dimensions. Together, MRI and CT may be used to characterize the relative contributions of airways disease and emphysema on overall lung function, providing a way to phenotype underlying disease processes in a way that conventional measurements of airflow, taken at the mouth, cannot. Importantly, structure-function measurements obtained from ^3He MRI and CT can be extracted from the whole-lung or from individual lung lobes, providing direct information on specific lung regions. In this thesis, my goal was to identify pulmonary imaging phenotypes to provide a better understanding of COPD pathophysiology in ex-smokers with and without airflow limitation. This thesis showed: 1) ex-smokers without airflow limitation had imaging evidence of subclinical lung and vascular disease, 2) pulmonary abnormalities in ex-smokers without airflow limitation were spatially related to airways disease and very mild emphysema, and, 3) in ex-smokers with COPD, there were distinct apical-basal lung phenotypes associated with disease severity. Collectively, these findings provide strong evidence that quantitative pulmonary imaging phenotypes may be used to characterize the underlying pathophysiology of very mild or early COPD and in patients with severe disease.

Keywords

Hyperpolarized Noble Gas, Magnetic Resonance Imaging, Computed Tomography,
Airways Disease, Emphysema, Chronic Obstructive Pulmonary Disease

Co-Authorship Statement

The following thesis contains three manuscripts published in peer-reviewed scientific journals. Chapter 2 is an original research article titled “Pulmonary Abnormalities and Carotid Atherosclerosis in Ex-smokers Without Airflow Limitation” and was published in *The Journal of Chronic Obstructive Pulmonary Disease* in 2014. This manuscript was co-authored by Damien Pike, Miranda Kirby, Tamas J. Lindenmaier, Khadija Sheikh, Casey E. Neron, Daniel G. Hackam, J. David Spence, Aaron Fenster, Nigel A. Paterson, Don D. Sin, Harvey O. Coxson and Grace Parraga. Chapter 3 is an original research article titled “Ventilation Heterogeneity in Ex-smokers Without Airflow Limitation” and was published in the journal *Academic Radiology* in 2015. This manuscript was co-authored by Damien Pike, Miranda Kirby, Fumin Guo, David G. McCormack and Grace Parraga. Chapter 4 is an original research article titled “Regional Heterogeneity of Chronic Obstructive Pulmonary Disease Phenotypes: Pulmonary ^3He Magnetic Resonance Imaging and Computed Tomography” and was published in *The Journal of Chronic Obstructive Pulmonary Disease* in 2016. This manuscript was co-authored by Damien Pike, Miranda Kirby, Rachel L. Eddy, Fumin Guo, Dante P.I. Capaldi, Alexei Ouriadov, David G. McCormack and Grace Parraga.

As the first author of these manuscripts, I assisted with the acquisition of data including carotid ultrasound, ^3He MRI and CT imaging and coaching study subjects through pulmonary function testing. I also contributed to the experimental design and the conception of the studies. I performed the statistical analyses, interpreted results and was responsible for drafting, revising and final approval of manuscripts. Dr. Miranda Kirby (Chapters 2 - 4), Tamas J. Lindenmaier (Chapter 2), Khadija Sheikh (Chapter 2), Dante P.I. Capaldi (Chapter 4), Rachel L. Eddy (Chapter 4) and Casey Neron (Chapter 2) assisted with the acquisition of data and helped draft the manuscripts they co-authored. Fumin Guo (Chapters 3, 4) provided assistance with image analysis and performed image registration of the data for the manuscripts he co-authored. Drs. Daniel G. Hackam (Chapter 2), J. David Spence (Chapter 2), Aaron Fenster (Chapter 2), Nigel A. Paterson (Chapter 2), Don D. Sin (Chapter 2), David G. McCormack (Chapters 3, 4), Alexei Ouriadov (Chapter 4) and Harvey O. Coxson (Chapters 2, 3) provided clinical and

medical imaging expertise and additional contributions to study design and statistical analyses of the respective manuscripts they co-authored and offered editorial assistance and helped with the final approval of the manuscripts they co-authored. Dr. Grace Parraga (Chapters 2-4), the principal investigator of all studies in this thesis, provided ongoing guidance and research assistance and contributed to the conception, design, data acquisition, data analysis and data interpretation for all manuscripts as well as manuscript drafting and final revisions of all work. She was also the guarantor of data integrity and responsible for Good Clinical Practice.

Pulmonary function test training and pulse oximetry measurements were performed by Sandra Blamires. Polarization of ^3He gas was performed by Andrew Wheatley, BSc. MRI acquisition and other imaging assistance was performed by Trevor Szekeres, MRT and David Reese, MRT.

To my mother, Cauline

Acknowledgments

First, I would like to acknowledge my supervisor Dr. Grace Parraga. I am extremely grateful for the guidance and support she has continuously offered me throughout graduate school. The experiences I have had as part of the London Lung Imaging Research Team will stay with me throughout all my future academic and professional endeavors and I will never forget the valuable lessons they taught me.

I would also like to thank all the members of my advisory committee for continuous support throughout my graduate studies. Drs. Daniel G. Hackam, David G. McCormack and Aaron Fenster always offered their assistance with my research and for that I am very thankful.

To the Parraga lab members, I have had an amazing time working with all of you. To Andrew Wheatley, thank you for training me to use polarization equipment and software that I would never have had a chance to do anywhere else in the world. To Sandra Blamires, thank you for pulmonary function test training and teaching me how to book and manage subjects and their visits. To Trevor Szekeres, thank you for going above and beyond to help me acquire MRI and CT scans for my research.

To all of my friends in London and colleagues at Western, thank you for being by my side the past few years. To Dr. Miranda Kirby, thank you for always being there to listen to my ideas and taking time out of your day to help. To Nikhil Kanhere who was my first roommate, thank you for showing me what it would be like to have a smarter, older brother. To Dan Buchanan, thank you for your ultrasound expertise and helping me with countless patient visits. To Dr. Amir Owrangi, thank you for being one of the nicest and funniest people I had the chance to become friends with during grad school. Many thanks to all of the other graduate students and staff members I have been fortunate enough to work with: Dr. Sarah Svenningsen for showing me what a relentless work ethic really is, Dr. Khadija Sheikh for answering my questions about MRI physics whenever I had them (which was everyday), Fumin Guo for his help and patience with teaching me how to write codes to analyze our images, Tamas Lindenmaier for all of his

help with acquiring and analyzing ultrasound scans and manuscript editing, Greg Paulin for conversations about medicine, Dante Capaldi for keeping me company with George and Wendy Hough for always helping me out. I also have to thank my friends Drs. Tom Hrinivich, Jeff Gaudet, Donna Murrell, Ashley Makala and Ian Connell for meaningful coffee breaks and conversations.

I would like to thank my Mom for her relentless encouragement. Your continuous support gave me the strength and confidence I needed to make it through the challenges of graduate school. To my Nan, thank you for always keeping me in your thoughts and to my aunts Gloria, Rose and Mary and uncles Randy, Arl and Joe thank you for always supporting me.

I am very grateful for the financial support I have received from an Ontario Graduate Scholarship (Queen Elizabeth II Scholarship in Science and Technology) and from the Canadian Institutes of Health Research (CIHR).

Table of Contents

Abstract	i
Co-Authorship Statement	iii
Dedication	v
Acknowledgments	vi
Table of Contents	viii
List of Appendices	xi
List of Tables	xii
List of Figures	xiii
List of Abbreviations	xv
CHAPTER 1	1
INTRODUCTION	1
1.1 Chronic Obstructive Pulmonary Disease: A Leading Cause of Death	
Worldwide.....	1
1.2 COPD: A Heterogeneous Disease of the Lung.....	4
1.2.1 Chronic Bronchitis	4
1.2.2 Small Airways Disease	5
1.2.3 Emphysema.....	7
1.2.4 COPD – Asthma Overlap.....	10
1.2.5 COPD – Bronchiectasis Overlap	10
1.3 COPD and Cardiovascular Disease	11
1.4 Subclinical COPD and Identifying Susceptible Individuals	14
1.4.1 Undiagnosed, Early and Subclinical COPD	14
1.4.2 Airflow Limitation in Obese and Overweight Individuals	15
1.4.3 Identifying Individuals Susceptible to Developing COPD.....	15
1.5 Pulmonary Function Tests	18
1.5.1 Spirometry.....	18
1.5.2 Plethysmography.....	19
1.5.3 Diffusing Capacity of the Lung	20
1.6 Measuring Exercise Capacity and Pulmonary Symptoms	21
1.6.1 The Six-Minute Walk Test.....	21

1.6.2	The St. George’s Respiratory Questionnaire	22
1.6.3	Modified Medical Research Council Dyspnea Scale.....	22
1.7	The Role of Imaging to Study COPD	24
1.7.1	High-resolution Computed Tomography of the Lung	24
1.7.2	Nuclear Medicine: Ventilation Scintigraphy	27
1.7.3	Pulmonary Magnetic Resonance Imaging	29
1.8	COPD Phenotypes	36
1.9	Thesis Hypothesis and Objectives	37
1.10	References.....	40
CHAPTER 2	51
2	Pulmonary Abnormalities and Carotid Atherosclerosis in Ex-Smokers Without Airflow Limitation.....	51
2.1	Introduction.....	51
2.2	Materials and Methods.....	52
2.2.1	Study subjects	52
2.2.2	Spirometry and plethysmography.....	53
2.2.3	Imaging	53
2.2.4	Image analysis.....	53
2.2.5	Statistics	54
2.3	Results.....	55
2.4	Discussion.....	62
2.5	References.....	65
CHAPTER 3	71
3	Ventilation Heterogeneity in Ex-smokers without Airflow Limitation.....	71
3.1	Introduction.....	71
3.2	Materials and Methods.....	72
3.2.1	Study Subjects.....	72
3.2.2	Spirometry and Plethysmography.....	73
3.2.3	Imaging	73
3.2.4	Image analysis.....	73
3.2.5	Statistics	74

3.3 Results.....	74
3.4 Discussion.....	83
3.5 References.....	87
CHAPTER 4.....	89
4 Regional Heterogeneity of Chronic Obstructive Pulmonary Disease Phenotypes: Pulmonary ³ He Magnetic Resonance Imaging and Computed Tomography.....	89
4.1 Introduction.....	89
4.2 Methods.....	90
4.2.1 Study Subjects.....	90
4.2.2 Spirometry and Plethysmography.....	91
4.2.3 Imaging.....	91
4.2.4 Image Analysis.....	92
4.2.5 Distribution of Emphysema and Ventilation Defects.....	93
4.2.6 Statistics.....	94
4.3 Results.....	94
4.4 Discussion.....	102
4.5 References.....	106
CHAPTER 5.....	111
5 Conclusions and Future Directions.....	111
5.1 Overview and Research Questions.....	111
5.2 Summary and Conclusions.....	111
5.3 Limitations.....	113
5.3.1 Study Specific Limitations.....	113
5.3.2 General Limitations.....	116
5.4 Future Directions.....	117
5.4.1 Longitudinal Hyperpolarized ³ He MRI of Ex-smokers With and Without Airflow Limitation.....	117
5.4.2 Hyperpolarized ³ He MRI Apparent Diffusion Coefficients: A Potential Tool to Evaluate Alpha-1 Antitrypsin Augmentation Therapy.....	119

5.4.3	Second-Order Texture Analysis of Hyperpolarized ^3He MR Images: Beyond the Ventilation Defect.....	121
5.5	References.....	128
APPENDIX	132

List of Appendices

APPENDIX A – Imaging Evidence of the Relationship Between Carotid Atherosclerosis and Chronic Obstructive Pulmonary Disease.....		132
APPENDIX B – Pulmonary Imaging Abnormalities in an Adult Case of Congenital Lobar Emphysema		172
APPENDIX C – Permissions for Reproduction of Scientific Articles		184
APPENDIX D – Research Ethics Board Approval Notices		191
APPENDIX E – Curriculum Vitae		194

List of Tables

Table 1-1. Leading Causes of Death Worldwide.....	1
Table 1-2. Worldwide leading causes of disability in 2004 and their predicted rank in 2030.....	2
Table 1-3. Grading of COPD severity based on post-bronchodilator spirometry	19
Table 1-4. Modified Medical Research Council (mMRC) Dyspnea Scale	22
Table 2-1. Demographic, pulmonary function, thoracic CT and carotid ultrasound data for all study subjects.....	56
Table 2-2. Multiple regression models for IMT, VWV and TPV	60
Table 3-1. Demographic, pulmonary function and imaging data	76
Table 3-2. Whole lung and regional measurements for ex-smokers with normal and elevated VDP	78
Table 3-3. Relationship of ³ He MRI VDP with airways disease and emphysema measurements.....	80
Table 4-1. Demographic and pulmonary function test measurements	94
Table 4-2. Imaging measurements.....	99
Table 4-3. ³ He MRI and CT apical-lung (AL) and basal-lung (BL) phenotype measurements.....	100
Table 4-4. Regional relationships for ventilation defects (VDP) and emphysema (RA ₉₅₀) for all subjects and by GOLD Grade	101
Table 5-1. Second-order texture measurements.....	124
Table 5-2. Second-order texture measurements for all study subjects	125

List of Figures

Figure 1-1. Hospitalizations and repeat hospitalizations by health condition	3
Figure 1-2. Diagram of airway tree including the conducting and respiratory zones and showing the airway generations.	6
Figure 1-3. Schematic of healthy, panlobular, centrilobular and paraseptal acini.....	9
Figure 1-4. Schematic of the mechanistic link between COPD and atherosclerosis.	13
Figure 1-5. Lung function decline over time in never-smokers, current-smokers and individuals who quit smoking.	17
Figure 1-6. Inspiratory – expiratory curve showing lung volumes measured by plethysmography.	20
Figure 1-7. Thoracic CT and segmented airway tree of a healthy volunteer and a COPD patient.	26
Figure 1-8. ^1H , ^3He and ^{129}Xe MRI of a healthy and COPD patient.....	31
Figure 1-9. Static-ventilation (SV) and apparent diffusion coefficient (ADC) ^3He MR images in a healthy volunteer and four COPD patients with increasing severity of airflow limitation.....	35
Figure 2-1. Representative ^3He MRI and 3DUS images for two never-smokers (S1 and S2) and two ex-smokers (S3 and S4).	57
Figure 2-2. Imaging phenotypes in asymptomatic ex-smokers and never-smokers.....	58
Figure 2-3. Never- and ex-smokers with $\text{IMT} \geq$ age-related upper limit of normal ($\text{IMT} > 97.5\%$ confidence interval (CI)) and subjects with $\text{IMT} <$ age-related normal limit ($\text{IMT} \leq 97.5$ CI).....	59
Figure 2-4. Relationships for carotid atherosclerosis and pulmonary VDP.	61
Figure 3-1. ^3He MRI Ventilation and CT airway trees in representative ex-smokers with normal (S1–S3) and abnormally-elevated VDP (S4–S6).	76
Figure 3-2. Whole lung and regional emphysema measurements in ex-smokers with normal (n=18) and abnormally-elevated VDP (n=42).	79
Figure 3-3. Relationships for whole lung and regional VDP with ^3He MRI emphysema measurements.....	81
Figure 3-4. Relationships for regional VDP with CT airways disease measurements.	82

Figure 4-1. Thoracic ^3He MRI and CT of COPD ex-smokers with representative apical- and basal-lung predominant ^3He ventilation defects and corresponding emphysema.....	97
Figure 4-2. GOLD Grade distribution of AL- and BL-predominant VDP and RA_{950} phenotypes	101
Figure 5-1. ^3He ventilation images in ex-smokers at baseline and follow-up (3yr).	118
Figure 5-2. ^3He ADC in alpha-1 antitrypsin patients & ex-smokers with emphysema at baseline and three-year follow-up.	120
Figure 5-3. ^3He static-ventilation and ^3He texture maps and measurements for a representative ex-smoker without airflow limitation, COPD subject and asthmatic subject.	122
Figure 5-4. Second-order texture analysis algorithm for hyperpolarized ^3He MR images	123

List of Abbreviations

¹⁹F	Fluorine
¹H	Proton / Hydrogen-1
³He	Helium-3
¹²⁹Xe	Xenon-129
^{81m}Kr	Metastable Krypton-81
^{99m}Tc	Metastable Technetium-99
6MWD	6 Minute Walk Distance
6MWT	6 Minute Walk Test
ADC	Apparent Diffusion Coefficient
AL	Apical Lung
ANOVA	One Way Analysis of Variance
ATS	American Thoracic Society
AUC	Area Under the Curve
BMI	Body Mass Index
BSA	Body Surface Area
BL	Basal Lung
CO	Carbon Monoxide
COPD	Chronic Obstructive Pulmonary Disease
COPDGene	Genetic Epidemiology of COPD Study
CT	Computed Tomography
CTS	Canadian Thoracic Society
DL_{CO}	Diffusing Capacity of the Lung for Carbon Monoxide
DTPA	Diethylaminetriaminepentacetic Acid
ECLIPSE	Evaluation of COPD Longitudinally to Identify Predictive Surrogate Endpoints Study
ERS	European Respiratory Society
ERV	Expiratory Reserve Volume
FBP	Filtered Back Projection
FEV₁	Forced Expiratory Volume in One Second
FOV	Field of View
FRV	Functional Residual Capacity
FVC	Forced Vital Capacity
GOLD	Global Initiative for Chronic Obstructive Lung Disease.
GLCM	Gray Level Co-occurrence Matrix
HIPAA	Health Insurance and Portability and Accountability Act
HU	Hounsfield Unit
IC	Inspiratory Capacity
IMT	Intima Median Thickness
IRV	Inspiratory Reserve Volume
LA	Lumen Area
LLL	Left Lower Lobe
LUL	Left Upper Lobe
mMRC	Modified British Medical Research Council

MESA	Multi-Ethnic Study of Atherosclerosis
MRI	Magnetic Resonance Imaging
mSv	MilliSieverts
NHANES	National Health and Nutrition Examination Survey
PD₁₅	Fifteenth Percentile on the CT Density Histogram
PIPEDA	Personal Information Protection and Electronic Documents Act
Pi10	Wall Thickness of Airways with Internal Perimeter of 10mm
RA₉₅₀	Relative Area of the Lung with Attenuation ≤ -950 HU
RLL	Right Lower Lobe
ROC	Receiver Operating Characteristic
RML	Right Middle Lobe
RV	Residual Volume
RUL	Right Upper Lobe
SGRQ	St. George's Respiratory Questionnaire
SPECT	Single Photon Emission Computed Tomography
TE	Echo Time
TLC	Total Lung Capacity
TPA	Total Plaque Area
TPV	Total Plaque Volume
TR	Repetition Time
US	Ultrasound
UTE	Ultra-Short Echo Time
VC	Vital Capacity
VDP	Ventilation Defect Percent
VWV	Vessel Wall Volume
VWT	Vessel Wall Plus Plaque Thickness
WA%	Airway Wall Area Percent
%_{pred}	Percent of Predicted Value

CHAPTER 1

INTRODUCTION

Chronic Obstructive Pulmonary Disease (COPD) is characterized by progressive airflow limitation caused by a combination of airways disease and emphysema due to inflammatory responses in the lung to noxious particles (1). The objective of Chapter 1 is to provide an overview of the global health burden imposed by COPD and the pathophysiology, symptoms and medical complications associated with the disease. Chapter 1 will also describe the conventional methodology for measuring pulmonary function and diagnosing COPD and discuss the use of pulmonary imaging for identifying clinically relevant COPD biomarkers and phenotypes.

1.1 Chronic Obstructive Pulmonary Disease: A Leading Cause of Death Worldwide

Chronic obstructive pulmonary disease (COPD) affects 10% of the adult population worldwide (2). A decade ago, COPD was the 4th leading cause of death in the world. At that time, based on global estimates of the rising use of tobacco smoke and biomass fuels, concomitant with the aging population, the World Health Organization (WHO) and others projected COPD to rise to the 3rd leading cause of death in the world between the years 2020 – 2030 (1, 3). Despite this threat, therapies and research efforts did not result in a reduced COPD mortality rate and it subsequently became the 3rd leading cause of death in the world in the year 2010, a decade earlier than expected (4).

Table 1-1. Leading Causes of Death Worldwide in 2012 (Adapted from The World Health Organization Report 2014 (5))

Rank	Disease	Deaths (millions)	% Deaths Worldwide
1	Ischemic Heart Disease	7.35	13.2
2	Cerebrovascular Disease	6.67	11.9
3	COPD	3.10	5.6
4	Lower Respiratory Infections	3.05	5.5
5	Respiratory Cancers	1.60	2.9

COPD also causes life-altering disability to those affected and is expected to become the 5th leading cause of disability worldwide by the year 2030 making it one of the fastest rising disability threats in the world (**Table 1-2**).

Table 1-2. Worldwide leading causes of disability in 2004 and their predicted rank in 2030 (Adapted from ‘The Global Burden of Disease: 2004 Update, World Health Organization’ (3))

2004 Rank*	Disease or Injury	2030 Rank*	Disease or Injury
1	Respiratory Infections	1	Depressive Disorders
2	Diarrhoeal Diseases	2	Heart Disease
3	Depressive Disorders	3	Traffic Accidents
4	Heart Disease	4	Cerebrovascular Disease
5	HIV / AIDS	5	COPD
6	Cerebrovascular Disease	6	Respiratory Infections
7	Premature birth	7	Hearing loss
8	Birth trauma	8	Vision problems
9	Traffic Accidents	9	HIV / AIDS
10	Neonatal Infections	10	Diabetes
13	COPD		

*Rank based on the disability adjusted life years (DALY), one DALY is equivalent to the loss of one year of full health

Given the staggering statistics on the mortality and disability rates, it is not surprising that COPD also has the highest rate for hospital admissions and readmissions among chronic illnesses in the United States, Canada and Europe (**Figure 1-1**) (6, 7).

Along with having a significant frequency of hospitalization, it is estimated that each hospitalized COPD exacerbation costs on average \$10,000 CAN and the overall national economic burden for COPD hospitalizations ranges from \$646 million to \$736 million each year (8). Unfortunately, these costs are expected to rise in tandem with the increasing burden of COPD disability over the next two decades.

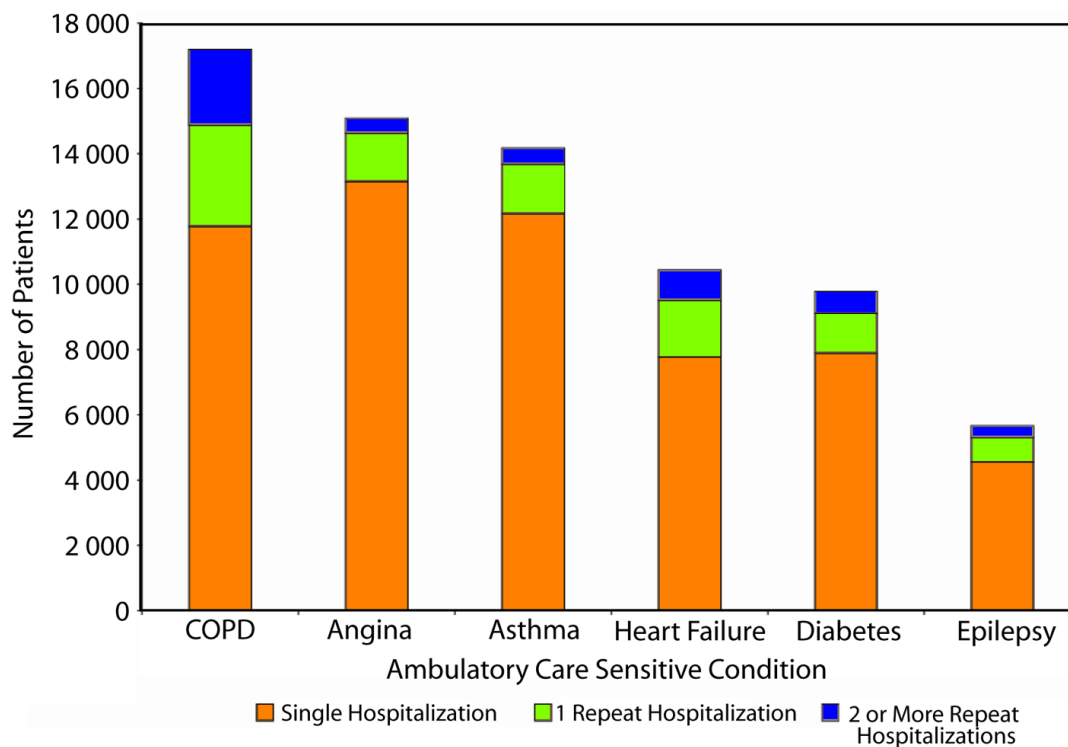


Figure 1-1. Hospitalizations and repeat hospitalizations by health condition
Adapted from the Canadian Institute for Health Information (CIHI) (6)

Collectively, these reports on the prevalence of COPD mortality, morbidity and disability have established that the burden of COPD is a global health issue. At the same time however, epidemiological studies are showing that anywhere from 20-80% of individuals with impaired lung function consistent with COPD are not diagnosed nor treated for the condition (9, 10). This may partly explain one reason why COPD is such a deadly and disabling disease as it suggests that individuals are not likely to seek care or treatment for their respiratory symptoms until their lung function has declined severely and may not be able to be adequately controlled with treatment or surgery. As will be explained in more detail in this thesis, another explanation for the high mortality and disability rates of COPD is related to poor characterization of pulmonary pathophysiology of at-risk individuals who may be in the early subclinical stages.

It has become obvious that there is room for improvement in regard to screening methods and diagnostic strategies for COPD. In the following subsections of the Introduction I

will provide background knowledge on pulmonary pathophysiology in the healthy and COPD lung with emphasis on the varying contributions of airways disease and emphysema from patient to patient. In the latter part of the introduction I will discuss conventional lung function testing and pulmonary imaging methods for characterizing, diagnosing and grading COPD. Chapters 2, 3 and 4 are original research investigations focused on identifying clinically meaningful pulmonary imaging biomarkers and phenotypes to provide a better understanding of airflow limitation in ex-smokers with and without COPD. Lastly Chapter 5, the Conclusion, will summarize the key pulmonary imaging findings from the studies in Chapters 2, 3 and 4 and discuss future work needed to address unanswered questions pertaining to pulmonary imaging abnormalities and their clinical relevance in ex-smokers with and without COPD.

1.2 COPD: A Heterogeneous Disease of the Lung

COPD is an umbrella term that encompasses airways disease and emphysema. Both airways disease and emphysema contribute differently to airflow limitation in each and every patient making the clinical presentation of COPD vary immensely among individuals who are demographically the same, who have the same smoking history and even among people with the same lung function and respiratory symptoms. Decades of research has been put in to characterizing the pathophysiological and biochemical processes in the airways and lung parenchyma involved in lung function decline. In this section I will discuss how pathophysiological changes to the airways and alveoli cause the irreversible airflow limitation characteristic of COPD

1.2.1 Chronic Bronchitis

Chronic bronchitis is characterized by extended periods of excessive cough and mucus and sputum production. The inflammation triggered by noxious particles (from cigarette smoke or other pollutants) in the large or central airways (> 4mm in diameter) is the key cause of bronchitis. The inflammatory response imposed by tobacco smoke triggers increased production of mucus and sputum with concomitant decrease in mucus clearance from the large central airways due to damage to the airway epithelial barrier.

There is also evidence that the bronchial walls thicken (causing the airway lumen to narrow) as a result of the abnormal accumulation of connective tissue within the medium and large airway walls (11). Methods have been developed (12) to diagnose chronic bronchitis based on the ratio of mucus gland to bronchial wall thickness (Reid Index) however a clinical definition based on the frequency and duration an individual experiences of a debilitating cough is more commonly used (1).

1.2.2 Small Airways Disease

The airways < 2mm in diameter are the major site of airflow obstruction in COPD (13). These are airways (bronchioles) beyond the fourth generation of branching (**Figure 1-2**). As the bronchial tree branches non-dichotomously, the number of airways with each successive generation increases and so does their total cross sectional area (14). The majority (75%) of airway resistance in the bronchial tree is attributable to the large (central) conducting airways (conducting airways > 2mm) while only a fraction of resistance is located in the small airways of the respiratory zone (15). Therefore, the small airways contribute very little to overall airway resistance. However, it is in these airways that disease can accumulate over long timeframes without having a significant effect on overall lung function and without causing noticeable respiratory symptoms (16).

As already mentioned in **1.2.1**, the introduction of toxins to airway epithelium increases mucus production, injures and impairs the mucociliary escalator and triggers an inflammatory response in the bronchi. This is true for the small airways also. The excess mucus and inflammatory markers (B cells, CD4 and CD8 lymphocytes) that are produced in response to the noxious particles accumulate and obstruct the small airways. There is also evidence that a portion of mucus present in the small airways in COPD may actually be aspirated there from the large and central airways (15). In addition to airway obstruction, the abnormal deposition of inflammatory cells and connective tissue in the small airway wall causes fibrosis of the airway wall and airway lumen obstruction in severe disease (13). The progression of COPD with respect to lung function decline from mild to severe grades has been most closely associated with the thickening of the airway wall and surrounding compartments and less closely related to the degree of inflammation and mucus secretion within the small airways (13).

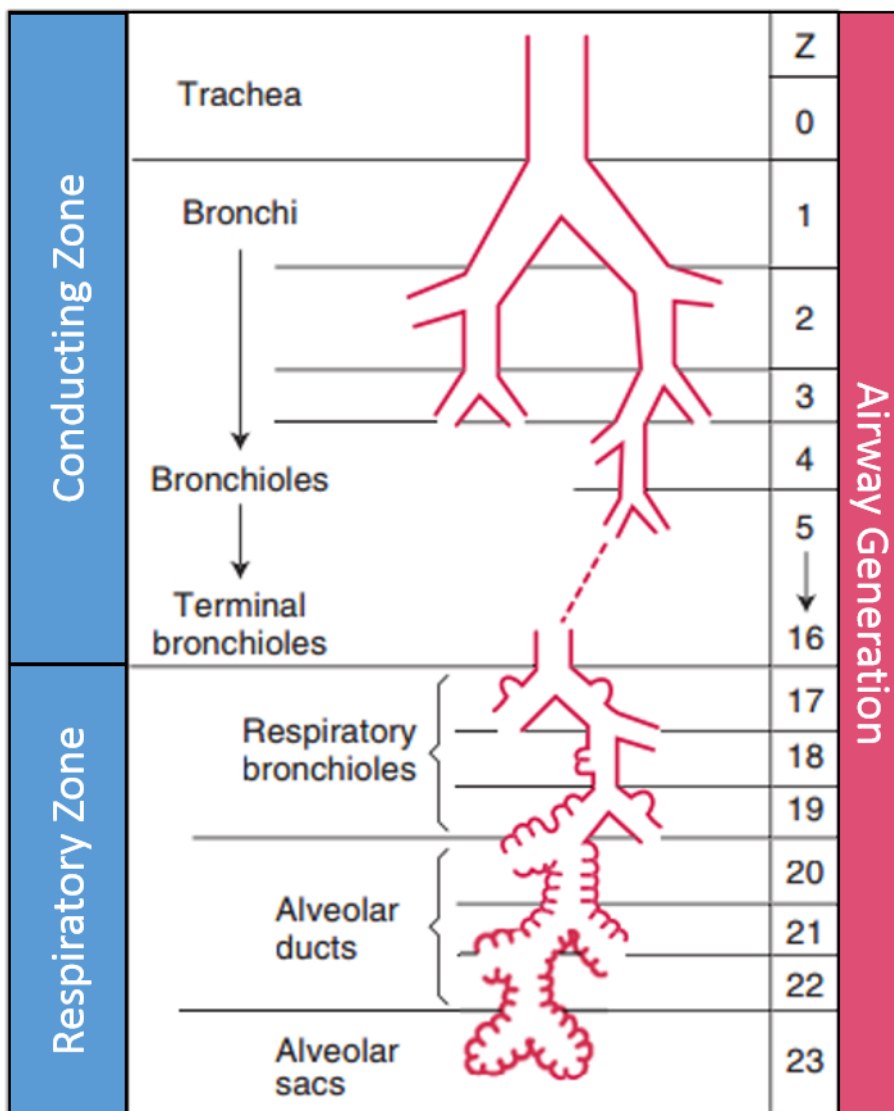


Figure 1-2. Diagram of airway tree including the conducting and respiratory zones and showing the airway generations. The conducting zone comprises the large and small central airways up to the 16th generation that do not participate in gas exchange. The transition and respiratory zone comprise airways >17th generation. Surface area increases with airways generation and gas exchange processes occur in the respiratory bronchioles, alveolar ducts and sacs. Reproduced from Respiratory Physiology: The Essentials, 8th Edition (14)

1.2.3 Emphysema

Emphysema is defined as dilation and destruction of lung parenchyma distal to the terminal bronchiole (17) (see **Figure 1-3**). In emphysema the airspaces involved in gas exchange enlarge and coalesce which reduces the surface area within the lung to carry out necessary gas exchange processes. There are several subphenotypes of emphysema which are named according to the lung units that are involved. *Centrilobular*, or *centriacinar* emphysema arises from damage and enlargement of the respiratory bronchioles (**Figure 1-2 and 1-3**) and is most commonly associated with cigarette smoking. Centrilobular emphysema predominantly occurs in the apical-lung and it is postulated that this is a result of the elevated ventilation (V) – perfusion (Q) ratio (V/Q) in this part of the lung (14). Since the ventilation largely outweighs perfusion (~3/1) in the apical lung, it is thought that noxious particles from cigarette smoke may be deposited in the distal airspaces without passing into the pulmonary circulation inducing inflammation and subsequent destruction of parenchymal tissue. A second form of emphysema, *panlobular* or *panacinar* emphysema, is more common in non-smoking related COPD and in particular alpha-1 antitrypsin deficiency (AATD). AATD is an autosomal hereditary disorder and the panlobular emphysema characteristic of AATD destroys the structure of the entire distal bronchiole starting with the alveolar ducts and sacs and gradually degrading the structure of the respiratory bronchiole (**Figure 1-2 and 1-3**) (18). AATD is a result of reduced serum levels of alpha-1 antitrypsin, a protease that is responsible for protecting the lung from proteolytic activity of neutrophil elastase. The unchecked levels of neutrophil elastase result in destruction of the alveolar walls. AATD associated panlobular emphysema has been found to occur predominantly in the highly perfused basal-lung region where neutrophils and proteases are circulating within the blood (18). Lastly, *paraseptal* emphysema is defined as dilation of the airspaces near or adjacent to the lung pleura and septa. In paraseptal emphysema the most peripheral airspaces (**Figure 1-2 and 1-3**) are destroyed but typically these emphysematous lesions are asymptomatic and not associated with cigarette smoke but with lung trauma such as pneumothorax (19).

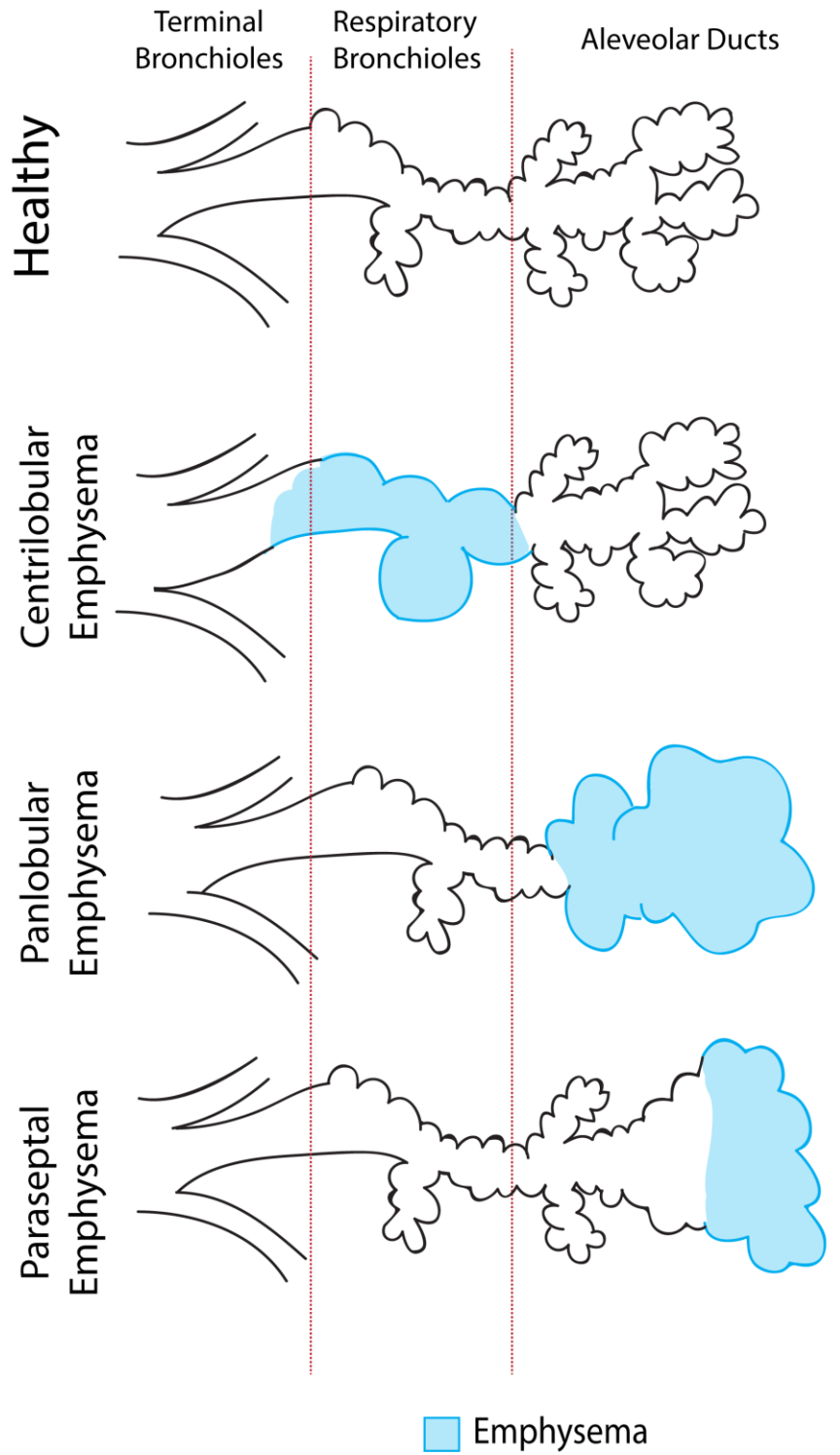


Figure 1-3. Schematic of healthy, panlobular, centrilobular and paraseptal acini.

1.2.4 COPD – Asthma Overlap

Although Asthma is not the direct focus of work presented in this thesis, a significant proportion of individuals who experience symptoms of COPD also exhibit symptoms consistent with Asthma. This clinical presentation has recently been termed ‘Asthma-COPD Overlap Syndrome (ACOS)’ and warrants explanation (20, 21). While COPD encompasses both an airway and emphysema component, asthma is characterized by inflammatory and hyperresponsive airways. Unlike in COPD, the airway obstruction in asthma is reversible with the use of inhaled corticosteroids and long-acting bronchodilators. Although there are clearly defined clinical characteristics to stratify asthma and COPD patients (20), these guidelines fail to acknowledge the spectrum of ACOS. This is an issue because based on these guidelines asthmatics are often excluded from large-scale and longitudinal COPD studies even if they are current- or ex-smokers. One study (22) found in a group of adults (> 55 yrs) with either COPD or asthma, 65% of subjects had overlap of asthma and COPD while only 16% and 21% of subjects had definite asthma or COPD respectively. There are many possible origins of the ‘overlap’ between asthma and COPD and most likely the origin is different for every patient with ACOS. It is widely known that asthma is most commonly diagnosed in childhood, but childhood respiratory disease is also closely linked to the development of impaired lung function and COPD later in life. At the same time, cigarette smoking and an asthma diagnosis are risk factors for the development of COPD, and cigarette smoking alone promotes asthma. Therefore there is substantial overlap even among the individual risk factors for asthma and COPD which may accumulate and increase the likelihood of developing just one of these diseases on its own (23, 24).

1.2.5 COPD – Bronchiectasis Overlap

Bronchiectasis is another chronic respiratory illness that has been closely linked with COPD. It is characterized by persistent bronchial sepsis due to irreversibly damaged and enlarged bronchi (25). The enlarged airways are injured in such a way that they are not able to clear mucus adequately. Mucus builds up within the large and small bronchi promoting a cycle of repeated lung infections. Each subsequent infection imposes more damage to the airways and a cyclical process ensues. There are many causes of

bronchiectasis ranging from abnormal congenital etiology and childhood development disorders to poorly healed respiratory infections. There is evidence that bronchiectasis is present in anywhere from 30% to 70% of patients with COPD (26-28) and those patients with concomitant COPD and bronchiectasis experience a more severe clinical course involving more hospitalizations and higher mortality (29). It is unclear what the exact underlying mechanisms involved in the development of co-occurring COPD and bronchiectasis are. It could be that the constant exposure to toxins in cigarette smoke repeatedly trigger respiratory infections promoting bronchiectic pathophysiology in the lungs of COPD patients. Another hypothesis is that the airway obstruction presented in bronchiectasis due to mucus plugging imposes airflow limitation severe enough to warrant a COPD diagnosis (30). It is not known for sure whether bronchiectasis is caused by COPD and repeated exposure to cigarette smoke or if the opposite is correct and COPD is a consequence of bronchiectasis pathophysiology. It seems likely that the same is true for ACOS and the exact cause of concomitant bronchiectasis and COPD is different for each patient.

1.3 COPD and Cardiovascular Disease

Over the past two decades there has been increasing evidence that both COPD and cardiovascular disease, and in particular vascular atherosclerosis are closely related. Large-scale epidemiological and experimental studies (31-35) have established that cardiovascular diseases and complications are the leading cause of hospitalization among COPD patients and are second only to lung cancer as the leading cause of death. Therefore it is clear that there is a serious burden of cardiovascular disease in COPD patients. Both COPD and cardiovascular disease share a common risk factor in cigarette smoke and air and gas pollution, however it is now known that the mechanistic link between cardiovascular and pulmonary disease pathophysiology extends beyond the toxicity imposed by inhaled toxins (32). The ‘lung permeability’ theory was recently proposed (36) as a potential mechanism for atherogenesis (atherosclerotic plaque development) in COPD patients. **Figure 1-4** presents a schematic of this mechanism. This concept suggests that inflammatory stress similar to what occurs in COPD patients

might cause the alveolar – capillary layer to become increasingly permeable to inflammatory mediators. These inflammatory markers, mainly the interleukins, are free to pass from the lungs into the systemic circulation where they trigger a secondary inflammatory response of procoagulant and inflammatory markers from the liver (C-reactive protein, fibrinogen, serum amyloid protein) that promote atherogenesis at various locations throughout the body. While this process may occur chronically in the inflamed COPD lung, cyclical insults of cigarette smoke would cause the alveolar – capillary layer to become chronically permeable, up-regulating the atherogenic response. Given this mechanistic hypothesis it seems plausible that there is a dose-response relationship between the severity of lung disease and vascular disease and several studies (35, 37-41) have confirmed that this is the case. The severity of atherosclerosis has been shown to be correlated with lung function decline whereby COPD patients have quantitatively more atherosclerotic plaque (37, 40, 42, 43) and more plaque that is vulnerable to rupture causing embolism and stroke (44). However it is not known for certain if cardiovascular disease causes COPD or vice-versa, and the question about ‘which comes first’ cannot yet be answered with certainty (45). What is known is that cardiovascular disease and acute ischemic events play one of the most important roles in the clinical course of COPD patients (46).

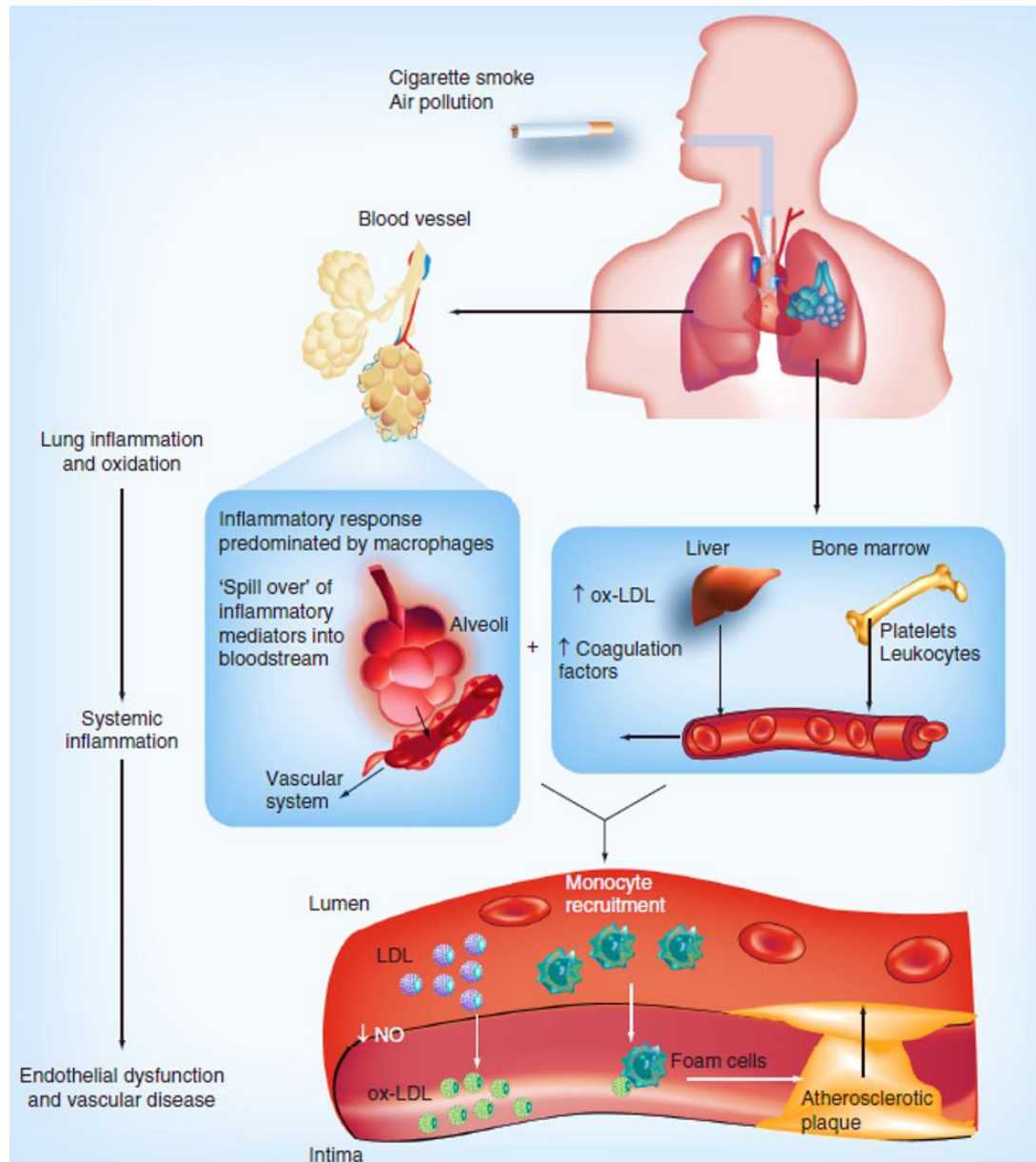


Figure 1-4. Schematic of the mechanistic link between COPD and atherosclerosis. Reproduced with permission from 'Imaging Evidence of the Relationship Between Atherosclerosis and Chronic Obstructive Pulmonary Disease' *Imaging in Medicine*; DOI: 10.2217/iim.13.70, 2013 (47)

1.4 Subclinical COPD and Identifying Susceptible Individuals

1.4.1 Undiagnosed, Early and Subclinical COPD

Typically, individuals with COPD present with obvious symptoms of airflow limitation including chronic cough, breathlessness and wheezing. These symptoms are related to the various contributions of airways disease and emphysema that reduce the ability to move air in and out of the lungs and participate in gas exchange. However there are many ex- and current-smokers who experience respiratory symptoms and may or may not have airflow limitation consistent with COPD and never receive treatment for a pulmonary condition. Ex- and current-smokers are most likely to encounter pulmonary function testing or be referred to a respirologist by a primary care provider only when pulmonary symptoms start to alter their exercise capacity and drastically impact their quality of life. A study in the province of Ontario, Canada reported that up to 75% of ex- and current-smokers had impaired lung function consistent with COPD but had not previously sought medical help for respiratory illness; (9) this may have reflected the fact that most of these individuals could still carry-out day-to-day activities. Unfortunately, other studies (48, 49) have recognized that COPD underdiagnosis is common in other countries as well. There are several reasons COPD might go undiagnosed and untreated in the general population. First, since lung function decline is a chronic process, it can take decades before obvious symptoms present. At the same time, many ex- and current-smokers often attribute impaired lung function to normal aging and not an indicator of respiratory illness. Second, certain individuals may be ‘protected’ from being diagnosed with airflow limitation because of anatomical or comorbid conditions that prevent them from performing diagnostic pulmonary function tests (to be discussed in **section 1.4.2**). Lastly, as was previously mentioned in **section 1.2.2**, the small airways are the major site of airflow obstruction in COPD, but these airways only account for a fraction of overall airway resistance. Given this, it has been speculated that disease processes can occur in the small airways or the ‘silent zones’ over very long timeframes without having a noticeable influence on lung function (16). Therefore it is likely that small airways

disease can accumulate without detection until a critical point is reached and overall lung function starts to decline rapidly.

1.4.2 Airflow Limitation in Obese and Overweight Individuals

Obesity, defined as a body mass index (BMI) greater than 30kg/m^2 , and being overweight is a biomarker for dyspnea which is one of the major and predominant symptoms of COPD (50). Therefore, breathlessness in overweight individuals might be directly related to their obesity or a manifestation of an underlying and untreated lung condition such as COPD. High BMI is associated with a decrease in functional residual capacity (FRC) and total lung capacity (TLC) due to the increase in adipose tissue in the thoracic trunk of affected individuals (51). The smaller lung capacity combined with increased adipose deposits cause impaired movement of the diaphragm, and reduced chest wall compliance and ultimately both the forced expiratory volume in one second (FEV_1) and forced vital capacity (FVC) decrease. It has also been reported that the decrease in FVC is more severe than FEV_1 , leading to a subsequent increase in FEV_1/FVC in these individuals (52, 53). Therefore overweight and obese individuals might be ‘protected’ from developing airflow limitation based on the FEV_1/FVC ratio due to extrapulmonary or anatomical impairment (50). As a result, many overweight individuals may go untreated due to the absence of a COPD diagnosis (on spirometry) even though they may experience dyspnea that is attributable to airflow limitation and not solely a symptom associated with being overweight. These individuals may make up a large percentage of people with ‘undiagnosed’ or very early or mild COPD. At the same time, it is difficult to know for sure if the symptoms these subjects experience are secondary only to obesity or directly related to impaired lung function – this is postulated to be the primary reason obese or overweight individuals do not seek further treatment from a respirologist beyond the primary care setting.

1.4.3 Identifying Individuals Susceptible to Developing COPD

The Fletcher and Peto curve (**Figure 1–5**) that describes the natural history of COPD popularized the concept that both smokers and non-smokers alike, reach and maintain

maximum lung function during the first half of adulthood before lung function starts to decline (54). Fletcher and Peto suggested that while both smokers and non-smokers experience a decline in lung function, smokers decline much more rapidly and develop airflow obstruction due to their rapidly declining trajectory. The concept of rapid declining lung function in smokers has been confirmed more recently but the rate of change in lung function over time is now known to be highly variable (55). Recently, the seminal findings of Fletcher and Peto were extended when it was suggested that there exists another group of individuals who develop COPD aside from ‘rapid decliners’. These individuals attain a low maximal lung function in adulthood and subsequently experience a rate of decline of lung function that is normal (similar to what is observed in non-smokers). This study found that among COPD patients, approximately half experienced a rapid-decline in lung function leading to airflow limitation while the other half reached a low maximal lung function before declining at a normal rate (56). This was an exciting finding because it suggested that lung function at young ages and maximally attained lung function in adulthood might serve as important biomarkers related to the development of COPD.

At the same time, it is clear that identifying which ‘trajectory’ an individual follows may not be enough to identify who will develop COPD. Many ex- and current-smokers have an ‘early’ or subclinical form of COPD that does not satisfy the criteria for a COPD diagnosis based on lung function or pulmonary symptoms. Disease might accumulate ‘silently’ (16) in the small airways (13) of the peripheral lung for many years without any symptomatic or lung function indications making it difficult to identify which trajectory an individual might follow (rapid decliner, normal decliner etc.). The identification of early and subclinical COPD in individuals who smoke or who have smoked has many benefits with respect to treatment planning and lifestyle change recommendations. Concomitant with the objectives of any COPD treatment plan, which are to reduce recurrent respiratory symptoms and prevent exacerbation episodes, the identification of very early forms of the disease can help individuals and their health care team put together a targeted therapy strategy to achieve the most optimal outcome for a certain individual at the onset of disease.

Unfortunately, as discussed in **section 1.4.1**, many smokers develop respiratory symptoms over the span of several years but may not consider them significant enough to seek help from a primary care provider who could help kickstart a treatment plan. In this way COPD progression may continue for decades before treatment begins at which point it may be in the severe and debilitating stages and be very difficult to manage. Furthermore, as will be described in more detail in **section 1.5**, conventional and gold-standard pulmonary function tests for assessing lung function and diagnosing COPD do not fully characterize small changes in lung function that might indicate very early or subclinical disease progression. Therefore the combination of very few individuals visiting the primary care setting along with poor characterization of small changes by gold-standard tools for diagnosing COPD makes the identification, treatment and longitudinal monitoring of COPD from the earliest stages extremely difficult in clinical practice.

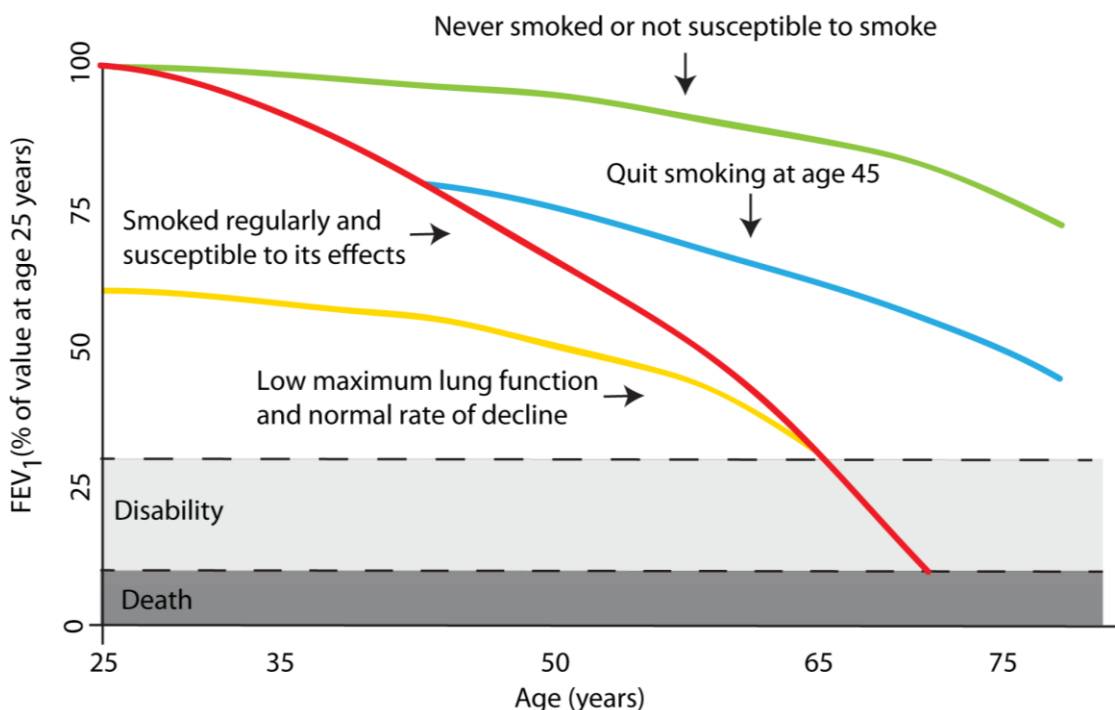


Figure 1–5. Lung function decline over time in never-smokers, current-smokers and individuals who quit smoking. Adapted from ‘The Natural History of Chronic Airflow Obstruction’ (54) and ‘Lung-Function Trajectories Leading to Chronic Obstructive Pulmonary Disease’ (56).

In the next section I will describe the methodology for measuring pulmonary function and diagnosing COPD. An overview of these methods will highlight the inherent drawbacks of these conventional breathing tests for characterizing the early and subclinical forms of COPD – another potential reason the prevalence of undiagnosis and undertreatment of COPD is so high.

1.5 Pulmonary Function Tests

Established methods for measuring pulmonary function focus on the assessment of expiratory flow volumes through spirometry, lung volumes through plethysmography and the diffusing capacity of the lungs.

1.5.1 Spirometry

Spirometry tests measure the volume of air an individual inhales or exhales as a function of time. Spirometry can be used to measure expiratory volumes and flow, although expiratory volumes are diagnostic for COPD. In particular, the spirometry measurements of the forced expiratory volume in one second (FEV_1) and the forced vital capacity (FVC) are the two most widely used measurements. FVC is the maximal volume of air that can be forcefully exhaled from maximal inspiration while FEV_1 is the maximal volume of air that is exhaled in just the first second of a forced expiration maneuver.

The American Thoracic Society (ATS) and European Respiratory Society (ERS) have collaborated to publish standards for which spirometry testing worldwide should follow when collecting measurements (57). First, since spirometry is the diagnostic test for both Asthma and COPD, measurements should always be collected by a trained and certified technician. Second, the spirometry test to measure FEV_1 and FVC is broken down into three distinct phases: 1) Maximal inspiration, 2) a ‘blast’ of exhalation and 3) continued exhalation until the end of the test. Third, for the test to be considered acceptable, a minimum of three forced expiration maneuvers repeatable to within 0.15L of each other must be performed. Lastly, ATS and ERS specify that the National Health and Nutrition

Examination Survey (NHANES III) reference standard equations be used to provide appropriate percent predicted spirometry values based on sex, age, height and ethnicity (58). This allows measurements to be recorded on a ‘percentage predicted’ (%_{pred}) scale from 0% to 100% (or higher) instead of interpreting raw volume measurements that vary greatly depending age, sex, height and ethnicity.

The global initiative for chronic obstructive lung disease (GOLD) has deemed spirometry as the diagnostic tool for COPD and grading disease severity (1). According to GOLD guidelines, assessing airflow limitation in an individual should be carried out after the administration of a short-acting inhaled bronchodilator. A post-bronchodilator FEV₁ consistently below 70% of the FVC (FEV₁/FVC < 70%) indicates that irreversible airflow limitation is present which warrants a COPD diagnosis. Once an individual’s measurements fall below the FEV₁/FVC < 70% threshold, their severity of airflow limitation is graded based on FEV₁ percent predicted. There are 4 grades of COPD disease severity as shown in **Table 1-3** and severity increases with each grade.

Table 1-3. Grading of COPD severity based on post-bronchodilator spirometry

<i>GOLD Grade</i>	<i>Severity</i>	<i>FEV₁/FVC < 70% and -</i>
GOLD 1	Mild	FEV ₁ % _{pred} ≥ 80%
GOLD 2	Moderate	50% ≤ FEV ₁ % _{pred} < 80%
GOLD 3	Severe	30% ≤ FEV ₁ % _{pred} ≤ 50%
GOLD 4	Very Severe	FEV ₁ % _{pred} < 30%

GOLD: Global initiative for chronic obstructive lung disease, FEV₁: Forced expiratory volume in one second, FVC: Forced vital capacity, %_{pred}: Percent of predicted value

1.5.2 Plethysmography

Plethysmography is used to measure lung volumes. Similar to spirometry, the ATS and ERS have specified guidelines (59) for measuring eight lung volumes as shown in **Figure 1-6**. The inspiratory reserve volume (IRV) is maximum volume that can be inhaled from the end of normal inspiration. The tidal volume (TV) is the volume of air an individual inhales or exhales during normal ‘tidal’ breathing. The expiratory reserve volume (ERV)

is the volume of air that can be exhaled from end-expiration of tidal breathing. The inspiratory vital capacity (IVC) is the volume of air that can be moved in and out of the lungs during full inspiration and full expiration. The residual volume (RV) is the amount of air or gas that remains in the lungs after maximal expiration. The inspiratory capacity (IC) is the maximum amount of air that can be inhaled from expiration during tidal breathing. The functional residual capacity (FRC) is the sum of RV and ERV, it is the amount of air remaining in the lungs at end expiration of tidal breathing. Finally, the total lung capacity (TLC) is the volume of air in the lungs after maximal inspiration.

Figure 1-6 shows an inspiratory – expiratory curve with all lung volumes labelled.

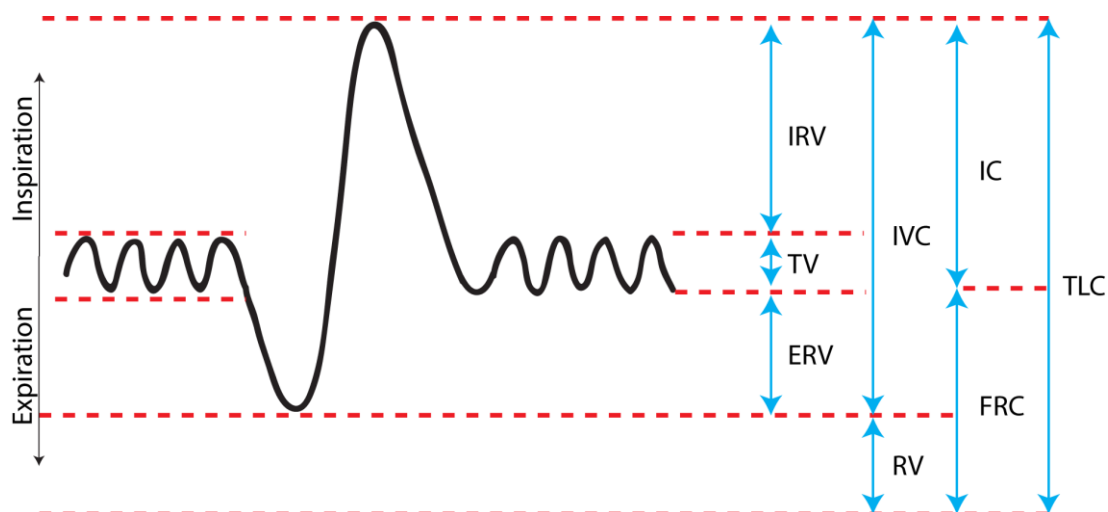


Figure 1-6. Inspiratory – expiratory curve showing lung volumes measured by plethysmography.

IRV: Inspiratory reserve volume, TV: Tidal volume, ERV: Expiratory reserve volume, IVC: Inspiratory vital capacity, RV: Residual volume, IC: Inspiratory capacity, FRC: Functional residual capacity, TLC: Total lung capacity

1.5.3 Diffusing Capacity of the Lung

The diffusing capacity of the lung for carbon monoxide is commonly used to evaluate pulmonary microcirculation and diffusion of gases across the alveolar – capillary membrane. There are two terms used for this measurement; the diffusing capacity for carbon monoxide (DL_{CO}) and the transfer factor for carbon monoxide (TL_{CO}). While

both are acceptable, there is no concrete consensus as to which term is the correct one, although it has been suggested, but not agreed upon, that TL_{CO} is more appropriate because the measurement does not solely reflect diffusion (60). Throughout the rest of this Thesis the DL_{CO} term will be used when referring to this measurement.

To measure diffusing capacity a trained technician coaches an individual through a maneuver involving 1) full exhalation to RV, 2) maximum inhalation to TLC, 3) a ~ 10 second breath-hold at TLC and 4) exhalation (61). During the inhalation step the test subject will inhale a gas mixture of helium (~10%), carbon monoxide (~0.3%) and room air (~85-90%). During the breath-hold step the carbon-monoxide and helium diffuse across the alveolar-capillary membrane throughout the lung. Finally, after the breath-hold the residual carbon-monoxide and helium is expired and this concentration is compared to the amount that was inhaled to estimate the amount of carbon monoxide that diffused into the pulmonary circulation. One important consideration when collecting DL_{CO} measurements is that the first bolus of air expired after the breath-hold was predominantly in the ‘anatomical dead-space’ of the large and central airways where gas exchange does not occur. Therefore, technology for measuring DL_{CO} discards this dead-space air (the volume of which is known through an equation: $2.2\text{ml} \cdot \text{kg body weight}$) and only collects the air which was in contact with the respiratory zone. In-line with the standardization of spirometry and plethysmography, the ATS and ERS have specified standards for the collection of DL_{CO} – TL_{CO} measurements as well (61).

1.6 Measuring Exercise Capacity and Pulmonary Symptoms

Measuring exercise capacity with a walk test and breathlessness and pulmonary symptoms through questionnaires can be used along with pulmonary function tests to better understand the impact of pulmonary function on daily activity.

1.6.1 The Six-Minute Walk Test

The six-minute walk test (6MWT) is an exercise test that is designed to measure the distance an individual can walk on a flat surface in six minutes (62). The test is supposed

to reflect the exercise capacity of activities a person would experience in their daily lives. Importantly, the results of the six-minute walk test, the six-minute walk distance (6MWD) in COPD patients have been shown to be reproducible, correlate with frequency of exacerbation episodes and mortality in COPD (63).

1.6.2 The St. George's Respiratory Questionnaire

The St. George's Respiratory Questionnaire (SGRQ) is used to measure the impact of respiratory disease on an individual's overall health, daily activities and perceived well-being (64). The questionnaire has four scores to rate the different components of respiratory disease: the symptoms score, the impact score, the activity score and the total score. For each component score the values range from zero to one-hundred with higher scores being more severe. Similar to other established measures of pulmonary function, SGRQ scores in COPD patients have been shown to be reproducible (64-66) and associated with other measures of pulmonary function (67).

1.6.3 Modified Medical Research Council Dyspnea Scale

The modified Medical Research Council (mMRC) dyspnea scale measures the impact of breathlessness on an individual's daily activity. The mMRC uses a straightforward scale of five grades ranging from 0 (no respiratory disability) to 4 (severe dyspnea with many limitations) to measure disability due to dyspnea (**Table 1-4**). It has been found that mMRC dyspnea scores are related to disease severity and predict all-cause mortality in COPD patients (68, 69).

Table 1-4. Modified Medical Research Council (mMRC) Dyspnea Scale (Adapted from 'Evaluation of Clinical Methods for Rating Dyspnea' (70))

<i>Grade</i>	<i>Description</i>
0	Not troubled with breathlessness except with strenuous exercise
1	Shortness of breath when hurrying on the level <i>or</i> walking up a slight hill
2	Walks slower than people of the same age on the level because of breathlessness <i>or</i> has to stop for breath when walking at own pace on the level
3	Stops for breath after walking ~100m <i>or</i> after a few minutes on the level
4	Too breathless to leave the house <i>or</i> breathless when dressing or undressing

1.7 The Role of Imaging to Study COPD

Although FEV₁ serves as the major endpoint for assessing the severity of airflow limitation and diagnosing COPD, it is clear that spirometry alone cannot fully characterize the heterogeneity of the disease. As previously mentioned in **Section 1.2**, COPD is an umbrella term encompassing large and small airways disease and emphysematous tissue destruction of the lung parenchyma, and the extent of each of these abnormalities vary from patient to patient (71). Therefore, simply measuring expiratory volumes at the mouth does not provide any regional information on lung pathophysiology nor indications on the relative contributions of airways disease and emphysema to lung function decline. In this regard, thoracic computed tomography (CT) and pulmonary magnetic resonance imaging (MRI) have emerged as robust and reliable tools for in vivo imaging of COPD. In recent years both CT and MRI have played important roles in advancing our knowledge on COPD heterogeneity and underlying pathophysiology and have simultaneously introduced the concept of radiological phenotyping to COPD to provide better stratification and targeted treatment options within COPD populations.

1.7.1 High-resolution Computed Tomography of the Lung

Conventional x-ray imaging is inherently limited to providing two-dimensional (2D) images of three-dimensional (3D) anatomical structures. CT technology overcomes this drawback by rotating the conventional x-ray tube around a patient to construct a 3D volume of the region of interest. The 3D volume created from the CT scan is made up of voxels (volume elements), each of which has a Hounsfield Unit (HU) associated with it based on the attenuation of x-rays through that region. The HU scale uses water as a reference, where water has a HU = 0, air has HU = -1000 and solid structures such as bone have HU > +1000 (72). Ultimately, CT provides 3D images of the anatomy based on density and since many tissues and organs within the body have different densities, good contrast can be achieved with conventional CT imaging.

As described in **Section 1.2**, one pathophysiological phenotype of COPD is emphysema. When the alveoli are destroyed, alveolar ducts and sacs coalesce and the distal airspaces

enlarge to ultimately cause a decrease in parenchymal density. Therefore, on CT images, emphysematous regions within the lung have attenuation values close to that of air (≤ -950 HU) and appear darker than the higher density parenchyma surrounding them. Extensive research and debate is ongoing to determine an optimal HU threshold to define emphysema on CT. Currently, the most commonly used HU threshold to identify emphysema is -950 HU, whereby regions of the lung with attenuation ≤ -950 HU are considered to be emphysematous. This threshold has been confirmed to correspond to emphysematous lesions on pulmonary histology of macroscopic (73) and microscopic (74) emphysema. **Figure 1-7** shows emphysematous lung regions ≤ -950 HU on CT in a healthy volunteer and a COPD patient. It is important to note that other thresholds are also in use for the purpose of identifying mild emphysema (-910 HU) and gas trapping on expiratory CT (-856 HU) (75-77). Another method for quantifying emphysema on CT is focused on the HU below which fifteen percent of all x-ray attenuation values fall (PD_{15}). Using this method, the measurement of emphysema is a HU not a percent of the lung as it is with the threshold cutoff. While both the threshold and percentile methods are widely used and considered appropriate for cross-sectional studies, the 15th percentile analysis is recommended for longitudinal studies because it is less sensitive to changes in CT scanner technology that may occur over time (78). At the same time, methods for quantitatively describing the size and distribution of emphysematous clusters (regions of RA_{950}) on CT have also emerged (79). The value of measuring these low attenuation clusters (LAC) relies on the concept that emphysematous lesions tend to coalesce and form larger clusters (bullae) as emphysema progresses. The total number of emphysematous clusters (clusters of voxels < -950 HU) is plotted against the cluster size in the log-log domain. The slopes of the plots can then be described by the power law and the value of the slope is obtained by linear regression and used to quantify the LAC. In this manner subjects with early or mild forms of emphysema have smaller and more emphysematous clusters and subsequently have a more negative LAC (higher slope) while COPD subjects who have larger emphysematous bullae and fewer total clusters have a more positive LAC (flatter slope).

Along with regionally mapping and quantifying emphysema within the lung, thoracic CT is also used to evaluate airway structure. By measuring the cross section of the airways,

measurements of the airway lumen and wall thickness can be assessed. The measurements of airway wall area percent (WA%) and lumen area (LA) were the first to be shown to significantly correlate with measures of lung function in COPD patients where the airway wall thickness increased and airway lumen area decreased as FEV₁ decreased (80). However this early work focused predominantly on measuring the large and central airways which do not reflect the main site of airflow obstruction in COPD. Subsequent studies have transitioned to measuring higher generation airways (81), counting the number of airways visible on CT (82) and estimating small airway dimensions (83). **Figure 1-7** shows CT airway trees in a healthy volunteer and COPD patient. Visibly, the COPD subject has few and thinner airways than the healthy subject.

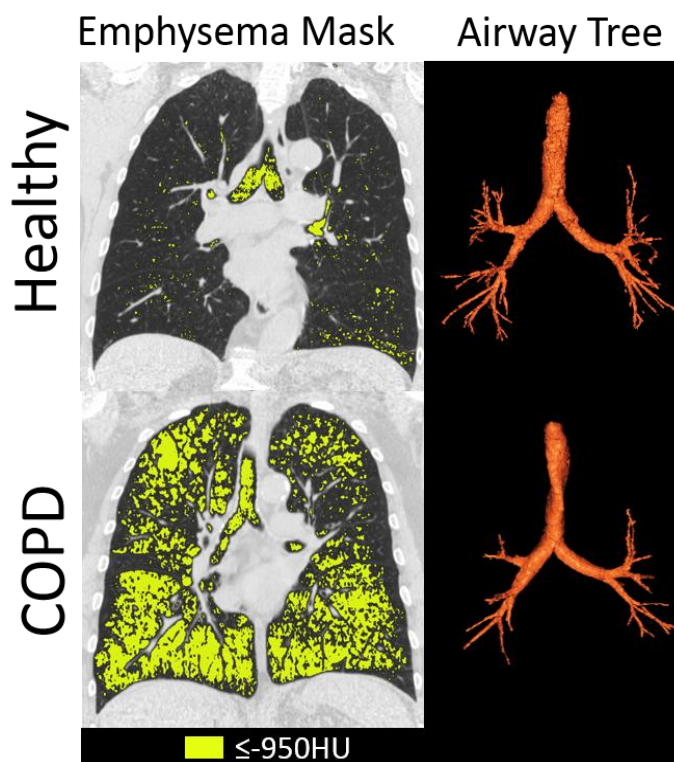


Figure 1-7. Thoracic CT and segmented airway tree of a healthy volunteer and a COPD patient.

Emphysema, or areas of the lung ≤ -950 HU on CT are shown in yellow. Compared to the healthy subject, the COPD patient has more severe emphysema and fewer airways present as measured by CT.

Lastly, an important consideration for using CT to evaluate and monitor COPD is the radiation dose associated with each scan. In COPD, longitudinal monitoring is necessary for evaluating disease progression or response to treatment or surgery. The radiation dose associated with a single conventional chest CT is estimated to be ~7 mSv which is equivalent to 2.8yr of natural background radiation (84). Therefore, if CT is the only option available for pulmonary imaging at a specific centre or within a region, it is clear that careful planning is required in order to longitudinally image a COPD patient because of the risk of radiation-induced cancers from cumulative dose of serial CT scans. One potential solution to the burden of radiation dose associated with chest CT scanning is the further development of iterative reconstruction techniques and their incorporation into clinical use instead of, or along with, filtered back projection (FBP) reconstruction approaches. Unlike FBP which is rapid and requires little computational processing, iterative approaches correct image data using a variety of models and require long computing times (85). Current iterative reconstruction techniques can produce thoracic CT images of similar or better quality (based on signal-to-noise ratio) using a lower dose than images acquired using FBP (86). The downside is that the reconstructive approach used during acquisition influences quantitative (and potentially qualitative) measurements of emphysema and airways disease. Therefore, scientists and clinicians would need to meet and overcome the challenge of standardizing reconstructive approaches across academic centres where large-scale and long-term follow-up studies are ongoing in order to compare and concatenate data.

1.7.2 Nuclear Medicine: Ventilation Scintigraphy

Single photon emission computed tomography (SPECT) is a tool that can provide information of pulmonary ventilation and perfusion through the use of radiolabeled aerosols and gases. In SPECT, gamma radiation from an injected or inhaled radiopharmaceutical is received by detectors which convert the radiation into visible light that can be used to produce an image based on its spatial and quantitative information. For pulmonary ventilation imaging using SPECT, a radiolabeled aerosol or gas inhaled at the mouth during tidal breathing is used to provide gamma energy necessary to create ventilation images. The most important consideration for ventilation imaging with

SPECT is the choice of which radiotracer to use. Within the past thirty years ^{99m}Tc -Technegas aerosol has emerged as the most widely used radiotracer for pulmonary SPECT. Other popular radiotracers used for pulmonary SPECT include ^{99m}Tc labelled with diethylaminetriaminepentacetic acid (DTPA), ^{133}Xe , and ^{81m}Kr . Unlike Technegas aerosol however, the laborious and expensive production along with their nuclear and physical properties have limited their use in ventilation studies. ^{133}Xe has a half-life on the order of days and low gamma radiation energy which has deterred its routine use. ^{81m}Kr on the other hand has an optimal gamma energy and short biological half-life making it suitable for ventilation imaging. However the availability of rubidium generators required to produce the metastable Kr are limited, expensive and require almost daily replacement so the production of ^{81m}Kr for ventilation imaging is often not feasible. At the same time an important consideration acknowledged by physicists and clinicians using these techniques was the size of these radiotracers being inhaled. Particles larger than $2\mu\text{m}$ are predominantly deposited in the large and central airways whereas particles $<1\mu\text{m}$ are deposited in the distal alveoli, therefore larger size radiotracers ($>1\mu\text{m}$) do not provide much information about distal lung regions when used for ventilation imaging. ^{99m}Tc -DTPA particles are $1\mu\text{m}$ - $2\mu\text{m}$ in size which has made it a popular alternative to ^{99m}Tc -Technegas aerosol. Technegas labelled with ^{99m}Tc is a newer solid aerosol type radiotracer with particle sizes ranging from $0.005\mu\text{m}$ - $0.2\mu\text{m}$ (87). The small size combined with Compton-scattering predominant gamma energy and easy and inexpensive production have made it the radiotracer of choice for ventilation scintigraphy. Several studies have compared the common radiotracers used for ventilation scintigraphy and have consistently reported superior results with ^{99m}Tc -Technegas (88-90). Importantly, both ^{99m}Tc -Technegas and ^{81m}Kr have been shown to produce similar quality ventilation images (91), however Technegas is favored due to its inexpensive and efficient production.

SPECT imaging of pulmonary ventilation has been used extensively for the assessment and diagnosis of pulmonary embolism but has not been widely exploited to evaluate and characterize COPD. Unlike CT (**Section 1.7.1**) techniques, SPECT pulmonary structure-function relationships and measurements in COPD are not as well established which has

limited its routine use in clinical practice and subsequently in large-scale epidemiological COPD studies.

1.7.3 Pulmonary Magnetic Resonance Imaging

Magnetic resonance imaging (MRI) is a tool that provides high-resolution images of the anatomy based on the magnetic properties of the protons in a tissue. Unlike CT, MRI does not require the use of ionizing radiation from x-ray beams or any other forms of contrast making it an attractive option for pulmonary imaging at first glance. However, the physical properties of the lungs are very different from other tissues in the body and pose unique challenges to generate clinically useful pulmonary images using conventional MRI methods.

When a sample containing protons is placed inside an MRI machine, the nuclear magnetic moment of the protons within the sample or tissue align with the magnetic field. To collect the signal necessary to generate an image a radiofrequency pulse (RF) is applied which tilts the protons nuclear magnetic moments away from its axis in the magnet. After this, the proton magnetization returns to its equilibrium state through longitudinal (T_1) and transverse (T_2) components of relaxation. Relaxation causes a changing magnetic field which induces a voltage in a receive coil (Faraday's Law of induction) that is spatially encoded to produce an MR image. The signal intensity in an MR image is proportional to the proton density of the sample being imaged (92).

The lungs have a tissue density that is approximately ten times lower than other tissues in the body, meaning they also have ten times lower proton density per gram of tissue compared to other tissues as well (93). Therefore, assuming perfect imaging conditions, the achievable MRI signal of the lungs is still ten-fold weaker than other tissues. Secondly, the lungs are almost entirely made up of air – tissue boundaries. Oxygen in room air is paramagnetic and in tissue it is diamagnetic and therefore there is a net magnetic susceptibility difference at each and every air – tissue boundary. This magnetic susceptibility difference spread over millions of air – tissue boundaries produces a highly inhomogeneous local magnetic field in the lungs which causes extremely fast relaxation of the protons after the initial RF pulse and associated with this, rapid signal decay. With

the combination of a low proton density and highly inhomogeneous local field within the lungs, conventional MRI methods such as those applied clinically to tissues like the brain or liver do not produce clinically relevant images of the lung parenchyma or airways. Until recently, this has limited the application of MRI to evaluate COPD predominantly to perfusion and hemodynamic studies using contrast-enhanced techniques (94). **Figure 1-8** shows conventional MR images in a healthy individual and a COPD patient. It is visibly obvious that the proton MR image does not provide a wealth of information on pulmonary parenchymal structure or function. However, an emerging series of MRI pulse sequences, called ‘ultra-short echo time’ (UTE) pulse sequences have been developed (95) and optimized to capture the rapidly decaying MR signal in the lung before it is lost. These UTE sequences are different from conventional proton MRI sequences in that they combine a fast RF pulse and rapid data acquisition steps to measure relaxation before it is completely lost. Recent research with UTE sequences suggests that UTE pulmonary MRI is capable of producing images of similar quality to thoracic CT (96).

Pulmonary MRI with hyperpolarized noble gases (^3He and ^{129}Xe) is another method of providing high-resolution images of the lungs that has gained traction in research settings over the past few decades. This MRI method is based on previous nuclear physics research (97) that recognized the potential for capturing MR signal from polarized ^3He and ^{129}Xe in the gaseous phase. This previous work showed that through a technique called ‘spin-exchange optical pumping’, collisions between ^3He or ^{129}Xe with gaseous rubidium could transfer angular momentum to the noble gas nuclei amplifying the achievable MR signal with these gases. In the early stages this work focused on using ^{129}Xe but became more common in ^3He due its ease in MR imaging compared to ^{129}Xe (98). Currently however this area of MRI research is transitioning back to ^{129}Xe owing to its lower cost and higher natural abundance over ^3He . Once the noble gas of choice is hyperpolarized, to collect images of the lungs an individual must inhale the gas and perform a short breath-hold while an MRI sequence collects the data. Several methods exist for doing this but the most commonly used method is to coach the patient to breathe the gas in from a bag (99). After a subject inhales the noble gas from the bag, there is an option of collecting ‘static-ventilation’ images or diffusion-weighted MR images, both of

which provide distinct measurements on lung pathophysiology. **Figure 1-8** shows ^3He (cyan) and ^{129}Xe (purple) static-ventilation MR images in a healthy volunteer and a COPD patient. Compared to the healthy subject, the COPD patient exhibits markedly greater ventilation heterogeneity on both ^3He and ^{129}Xe images.

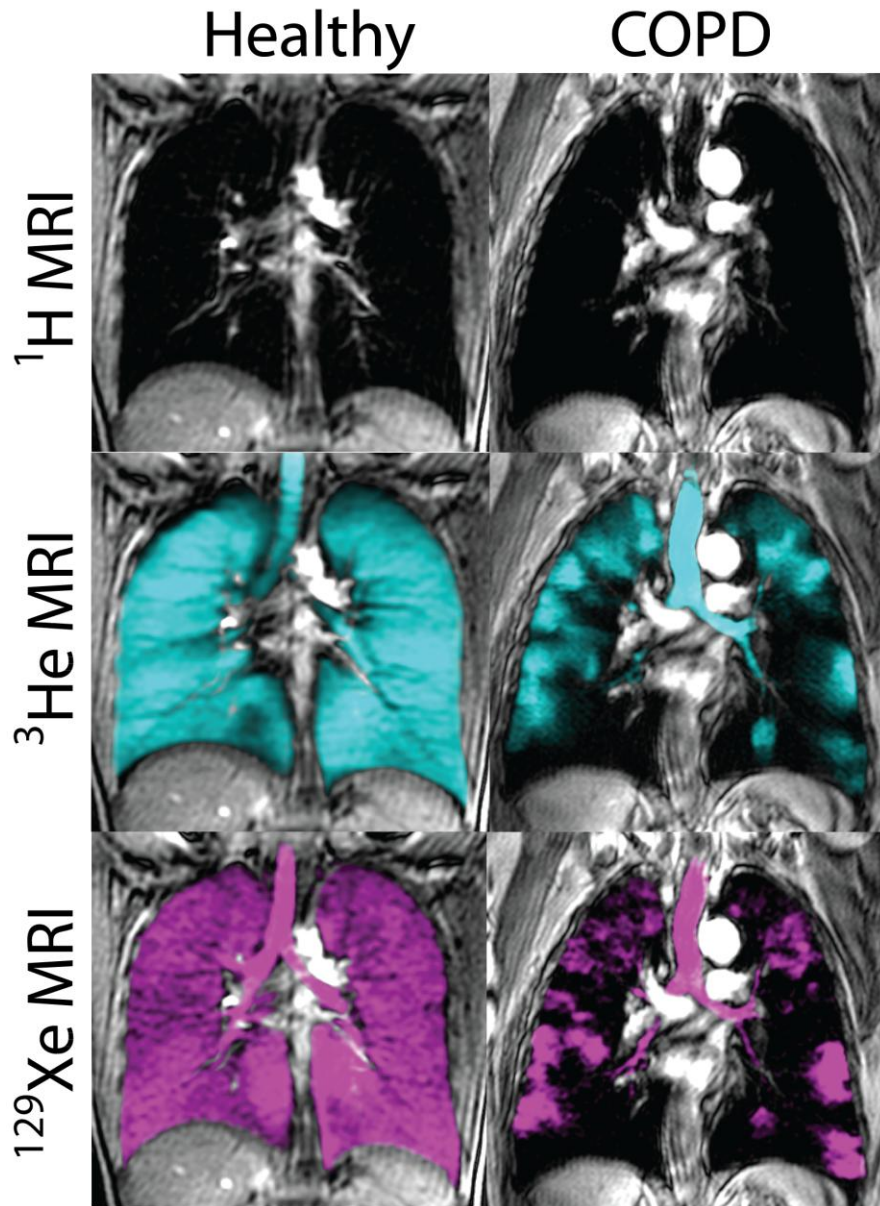


Figure 1-8. ^1H , ^3He and ^{129}Xe MRI of a healthy and COPD patient.

Reproduced with permission from 'Imaging Evidence of the Relationship Between Atherosclerosis and Chronic Obstructive Pulmonary Disease' *Imaging in Medicine*; DOI: 10.2217/iim.13.70, 2013 (47).

Static-ventilation hyperpolarized noble gas images show which regions of the lung participate in ventilation. Several studies have confirmed that static-ventilation MR images show that healthy non-smoking subjects without airflow limitation exhibit homogeneous ventilation signal throughout their lungs (shown in **Figure 1-8** and **1-9**) (100, 101). In contrast, in subjects with COPD, it has been observed (101-104) that ventilation signal is heterogeneous with many regions within the lung not receiving any ventilation at all. Importantly, these regions of signal void or ‘ventilation defects’ have also been shown to be reproducible over time (105). Ventilation defects have become central to image analysis techniques for quantifying disease on noble gas MR images since they are speculated to represent regions of the lung with underlying disease. Initially, visual grading of ventilated and unventilated regions was used to evaluate disease severity from noble gas MR images (101), but more recently, methods that normalize the volume of ventilation defects to the total thoracic cavity volume to calculate a ventilation defect percent (VDP) have become more common (106).

Diffusion-weighted MRI is a tool that provides information on the movement of nuclei in a sample. With regards to hyperpolarized noble gas MRI of the lung, diffusion-weighted methods have been harnessed to provide details on alveolar microstructure (107). After the gas is inhaled, diffusion-weighted MRI pulse sequences can be applied to sensitize the data acquisition to the diffusion of gas within the alveoli. Over a pre-specified time-interval, the gas nuclei move within the airspaces, bouncing off the alveolar walls. Diffusion-weighted sequences provide information pertaining to the distance the nuclei travel per unit time within the airspaces. Ultimately, this type of imaging is used to calculate the apparent diffusion coefficient (ADC) that reflects the amount of restriction of the gas nuclei in the distal lung airspaces. These are valuable measurements for assessing structural changes to the lungs in COPD because emphysematous destruction is characterized by airspace enlargement. Previous work (107-110) has established that noble gas MRI ADC measurements are correlated with lung function in COPD and importantly, the ADC measures of microstructure seem to be more sensitive to early- or pre-clinical changes to lung structure than conventional pulmonary function testing and CT (111).

Figure 1-9 shows ^3He static-ventilation and diffusion-weighted MR images in a healthy subject and four COPD patients with increasing grades of severity. In the healthy subject, the ventilation pattern is homogeneous throughout the lung with the lung periphery and contour of the diaphragm clearly visualized by the ^3He gas. Similarly, in the healthy subject the ADC map shows low ADC throughout the lung. In contrast, in the COPD subjects the ventilation signal becomes increasingly heterogeneous with more and larger ventilation defects visible in more severe grades of disease. Concomitant with the increasing ventilation heterogeneity, ADC maps get brighter (worse) indicative of worse microstructural emphysema with increasing disease severity.

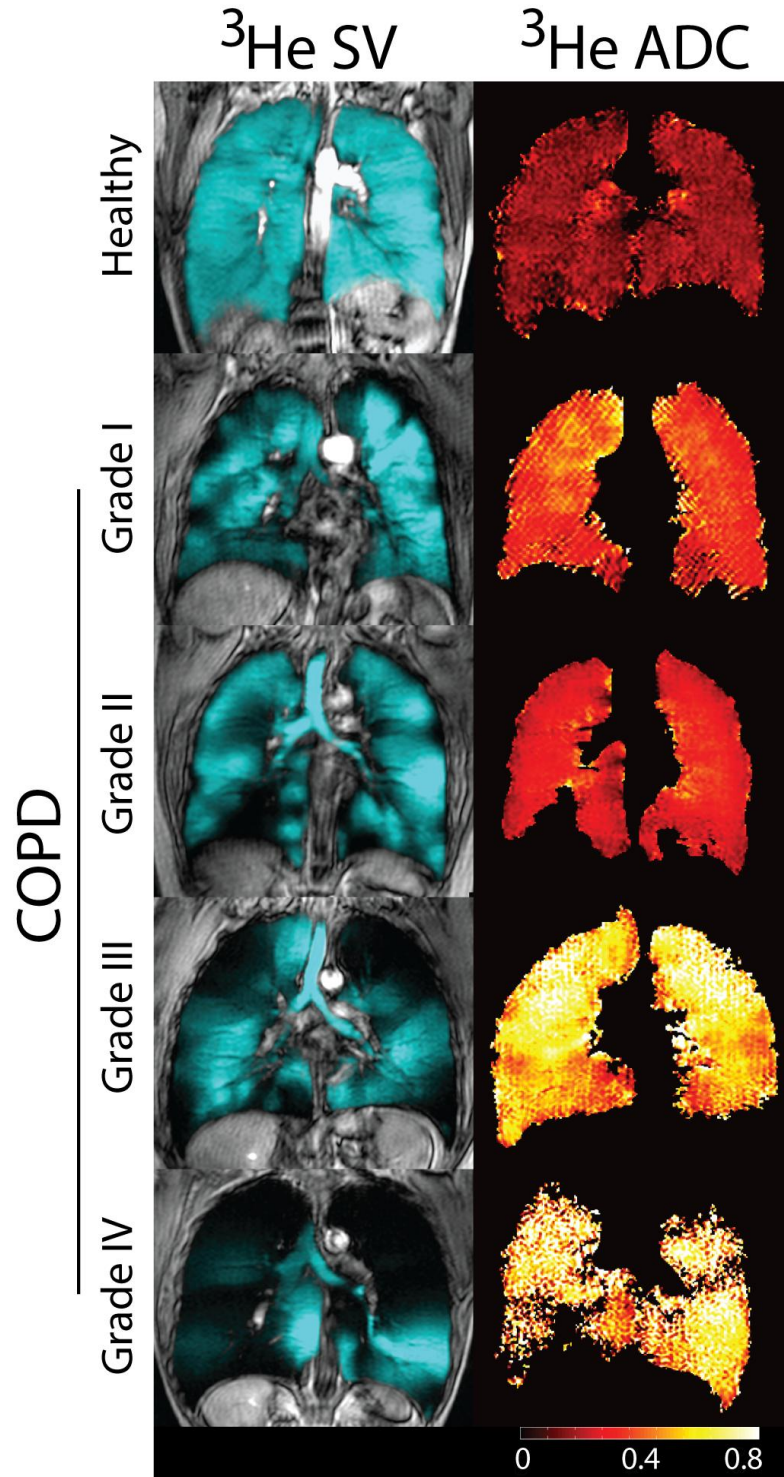


Figure 1-9. Static-ventilation (SV) and apparent diffusion coefficient (ADC) ^3He MR images in a healthy volunteer and four COPD patients with increasing severity of airflow limitation.

Reproduced with permission from 'Imaging Evidence of the Relationship Between Atherosclerosis and Chronic Obstructive Pulmonary Disease' *Imaging in Medicine*; DOI: 10.2217/im. 13.70, 2013 (47).

1.8 COPD Phenotypes

It is now known that the relative contributions of airways disease and emphysema on airflow limitation vary greatly from patient to patient (71). With this emerging knowledge, phenotyping COPD patients based on underlying pathophysiology has become an attractive concept as it would allow scientists and clinicians to stratify patients into distinct groups to study clinical features and form targeted treatment plans. At the same time, advances in quantitative pulmonary imaging with CT and MRI have become the methods of choice for identifying distinct COPD phenotypes. Since imaging is well suited to measure airway dimensions and quantify the severity of emphysema, imaging studies have focused on three phenotypes in particular; an emphysema – predominant phenotype, an airways disease – predominant phenotype and a mixed airways disease – emphysema phenotype. Whether or not an individual phenotype predicts worse pulmonary function or outcomes is an area of active research but studies have shown distinct clinical features among different phenotypes (112). For example, it has been shown that patients with predominant emphysema have worse exercise capacity, tend to have more exacerbations and have more rapid disease progression than patients with airways disease (113, 114). While it has also been found that subjects with predominant airways disease exhibit worse overall symptoms including coughing and wheezing (114). However, a combination of both airways disease and emphysema appears to be associated with the highest risk of exacerbations and debilitating respiratory symptoms (113). Interestingly the development of a predominant phenotype does not appear to be related to smoking history, whereby patients who have the same number of pack years may develop either emphysema or airways disease or a mix of the two. Given this, it seems likely that there is an important genetic component which determines the phenotype individuals will develop during the course of the disease and several studies have provided evidence of this (115, 116).

Along with whole-lung phenotyping methods, ‘regional’ emphysema phenotyping studies have also emerged (117-120). These studies are motivated by the fact that patients with the same amount of emphysema show high heterogeneity in clinical features. Unfortunately, phenotyping patients based on the spatial location of emphysema has

yielded inconsistent results and the clinical relevance of emphysema distribution is still not entirely clear.

Given that smoking history is not associated with the development of a particular COPD phenotype over another, it seems plausible that the different pathophysiological and biochemical construction of the lungs between males and females might be partly responsible for phenotype heterogeneity among cohorts. Currently, more females than males have COPD. It is not known for sure what has caused the drastic increase in COPD diagnoses among females over the past few decades, but one hypothesis attributes the rising incidence of COPD among females to their steadily increasing use of cigarette smoking since World War II (121). In line with this theory, biochemical and epidemiological studies suggest that female lungs are more susceptible to the toxic effects of cigarette smoke than males (122). With regards to COPD phenotypes, it has been found that females predominantly suffer from airways disease while males have more emphysema (123, 124). A better understanding of the connection between COPD phenotype and sex might serve as a valuable endpoint to treat COPD, and sophisticated imaging techniques may provide valuable information on this relationship in the future (123, 125, 126).

The two major goals of COPD therapy are 1) to alleviate respiratory symptoms and 2) to prevent or avoid exacerbation episodes. Phenotyping COPD patients has the potential to do both of these things. However, many questions remain unanswered with regards to the origins of COPD phenotypes in pre- or sub-clinical disease. It seems likely that if we could develop a better understanding of the origins and progression of lung disease phenotypes as they occur in pre- or subclinical stages, we would be able to create patient-specific treatment plans to better satisfy the two major goals of COPD therapy.

1.9 Thesis Hypothesis and Objectives

The prevalence and underdiagnosis of COPD and shortcomings of COPD treatments may be attributable to the paucity of information that exists on early- or subclinical structural

and functional changes to the lungs of ex- or current-smokers. This may be partly due to the fact that imaging studies have focused on cohorts with diagnosed and established COPD to provide a better understanding of pathophysiology in disease and less on susceptible individuals without airflow limitation (127). Furthermore, most histological investigations on the underlying origins of disease and disease progression have also been biased to post-mortem or post-surgical specimens of excised lung tissue from localized regions of the lung (13, 128, 129). Therefore, there is little information available regarding susceptible groups of ex-smokers without evidence of airflow limitation. This would help to provide a better understanding on pre- or subclinical COPD pathophysiology and perhaps strategies on how to treat it. Pulmonary imaging with hyperpolarized ^3He MRI and CT can provide high-resolution images and quantitative measurements of pulmonary ventilation, alveolar microstructure and macroscopic emphysema. Therefore, the overarching goal of this thesis was to exploit sensitive and direct pulmonary imaging measurements in ex-smokers without airflow limitation to better characterize and phenotype early- or subclinical forms of COPD.

As described in **Section 1.3**, there is strong evidence to support underlying mechanistic links between COPD and cardiovascular disease. Studies investigating the relationship between comorbid vascular and lung disease have predominantly focused on either cardiovascular disease or COPD patients who have a long-standing diagnosis of either condition. Therefore, while it has been established that a relationship between lung function decline and cardiovascular disease exists, little is known about the pre- or subclinical origins of this comorbid relationship. Furthermore, few studies have exploited pulmonary structural and functional imaging with MRI and CT to characterize whether a particular COPD phenotype is associated with cardiovascular disease complications. Hence, the aim of **Chapter 2** was to evaluate ^3He MRI, CT and carotid ultrasound data from ex- and never-smokers without airflow limitation or diagnosis of cardiovascular disease to provide a better understanding of the pathophysiological link between subclinical COPD and vascular disease. We hypothesized that ex- and never-smokers without airflow limitation would show pulmonary imaging evidence of airways disease that would be related to subclinical atherosclerosis independently of smoking history.

Findings in **Chapter 2** showed that ex-smokers without spirometry evidence of airflow limitation showed evidence of pre- or subclinical lung disease on ^3He MR images. In that study, ex-smokers without airflow limitation had significantly higher ^3He VDP than never-smokers but were not different with regards to pulmonary function test measurements. This suggested that ex-smokers without airflow limitation have pre- or subclinical airways disease and/or emphysema that is apparent on ^3He MRI but not with spirometry or other breathing tests. In **Chapter 3** our objective was to improve our understanding of the underlying lung disease phenotype that cause ^3He ventilation defects in ex-smokers without airflow limitation by using regional ^3He MRI ventilation and diffusion-weighted measurements and regional CT airway and emphysema measurements. Owing to research that suggested airway obstruction and obliteration is the dominant COPD phenotype in mild disease, we hypothesized that ^3He ventilation defects in ex-smokers without airflow limitation would be spatially and quantitatively related to airway remodeling but not emphysema.

The study in **Chapter 3** showed that hyperpolarized ^3He ventilation heterogeneity is present in ex-smokers without airflow limitation and the underlying etiology of ventilation defects in such subjects could be phenotyped using regional MRI and CT measurements. We therefore wanted to use regional MRI and CT measurements to phenotype ex-smokers with a COPD diagnosis. It is widely known that ex-smokers with COPD exhibit ventilation defects and emphysema throughout the lung, however the clinical relevance of the spatial location of ventilation heterogeneity and emphysema within the lung is not completely understood. Our objective in **Chapter 4** was to phenotype ex-smokers with COPD based on the apical-to-basal distribution of ventilation abnormalities and emphysema to better understand how regional phenotypes change as COPD progresses. Data presented in **Chapter 4** show that with increasing disease severity there is a basal-to-apical progression of ventilation abnormalities and an apical-to-basal progression of emphysema, suggestive of distinct apical-basal lung COPD phenotypes.

Lastly, **Chapter 5** will provide an overview and summary of the findings and conclusions from Chapters 2-4, address study specific and general limitations of the imaging studies presented in this thesis and provide motivation for future imaging studies in COPD.

1.10 References

1. Vestbo J, Hurd SS, Agusti AG, Jones PW, Vogelmeier C, Anzueto A, et al. Global strategy for the diagnosis, management, and prevention of chronic obstructive pulmonary disease: GOLD executive summary. *American journal of respiratory and critical care medicine*. 2013;187(4):347-65.
2. Buist AS, McBurnie MA, Vollmer WM, Gillespie S, Burney P, Mannino DM, et al. International variation in the prevalence of COPD (the BOLD Study): a population-based prevalence study. *Lancet*. 2007;370(9589):741-50.
3. Organization WH. *The Global Burden of Disease: 2004 Update*. Switzerland: WHO Press; 2008.
4. Lozano R, Naghavi M, Foreman K, Lim S, Shibuya K, Aboyans V, et al. Global and regional mortality from 235 causes of death for 20 age groups in 1990 and 2010: a systematic analysis for the Global Burden of Disease Study 2010. *Lancet*. 2012;380(9859):2095-128.
5. Organization WH. *Global Health Estimates 2014 Summary Tables: Death by Cause, Age and Sex 2000-2012* 2014.
6. Canadian Institute for Health Information: *Health Indicators 2008*. Ottawa: 2008.
7. Society TCT. *The Human and Economic Burden of COPD: A Leading Cause of Hospital Admission in Canada*. 2010.
8. Mittmann N, Kuramoto L, Seung SJ, Haddon JM, Bradley-Kennedy C, Fitzgerald JM. The cost of moderate and severe COPD exacerbations to the Canadian healthcare system. *Respir Med*. 2008;102(3):413-21.
9. Hill K, Goldstein RS, Guyatt GH, Blouin M, Tan WC, Davis LL, et al. Prevalence and underdiagnosis of chronic obstructive pulmonary disease among patients at risk in primary care. *CMAJ*. 2010;182(7):673-8.
10. Bednarek M, Maciejewski J, Wozniak M, Kuca P, Zielinski J. Prevalence, severity and underdiagnosis of COPD in the primary care setting. *Thorax*. 2008;63(5):402-7.
11. Dunnill MS, Massarella GR, Anderson JA. A comparison of the quantitative anatomy of the bronchi in normal subjects, in status asthmaticus, in chronic bronchitis, and in emphysema. *Thorax*. 1969;24(2):176-9.

12. Reid L. Measurement of the bronchial mucous gland layer: a diagnostic yardstick in chronic bronchitis. *Thorax*. 1960;15:132-41.
13. Hogg JC, Chu F, Utokaparch S, Woods R, Elliott WM, Buzatu L, et al. The nature of small-airway obstruction in chronic obstructive pulmonary disease. *N Engl J Med*. 2004;350(26):2645-53.
14. West JB. *Respiratory Physiology: The Essentials* (8th Edition): Lippincott Williams and Wilkins; 2008.
15. Hogg JC. Pathophysiology of airflow limitation in chronic obstructive pulmonary disease. *Lancet*. 2004;364(9435):709-21.
16. Mead J. The lung's "quiet zone". *The New England journal of medicine*. 1970;282(23):1318.
17. Snider G. The definition of emphysema; report of a National Heart, Lung and Blood Institute. Division of Lung Diseases. Workshop. *Am Rev Respir Dis*. 1985;132:182-5.
18. Kohnlein T, Welte T. Alpha-1 antitrypsin deficiency: pathogenesis, clinical presentation, diagnosis, and treatment. *Am J Med*. 2008;121(1):3-9.
19. Takahashi M, Fukuoka J, Nitta N, Takazakura R, Nagatani Y, Murakami Y, et al. Imaging of pulmonary emphysema: a pictorial review. *Int J Chron Obstruct Pulmon Dis*. 2008;3(2):193-204.
20. Global Initiative for Asthma (GINA) and Global Initiative for Chronic Obstructive Pulmonary Disease (GOLD). *Diagnosis of Disease of Chronic Airflow Limitation: Asthma, COPD and Asthma-COPD Overlap Syndrome (ACOS)*. 2015.
21. Drazen JM, Postma DS, Rabe KF. The asthma-COPD overlap syndrome. *New England Journal of Medicine*. 2015;373(13):1241-9.
22. Gibson PG, Simpson JL. The overlap syndrome of asthma and COPD: what are its features and how important is it? *Thorax*. 2009;64(8):728-35.
23. James AL, Palmer LJ, Kicic E, Maxwell PS, Lagan SE, Ryan GF, et al. Decline in lung function in the Busselton Health Study: the effects of asthma and cigarette smoking. *Am J Respir Crit Care Med*. 2005;171(2):109-14.
24. Lange P, Parner J, Vestbo J, Schnohr P, Jensen G. A 15-year follow-up study of ventilatory function in adults with asthma. *N Engl J Med*. 1998;339(17):1194-200.
25. Chalmers JD, Goeminne P, Aliberti S, McDonnell MJ, Lonni S, Davidson J, et al. The bronchiectasis severity index. An international derivation and validation study. *Am J Respir Crit Care Med*. 2014;189(5):576-85.

26. Smith IE, Jurriaans E, Diederich S, Ali N, Shneerson JM, Flower CD. Chronic sputum production: correlations between clinical features and findings on high resolution computed tomographic scanning of the chest. *Thorax*. 1996;51(9):914-8.
27. O'Brien C, Guest PJ, Hill SL, Stockley RA. Physiological and radiological characterisation of patients diagnosed with chronic obstructive pulmonary disease in primary care. *Thorax*. 2000;55(8):635-42.
28. Currie DC, Cooke JC, Morgan AD, Kerr IH, Delany D, Strickland B, et al. Interpretation of bronchograms and chest radiographs in patients with chronic sputum production. *Thorax*. 1987;42(4):278-84.
29. Gatheral T, Kumar N, Sansom B, Lai D, Nair A, Vlahos I, et al. COPD-related bronchiectasis; independent impact on disease course and outcomes. *COPD*. 2014;11(6):605-14.
30. Blasi F, Chalmers JD, Aliberti S. COPD and bronchiectasis: phenotype, endotype or co-morbidity? *COPD*. 2014;11(6):603-4.
31. Anthonisen NR, Skeans MA, Wise RA, Manfreda J, Kanner RE, Connett JE, et al. The effects of a smoking cessation intervention on 14.5-year mortality: a randomized clinical trial. *Ann Intern Med*. 2005;142(4):233-9.
32. Sin DD, MacNee W. Chronic obstructive pulmonary disease and cardiovascular diseases: a "vulnerable" relationship. *American journal of respiratory and critical care medicine*. 2013;187(1):2-4.
33. Sin DD, Man SF. Chronic obstructive pulmonary disease as a risk factor for cardiovascular morbidity and mortality. *Proc Am Thorac Soc*. 2005;2(1):8-11.
34. Sin DD, Man SF. Why are patients with chronic obstructive pulmonary disease at increased risk of cardiovascular diseases? The potential role of systemic inflammation in chronic obstructive pulmonary disease. *Circulation*. 2003;107(11):1514-9.
35. Schroeder EB, Welch VL, Evans GW, Heiss G. Impaired lung function and subclinical atherosclerosis. The ARIC Study. *Atherosclerosis*. 2005;180(2):367-73.
36. Van Eeden S, Leipsic J, Paul Man SF, Sin DD. The relationship between lung inflammation and cardiovascular disease. *American journal of respiratory and critical care medicine*. 2012;186(1):11-6.
37. Iwamoto H, Yokoyama A, Kitahara Y, Ishikawa N, Haruta Y, Yamane K, et al. Airflow limitation in smokers is associated with subclinical atherosclerosis. *American journal of respiratory and critical care medicine*. 2009;179(1):35-40.
38. Barr RG, Ahmed FS, Carr JJ, Hoffman EA, Jiang R, Kawut SM, et al. Subclinical atherosclerosis, airflow obstruction and emphysema: the MESA Lung Study. *The European respiratory journal*. 2012;39(4):846-54.

39. Engstrom G, Hedblad B, Valind S, Janzon L. Asymptomatic leg and carotid atherosclerosis in smokers is related to degree of ventilatory capacity: longitudinal and cross-sectional results from 'Men born in 1914', Sweden. *Atherosclerosis*. 2001;155(1):237-43.
40. Kim SJ, Yoon DW, Lee EJ, Hur GY, Jung KH, Lee SY, et al. Carotid atherosclerosis in patients with untreated chronic obstructive pulmonary disease. *Int J Tuberc Lung Dis*. 2011;15(9):1265-70, i.
41. Zureik M, Kauffmann F, Touboul PJ, Courbon D, Ducimetiere P. Association between peak expiratory flow and the development of carotid atherosclerotic plaques. *Arch Intern Med*. 2001;161(13):1669-76.
42. Frantz S, Nihlen U, Dencker M, Engstrom G, Lofdahl CG, Wollmer P. Atherosclerotic plaques in the internal carotid artery and associations with lung function assessed by different methods. *Clin Physiol Funct Imaging*. 2012;32(2):120-5.
43. van Gestel YR, Flu WJ, van Kuijk JP, Hoeks SE, Bax JJ, Sin DD, et al. Association of COPD with carotid wall intima-media thickness in vascular surgery patients. *Respir Med*. 2010;104(5):712-6.
44. Lahousse L, van den Bouwhuijsen QJ, Loth DW, Joos GF, Hofman A, Witteman JC, et al. Chronic obstructive pulmonary disease and lipid core carotid artery plaques in the elderly: the Rotterdam Study. *American journal of respiratory and critical care medicine*. 2013;187(1):58-64.
45. Sabit R, Shale DJ. Vascular structure and function in chronic obstructive pulmonary disease: a chicken and egg issue? *American journal of respiratory and critical care medicine*. 2007;176(12):1175-6.
46. Sin DD, Wu L, Man SF. The relationship between reduced lung function and cardiovascular mortality: a population-based study and a systematic review of the literature. *Chest*. 2005;127(6):1952-9.
47. Pike D, Lindenmaier TJ, Sin DD, Parraga G. Imaging evidence of the relationship between atherosclerosis and chronic obstructive pulmonary disease. *Imaging in Medicine*. 2014;6(1):53-73.
48. Lindberg A, Bjerg A, Ronmark E, Larsson LG, Lundback B. Prevalence and underdiagnosis of COPD by disease severity and the attributable fraction of smoking Report from the Obstructive Lung Disease in Northern Sweden Studies. *Respir Med*. 2006;100(2):264-72.
49. Shahab L, Jarvis MJ, Britton J, West R. Prevalence, diagnosis and relation to tobacco dependence of chronic obstructive pulmonary disease in a nationally representative population sample. *Thorax*. 2006;61(12):1043-7.

50. Colak Y, Marott JL, Vestbo J, Lange P. Overweight and obesity may lead to under-diagnosis of airflow limitation: findings from the Copenhagen City Heart Study. *COPD*. 2015;12(1):5-13.
51. O'Donnell DE, Ciavaglia CE, Neder JA. When obesity and chronic obstructive pulmonary disease collide. Physiological and clinical consequences. *Ann Am Thorac Soc*. 2014;11(4):635-44.
52. Lazarus R, Sparrow D, Weiss ST. Effects of obesity and fat distribution on ventilatory function: the normative aging study. *Chest*. 1997;111(4):891-8.
53. O'Donnell DE, Deesomchok A, Lam Y-M, Guenette JA, Amornputtisathaporn N, Forkert L, et al. Effects of BMI on static lung volumes in patients with airway obstruction. *CHEST Journal*. 2011;140(2):461-8.
54. Fletcher C, Peto R. The natural history of chronic airflow obstruction. *Br Med J*. 1977;1(6077):1645-8.
55. Vestbo J, Edwards LD, Scanlon PD, Yates JC, Agusti A, Bakke P, et al. Changes in Forced Expiratory Volume in 1 Second over Time in COPD. *New England Journal of Medicine*. 2011;365(13):1184-92.
56. Lange P, Celli B, Agusti A, Boje Jensen G, Divo M, Faner R, et al. Lung-Function Trajectories Leading to Chronic Obstructive Pulmonary Disease. *N Engl J Med*. 2015;373(2):111-22.
57. Miller MR, Hankinson J, Brusasco V, Burgos F, Casaburi R, Coates A, et al. Standardisation of spirometry. *The European respiratory journal*. 2005;26(2):319-38.
58. Sood A, Dawson BK, Henkle JQ, Hopkins-Price P, Quails C. Effect of change of reference standard to NHANES III on interpretation of spirometric 'abnormality'. *Int J Chron Obstruct Pulmon Dis*. 2007;2(3):361-7.
59. Wanger J, Clausen JL, Coates A, Pedersen OF, Brusasco V, Burgos F, et al. Standardisation of the measurement of lung volumes. *Eur Respir J*. 2005;26(3):511-22.
60. Fitting JW. Transfer factor for carbon monoxide: a glance behind the scene. *Swiss Med Wkly*. 2004;134(29-30):413-8.
61. Macintyre N, Crapo RO, Viegi G, Johnson DC, van der Grinten CP, Brusasco V, et al. Standardisation of the single-breath determination of carbon monoxide uptake in the lung. *Eur Respir J*. 2005;26(4):720-35.
62. Laboratories ACoPSfCPF. ATS statement: guidelines for the six-minute walk test. *American Journal of Respiratory and Critical Care Medicine*. 2002;166(1):111.
63. Polkey MI, Spruit MA, Edwards LD, Watkins ML, Pinto-Plata V, Vestbo J, et al. Six-minute-walk test in chronic obstructive pulmonary disease: minimal clinically

- important difference for death or hospitalization. *Am J Respir Crit Care Med*. 2013;187(4):382-6.
64. Jones PW, Quirk FH, Baveystock CM, Littlejohns P. A self-complete measure of health status for chronic airflow limitation. The St. George's Respiratory Questionnaire. *Am Rev Respir Dis*. 1992;145(6):1321-7.
65. Jones PW, Quirk FH, Baveystock CM. The St George's Respiratory Questionnaire. *Respir Med*. 1991;85 Suppl B:25-31; discussion 3-7.
66. Meguro M, Barley EA, Spencer S, Jones PW. Development and Validation of an Improved, COPD-Specific Version of the St. George Respiratory Questionnaire. *Chest*. 2007;132(2):456-63.
67. Westwood M, Bourbeau J, Jones PW, Cerulli A, Capkun-Niggli G, Worthy G. Relationship between FEV1 change and patient-reported outcomes in randomised trials of inhaled bronchodilators for stable COPD: a systematic review. *Respir Res*. 2011;12:40.
68. Mahler DA, Ward J, Waterman LA, McCusker C, ZuWallack R, Baird JC. Patient-reported dyspnea in COPD reliability and association with stage of disease. *CHEST Journal*. 2009;136(6):1473-9.
69. Casanova C, Marin JM, Martinez-Gonzalez C, de Lucas-Ramos P, Mir-Viladrich I, Cosio B, et al. Differential Effect of Modified Medical Research Council Dyspnea, COPD Assessment Test, and Clinical COPD Questionnaire for Symptoms Evaluation Within the New GOLD Staging and Mortality in COPD. *CHEST Journal*. 2015;148(1):159-68.
70. Mahler DA, Wells CK. Evaluation of clinical methods for rating dyspnea. *CHEST Journal*. 1988;93(3):580-6.
71. Agusti A, Calverley P, Celli B, Coxson HO, Edwards LD, Lomas DA, et al. Characterisation of COPD heterogeneity in the ECLIPSE cohort. *Respir Res*. 2010;11(1):122-36.
72. Lynch DA, Boisselle, P. A. *CT of the Airways*. Springer. 2008.
73. Gevenois PA, De Maertelaer V, De Vuyst P, Zanen J, Yernault J-C. Comparison of computed density and macroscopic morphometry in pulmonary emphysema. *American journal of respiratory and critical care medicine*. 1995;152(2):653-7.
74. Gevenois PA, De Vuyst P, de Maertelaer V, Zanen J, Jacobovitz D, Cosio MG, et al. Comparison of computed density and microscopic morphometry in pulmonary emphysema. *American journal of respiratory and critical care medicine*. 1996;154(1):187-92.

75. Coxson HO, Leipsic J, Parraga G, Sin DD. Using Pulmonary Imaging to Move Chronic Obstructive Pulmonary Disease beyond FEV1. *Am J Respir Crit Care Med*. 2014;190(2):135-44.
76. Muller NL, Staples CA, Miller RR, Abboud RT. "Density mask". An objective method to quantitate emphysema using computed tomography. *Chest*. 1988;94(4):782-7.
77. Zach JA, Newell JD, Jr., Schroeder J, Murphy JR, Curran-Everett D, Hoffman EA, et al. Quantitative computed tomography of the lungs and airways in healthy nonsmoking adults. *Invest Radiol*. 2012;47(10):596-602.
78. Coxson HO. Quantitative chest tomography in COPD research: chairman's summary. *Proc Am Thorac Soc*. 2008;5(9):874-7.
79. Mishima M, Hirai T, Itoh H, Nakano Y, Sakai H, Muro S, et al. Complexity of terminal airspace geometry assessed by lung computed tomography in normal subjects and patients with chronic obstructive pulmonary disease. *Proc Natl Acad Sci U S A*. 1999;96(16):8829-34.
80. Nakano Y, Muro S, Sakai H, Hirai T, Chin K, Tsukino M, et al. Computed tomographic measurements of airway dimensions and emphysema in smokers. Correlation with lung function. *American journal of respiratory and critical care medicine*. 2000;162(3 Pt 1):1102-8.
81. Hackx M, Bankier AA, Gevenois PA. Chronic obstructive pulmonary disease: CT quantification of airways disease. *Radiology*. 2012;265(1):34-48.
82. Diaz AA, Valim C, Yamashiro T, Estepar RS, Ross JC, Matsuoka S, et al. Airway count and emphysema assessed by chest CT imaging predicts clinical outcome in smokers. *Chest*. 2010;138(4):880-7.
83. Nakano Y, Wong JC, de Jong PA, Buzatu L, Nagao T, Coxson HO, et al. The prediction of small airway dimensions using computed tomography. *American journal of respiratory and critical care medicine*. 2005;171(2):142-6.
84. Mayo JR, Aldrich J, Muller NL, Fleischner S. Radiation exposure at chest CT: a statement of the Fleischner Society. *Radiology*. 2003;228(1):15-21.
85. Hara AK, Paden RG, Silva AC, Kujak JL, Lawder HJ, Pavlicek W. Iterative reconstruction technique for reducing body radiation dose at CT: feasibility study. *American Journal of Roentgenology*. 2009;193(3):764-71.
86. Leipsic J, Nguyen G, Brown J, Sin D, Mayo JR. A prospective evaluation of dose reduction and image quality in chest CT using adaptive statistical iterative reconstruction. *American Journal of Roentgenology*. 2010;195(5):1095-9.
87. Bajc M, Jogi J. Quantitative Ventilation/Perfusion Tomography: The Foremost Technique for Pulmonary Embolism Diagnosis. *Pulmonary Embolism: InTech*; 2012.

88. Magnant J, Vecellio L, de Monte M, Grimbert D, Valat C, Boissinot E, et al. Comparative analysis of different scintigraphic approaches to assess pulmonary ventilation. *J Aerosol Med.* 2006;19(2):148-59.
89. Jogi J, Jonson B, Ekberg M, Bajc M. Ventilation-perfusion SPECT with ^{99m}Tc-DTPA versus Technegas: a head-to-head study in obstructive and nonobstructive disease. *J Nucl Med.* 2010;51(5):735-41.
90. Hartmann IJ, Hagen PJ, Stokkel MP, Hoekstra OS, Prins MH. Technegas versus (^{81m}Kr) ventilation-perfusion scintigraphy: a comparative study in patients with suspected acute pulmonary embolism. *J Nucl Med.* 2001;42(3):393-400.
91. Bajc MaJ, J. Quantitative Ventilation/Perfusion Tomography: The Foremost Technique for Pulmonary Embolism Diagnosis. 2012.
92. McRobbie DW, Moore, E. A., Graves, M. J. and Graves, M. R. MRI: From Picture to Proton. Cambridge University Press. 2006.
93. Wild J, Marshall H, Bock M, Schad L, Jakob P, Puderbach M, et al. MRI of the lung (1/3): methods. *Insights into imaging.* 2012;3(4):345-53.
94. Ley-Zaporozhan J, Ley S, Kauczor H-U. Proton MRI in COPD. *COPD: Journal of Chronic Obstructive Pulmonary Disease.* 2007;4(1):55-65.
95. Johnson KM, Fain SB, Schiebler ML, Nagle S. Optimized 3D ultrashort echo time pulmonary MRI. *Magnetic Resonance in Medicine.* 2013;70(5):1241-50.
96. Ma W, Sheikh K, Svenningsen S, Pike D, Guo F, Etemad-Rezai R, et al. Ultra-short echo-time pulmonary MRI: Evaluation and reproducibility in COPD subjects with and without bronchiectasis. *J Magn Reson Imaging.* 2014.
97. Albert MS, Cates GD, Driehuys B, Happer W, Saam B, Springer CS, Jr., et al. Biological magnetic resonance imaging using laser-polarized ¹²⁹Xe. *Nature.* 1994;370(6486):199-201.
98. Mugler JP, Altes TA. Hyperpolarized ¹²⁹Xe MRI of the human lung. *Journal of Magnetic Resonance Imaging.* 2013;37(2):313-31.
99. Kirby M, Parraga G. Pulmonary functional imaging using hyperpolarized noble gas MRI: six years of start-up experience at a single site. *Academic radiology.* 2013;20(11):1344-56.
100. Sheikh K, Paulin GA, Svenningsen S, Kirby M, Paterson NA, McCormack DG, et al. Pulmonary ventilation defects in older never-smokers. *J Appl Physiol (1985).* 2014;117(3):297-306.

101. Woodhouse N, Wild JM, Paley MN, FICHELE S, Said Z, Swift AJ, et al. Combined helium-3/proton magnetic resonance imaging measurement of ventilated lung volumes in smokers compared to never-smokers. *J Magn Reson Imaging*. 2005;21(4):365-9.
102. Kirby M, Mathew L, Heydarian M, Etemad-Rezai R, McCormack DG, Parraga G. Chronic obstructive pulmonary disease: quantification of bronchodilator effects by using hyperpolarized (3)He MR imaging. *Radiology*. 2011;261(1):283-92. Epub 2011/08/05.
103. Kirby M, Mathew L, Wheatley A, Santyr GE, McCormack DG, Parraga G. Chronic obstructive pulmonary disease: longitudinal hyperpolarized (3)He MR imaging. *Radiology*. 2010;256(1):280-9.
104. Kirby M, Svenningsen S, Owrangi A, Wheatley A, Farag A, Ouriadov A, et al. Hyperpolarized 3He and 129Xe MR imaging in healthy volunteers and patients with chronic obstructive pulmonary disease. *Radiology*. 2012;265(2):600-10.
105. Mathew L, Evans A, Ouriadov A, Etemad-Rezai R, Fogel R, Santyr G, et al. Hyperpolarized 3He magnetic resonance imaging of chronic obstructive pulmonary disease: reproducibility at 3.0 tesla. *Acad Radiol*. 2008;15(10):1298-311.
106. Kirby M, Heydarian M, Svenningsen S, Wheatley A, McCormack DG, Etemad-Rezai R, et al. Hyperpolarized 3He magnetic resonance functional imaging semiautomated segmentation. *Acad Radiol*. 2012;19(2):141-52.
107. Fain SB, Altes TA, Panth SR, Evans MD, Waters B, Mugler JP, 3rd, et al. Detection of age-dependent changes in healthy adult lungs with diffusion-weighted 3He MRI. *Acad Radiol*. 2005;12(11):1385-93.
108. Stavngaard T, Sogaard LV, Batz M, Schreiber LM, Dirksen A. Progression of emphysema evaluated by MRI using hyperpolarized (3)He (HP (3)He) measurements in patients with alpha-1-antitrypsin (A1AT) deficiency compared with CT and lung function tests. *Acta Radiol*. 2009;50(9):1019-26. Epub 2009/10/30.
109. Swift AJ, Wild JM, FICHELE S, Woodhouse N, Fleming S, Waterhouse J, et al. Emphysematous changes and normal variation in smokers and COPD patients using diffusion 3He MRI. *Eur J Radiol*. 2005;54(3):352-8.
110. Woods JC, Choong CK, Yablonskiy DA, Bentley J, Wong J, Pierce JA, et al. Hyperpolarized 3He diffusion MRI and histology in pulmonary emphysema. *Magn Reson Med*. 2006;56(6):1293-300.
111. Wang C, Mugler JP, 3rd, de Lange EE, Patrie JT, Mata JF, Altes TA. Lung injury induced by secondhand smoke exposure detected with hyperpolarized helium-3 diffusion MR. *J Magn Reson Imaging*. 2014;39(1):77-84.
112. Han MK, Agusti A, Calverley PM, Celli BR, Criner G, Curtis JL, et al. Chronic obstructive pulmonary disease phenotypes: the future of COPD. *Am J Respir Crit Care Med*. 2010;182(5):598-604.

113. Han MK, Kazerooni EA, Lynch DA, Liu LX, Murray S, Curtis JL, et al. Chronic obstructive pulmonary disease exacerbations in the COPDGene study: associated radiologic phenotypes. *Radiology*. 2011;261(1):274-82.
114. Han MK. Clinical correlations of computed tomography imaging in chronic obstructive pulmonary disease. *Ann Am Thorac Soc*. 2013;10 Suppl:S131-7.
115. Zhou JJ, Cho MH, Castaldi PJ, Hersh CP, Silverman EK, Laird NM. Heritability of chronic obstructive pulmonary disease and related phenotypes in smokers. *American journal of respiratory and critical care medicine*. 2013;188(8):941-7.
116. Manichaikul A, Hoffman EA, Smolonska J, Gao W, Cho MH, Baumhauer H, et al. Genome-wide study of percent emphysema on computed tomography in the general population. The Multi-Ethnic Study of Atherosclerosis Lung/SNP Health Association Resource Study. *American journal of respiratory and critical care medicine*. 2014;189(4):408-18.
117. Gietema HA, Zanen P, Schilham A, van Ginneken B, van Klaveren RJ, Prokop M, et al. Distribution of emphysema in heavy smokers: impact on pulmonary function. *Respir Med*. 2010;104(1):76-82.
118. Ju J, Li R, Gu S, Leader JK, Wang X, Chen Y, et al. Impact of emphysema heterogeneity on pulmonary function. *PLoS One*. 2014;9(11):e113320.
119. Mohamed Hoesein FA, van Rikxoort E, van Ginneken B, de Jong PA, Prokop M, Lammers JW, et al. Computed tomography-quantified emphysema distribution is associated with lung function decline. *Eur Respir J*. 2012;40(4):844-50.
120. Mair G, Miller JJ, McAllister D, Maclay J, Connell M, Murchison JT, et al. Computed tomographic emphysema distribution: relationship to clinical features in a cohort of smokers. *Eur Respir J*. 2009;33(3):536-42.
121. Sin DD, Cohen SB, Day A, Coxson H, Pare PD. Understanding the biological differences in susceptibility to chronic obstructive pulmonary disease between men and women. *Proc Am Thorac Soc*. 2007;4(8):671-4.
122. Gan WQ, Man SF, Postma DS, Camp P, Sin DD. Female smokers beyond the perimenopausal period are at increased risk of chronic obstructive pulmonary disease: a systematic review and meta-analysis. *Respir Res*. 2006;7:52.
123. Martinez FJ, Curtis JL, Sciruba F, Mumford J, Giardino ND, Weinmann G, et al. Sex differences in severe pulmonary emphysema. *American journal of respiratory and critical care medicine*. 2007;176(3):243-52.
124. Tam A, Churg A, Wright JL, Zhou S, Kirby M, Coxson HO, et al. Sex Differences in Airway Remodeling in a Mouse Model of Chronic Obstructive Pulmonary Disease. *American journal of respiratory and critical care medicine*. 2015(ja).

125. Kirby M, Zhang W, Laratta PK, Sin DD, Lam S, Coxson HO, editors. Sex differences in chronic obstructive pulmonary disease evaluated using optical coherence tomography. SPIE BiOS; 2014: International Society for Optics and Photonics.
126. Sverzellati N, Calabro E, Randi G, La Vecchia C, Marchiano A, Kuhnigk JM, et al. Sex differences in emphysema phenotype in smokers without airflow obstruction. *The European respiratory journal*. 2009;33(6):1320-8.
127. Celli BR, Decramer M, Wedzicha JA, Wilson KC, Agustí A, Criner GJ, et al. An official American Thoracic Society/European Respiratory Society statement: research questions in chronic obstructive pulmonary disease. *American journal of respiratory and critical care medicine*. 2015;191(7):e4-e27.
128. Hogg JC, Macklem PT, Thurlbeck WM. The resistance of collateral channels in excised human lungs. *J Clin Invest*. 1969;48(3):421-31.
129. McDonough JE, Yuan R, Suzuki M, Seyednejad N, Elliott WM, Sanchez PG, et al. Small-airway obstruction and emphysema in chronic obstructive pulmonary disease. *N Engl J Med*. 2011;365(17):1567-75.

CHAPTER 2

To provide a better understanding of the mechanistic links between pre- or sub-clinical atherosclerosis and chronic obstructive pulmonary disease we acquired three-dimensional carotid ultrasound and pulmonary hyperpolarized ^3He magnetic resonance imaging measurements in ex- and never-smokers without clinical evidence of vascular or pulmonary disease.

The contents of this chapter have been previously published in COPD: Journal of Chronic Obstructive Pulmonary Disease (JCOPD) and permission to reproduce the article was granted by Taylor and Francis Publishing Group on behalf of JCOPD and is provided in Appendix D.

D Pike, M Kirby, TJ Lindenmaier, K Sheikh, C Neron, DG Hackam, JD Spence, A Fenster, NAM Paterson, HO Coxson, DG McCormack, DD Sin and G Parraga. Pulmonary Abnormalities and Carotid Atherosclerosis in Ex-smokers without Airflow Limitation. Journal of Chronic Obstructive Pulmonary Disease; DOI: 10.3109: 1-0, 2014

2 Pulmonary Abnormalities and Carotid Atherosclerosis in Ex-Smokers Without Airflow Limitation

2.1 Introduction

Cardiovascular disease is the single largest cause of hospitalization in patients with mild and moderate chronic obstructive pulmonary disease (COPD), and after lung cancer, the leading cause of death (1, 2). In addition, in COPD patients, there is a dose-response relationship for pulmonary structure-function abnormalities with carotid atherosclerosis (3-8), coronary artery calcification (9-12) and vascular dysfunction (13-16). While these studies have shown the presence of cardiovascular disease in patients with COPD that cannot be explained by smoking history alone (3, 4, 6-8, 17), the mechanisms by which cardiovascular disease may be accelerated in COPD are not clear, nor is our understanding of these relationships in early or milder subclinical stages.

While the diagnosis and monitoring of COPD is mainly based on spirometry measurements of airflow obstruction (18, 19), such measurements cannot fully characterize the pathophysiological changes that occur in obstructive lung disease (20). These include regional small-airways disease and microstructural changes in the terminal

bronchi and parenchyma. In this regard, regional imaging measurements provided by hyperpolarized ^3He magnetic resonance imaging (MRI) are highly sensitive to pulmonary abnormalities in asymptomatic ex-smokers (21, 22) and never-smokers with second-hand smoke exposure (23). Similarly, airway morphology and parenchyma density x-ray computed tomography (CT) measurements from the ECLIPSE (24) and COPDGene (25) studies showed the utility of CT phenotypes (26) for stratifying COPD patients (27-29).

Cardiovascular disease, predominated by large vessel atherosclerosis, is associated with obstructive lung disease (30, 31) that can be regionally and quantitatively evaluated using carotid ultrasound (US). The burden of atherosclerosis can be quantified (32) using carotid intima-media thickness (IMT) measurements and this is believed to reflect medial hypertrophy and intima abnormalities, and importantly, IMT correlates with cardiovascular outcomes (32, 33). In a similar manner, three-dimensional ultrasound (3DUS) carotid atherosclerosis measurements (34) of carotid wall and plaque abnormalities are sensitive predictors of cardiovascular risk (35-37) and in some patients, these provide a better estimate of plaque burden and risk (37).

There is a paucity of direct evidence relating subclinical lung disease and atherosclerosis in otherwise healthy ex-smokers. To provide a better understanding of the relationship between carotid atherosclerosis and pulmonary abnormalities common to ex-smokers with obstructive lung disease, our objective was to acquire highly sensitive pulmonary and carotid 3D imaging measurements in never- and ex-smokers with normal pulmonary function. We hypothesized that quantitative 3D imaging phenotypes would provide a way to tease out potential relationships for early or mild sub-clinical emphysema or airways disease with atherosclerosis in subjects at risk.

2.2 Materials and Methods

2.2.1 Study subjects

Ex-smokers (≥ 10 pack-year smoking history) without symptoms or a physician-diagnosis of COPD and normal spirometry ($\text{FEV}_1/\text{FVC} \geq 70\%$) as well as never-smokers (< 1 pack-year smoking history) with no history of chronic respiratory or significant or uncontrolled

cardiovascular disease between 50-90 years of age were recruited. These subjects enrolled in response to advertisements placed within the community and at local healthy aging exercise and atherosclerosis prevention clinics. All subjects provided written informed consent to a protocol approved by a local research ethics board and Health Canada.

2.2.2 Spirometry and plethysmography

Spirometry, plethysmography and diffusing capacity of carbon monoxide (DL_{CO}) measurements were performed according to the American Thoracic Society guidelines (19). An ndd EasyOne spirometer (ndd Medizintechnik AG, Zurich, Switzerland) was used to measure FEV_1 and FVC. Whole body plethysmography was performed for lung volumes and DL_{CO} measurements were recorded using a gas analyzer (MedGraphics Corporation, St. Paul, Minnesota, USA).

2.2.3 Imaging

High-resolution B-mode ultrasound (US) images were acquired (ATL HDI 5000; Philips, Bothel, Washington, USA) as previously described (38) using a 50 mm L12-5 MHz transducer (frequency=8.5 MHz, Philips). Gain, focal points and time-depth compensation were optimized by the sonographer taking into consideration neck size, carotid anatomy and tissue depth. Two dimensional images were reconstructed into a 3D volume as previously described (39, 40). MRI was performed on a whole body 3.0 Tesla Discovery 750MR (General Electric Health Care, Milwaukee, Wisconsin, USA) MRI system. 1H and 3He MRI were performed as previously described (41) with the subject in an inspiration breath-hold (FRC+1L). For ex-smokers only, computed tomography (CT) was acquired within 10 minutes of MRI and at the same lung volume (FRC+1L) to ensure similar parenchymal distension in a method previously described (41).

2.2.4 Image analysis

Carotid IMT was measured from the longitudinal plane of the 3DUS volume using Prowin 24.0 software (Medical Technologies International Inc., Palm Desert, California,

USA) as previously described (42). Carotid total plaque volume (TPV) and vessel wall volume (VWV) were measured as previously described (43).

³He MRI ventilation defect percent (VDP) and apparent diffusion coefficients (ADC) were measured using semi-automated segmentation generated using custom-built software in MATLAB R2007b (The Math-works Inc., Natick, Massachusetts, USA) as previously described (44, 45). CT volumes were analyzed using Pulmonary Workstation 2.0 (PW2, VIDA Diagnostics Inc., Coralville, Iowa, USA). Pulmonary CT images were analyzed for airway dimensions including wall area percent (WA%), lumen area (LA) and standardized wall thickness of airways with an inner perimeter of 10 mm (Pi10) (46). In addition, the relative area of the lung with CT attenuation values less than -950HU (RA₉₅₀) and total airway count were also measured using PW2.

2.2.5 Statistics

Normality of data was tested using the Shapiro-Wilk test and when significant, the Mann-Whitney U test for nonparametric data was performed using SPSS Statistics V20.0 (SPSS Inc., Chicago, Illinois, USA). Unpaired two tailed t-test comparisons were performed using GraphPad Prism V4.0 (GraphPad Software Inc., California, USA) and Welch's correction used when the F test for equal variances was significant. The Holm-Bonferroni correction (47) was performed for multiple unpaired t-test comparisons. Multiple regression analyses were performed in SPSS to determine the relationship between carotid US measurements with ³He MRI VDP and pulmonary function parameters. Partial correlations were computed using SPSS. Multiple regression and correlation models were adjusted for age, BMI and DL_{CO} since these parameters are established risk factors for cardiovascular and pulmonary diseases (8, 48). Results were considered significant when the probability of two-tailed type I error was less than 5% (p<0.05) and summary data are presented as mean ± SD unless otherwise indicated.

2.3 Results

As shown in **Table 2-1**, 61 subjects including 27 ex-smokers (73 ± 9 yr, 18 male) and 34 never-smokers (72 ± 6 yr, 18 male) were evaluated. Except for BMI, ($p=0.001$) there were no significant differences between subject groups for demographic characteristics.

Table 2-1. Demographic, pulmonary function, thoracic CT and carotid ultrasound data for all study subjects

	Ex-smokers n=27	Never-smokers n=34	Significance of Difference p*
Age yrs (\pm SD)	73 (9)	72 (6)	1.0
Male n	18	18	-
BMI kg·m ⁻² (\pm SD)	30 (3)	27 (3)	0.001
Pack years (\pm SD)	27 (18)	-	-
Years quit (\pm SD)	26 (6)	-	-
FEV ₁ % _{pred} (\pm SD)	106 (16)	106 (18)	0.89
FVC % _{pred} (\pm SD)	97 (13)	101 (17)	1.0
FEV ₁ /FVC (\pm SD)	81 (7)	77 (5)	0.36
TLC % _{pred} (\pm SD)	102 (14)	106 (15)	1.0
IC % _{pred} (\pm SD)	107 (14)	107 (22)	1.0
RV % _{pred} (\pm SD)	110 (26)	109 (29)	1.0
RV/TLC (\pm SD)	42 (7)	39 (13)	0.96
Raw% _{pred} (\pm SD)	115 (72)	76 (34)	0.11
DL _{CO} % _{pred} (\pm SD)	83 (17)	87 (20)	1.0
ADC cm ² /s (\pm SD)	0.29 (0.04) ¹	0.26 (0.03) ²	0.20
VDP % (\pm SD)	7 (3) ¹	3 (2) ²	0.001
IMT mm (\pm SD)	0.84 (0.10)	0.77 (0.09)	0.11
TPV mm ³ (\pm SD)	250 (200)	60 (90)	0.002
VWV mm ³ (\pm SD)	910 (190) ³	890 (170) ⁴	1.0
5 th gen. WA% (\pm SD)	61 (2)	-	-
5 th gen. LA mm ² (\pm SD)	17 (11)	-	-
Pi10 mm (\pm SD)	4.1 (0.17)	-	-
RA ₉₅₀ % (\pm SD)	1.5 (1.4)	-	-
Airway Count n (\pm SD)	127 (35)		

BMI: Body mass index, FEV₁: Forced expiratory volume in one second, FVC: Forced vital capacity, TLC: Total lung capacity, IC: Inspiratory capacity, RV: Residual volume, Raw: Airways resistance, DL_{CO}: Diffusing capacity for carbon monoxide, ADC: Apparent diffusion coefficient, VDP: Ventilation defect percentage, IMT: Intima-media thickness, TPV: Total plaque volume, VWV: Vessel wall volume, 5th gen.: Fifth generation airway, WA%: Airway wall area percentage, LA: Airway lumen area, Pi10: Standardized wall thickness of airways with an inner perimeter of 10mm, RA₉₅₀: Relative area of the lung with attenuation values below -950HU, SD: Standard deviation, %pred: Percent of predicted value

*Data are Holm-Bonferroni corrected p-values for unpaired t-test comparisons

¹n=26, ²n=29, ³n=22, ⁴n=30

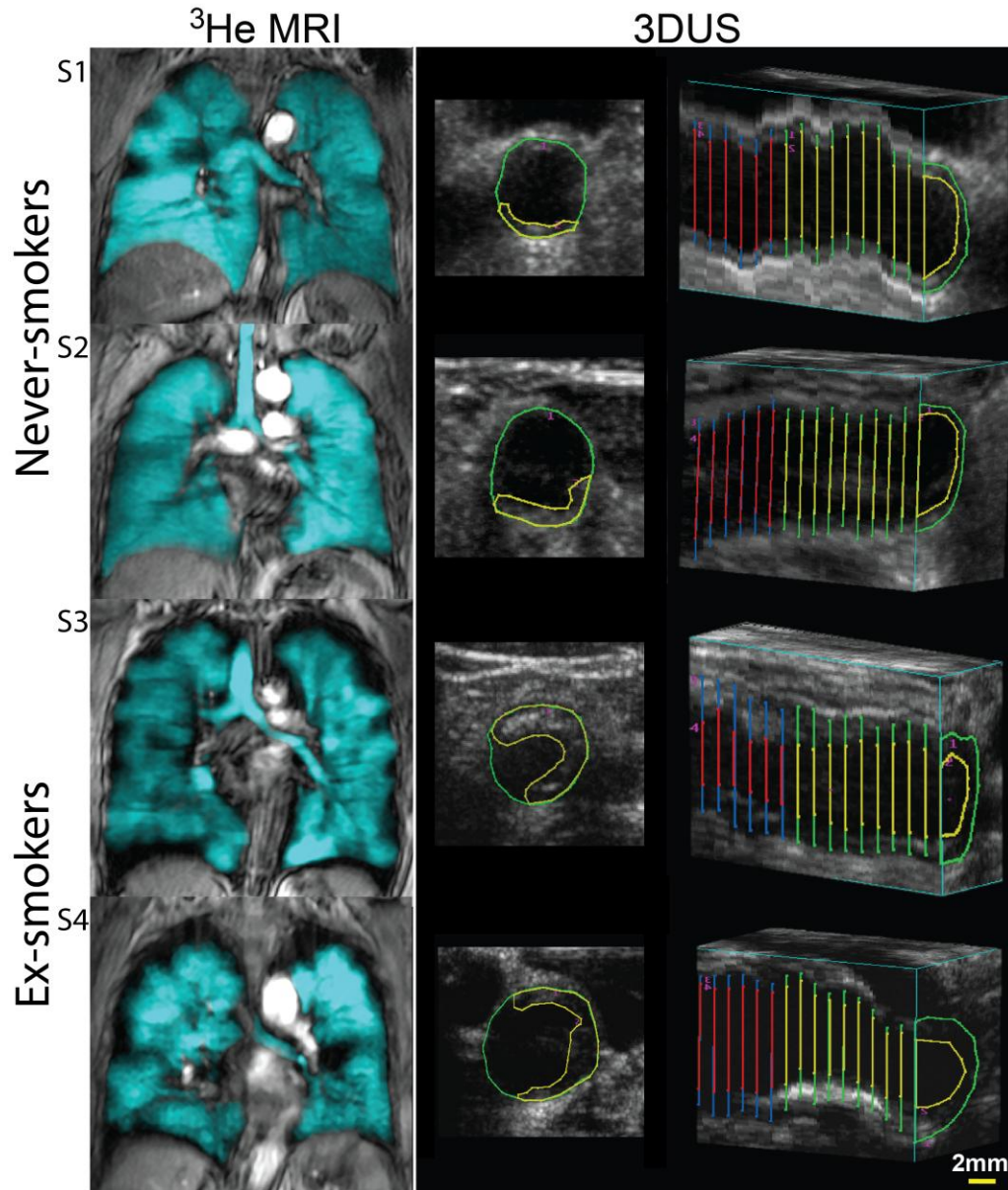


Figure 2-1. Representative ^3He MRI and 3DUS images for two never-smokers (S1 and S2) and two ex-smokers (S3 and S4). Never-smoker S1 is a 67-year old female with $\text{FEV}_1=120\%$, $\text{FEV}_1/\text{FVC}=0.77$, ^3He MRI $\text{VDP}=3\%$, $\text{TPV}=20\text{mm}^3$ and $\text{IMT}=0.79\text{mm}$. Never-smoker S2 is a 68-year old male with $\text{FEV}_1=93\%$, $\text{FEV}_1/\text{FVC}=0.79$, ^3He MRI $\text{VDP}=2\%$, $\text{TPV}=30\text{mm}^3$ and $\text{IMT}=0.73\text{mm}$. Ex-smoker S3 is a 79-year old female with $\text{FEV}_1=88\%$, $\text{FEV}_1/\text{FVC}=0.71$, $\text{VDP}=8\%$, $\text{TPV}=500\text{mm}^3$ and $\text{IMT}=0.94\text{mm}$. Ex-smoker S4 is a 85-year old male with $\text{FEV}_1=139\%$, $\text{FEV}_1/\text{FVC}=0.79$, $\text{VDP}=8\%$, $\text{TPV}=340\text{mm}^3$ and $\text{IMT}=0.96\text{mm}$. The axial 3DUS image of the common carotid artery shows the intima-lumen boundary in green and carotid plaque-lumen boundary in yellow. The longitudinal 3DUS carotid image shows IMT segmentation of the common carotid artery.

Figure 2-1 shows ^3He MRI centre coronal slices and 3DUS axial and longitudinal images for representative ex- and never-smokers. ^3He MRI ventilation images show homogeneous ventilation in never-smokers, whereas there is heterogeneous signal intensity with visually obvious ventilation defects in ex-smokers. 3DUS axial images show carotid plaque that is qualitatively greater in the two ex-smokers.

Quantitative results are provided in **Figure 2-2** and **Table 2-1** that show that the ex-smokers subgroup had significantly greater TPV, ($250\pm 200\text{mm}^3$, $p=0.002$) and ^3He MRI VDP, ($7\pm 3\%$, $p=0.001$) than never-smokers. No significant differences were observed for VWV ($p=1.0$), IMT ($p=0.11$), ADC ($p=0.20$) or FEV_1 ($p=0.89$). For ex-smokers, CT mean RA_{950} ($1.5\pm 1.4\%$), airway wall thickness at an internal perimeter of 10mm (Pi_{10} , $4.1\pm 0.17\text{mm}$), $\text{WA}\%$ ($61\pm 2\%$), and LA ($17\pm 11\text{mm}^2$) were within normal range as previously published (49, 50).

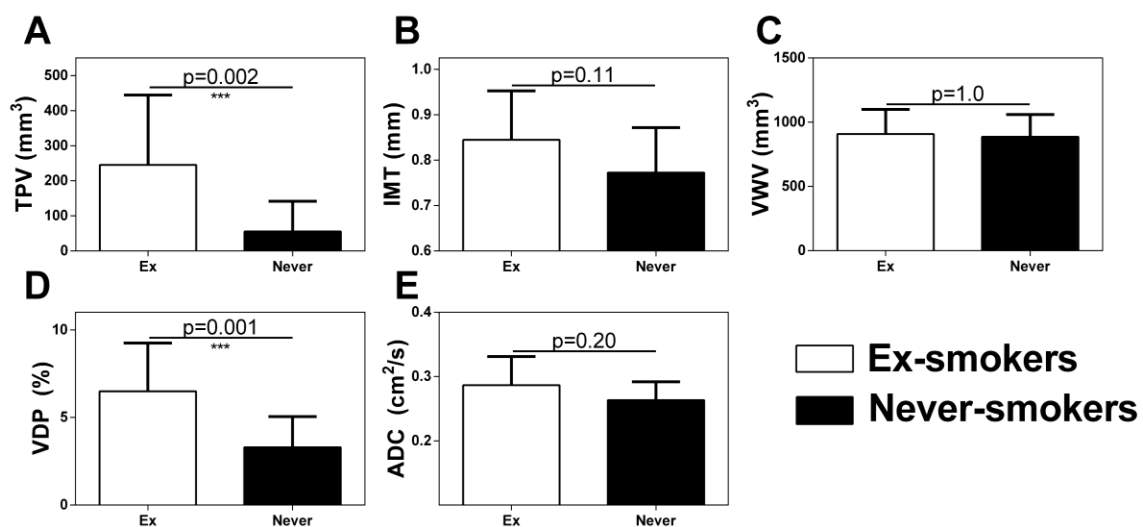


Figure 2-2. Imaging phenotypes in asymptomatic ex-smokers and never-smokers. Ex-smokers have significantly greater: A) TPV ($p=0.002$) and D) VDP ($p=0.001$) than never-smokers. No significant differences were observed for: B) IMT ($p=0.11$), C) VWV ($p=1.0$), E) ADC ($p=0.20$). Holm-Bonferroni corrected p-values are shown.

Using previously established age-normalized values for IMT (51), 28 subjects (15 ex-smokers and 13 never-smokers, 28/61=46%) exceeded the upper limit of normal for IMT and 33 subjects (12 ex-smokers and 21 never-smokers, 33/61=54%) had normal IMT. As shown in **Figure 2-3**, subjects with abnormally elevated IMT had significantly greater VDP ($p=0.04$) than subjects with normal IMT, but the two subgroups were not significantly different with respect to ADC ($p=0.06$), $FEV_1\%_{pred}$ ($p=1.0$) or $DL_{CO}\%_{pred}$ ($p=0.85$). CT measurements for the 15 ex-smokers with abnormal IMT were not significantly different than ex-smokers with normal IMT for RA_{950} ($p=0.96$), $WA\%$ ($p=0.66$) or LA ($p=0.63$).

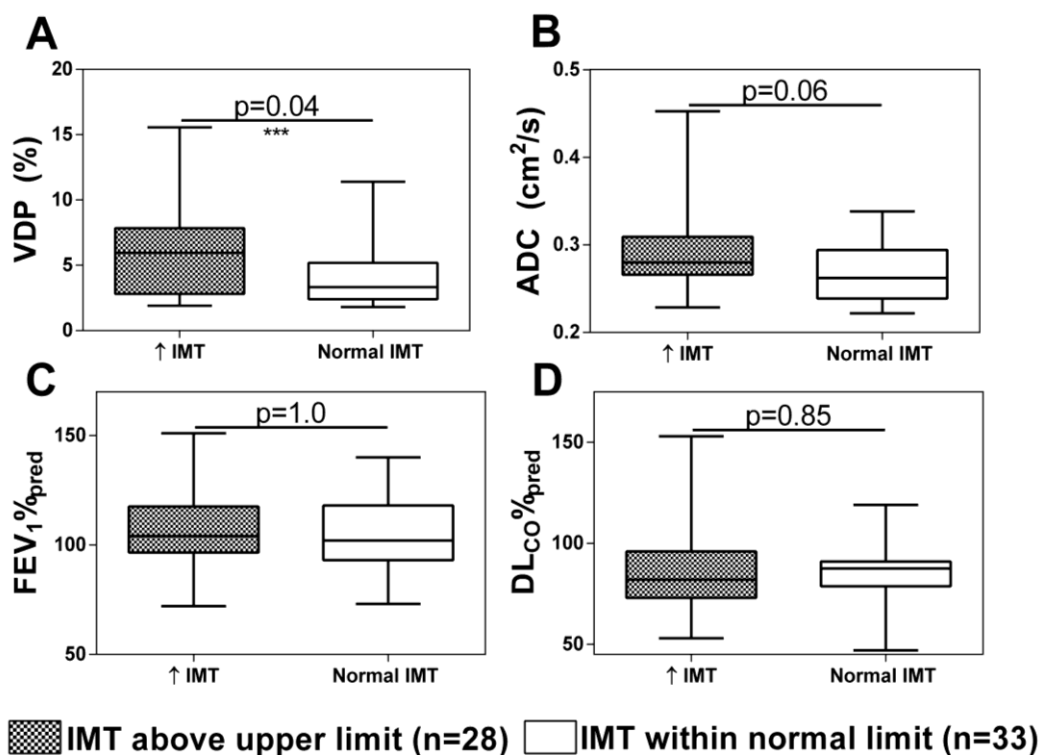


Figure 2-3. Never- and ex-smokers with $IMT \geq$ age-related upper limit of normal ($IMT >97.5\%$ confidence interval (CI)) and subjects with $IMT <$ age-related normal limit ($IMT \leq 97.5$ CI). A) Subjects with abnormally elevated IMT have statistically significantly different 3He MRI VDP ($p=0.04$) than subjects with normal IMT. No significant differences were observed for: B) ADC ($p=0.06$), C) FEV_1 ($p=1.0$) or D) DL_{CO} ($p=0.85$). Comparisons displayed are Holm-Bonferroni corrected p-values.

As shown in **Figure 2-4**, univariate Pearson correlations between ^3He MRI VDP and carotid ultrasound measurements revealed a moderate significant relationship for VDP with carotid IMT ($r=0.42$, $p=0.004$), TPV ($r=0.41$, $p=0.006$) and VWV ($r=0.40$, $p=0.007$). Multivariate regression models for IMT, VWV and TPV are provided in **Table 2-2**. VDP was a significant determinant of IMT ($\beta=0.41$, $p=0.001$), VWV ($\beta=0.45$, $p=0.003$) and TPV ($\beta=0.38$, $p=0.005$). For the ex-smokers alone, CT-derived measurements including RA_{950} and airway count, WA%, LA and Pi10 did not correlate with carotid US measurements of IMT, TPV and VWV.

Table 2-2. Multiple regression models for IMT, VWV and TPV

	IMT		VWV		TPV	
	β	p	β	p	β	p
Age	0.005	0.02	-0.08	0.63	0.18	0.20
BMI	0.20	0.11	-0.11	0.44	0.09	0.47
FEV ₁	-0.03	0.81	0.21	0.18	0.10	0.48
DL _{CO}	0.15	0.22	-0.08	0.59	-0.10	0.46
VDP	0.41	0.001	0.45	0.003	0.38	0.005

Dependent Variables: IMT, $r^2=0.27$, $p=0.001$; VWV, $r^2=0.21$, $p=0.08$; TPV, $r^2=0.16$, $p=0.02$

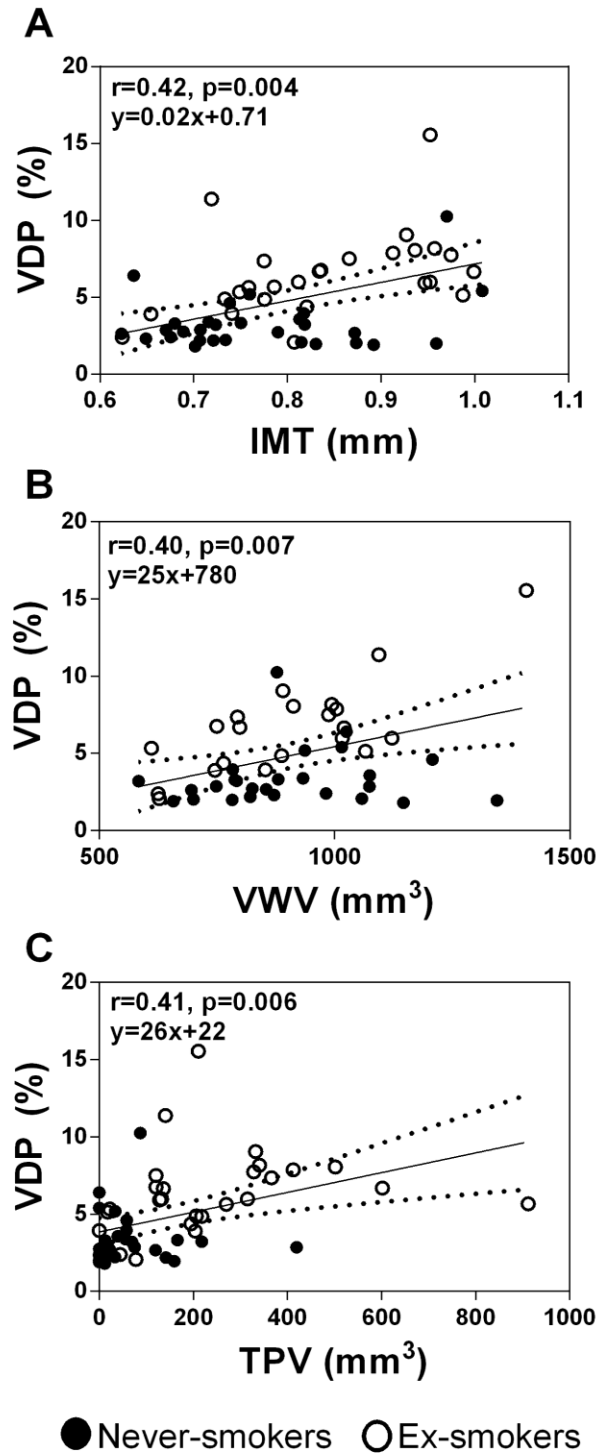


Figure 2-4. Relationships for carotid atherosclerosis and pulmonary VDP. Significant relationships between ³He MRI VDP and: A) carotid IMT ($r=0.42, p=0.004$), B) VWV ($r=0.40, p=0.007$) and C) TPV ($r=0.41, p=0.006$).

2.4 Discussion

We tested the hypothesis that atherosclerosis and pulmonary structure-function measurements were significantly different in ex-smokers without airflow limitation or symptoms consistent with COPD than in never-smokers. We observed: 1) ex-smokers had significantly greater carotid TPV and worse ^3He VDP than never-smokers, but were not significantly different with respect to pulmonary function test measurements, 2) 28 subjects including 15 ex- and 13 never-smokers with abnormally elevated IMT had significantly worse VDP but ADC, FEV_1 , DL_{CO} and CT measurements were not different compared to subjects with normal IMT, 3) ^3He VDP was significantly related to carotid atherosclerosis measurements (IMT, VWV and TPV) but pulmonary function tests were not, and 4), multivariate regression models showed that VDP, a measurement of small airway function, was the only significant determinant of carotid artery IMT, VWV and TPV.

In these older subjects without COPD, we observed, as expected, that spirometry and plethysmography measurements were not different in ex- and never-smokers, but importantly ^3He VDP was significantly worse for ex-smokers. This finding is concordant with previous findings in asymptomatic ex-smokers that showed significant differences in ^3He MRI ventilation defects compared to never-smokers (22). Although we did not observe differences between subgroups for ^3He MRI ADC, abnormally elevated ^3He ADC has been previously reported in asymptomatic smokers (21) and never-smokers with second-hand smoke exposure (23). Our finding of abnormal ^3He ventilation in the absence of abnormal DL_{CO} , ADC or CT RA_{950} in ex-smokers is in agreement with the notion that “silent” airway disease (20) and small airway remodeling (52) may be the source of ventilation defects in these subjects. We think that the significant differences observed for VDP in the absence of differences in DL_{CO} , ADC or RA_{950} suggests mild, sub-clinical airway abnormalities, although we must point out that a definitive structure-function etiology for ^3He ventilation defects (46, 53, 54) is yet to be determined. It is also worth noting that for the healthy ex-smokers evaluated here, there was no CT evidence of emphysema or airways disease and such values were in agreement with those reported in healthy non-smokers in the COPDGene study (49, 50). This finding

underscores the sensitivity of ^3He MRI ventilation measurements for detecting functional abnormalities that may not be apparent using CT or spirometry.

Previous work in COPD patients (3, 4, 6, 7, 17, 55, 56) reported a relationship for IMT with FEV_1 and emphysema measurements, but this was not observed here in ex-smokers without COPD. We were likely underpowered to detect differences in IMT between subgroups as these previous studies investigating IMT in COPD and healthy older subjects used sample sizes ranging from 305 to 14,480 subjects. On the other hand, significantly elevated 3DUS TPV in ex-smoker subgroup was consistent with previous work (35, 36) that showed smaller sample sizes can be used when employing 3D measurements of plaque as compared to IMT. Although no difference was observed for IMT between ex- and never-smokers, when age-normalized IMT values were used to stratify subjects (51), subjects with abnormal IMT had significantly worse VDP. This finding suggests that in both never- and ex-smokers with elevated IMT, there is evidence of mild, subclinical airways disease that may be related to factors other than cigarette smoking.

We also observed significant univariate relationships for ^3He VDP with carotid artery IMT, TPV and VWV, consistent with previous studies that showed relationships between spirometry measurements and carotid IMT (3, 4, 6, 17, 55, 56), although this is the first report of such relationships in subjects with normal pulmonary function. Similarly, multivariate regression models that controlled for cardiovascular and pulmonary disease risk factors showed that VDP was the only significant determinant of carotid artery IMT, VWV and TPV. It is also important to note that carotid TPV and VWV provide measurements of intima echogenic (TPV and VWV) and echolucent (VWV) plaque (38, 57, 58). Hence, these relationships between VDP and IMT, VWV and TPV suggest that in this relatively small group of never- and ex-smokers, mild, subclinical airways disease may be related to carotid plaque burden and wall thickening. While it was recently shown that COPD patients may have atherosclerotic plaque characteristics that make them more vulnerable to rupture (6), we did not evaluate carotid plaque composition here. The significant carotid plaque burden quantified in some of the ex-smokers investigated here may be amenable to more complex image methods (59) to develop a better understanding

of plaque composition/texture and outcomes. We acknowledge that the main limitation of this study was the relatively small sample size of never- and ex-smokers, and that this may have limited our power to detect any potential differences in IMT and FEV₁ between subgroups. Certainly, one of the strengths of 3D imaging is that significantly different measurements can be detected in small groups of subjects, because of the high dynamic range and sensitivity of 3D measurements to structure-function abnormalities. This is an important consideration when powering studies to detect differences in small groups of subjects. Finally, we cannot infer the temporal or causal nature of carotid and pulmonary abnormalities in this cross-sectional evaluation. Questions related to “which came first” still need to be answered in longitudinal natural disease and intervention studies (60).

In conclusion, we acquired sensitive 3D imaging measurements of atherosclerosis and pulmonary structure-function in order to illuminate potential relationships between early or mild sub-clinical pulmonary disease with atherosclerosis in otherwise healthy ex-smokers. Although a number of studies have provided evidence that pulmonary and carotid abnormalities are both present and related in COPD patients, here, this important relationship was shown in never- and ex-smokers with normal pulmonary function. Whilst the clinical relevance of these observations is not yet clear, these data suggest that lung abnormalities and carotid atherosclerosis in never- and ex-smokers without airflow limitation may be directly related. As our knowledge of comorbid lung and vascular disease increases, such findings may potentially have implications for patient management decision strategies in preclinical stages.

2.5 References

1. Anthonisen NR, Skeans MA, Wise RA, Manfreda J, Kanner RE, Connett JE, et al. The effects of a smoking cessation intervention on 14.5-year mortality: a randomized clinical trial. *Ann Intern Med.* 2005;142(4):233-9.
2. Sidney S, Sorel M, Quesenberry CP, Jr., DeLuise C, Lanes S, Eisner MD. COPD and incident cardiovascular disease hospitalizations and mortality: Kaiser Permanente Medical Care Program. *Chest.* 2005;128(4):2068-75.
3. Iwamoto H, Yokoyama A, Kitahara Y, Ishikawa N, Haruta Y, Yamane K, et al. Airflow limitation in smokers is associated with subclinical atherosclerosis. *American journal of respiratory and critical care medicine.* 2009;179(1):35-40.
4. Barr RG, Ahmed FS, Carr JJ, Hoffman EA, Jiang R, Kawut SM, et al. Subclinical atherosclerosis, airflow obstruction and emphysema: the MESA Lung Study. *The European respiratory journal.* 2012;39(4):846-54.
5. Engstrom G, Hedblad B, Valind S, Janzon L. Asymptomatic leg and carotid atherosclerosis in smokers is related to degree of ventilatory capacity: longitudinal and cross-sectional results from 'Men born in 1914', Sweden. *Atherosclerosis.* 2001;155(1):237-43.
6. Lahousse L, van den Bouwhuijsen QJ, Loth DW, Joos GF, Hofman A, Witteman JC, et al. Chronic obstructive pulmonary disease and lipid core carotid artery plaques in the elderly: the Rotterdam Study. *American journal of respiratory and critical care medicine.* 2013;187(1):58-64.
7. van Gestel YR, Flu WJ, van Kuijk JP, Hoeks SE, Bax JJ, Sin DD, et al. Association of COPD with carotid wall intima-media thickness in vascular surgery patients. *Respir Med.* 2010;104(5):712-6.
8. Frantz S, Nihlen U, Dencker M, Engstrom G, Lofdahl CG, Wollmer P. Atherosclerotic plaques in the internal carotid artery and associations with lung function assessed by different methods. *Clin Physiol Funct Imaging.* 2012;32(2):120-5.
9. Dransfield MT, Huang F, Nath H, Singh SP, Bailey WC, Washko GR. CT emphysema predicts thoracic aortic calcification in smokers with and without COPD. *COPD.* 2010;7(6):404-10.
10. Chae EJ, Seo JB, Oh YM, Lee JS, Jung Y, Lee SD. Severity of systemic calcified atherosclerosis is associated with airflow limitation and emphysema. *J Comput Assist Tomogr.* 2013;37(5):743-9.
11. McAllister DA, MacNee W, Duprez D, Hoffman EA, Vogel-Claussen J, Criqui MH, et al. Pulmonary function is associated with distal aortic calcium, not proximal aortic distensibility. *MESA lung study. COPD.* 2011;8(2):71-8.

12. Rasmussen T, Kober L, Pedersen JH, Dirksen A, Thomsen LH, Stender S, et al. Relationship between chronic obstructive pulmonary disease and subclinical coronary artery disease in long-term smokers. *Eur Heart J Cardiovasc Imaging*. 2013.
13. Wells JM, Washko GR, Han MK, Abbas N, Nath H, Marmar AJ, et al. Pulmonary arterial enlargement and acute exacerbations of COPD. *N Engl J Med*. 2012;367(10):913-21.
14. Barr RG, Mesia-Vela S, Austin JH, Basner RC, Keller BM, Reeves AP, et al. Impaired flow-mediated dilation is associated with low pulmonary function and emphysema in ex-smokers: the Emphysema and Cancer Action Project (EMCAP) Study. *American journal of respiratory and critical care medicine*. 2007;176(12):1200-7.
15. Cinarka H, Kayhan S, Gumus A, Durakoglugil ME, Erdogan T, Ezberci I, et al. Arterial stiffness measured by carotid femoral pulse wave velocity is associated with disease severity in chronic obstructive pulmonary disease. *Respir Care*. 2013.
16. Sabit R, Bolton CE, Edwards PH, Pettit RJ, Evans WD, McEniery CM, et al. Arterial stiffness and osteoporosis in chronic obstructive pulmonary disease. *American journal of respiratory and critical care medicine*. 2007;175(12):1259-65.
17. Kim SJ, Yoon DW, Lee EJ, Hur GY, Jung KH, Lee SY, et al. Carotid atherosclerosis in patients with untreated chronic obstructive pulmonary disease. *Int J Tuberc Lung Dis*. 2011;15(9):1265-70, i.
18. Karkhanis VS, Joshi JM. Spirometry in chronic obstructive lung disease (COPD). *J Assoc Physicians India*. 2012;60 Suppl:22-6.
19. Miller MR, Hankinson J, Brusasco V, Burgos F, Casaburi R, Coates A, et al. Standardisation of spirometry. *The European respiratory journal*. 2005;26(2):319-38.
20. Hogg JC, Chu F, Utokaparch S, Woods R, Elliott WM, Buzatu L, et al. The nature of small-airway obstruction in chronic obstructive pulmonary disease. *N Engl J Med*. 2004;350(26):2645-53.
21. Swift AJ, Wild JM, Fischele S, Woodhouse N, Fleming S, Waterhouse J, et al. Emphysematous changes and normal variation in smokers and COPD patients using diffusion 3He MRI. *Eur J Radiol*. 2005;54(3):352-8.
22. Woodhouse N, Wild JM, Paley MN, Fischele S, Said Z, Swift AJ, et al. Combined helium-3/proton magnetic resonance imaging measurement of ventilated lung volumes in smokers compared to never-smokers. *J Magn Reson Imaging*. 2005;21(4):365-9.
23. Wang C MJPI, de Lange E and Altes T A, editor Elevated short-time-scale hyperpolarized helium-3 diffusion in secondhand smokers. *International Society of Magnetic Resonance in Medicine Proceedings 2012*; 2012.

24. Vestbo J, Anderson W, Coxson HO, Crim C, Dawber F, Edwards L, et al. Evaluation of COPD Longitudinally to Identify Predictive Surrogate End-points (ECLIPSE). *The European respiratory journal*. 2008;31(4):869-73.
25. Regan EA, Hokanson JE, Murphy JR, Make B, Lynch DA, Beaty TH, et al. Genetic epidemiology of COPD (COPDGene) study design. *COPD*. 2010;7(1):32-43.
26. Gietema HA, Muller NL, Fauerbach PV, Sharma S, Edwards LD, Camp PG, et al. Quantifying the extent of emphysema: factors associated with radiologists' estimations and quantitative indices of emphysema severity using the ECLIPSE cohort. *Acad Radiol*. 2011;18(6):661-71.
27. Han MK, Kazerooni EA, Lynch DA, Liu LX, Murray S, Curtis JL, et al. Chronic obstructive pulmonary disease exacerbations in the COPDGene study: associated radiologic phenotypes. *Radiology*. 2011;261(1):274-82.
28. Galban CJ, Han MK, Boes JL, Chughtai KA, Meyer CR, Johnson TD, et al. Computed tomography-based biomarker provides unique signature for diagnosis of COPD phenotypes and disease progression. *Nat Med*. 2012;18(11):1711-5.
29. Hersh CP, Washko GR, Estepar RS, Lutz S, Friedman PJ, Han MK, et al. Paired inspiratory-expiratory chest CT scans to assess for small airways disease in COPD. *Respir Res*. 2013;14:42.
30. Van Eeden S, Leipsic J, Paul Man SF, Sin DD. The relationship between lung inflammation and cardiovascular disease. *American journal of respiratory and critical care medicine*. 2012;186(1):11-6.
31. Man SF, Van Eeden S, Sin DD. Vascular risk in chronic obstructive pulmonary disease: role of inflammation and other mediators. *Can J Cardiol*. 2012;28(6):653-61.
32. Stein JH, Korcarz CE, Hurst RT, Lonn E, Kendall CB, Mohler ER, et al. Use of carotid ultrasound to identify subclinical vascular disease and evaluate cardiovascular disease risk: a consensus statement from the American Society of Echocardiography Carotid Intima-Media Thickness Task Force. Endorsed by the Society for Vascular Medicine. *J Am Soc Echocardiogr*. 2008;21(2):93-111; quiz 89-90.
33. Polak JF, Pencina MJ, Pencina KM, O'Donnell CJ, Wolf PA, D'Agostino RB, Sr. Carotid-wall intima-media thickness and cardiovascular events. *N Engl J Med*. 2011;365(3):213-21.
34. Mallett C, House AA, Spence JD, Fenster A, Parraga G. Longitudinal ultrasound evaluation of carotid atherosclerosis in one, two and three dimensions. *Ultrasound Med Biol*. 2009;35(3):367-75.
35. Inaba Y, Chen JA, Bergmann SR. Carotid plaque, compared with carotid intima-media thickness, more accurately predicts coronary artery disease events: a meta-analysis. *Atherosclerosis*. 2012;220(1):128-33.

36. Spence JD. Carotid plaque measurement is superior to IMT Invited editorial comment on: carotid plaque, compared with carotid intima-media thickness, more accurately predicts coronary artery disease events: a meta-analysis-Yoichi Inaba, M.D., Jennifer A. Chen M.D., Steven R. Bergmann M.D., Ph.D. *Atherosclerosis*. 2012;220(1):34-5.
37. Wannarong T, Parraga G, Buchanan D, Fenster A, House AA, Hackam DG, et al. Progression of carotid plaque volume predicts cardiovascular events. *Stroke*. 2013;44(7):1859-65.
38. Buchanan DN, Lindenmaier T, McKay S, Bureau Y, Hackam DG, Fenster A, et al. The relationship of carotid three-dimensional ultrasound vessel wall volume with age and sex: comparison to carotid intima-media thickness. *Ultrasound Med Biol*. 2012;38(7):1145-53.
39. Fenster A, Downey DB. Three-dimensional ultrasound imaging. *Annu Rev Biomed Eng*. 2000;2:457-75.
40. Landry A, Fenster A. Theoretical and experimental quantification of carotid plaque volume measurements made by three-dimensional ultrasound using test phantoms. *Med Phys*. 2002;29(10):2319-27.
41. Kirby M, Svenningsen S, Owrangi A, Wheatley A, Farag A, Ouriadov A, et al. Hyperpolarized ³He and ¹²⁹Xe MR imaging in healthy volunteers and patients with chronic obstructive pulmonary disease. *Radiology*. 2012;265(2):600-10.
42. Shai I, Spence JD, Schwarzfuchs D, Henkin Y, Parraga G, Rudich A, et al. Dietary intervention to reverse carotid atherosclerosis. *Circulation*. 2010;121(10):1200-8.
43. Ukwatta E, Awad J, Ward AD, Buchanan D, Samarabandu J, Parraga G, et al. Three-dimensional ultrasound of carotid atherosclerosis: semiautomated segmentation using a level set-based method. *Med Phys*. 2011;38(5):2479-93.
44. Kirby M, Heydarian M, Svenningsen S, Wheatley A, McCormack DG, Etemad-Rezai R, et al. Hyperpolarized ³He magnetic resonance functional imaging semiautomated segmentation. *Acad Radiol*. 2012;19(2):141-52.
45. Kirby M, Heydarian M, Wheatley A, McCormack DG, Parraga G. Evaluating bronchodilator effects in chronic obstructive pulmonary disease using diffusion-weighted hyperpolarized helium-3 magnetic resonance imaging. *J Appl Physiol*. 2012;112(4):651-7.
46. Nakano Y, Wong JC, de Jong PA, Buzatu L, Nagao T, Coxson HO, et al. The prediction of small airway dimensions using computed tomography. *American journal of respiratory and critical care medicine*. 2005;171(2):142-6.
47. Van Belle GF, L.; Heagerty, P.; Lumley, T. *Multiple Comparisons Biostatistics a methodology for health sciences* 2nd ed. Seattle, Washington: Wiley-Interscience; 2004.

48. van den Bouwhuijsen QJ, Vernooij MW, Hofman A, Krestin GP, van der Lugt A, Witteman JC. Determinants of magnetic resonance imaging detected carotid plaque components: the Rotterdam Study. *Eur Heart J*. 2012;33(2):221-9.
49. Schroeder JD, McKenzie AS, Zach JA, Wilson CG, Curran-Everett D, Stinson DS, et al. Relationships Between Airflow Obstruction and Quantitative CT Measurements of Emphysema, Air Trapping, and Airways in Subjects With and Without Chronic Obstructive Pulmonary Disease. *AJR Am J Roentgenol*. 2013;201(3):W460-70.
50. Zach JA, Newell JD, Jr., Schroeder J, Murphy JR, Curran-Everett D, Hoffman EA, et al. Quantitative computed tomography of the lungs and airways in healthy nonsmoking adults. *Invest Radiol*. 2012;47(10):596-602.
51. Lim TK, Lim E, Dwivedi G, Kooner J, Senior R. Normal value of carotid intima-media thickness--a surrogate marker of atherosclerosis: quantitative assessment by B-mode carotid ultrasound. *J Am Soc Echocardiogr*. 2008;21(2):112-6.
52. McDonough JE, Yuan R, Suzuki M, Seyednejad N, Elliott WM, Sanchez PG, et al. Small-airway obstruction and emphysema in chronic obstructive pulmonary disease. *N Engl J Med*. 2011;365(17):1567-75.
53. Coxson HO, Eastwood PR, Williamson JP, Sin DD. Phenotyping airway disease with optical coherence tomography. *Respirology*. 2011;16(1):34-43.
54. Woods JC, Choong CK, Yablonskiy DA, Bentley J, Wong J, Pierce JA, et al. Hyperpolarized ³He diffusion MRI and histology in pulmonary emphysema. *Magn Reson Med*. 2006;56(6):1293-300.
55. Schroeder EB, Welch VL, Evans GW, Heiss G. Impaired lung function and subclinical atherosclerosis. The ARIC Study. *Atherosclerosis*. 2005;180(2):367-73.
56. Ebrahim S, Papacosta O, Whincup P, Wannamethee G, Walker M, Nicolaides AN, et al. Carotid plaque, intima media thickness, cardiovascular risk factors, and prevalent cardiovascular disease in men and women: the British Regional Heart Study. *Stroke*. 1999;30(4):841-50.
57. Schminke U, Hilker L, Motsch L, Griewing B, Kessler C. Volumetric assessment of plaque progression with 3-dimensional ultrasonography under statin therapy. *J Neuroimaging*. 2002;12(3):245-51.
58. Ainsworth CD, Blake CC, Tamayo A, Beletsky V, Fenster A, Spence JD. 3D ultrasound measurement of change in carotid plaque volume: a tool for rapid evaluation of new therapies. *Stroke*. 2005;36(9):1904-9.
59. Awad J, Krasinski A, Parraga G, Fenster A. Texture analysis of carotid artery atherosclerosis from three-dimensional ultrasound images. *Med Phys*. 2010;37(4):1382-91.

60. Sabit R, Shale DJ. Vascular structure and function in chronic obstructive pulmonary disease: a chicken and egg issue? *American journal of respiratory and critical care medicine*. 2007;176(12):1175-6.

CHAPTER 3

The study in Chapter 2 showed how hyperpolarized ^3He MRI reveals clinically relevant ventilation defects in the lungs of ex-smokers without airflow limitation. This suggests that ex-smokers without spirometry evidence of COPD may suffer from a form of pre- or sub-clinical obstructive lung disease attributable to airway and/or parenchymal abnormalities which are not detected using conventional spirometry or plethysmography. Here, we aimed to provide a better understanding of the underlying pathophysiology of ventilation defects in ex-smokers without airflow limitation by collecting regional ^3He ventilation and diffusion-weighted imaging data, as well as regional thoracic computed tomography airway and emphysema measurements in ex-smokers without airflow limitation.

The contents of this chapter have been previously published in Academic Radiology and permission to reproduce the article was granted by Elsevier Publishing and is provided in Appendix D.

D Pike, M Kirby, F Guo, DG McCormack and G Parraga. Ventilation Heterogeneity in Ex-smokers without Airflow Limitation. Academic Radiology; DOI: 10.1017/j.acra.2015.04.006

3 Ventilation Heterogeneity in Ex-smokers without Airflow Limitation

3.1 Introduction

Chronic obstructive pulmonary disease (COPD) is characterized by irreversible airflow limitation caused by small airway remodeling, airway obliteration (1) and emphysematous tissue destruction (2). COPD is typically diagnosed after respiratory symptoms become obvious and intolerable (3), and this usually occurs when spirometry measurements of lung function reflect airflow limitation and obstruction. However it is well-understood that ex- and current-smokers may report normal lung function (3) and mild symptoms and this may represent an early or ‘subclinical’ phase. A deep understanding of the underlying morphological changes that accompany this ‘subclinical’ phase is lacking, mainly because methods for evaluating pulmonary function cannot detect very mild or early structure-function abnormalities.

Hyperpolarized ^3He magnetic resonance imaging (MRI) ventilation heterogeneity has been shown in healthy older subjects (4) and patients with COPD (5) and asthma (6). To

evaluate the underlying anatomical and structural determinants of ventilation heterogeneity, thoracic x-ray computed tomography (CT) has been used to help determine the spatial relationship of airways disease and emphysema with ventilation abnormalities. For example, recent work (7) provided evidence that in COPD, ^3He ventilation defects represent regions of emphysema and airways disease and that this relationship depends on disease severity. In asthma (6), ^3He ventilation heterogeneity was also shown to be spatially related to abnormally remodeled airways. Whilst previous work reported the presence of ventilation heterogeneity in ex-smokers with normal spirometry (8), the underlying etiology and clinical relevance of these findings is not well-understood.

In order to better understand the pathophysiological features of ventilation heterogeneity in the ‘subclinical phase’ of obstructive lung disease in otherwise normal healthy ex-smokers, we evaluated a group of well-characterized ex-smokers without airflow limitation using both MRI and CT. Based on previous work using micro-CT that suggested that airway obstruction and obliteration may provide the dominant contribution to airflow limitation in COPD (1), we hypothesized that in normal ex-smokers, ^3He ventilation abnormalities would be spatially and quantitatively related to airway remodeling and not emphysema.

3.2 Materials and Methods

3.2.1 Study Subjects

Study participants provided written informed consent to a protocol approved by a local research ethics board and Health Canada and was compliant with the Personal Information Protection and Electronic Documents Act (PIPEDA, Canada) and Health Insurance Portability and Accountability Act (HIPAA, USA). Research volunteers were recruited from a tertiary health care practice. Each visit was completed in approximately two hours when spirometry, plethysmography, the six-minute walk test (6MWT), St. George’s Respiratory Questionnaire (SGRQ), ^3He MRI and CT were completed.

3.2.2 Spirometry and Plethysmography

Spirometry was performed according to the American Thoracic Society guidelines (9). Whole-body plethysmography was used to measure lung volumes (MedGraphics Corporation, St. Paul, Minnesota, USA) and the attached gas analyzer was used to measure diffusing capacity of the lung for carbon monoxide (DL_{CO}).

3.2.3 Imaging

MRI was performed on a 3T Discovery MR750 (General Electric Health Care, Milwaukee, Wisconsin, USA) system with subjects in inspiratory breath hold at functional residual capacity (FRC)+1L. 1H MRI was acquired prior to 3He MRI after inhalation of 1L high purity, medical grade nitrogen (N_2) from FRC using the whole-body radiofrequency coil and a fast spoiled gradient-recalled-echo sequence (10). 3He MRI was acquired with subjects in inspiratory breath-hold after inhalation from FRC of a 1L mixture of hyperpolarized 3He (5ml/kg body weight) diluted with N_2 . 3He static-ventilation and diffusion-weighted MRI was performed as previously described (10, 11).

CT was acquired within 30 minutes of MRI using a 64 slice Lightspeed VCT system (General Electric Health Care, Milwaukee, Wisconsin, USA) and a single spiral acquisition from apex to base with the subjects in the supine position. Subjects were transported to the CT suite by wheelchair to prevent the potential for exercise-induced changes between MRI and CT image acquisitions. CT was acquired during inspiratory breath-hold of FRC+1L of N_2 as previously described (12). The total effective dose was 1.8 mSv as calculated using manufacturer settings and the ImPACT CT dosimetry calculator based on Health Protection Agency (UK) NRPB-SR250.

3.2.4 Image analysis

Ventilation heterogeneity or regions of “signal void” were quantified as 3He ventilation defect percent (VDP) using semi-automated software generated in MATLAB (Mathworks, Natick, Massachusetts, USA) as previously described (13). Lobar VDP was generated by registering the segmented thoracic CT lobe mask from VIDA Pulmonary

Workstation 2.0 (VIDA Diagnostics Inc., Coralville, Iowa, USA) to ^3He MRI ventilation images using deformable registration, and generating VDP for each lobe (right upper lobe (RUL), right middle lobe (RML), right lower lobe (RLL), left upper lobe (LUL), left lower lobe (LLL)) using hierarchical k-means clustering (13). All ex-smokers were classified on the basis of the 95% confidence interval for VDP in healthy elderly never-smokers of 4.3% as previously described (4). Therefore, ex-smokers with $\text{VDP} < 4.3\%$ were classified as normal whereas ex-smokers with $\text{VDP} \geq 4.3\%$ were classified as having abnormally-elevated VDP. ^3He MRI apparent diffusion coefficients (ADC) were generated as previously described (11).

CT volumes were evaluated using Pulmonary Workstation 2.0 to generate airway wall area percent (WA%), lumen area (LA) and airway count. It was previously shown that airway lumen area is related to body surface area (BSA) (14, 15) and therefore LA was normalized to BSA (LA/BSA). CT WA%, LA and LA/BSA were measured for subsegmental bronchi including RB1, RB5, RB8, LB1 and LB8 airways because each of these feed individual lobes (RB1-RUL, RB5-RML, RB8-RLL, LB1-LUL and LB8-LLL) and they were measureable for each subject. Emphysema was also measured using Pulmonary Workstation 2.0 including the relative area of the lung with attenuation ≤ -950 Hounsfield units (HU) (RA_{950}) for whole-lung and each individual lung lobe.

3.2.5 Statistics

All tests were performed in IBM SPSS V22 (SPSS Inc., Chicago, Illinois, USA). Normality was tested using the Shapiro-Wilk test. A one-way analysis of variance (ANOVA) was used to compare multiple parameters and univariate comparisons were investigated using unpaired two-tailed t-tests (parametric data) or Mann-Whitney U tests (non-parametric data). Spearman correlations were performed for non-parametric data.

3.3 Results

A summary of demographic, pulmonary function test and imaging measurements is provided in **Table 3-1** for all 60 subjects, while **Supplemental Table 3I-1** (online) provides a subject listing of data. All participants reported normal spirometry

measurements ($FEV_1=104\pm 13\%$, $FEV_1/FVC=80\pm 6\%$) and no subjects reported Global initiative for Chronic Obstructive Lung Disease (GOLD) unclassified COPD (16). Eighteen subjects ($18/60=30\%$) reported normal VDP and 42 ($42/60=70\%$) subjects reported abnormally-elevated VDP. As shown in **Figure 3-1** for four representative subjects, volunteers with normal VDP showed small or no ventilation defects along the periphery of the lung, whereas participants with abnormally-elevated VDP showed evidence of patchy ventilation throughout the lung and on the periphery. The qualitative spatial relationship for patchy ventilation and subsegmental airway morphology reconstructed from CT is also shown in **Figure 3-1**.

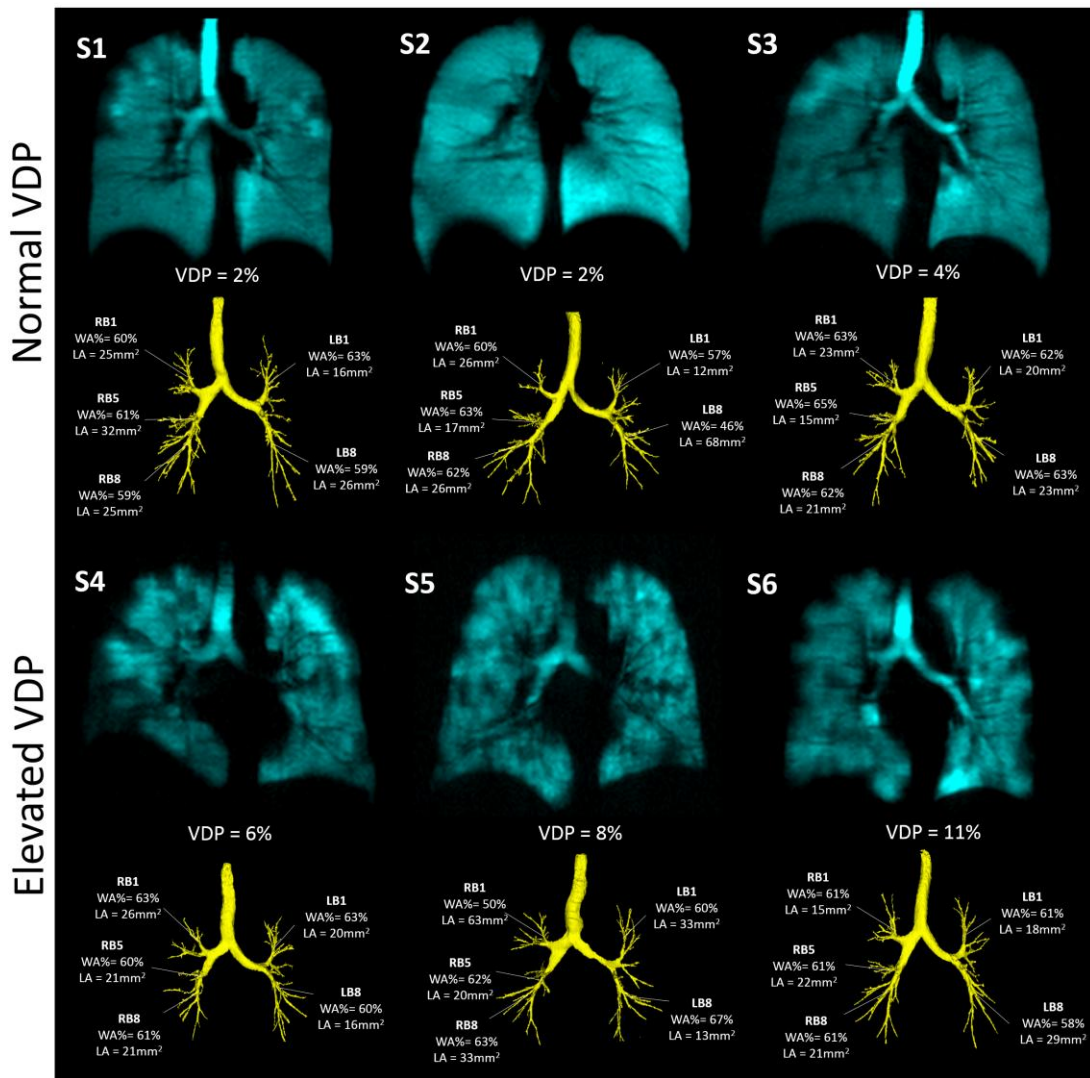


Figure 3-1. ^3He MRI Ventilation and CT airway trees in representative ex-smokers with normal (S1–S3) and abnormally-elevated VDP (S4–S6). S1=70y female, 12 pack years, FEV₁=93% and VDP=2%. S2=59y female, 18 pack years, FEV₁=97% and VDP=2%. S3=51y female, 20 pack years, FEV₁=103% and VDP=4%. S4=74y male, 50 pack years, FEV₁=89% and VDP=6%. S5=79y male, 10 pack years, FEV₁=88% and VDP=8%. S6=74y male, 60 pack years, FEV₁=95% and VDP=11%.

As shown in **Table 3-1**, subjects with abnormally-elevated VDP were not significantly different ($p>0.05$) with respect to pulmonary function test or CT measurements but they did report significantly greater ($p=0.02$) ^3He ADC than subjects with normal VDP.

Table 3-1. Demographic, pulmonary function and imaging data

Parameter (\pm SD)	All (n=60)	Normal VDP (n=18)	Elevated VDP (n=42)
Age yr	69 (9)	67 (10)	70 (9)
Male n (%)	38 (63)	9 (50)	29 (69)
Pack years	28 (16)	27 (14)	28 (17)
BMI kg/m ²	29 (4)	29 (5)	30 (4)
FVC% _{pred}	97 (13)	100 (10)	95 (14)
FEV ₁ % _{pred}	104 (13)	106 (12)	102 (14)
FEV ₁ /FVC %	80 (6)	80 (6)	80 (6)
RV/TLC% _{pred}	103 (15)	104 (12)	103 (16)
DL _{CO} % _{pred}	80 (20)	87 (16)	77 (22)
6MWD m	404 (95)	433 (81)	392 (98)
SGRQ total	36 (26)	22 (20)	23 (22)
WA %	65 (2)	65 (2)	65 (2)
LA mm ²	14 (3)	13 (2)	14 (4)
LA/BSA mm ² /m ²	7 (2)	7 (1)	7 (2)
Airway count	115 (37)	106 (28)	119 (40)
RA ₉₅₀ %	1.2 (1.0)	0.8 (0.5)	1.4 (1.1)
VDP %	6 (3)	3 (1)	7 (3) [†]
ADC cm ² /s	0.28 (0.04)	0.26 (0.03)	0.29 (0.03) [†]

BMI: Body mass index, FVC: Forced vital capacity, FEV₁: Forced expiratory volume in one second, RV: Residual volume, TLC: Total lung capacity, DL_{CO}: Diffusing capacity for carbon monoxide, SGRQ: St. Georges Respiratory Questionnaire, 6MWD: Six minute walk distance, WA%: Mean fifth generation airway wall area percent, LA: Mean fifth generation airway lumen area, BSA: Body surface area, RA₉₅₀: Relative area of the lung parenchyma with attenuation $\leq -950\text{HU}$, VDP: ^3He MRI ventilation defect percent, ADC: ^3He MRI apparent diffusion coefficient, SD: standard deviation
[†]Significantly different $p<0.05$

Table 3-2 shows quantitative airway morphology and emphysema measurements for subjects with normal and abnormally-elevated VDP. No significant differences were observed for whole-lung airway (mean of fifth generation airways) WA% ($p=0.88$), LA ($p=0.50$) or LA/BSA ($p=0.57$) and this was consistent in all lung lobes. **Table 3-2** and **Figure 3-2** show that only ^3He MRI ADC was significantly greater in the apical lung (RUL: $p=0.02$, RML: $p=0.04$ and LUL: $p=0.009$) in subjects with elevated VDP.

Table 3-3 shows the relationships for VDP with airway morphology and emphysema measurements. Whole lung VDP was significantly correlated with whole lung ADC ($r=0.40$, $p=0.001$) and whole lung RA_{950} ($r=0.34$, $p=0.008$). As shown in **Table 3-3** and in more detail in **Figure 3-3**, regional VDP correlated with regional ADC in each of the lung lobes (RUL: $r=0.32$, $p=0.01$, RML: $r=0.46$, $p=0.002$, RLL: $r=0.38$, $p=0.003$, LUL: $r=0.35$, $p=0.006$ and LLL: $r=0.37$, $p=0.004$). As shown in Table 3, whole lung VDP did not correlate with whole lung (mean of fifth generation airways) WA%, LA or LA/BSA. There were no significant correlations for regional VDP and airway morphological measurements in the RML (RB5 morphology), LUL (LB1 morphology) or LLL (LB8 morphology). However, as shown **Figure 3-4** in more detail, RUL VDP significantly correlated RB1 morphological measurements (LA: $r=-0.37$, $p=0.004$, LA/BSA: $r=-0.42$, $p=0.0008$) and RLL VDP significantly correlated with RB8 morphological measurements (WA%: $r=0.28$, $p=0.03$, LA: $r=-0.28$, $p=0.03$, LA/BSA: $r=-0.37$, $p=0.004$).

Table 3-2. Whole lung and regional measurements for ex-smokers with normal and elevated VDP

Parameter (\pm SD)	Normal VDP (n=18)	Elevated VDP (n=42)	p-value
<i>Whole Lung</i>			
**WA%	65 (2)	65 (2)	0.88
**LA mm ²	13 (2)	14 (4)	0.50
**LA/BSA mm ² /m ²	7 (1)	7 (2)	0.57
VDP %	3 (1)	7 (3)	<0.0001
ADC cm ² /s	0.26 (0.03)	0.29 (0.03)	0.02
RA ₉₅₀ %	0.8 (0.5)	1.4 (1.1)	0.08
<i>Right upper lobe</i>			
RB1 WA%	62 (2)	61 (4)	0.29
RB1 LA mm ²	25 (5)	25 (11)	0.64
RB1 LA/BSA mm ² /m ²	13 (3)	13 (6)	0.39
VDP %	3 (2)	5 (4)	0.02
ADC cm ² /s	0.24 (0.03)	0.27 (0.03)	0.02
RA ₉₅₀ %	0.7 (0.6)	1.2 (1.2)	0.08
<i>Right middle Lobe</i>			
RB5 WA%	63 (4)	62 (4)	0.25
RB5 LA mm ²	22 (13)	21 (8)	0.80
RB5 LA/BSA mm ² /m ²	12 (7)	11 (4)	0.99
VDP %	6 (9)	9 (10)	0.04
ADC cm ² /s	0.24 (0.03)	0.27 (0.04)	0.04
RA ₉₅₀ %	1.6 (1.0)	2.0 (1.8)	0.79
<i>Right lower lobe</i>			
RB8 WA%	62 (3)	62 (3)	0.43
RB8 LA mm ²	21 (8)	21 (7)	0.99
RB8 LA/BSA mm ² /m ²	11 (5)	11 (4)	0.67
VDP %	5 (3)	8 (6)	0.02
ADC cm ² /s	0.25 (0.03)	0.27 (0.03)	0.07
RA ₉₅₀ %	0.6 (0.4)	1.0 (1.0)	0.42
<i>Left Upper Lobe</i>			
LB1 WA%	63 (3)	63 (3)	0.52
LB1 LA mm ²	15 (4)	18 (6)	0.19
LB1 LA/BSA mm ² /m ²	8 (2)	9 (3)	0.34
VDP %	4 (4) (3)	8 (8)	0.02
ADC cm ² /s	0.25 (0.03)	0.28 (0.04)	0.009
RA ₉₅₀ %	1.0 (0.6)	1.8 (1.7)	0.22
<i>Left Lower Lobe</i>			
LB8 WA%	59 (4)	60 (4)	0.68
LB8 LA mm ²	30 (11)	28 (12)	0.27
LB8 LA/BSA mm ² /m ²	17 (8)	14 (6)	0.13
VDP %	3 (1)	7 (3)	<0.0001
ADC cm ² /s	0.25 (0.03)	0.27 (0.04)	0.07
RA ₉₅₀ %	0.7 (0.4)	1.1 (1.1)	0.42

WA%: Wall area percent, LA: Lumen area, BSA: Body surface area, RB1: Right upper lobe apical bronchus, RB5: Right middle lobe lateral bronchus, RB8: Right lower lobe subsegmental bronchus, LB1: Left upper lobe apical bronchus, LB8: Left lower lobe subsegmental bronchus, RA₉₅₀: Relative area of the lung parenchyma with attenuation \leq -

950HU, VDP: ^3He MRI ventilation defect percent, ADC: ^3He MRI apparent diffusion coefficient, **Mean of fifth generation airway

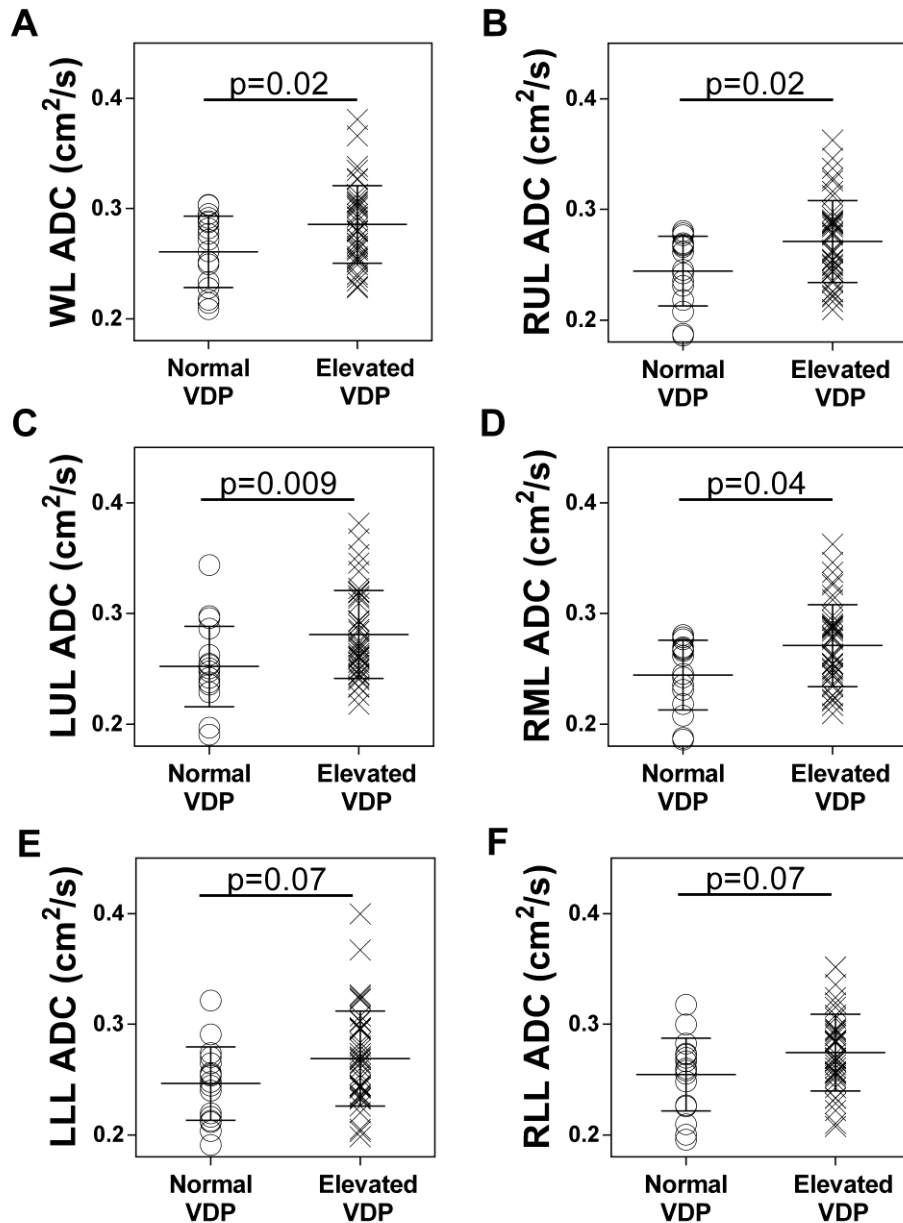


Figure 3-2. Whole lung and regional emphysema measurements in ex-smokers with normal (n=18) and abnormally-elevated VDP (n=42). ADC was significantly greater in apical lung in subjects with elevated VDP. A) Whole lung ADC (p=0.02), B) Right upper lobe ADC (p=0.02), C) Left upper lobe ADC (p=0.009), D) Right middle lobe ADC (p=0.04), E) Left lower lobe ADC (p=0.07), F) Right lower lobe ADC (p=0.07).

Table 3-3. Relationship of ³He MRI VDP with airways disease and emphysema measurements

	Spearman r	p
<i>Whole Lung VDP</i>		
**WA%	0.002	0.99
**LA	0.04	0.76
**LA/BSA	-0.04	0.75
ADC	0.40	0.001
RA ₉₅₀	0.34	0.008
<i>Right Upper Lobe VDP</i>		
RB1 WA%	0.24	0.06
RB1 LA	-0.37	0.004
RB1 LA/BSA	-0.42	0.0008
ADC	0.32	0.01
RA ₉₅₀	0.15	0.27
<i>Right Middle Lobe VDP</i>		
RB5 WA%	-0.11	0.40
RB5 LA	-0.003	0.98
RB5 LA/BSA	-0.02	0.91
ADC	0.46	0.002
RA ₉₅₀	0.24	0.07
<i>Right Lower Lobe VDP</i>		
RB8 WA%	0.28	0.03
RB8 LA	-0.28	0.03
RB8 LA/BSA	-0.37	0.004
ADC	0.38	0.003
RA ₉₅₀	0.21	0.11
<i>Left Upper Lobe VDP</i>		
LB1 WA%	0.07	0.62
LB1 LA	0.13	0.33
LB1 LA/BSA	-0.01	0.94
ADC	0.35	0.006
RA ₉₅₀	0.23	0.08
<i>Left Lower Lobe VDP</i>		
LB8 WA%	0.04	0.73
LB8 LA	0.05	0.68
LB8 LA/BSA	-0.02	0.86
ADC	0.37	0.004
RA ₉₅₀	0.26	0.05

WA%: Wall area percent, LA: Lumen area, BSA: Body surface area WL; Whole lung, RB1: Right upper lobe apical bronchus, RB5: Right middle lobe lateral bronchus, RB8: Right lower lobe subsegmental bronchus, LB1: Left upper lobe apical bronchus, LB8: Left lower lobe subsegmental bronchus, RA₉₅₀: Relative area of the lung parenchyma with attenuation ≤ -950 HU, VDP: ³He MRI ventilation defect percent, ADC: ³He MRI apparent diffusion coefficient, **Mean of fifth generation airways

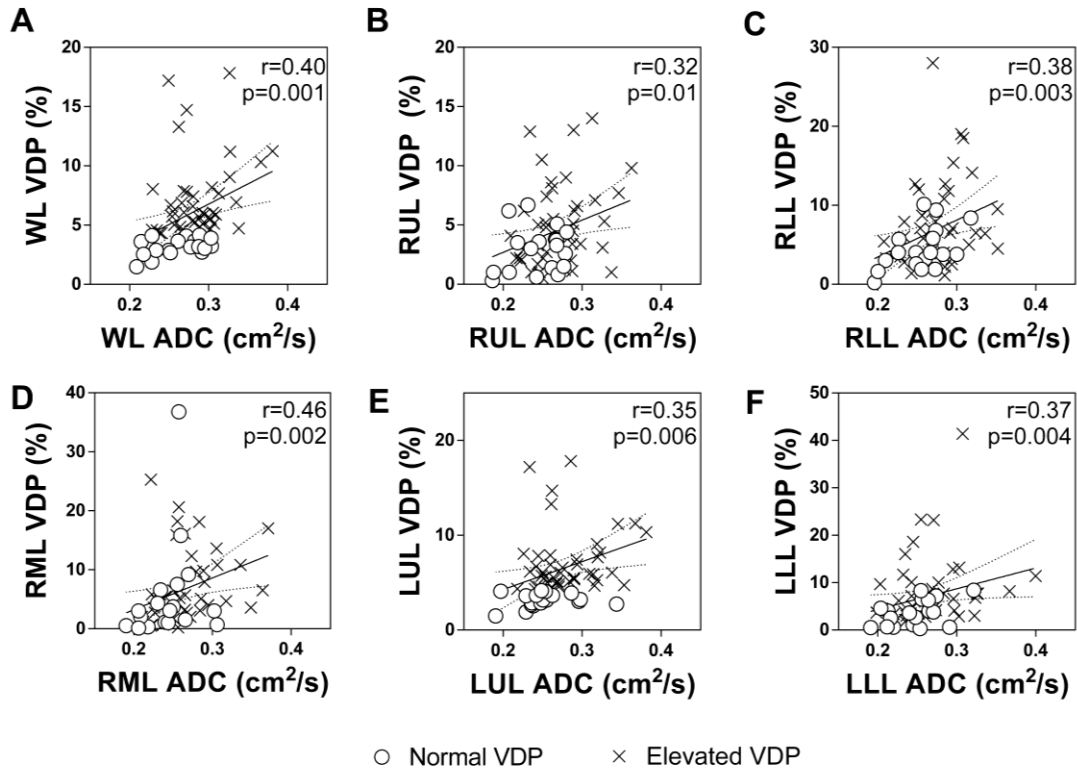


Figure 3-3. Relationships for whole lung and regional VDP with ³He MRI emphysema measurements. A) Whole lung (WL) VDP correlated with WL ADC ($r=0.40$, $p=0.001$), B) RUL VDP correlated with RUL ADC ($r=0.32$, $p=0.01$), C) RLL VDP correlated with RLL ADC ($r=0.38$, $p=0.003$), D) RML VDP correlated with RML ADC ($r=0.46$, $p=0.002$), E) LUL VDP correlated with LUL ADC ($r=0.35$, $p=0.006$), F) LLL VDP correlated with LLL ADC ($r=0.37$, $p=0.004$).

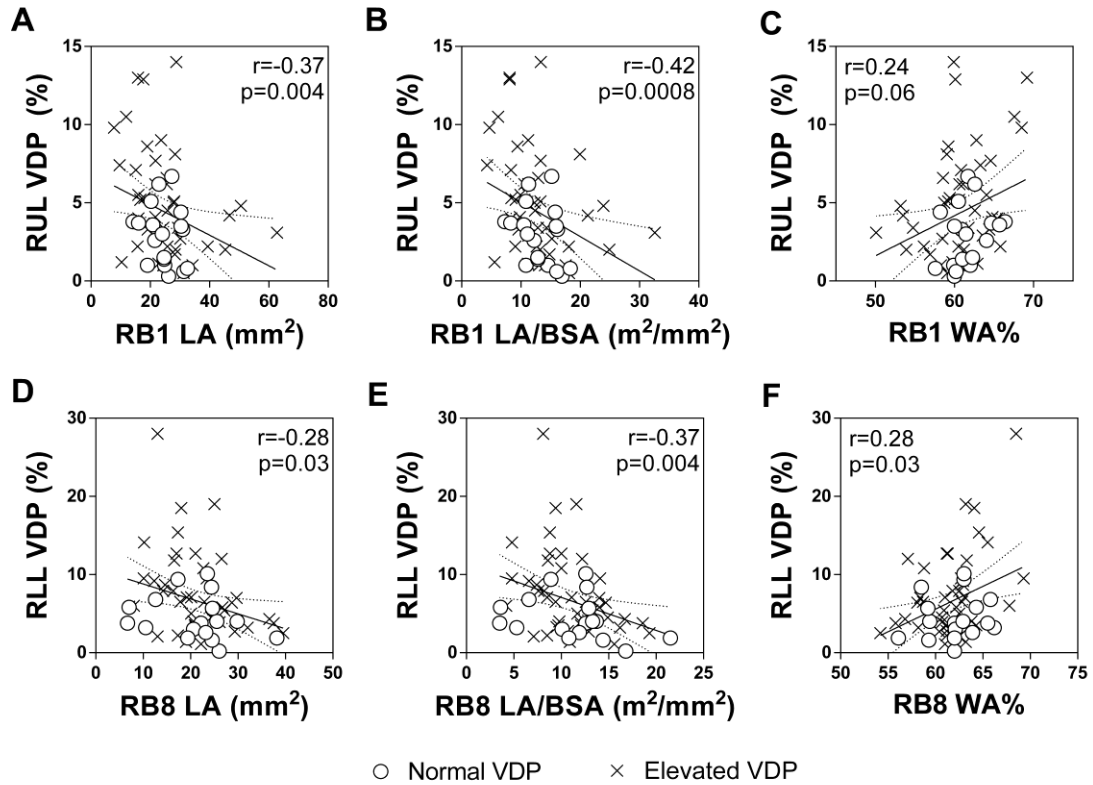


Figure 3-4. Relationships for regional VDP with CT airways disease measurements. Right upper lobe (RUL) VDP correlated with A) RB1 LA ($r = -0.37$, $p = 0.004$), B) RB1 LA/BSA ($r = -0.42$, $p = 0.0008$) but not C) RB1 WA% ($r = 0.24$, $p = 0.06$). Right lower lobe (RLL) VDP correlated with D) RB8 LA ($r = -0.28$, $p = 0.03$), E) RB8 LA/BSA ($r = -0.37$, $p = 0.004$) and F) RB8 WA% ($r = 0.28$, $p = 0.03$).

3.4 Discussion

We acquired ^3He MRI and CT in 60 ex-smokers without airflow limitation and made the following observations: 1) 42 of 60 volunteers reported abnormally-elevated ^3He VDP and these subjects reported normal airflow and lung volume measurements that were not significantly different from 18 ex-smokers with normal VDP, 2) there was significantly greater (worse) apical lung ^3He ADC in the 42 ex-smokers with abnormally-elevated VDP as compared to ex-smokers with normal VDP, but there were no other imaging differences between the subgroups, 3) ^3He VDP was significantly correlated with whole lung and regional ADC, and, 4) whole lung ^3He VDP was not correlated with whole lung airway morphological measurements, although RUL and RLL VDP was associated with thicker airway walls (WA%) and narrowed airway lumen (LA) in those regions of interest.

We observed that 42 ex-smokers reported VDP \geq 95% confidence interval for VDP in never-smokers (4). Although all participants had a significant smoking history (mean pack years=28), spirometry, plethysmography and CT showed no evidence of lung function decline or lung destruction and these same measurements showed no significant differences in subjects with elevated VDP compared to subjects with normal VDP. Previous work (8) in 'healthy' smokers showed significantly different MRI ventilation measurements as compared to never-smokers and COPD smokers and our findings build on this previous work by showing that ex-smokers with abnormally-elevated VDP also showed significantly greater whole-lung and apical lung ^3He ADC. These MRI findings were not observed using CT measurements of emphysema. In this regard, it is important to note that ^3He ADC provides a surrogate measure of microstructural emphysema (17) and was previously shown to be sensitive to very mild emphysematous changes by detecting differences in subjects exposed only to second-hand smoke (18). We observed that subjects with elevated VDP reported greater whole-lung and apical lung ^3He ADC. Previous work (19) evaluated the anatomical ADC distribution in more severe COPD and established the presence of elevated ADC in the apical lung regions and this is in agreement with predominant centrilobular emphysema in such patients. However to our knowledge the spatial distribution of ADC in ex-smokers without COPD has not yet been

evaluated. We did not observe differences in CT emphysema (RA_{950}) measurements. However, previous research (20) showed that CT-derived emphysema measurements may underestimate the extent of emphysema in very mild disease. The mean RA_{950} in the ex-smokers in our study was very low (mean $RA_{950} = 1.2\%$) and this may reflect why CT RA_{950} was not significantly different between subgroups. Nevertheless, these results suggest that ex-smokers with a significant smoking history and abnormal ^3He VDP but without airflow limitation may also have a mild or subclinical form of centrilobular emphysema that is not detected using CT or conventional pulmonary function tests.

Whole lung and regional VDP were correlated with ADC which suggests that ventilation abnormalities and very mildly abnormal parenchyma co-existed in these otherwise normal ex-smokers. We evaluated regional (lobar) correlations for ^3He VDP and ADC because a direct spatial comparison previously described in COPD patients (7) was not feasible here. This previous approach (7) evaluated the direct spatial relationship between ^3He ventilation defects and emphysema by evaluating the overlap of RA_{950} (emphysema) regions and ^3He ventilation defects. As compared with COPD patients with severe emphysema ($RA_{950} > 15\%$), the ex-smokers here reported very low or normal RA_{950} and therefore the spatial overlap of ^3He ventilation defects and RA_{950} could not be evaluated. We wonder about the long-term consequences of these very mild abnormalities in ventilation and emphysema measurements and whether these are predictors of a transition to COPD. Future longitudinal evaluations in these subjects are warranted and will be undertaken.

It was not expected that whole-lung airway measurements would show differences between subgroups since it is widely appreciated that obstructive disease is regionally (and not uniformly) distributed in the lung (21). However it was surprising that we did not detect or measure abnormal or different regional airway morphologies in the ex-smokers with abnormally elevated VDP, especially since whole-lung and lobar VDP was significantly greater in these participants. We think one explanation for this may be related to the airways we measured and the fact that they may not have been distal enough to reflect such mild disease. We did observe that RUL and RLL VDP were significantly correlated with RB1 and RB8 airway morphological abnormalities, but these

relationships were not significant in the other lung lobes. Nonetheless, the finding that airway walls thicken and airway lumens narrow with increasing ventilation heterogeneity in the RUL and RLL suggests a relationship between airway morphology and ventilation in these ex-smokers without COPD. These findings also highlight some of the limitations of CT and advantages of MRI for pulmonary imaging and characterization of very mild lung disease. As described elsewhere (22, 23), CT measurements are limited because of the inherent spatial resolution limit achievable on thoracic CT scans. On the other hand, MRI ADC provides a way to reveal subtle parenchymal changes to the alveolar microstructure and the subjects in our study certainly exemplify a patient group in whom MRI is highly advantageous.

We must acknowledge several limitations to our study. First, we measured five individual subsegmental airways (RB1, RB5, RB8, LB1 and LB8) and not all subsegmental airways. We chose these five airways in particular because they were most easily visible and measurable on thoracic CT and because they lead to the individual lung lobes of interest. While it is possible to quantitatively evaluate more distal subsegmental airways, the reproducibility of this in all subjects would be difficult to determine. Second, our findings were derived on a VDP threshold determined in never-smokers from a previous ^3He MRI study (4). The range of VDP for all subjects in our study was 2% - 18% and the VDP data distribution was not normally distributed, but reflected a Poisson distribution centered at 5-6%. This partially explains why 42 of 60 subjects reported abnormal VDP. If this threshold was greater, for example 5%, 33 of 60 subjects would have reported abnormally-elevated VDP. Nevertheless, the results of our analysis point to very mild emphysema and airways disease in ex-smokers without airflow limitation. We must also acknowledge that ^3He MRI may only be employed at a limited number of research centres worldwide due to the limited supply of ^3He gas and need for specialized equipment and software. However, pulmonary functional MRI using hyperpolarized ^{129}Xe is emerging as an attractive alternative with the potential for implementation and translation. In this regard, longitudinal measurements in these 60 ex-smokers will be undertaken using ^{129}Xe and more conventional ^1H MRI methods. We also recognize that although this study evaluated 60 ex-smokers – a relatively large study by MRI standards, the sample size may have limited our ability to detect significant

relationships for CT airway morphology and emphysema measurements between subgroups. Finally, while this study did not evaluate current smokers (with or without airflow limitation), future work investigating MRI ventilation measurements in current-smokers would also provide an understanding of acute effects of cigarette smoke on pulmonary ventilation.

In conclusion, in ex-smokers without airflow limitation, ^3He MRI identified a subgroup with abnormally elevated ventilation defect percent – a measure of ventilation heterogeneity. While there were no other pulmonary function or CT differences in ex-smokers with normal or abnormal VDP, there was significantly different MRI ADC and there was a relationship for whole-lung and regional VDP with ADC and for regional VDP with regional CT airway morphological abnormalities. Taken together, these data suggest that ex-smokers with normal airflow and lung volumes may represent a subclinical COPD phenotype that warrants further longitudinal investigation.

3.5 References

1. Hogg JC, Chu F, Utokaparch S, Woods R, Elliott WM, Buzatu L, et al. The nature of small-airway obstruction in chronic obstructive pulmonary disease. *N Engl J Med*. 2004;350(26):2645-53.
2. McDonough JE, Yuan R, Suzuki M, Seyednejad N, Elliott WM, Sanchez PG, et al. Small-airway obstruction and emphysema in chronic obstructive pulmonary disease. *N Engl J Med*. 2011;365(17):1567-75.
3. Vestbo J, Hurd SS, Agusti AG, Jones PW, Vogelmeier C, Anzueto A, et al. Global strategy for the diagnosis, management, and prevention of chronic obstructive pulmonary disease: GOLD executive summary. *American journal of respiratory and critical care medicine*. 2013;187(4):347-65.
4. Sheikh K, Paulin GA, Svenningsen S, Kirby M, Paterson NA, McCormack DG, et al. Pulmonary ventilation defects in older never-smokers. *J Appl Physiol* (1985). 2014;117(3):297-306.
5. Kirby M, Mathew L, Heydarian M, Etemad-Rezai R, McCormack DG, Parraga G. Chronic obstructive pulmonary disease: quantification of bronchodilator effects by using hyperpolarized (3)He MR imaging. *Radiology*. 2011;261(1):283-92. Epub 2011/08/05.
6. Svenningsen S, Kirby M, Starr D, Coxson HO, Paterson NA, McCormack DG, et al. What are ventilation defects in asthma? *Thorax*. 2014;69(1):63-71.
7. Kirby M, Pike D, Coxson HO, McCormack DG, Parraga G. Hyperpolarized 3He Ventilation Defects Used to Predict Pulmonary Exacerbations in Mild to Moderate Chronic Obstructive Pulmonary Disease. *Radiology*. 2014:140161.
8. Woodhouse N, Wild JM, Paley MN, FICHELE S, Said Z, Swift AJ, et al. Combined helium-3/proton magnetic resonance imaging measurement of ventilated lung volumes in smokers compared to never-smokers. *J Magn Reson Imaging*. 2005;21(4):365-9.
9. Miller MR, Hankinson J, Brusasco V, Burgos F, Casaburi R, Coates A, et al. Standardisation of spirometry. *The European respiratory journal*. 2005;26(2):319-38.
10. Svenningsen S, Kirby M, Starr D, Leary D, Wheatley A, Maksym GN, et al. Hyperpolarized (3) He and (129) Xe MRI: differences in asthma before bronchodilation. *J Magn Reson Imaging*. 2013;38(6):1521-30.
11. Kirby M, Heydarian M, Wheatley A, McCormack DG, Parraga G. Evaluating bronchodilator effects in chronic obstructive pulmonary disease using diffusion-weighted hyperpolarized helium-3 magnetic resonance imaging. *J Appl Physiol*. 2012;112(4):651-7.

12. Owrangi AM, Etemad-Rezai R, McCormack DG, Cunningham IA, Parraga G. Computed tomography density histogram analysis to evaluate pulmonary emphysema in ex-smokers. *Acad Radiol*. 2013;20(5):537-45.
13. Kirby M, Heydarian M, Svenningsen S, Wheatley A, McCormack DG, Etemad-Rezai R, et al. Hyperpolarized ³He magnetic resonance functional imaging semiautomated segmentation. *Acad Radiol*. 2012;19(2):141-52.
14. Niimi A, Matsumoto H, Amitani R, Nakano Y, Mishima M, Minakuchi M, et al. Airway wall thickness in asthma assessed by computed tomography: relation to clinical indices. *American journal of respiratory and critical care medicine*. 2000;162(4):1518-23.
15. West JB. *Respiratory Physiology: The Essentials (8th Edition)*: Lippincott Williams and Wilkins; 2008.
16. Wan ES, Hokanson JE, Murphy JR, Regan EA, Make BJ, Lynch DA, et al. Clinical and radiographic predictors of GOLD-unclassified smokers in the COPD Gene study. *American journal of respiratory and critical care medicine*. 2011;184(1):57-63.
17. Yablonskiy DA, Sukstanskii AL, Woods JC, Gierada DS, Quirk JD, Hogg JC, et al. Quantification of lung microstructure with hyperpolarized ³He diffusion MRI. *J Appl Physiol*. 2009;107(4):1258-65.
18. Wang C, Mugler JP, 3rd, de Lange EE, Patrie JT, Mata JF, Altes TA. Lung injury induced by secondhand smoke exposure detected with hyperpolarized helium-3 diffusion MR. *J Magn Reson Imaging*. 2014;39(1):77-84.
19. Evans A, McCormack D, Ouriadov A, Etemad-Rezai R, Santyr G, Parraga G. Anatomical distribution of ³He apparent diffusion coefficients in severe chronic obstructive pulmonary disease. *J Magn Reson Imaging*. 2007;26(6):1537-47. Epub 2007/10/31.
20. Miller RR, Muller NL, Vedal S, Morrison NJ, Staples CA. Limitations of computed tomography in the assessment of emphysema. *Am Rev Respir Dis*. 1989;139(4):980-3.
21. Coxson HO, Leipsic J, Parraga G, Sin DD. Using Pulmonary Imaging to Move Chronic Obstructive Pulmonary Disease beyond FEV1. *Am J Respir Crit Care Med*. 2014;190(2):135-44.
22. Coxson HO. Quantitative chest tomography in COPD research: chairman's summary. *Proc Am Thorac Soc*. 2008;5(9):874-7.
23. Coxson HO. Quantitative computed tomography assessment of airway wall dimensions: current status and potential applications for phenotyping chronic obstructive pulmonary disease. *Proc Am Thorac Soc*. 2008;5(9):940-5.

CHAPTER 4

In Chapter 3 we observed that hyperpolarized ^3He MRI ventilation abnormalities in ex-smokers without chronic obstructive pulmonary disease (COPD) were spatially related to airways disease and microstructural emphysema. Results from Chapters 2 and 3 and previous research from our group and others established that individuals with COPD exhibit ventilation abnormalities and emphysema throughout the lung. Therefore we were interested in how individuals could be grouped into clinically meaningful phenotypes based on the location of pulmonary abnormalities within the lung and furthermore, how these regional phenotypes might change with disease progression. Therefore, here we used ^3He MRI and CT to phenotype COPD ex-smokers based on the apical – basal distribution of ventilation abnormalities and emphysema and evaluate the change in phenotype with disease progression.

The contents of this chapter have been published in COPD: Journal of Chronic Obstructive Pulmonary Disease (JCOPD) and permission to reproduce the article was granted by Taylor and Francis Publishing Group on behalf of JCOPD and is provided in Appendix D.

D Pike, M Kirby, RL Eddy, F Guo, DPI Capaldi, A Ouriadov, DG McCormack, and G Parraga. Regional Heterogeneity of Chronic Obstructive Pulmonary Disease Phenotypes: Pulmonary ^3He Magnetic Resonance Imaging and Computed Tomography; DOI: 10.3109/15412555.2015.1123682

4 Regional Heterogeneity of Chronic Obstructive Pulmonary Disease Phenotypes: Pulmonary ^3He Magnetic Resonance Imaging and Computed Tomography

4.1 Introduction

Chronic obstructive pulmonary disease (COPD) is characterized by irreversible airflow obstruction, mainly due to airways disease, emphysema, or a combination of airway and parenchymal abnormalities (1). While both airways disease and emphysema influence the clinical course of COPD, the emphysema phenotype is associated with more rapid disease progression, more frequent exacerbation episodes and significantly worse mortality than the airways disease phenotype (2-4). In this regard, high-resolution computed tomography (CT) has emerged as a robust method for quantifying and spatially mapping emphysema and its progression (5-7). At the same time, heterogeneity in the

clinical presentation of patients (8, 9) with the same lung function and emphysema measurements, has prompted several CT studies (10-19) to provide a better understanding of the clinical relevance of the spatial distribution of emphysema. While these previous studies have yielded important results, the clinical relevance and physiological outcomes associated with different emphysema (10, 14, 17, 20) and airways disease (21, 22) distribution is not well-understood.

Hyperpolarized ^3He magnetic resonance imaging (MRI) has emerged as another imaging approach for quantifying airways disease and emphysema phenotypes in COPD (23-25). ^3He and ^{129}Xe MRI ventilation imaging readily identifies regions of signal void (26) that are believed to reflect poorly ventilated regions of the parenchyma (27). In COPD patients, ^3He ventilation defects are highly reproducible over long periods of time in stable patients (28), predict COPD exacerbations (29), and diminish in response to short-acting bronchodilator therapy (30) and bronchoscopic lung volume reduction using stents (31). Previous work (32) showed that ^3He ventilation defects in asthma are spatially related to abnormal airway morphology and it has been suggested (29) that in COPD, ventilation defects may be related to airways disease, emphysema or a combination of both. However, the relationship of the distribution of ^3He ventilation defects and progression of COPD has not yet been investigated. Therefore, our objective here was to investigate the relationship between COPD severity and the spatial distribution of ventilation defects measured using MRI and emphysema measured using CT in a relatively large group of COPD ex-smokers.

4.2 Methods

4.2.1 Study Subjects

This study was registered as NCT02279329 (ClinicalTrials.gov, National Institute of Health, Maryland, USA). Study subjects with a clinical diagnosis of COPD provided written informed consent to a protocol that was compliant with the Personal Information Protection and Electronic Documents Act (PIPEDA, Canada) and Health Insurance Portability and Accountability Act (HIPAA, USA) and approved by a local research ethics board and Health Canada. Each two-hour visit consisted of spirometry,

plethysmography, the six-minute-walk-test (6MWT) for the six-minute walk distance (6MWD), St. George's Respiratory Questionnaire (SGRQ), ^3He MRI and inspiratory CT. Subjects were clinically diagnosed and classified according to the Global Initiative for Chronic Obstructive Lung Disease (GOLD) criteria (33) and/or clinical symptoms over a 3 month period in addition to a smoking history of >10 pack years.

4.2.2 Spirometry and Plethysmography

Spirometry measurements, including the forced expiratory volume in one second (FEV_1) and forced vital capacity (FVC), were acquired according to the American Thoracic Society guidelines (34). Whole-body plethysmography was used to measure lung volumes (residual volume (RV) and total lung capacity (TLC)) (MedGraphics Corporation, St. Paul, Minnesota, USA) and a stand-alone gas analyzer (attached to plethysmograph) was used to measure diffusing capacity of the lung for carbon monoxide (DL_{CO}).

4.2.3 Imaging

Subjects were randomized to first receive either MRI or CT and image acquisition was performed within 15 minutes of each other. For both MRI and CT, image acquisition was completed within 5-7 minutes of patients being made comfortable in a supine position. MRI was performed using a 3.0 Tesla Discovery MR750 (General Electric Health Care, Milwaukee, Wisconsin, USA) system, as previously described (35), using a whole-body gradient set with a maximum gradient amplitude of 1.94G/cm and a single-channel, rigid elliptical transmit/receive chest coil (Rapid Biomedical GmbH, Rimpar, Germany) with patients in inspiratory breath-hold at functional residual capacity (FRC) + 1L. Anatomical ^1H MRI was acquired prior to ^3He MRI after inhalation of 1L medical grade nitrogen (N_2) from FRC using the whole-body radiofrequency coil and a ^1H fast-spoiled, gradient-recalled-echo sequence using a partial echo [16s total data acquisition, posterior to anterior repetition time (TR)/echo times (TE)/flip angle=4.7ms/1.2ms/ 30° , field of view (FOV)=40x40cm, bandwidth 24.4 kHz, matrix=128x80, 15-17 slices, 15mm slice thickness, zero gap] as previously described (35). ^3He static-ventilation MR images were acquired with a mixture of hyperpolarized ^3He (5ml/kg body weight) diluted to 1L with

N₂ and using a fast-gradient echo method using a partial echo [14s total data acquisition, posterior to anterior, TR/TE/flip angle=4.3ms/1.4ms/7°, FOV=40x40cm, bandwidth=48.8kHz, matrix=128x80, 15-17 slices, 15mm slice thickness, zero gap]. ³He diffusion-weighted MRI was also performed as previously described (27), however we did not evaluate apparent diffusion coefficients (ADCs) as estimates of emphysema because these values only report from regions of normal ventilation which would have biased the ADC-based emphysema estimates.

CT was acquired using a 64 slice Lightspeed VCT system (General Electric Health Care, Milwaukee, Wisconsin, USA) using a single spiral acquisition from apex to base (64×0.625mm collimation, 120kVp, 100mA, tube rotation time=500ms, pitch=1.25, standard reconstruction kernel and 1.25mm slice thickness). All subjects were transported from the MRI suite to the CT suite by wheelchair to prevent the potential of any exercise-induced dilatation of the airways or lung parenchyma. CT was acquired during inspiratory breath-hold of high-purity, medical grade N₂ at the same volume as MRI (FRC+1L) as previously described (36) to enable direct comparison to MR images. The total effective dose for each CT scan was 1.8 mSv as calculated using manufacturer settings and the ImPACT CT dosimetry calculator based on Health Protection Agency (UK) NRPB-SR250.

4.2.4 Image Analysis

Hyperpolarized ³He MR static-ventilation images were used to generate whole-lung ³He ventilation defect percent (VDP) using semi-automated software generated using MATLAB (Mathworks, Natick, Massachusetts, USA) (37).

Inspiratory CT images were evaluated using VIDA Pulmonary Workstation 2.0 (VIDA Diagnostics, Coralville, Iowa, USA). Emphysema was measured for whole-lung and individual lung lobes using the relative area of the lung parenchyma with attenuation \leq -950 Hounsfield units (HU) (RA₉₅₀). Airway wall area percent for the 5th generation airways (WA%) and airway wall thickness for airways with an internal perimeter of 10mm (Pi10) were estimated as previously described (38).

Ventilation defect percent for each lung lobe (right upper lobe (RUL), right lower lobe (RLL), left upper lobe (LUL), left lower lobe (LLL)) was generated by registering the thoracic CT segmentation of the lung lobes (VIDA Pulmonary Workstation 2.0) to ^3He MRI ventilation images using deformable registration as previously described (39).

4.2.5 Distribution of Emphysema and Ventilation Defects

Apical-lung (AL) and basal-lung (BL) predominant emphysema phenotypes were defined using a method adapted from a previously described technique (10) whereby RA_{950} in the BL ($RA_{950BL} = RA_{950RLL} + RA_{950LLL}$) and RA_{950} in the AL ($RA_{950AL} = RA_{950RUL} + RA_{950LUL}$) were used to generate the difference between AL and BL RA_{950} (ΔRA_{950}). A positive ΔRA_{950} was indicative of AL-predominant distribution, and a negative ΔRA_{950} indicated BL-predominant emphysema distribution such that:

$$AL\text{-predominant emphysema: } RA_{950AL} - RA_{950BL} = + \Delta RA_{950} \quad (1)$$

$$BL\text{-predominant emphysema: } RA_{950AL} - RA_{950BL} = - \Delta RA_{950} \quad (2)$$

In a similar manner, regional ^3He VDP was used to identify AL- and BL-predominant ^3He ventilation defect phenotypes. The ventilation defect percent in BL ($VDP_{BL} = VDP_{RLL} + VDP_{LLL}$) was subtracted from the ventilation defect percent in the AL ($VDP_{AL} = VDP_{RUL} + VDP_{LUL}$) to generate the difference between AL- and BL-VDP (ΔVDP), whereby a positive ΔVDP indicated an AL-predominant distribution of ventilation defects and a negative ΔVDP indicated a BL-predominant distribution of ventilation defects such that:

$$AL\text{-predominant ventilation defects: } VDP_{AL} - VDP_{BL} = + \Delta VDP \quad (3)$$

$$BL\text{-predominant ventilation defects: } VDP_{AL} - VDP_{BL} = - \Delta VDP \quad (4)$$

All participants were classified in AL- and BL-predominant subgroups using both CT and ^3He MRI measurements for all lobes except the right middle lobe (RML) because recent research (40) has shown that the RML contributes disproportionately to imaging measurements of emphysema.

4.2.6 Statistics

All statistical tests were performed in IBM SPSS V22 (SPSS Inc., Chicago, Illinois, USA). A one-way analysis of variance (ANOVA) was used to compare parameters between COPD grades of severity. Comparisons between imaging measurements of AL and BL subgroups were performed using unpaired t-tests with Holm-Bonferroni corrections to adjust for family-wise error. Pearson correlations were used for univariate analyses and p-values were adjusted for family-wise error. All statistical figures were created in GraphPad Prism V6 (GraphPad Software Inc., La Jolla, California, USA).

4.3 Results

We evaluated 100 COPD ex-smokers (n=22 GOLD I, n=46 GOLD II and n=32 GOLD III/IV). **Table 4-1** shows the demographic and pulmonary function measurements for all subjects and stratified by GOLD grade severity. Measurements of pulmonary function and volumes including FEV₁, FVC, FEV₁/FVC, RV, RV/TLC and DL_{CO} worsened with increasing GOLD grade severity (all p<0.0001). Similarly, SGRQ total score increased (p<0.0001) and 6MWD decreased (p=0.001) with increasing disease severity.

Table 4-1. Demographic and pulmonary function test measurements

Parameter (±SD)	All (n=100)	GOLD I (n=22)	GOLD II (n=46)	GOLD III/IV (n=32)	p*
Age yr	71 (8)	75 (7)	70 (8)	70 (8)	0.03
Male n (%)	65 (65)	19 (86)	27 (59)	19 (59)	0.06
Pack years	50 (30)	48 (36)	48 (27)	54 (31)	0.6
BMI kg/m ²	27 (4)	28 (4)	27 (4)	26 (5)	0.3
6MWD m	377 (91) ¹	419 (47) ²	388 (90) ³	323 (98) ⁴	0.001
FEV ₁ % _{pred}	62 (23)	95 (12)	64 (9)	36 (7)	<0.0001
FVC% _{pred}	90 (20)	109 (12)	92 (14)	73 (16)	<0.0001
FEV ₁ /FVC %	50 (12)	63 (5)	52 (8)	37 (8)	<0.0001
RV% _{pred}	160 (48)	123 (30)	148 (34)	202 (45)	<0.0001
RV/TLC % _{pred}	133 (27)	107 (18)	127 (17)	159 (22)	<0.0001
DL _{CO} % _{pred}	55 (20)	69 (19)	57 (16)	42 (18)	<0.0001
SGRQ Total Score	40 (19)	23 (16)	37 (14)	56 (12)	<0.0001

BMI: Body mass index, FEV₁: Forced expiratory volume in one second, FVC: Forced vital capacity, RV: Residual volume, TLC: Total lung capacity, DL_{CO}: Diffusing

capacity for carbon monoxide, SGRQ: St. George's Respiratory Questionnaire, 6MWD: Six-minute walk distance, ¹n=91, ²n=21, ³n=44, ⁴n=26, *ANOVA corrected p-value

Figure 4-1 shows ^3He MR static-ventilation and CT images for COPD ex-smokers stratified by GOLD grade with ventilation defects and corresponding emphysema. ^3He ventilation is shown in cyan and emphysema is shown using an RA_{950} mask (voxels \leq 950HU in yellow). It was visibly obvious that ex-smokers (S1, S2, S3, S4 and S5) with BL-predominant ^3He ventilation defects showed ventilation heterogeneity in the lower lung lobes while ex-smokers (S6, S7, S8, S9 and S10) with AL-predominant ^3He ventilation defects had ventilation abnormalities localized to the upper lung lobes. At the same time, corresponding CT emphysema masks were not spatially concordant with the BL and AL ventilation defect phenotypes in milder COPD (as shown in subjects S1 and S2 as well as in S6 and S7). However in moderate-severe grade ex-smokers (such as S3, S4 and S5 and also S8, S9 and S10) the spatial relationship between ventilation defects and CT RA_{950} was more obvious.

Table 4-2 provides a summary of whole-lung and regional RA_{950} and VDP as well as airway measurements for all study subjects and stratified by GOLD grade. Whole-lung and regional RA_{950} (RUL, RLL, LUL, LLL, $\text{RA}_{950\text{AL}}$, $\text{RA}_{950\text{BL}}$) were significantly worse (all $p < 0.05$) with increasing GOLD grade. Similarly, whole-lung and regional VDP (RUL, RLL, LUL, LLL, VDP_{AL} , VDP_{BL}) was significantly worse (all $p < 0.05$ except LLL VDP $p = 0.05$) with increasing disease severity. No significant differences were observed for ΔRA_{950} ($p = 0.7$) or ΔVDP ($p = 0.9$) between GOLD grades and there were no differences for airway Pi_{10} ($p = 0.6$) or mean fifth generation $\text{WA}\%$ ($p = 0.5$) or LA ($p = 1.0$) between GOLD grades. Women had significantly decreased VDP in the RLL and LLL and significantly different VDP_{BL} and ΔVDP compared to men for GOLD II and GOLD III/IV while no significant differences were observed for the 3 women in the GOLD I subgroup (data not shown).

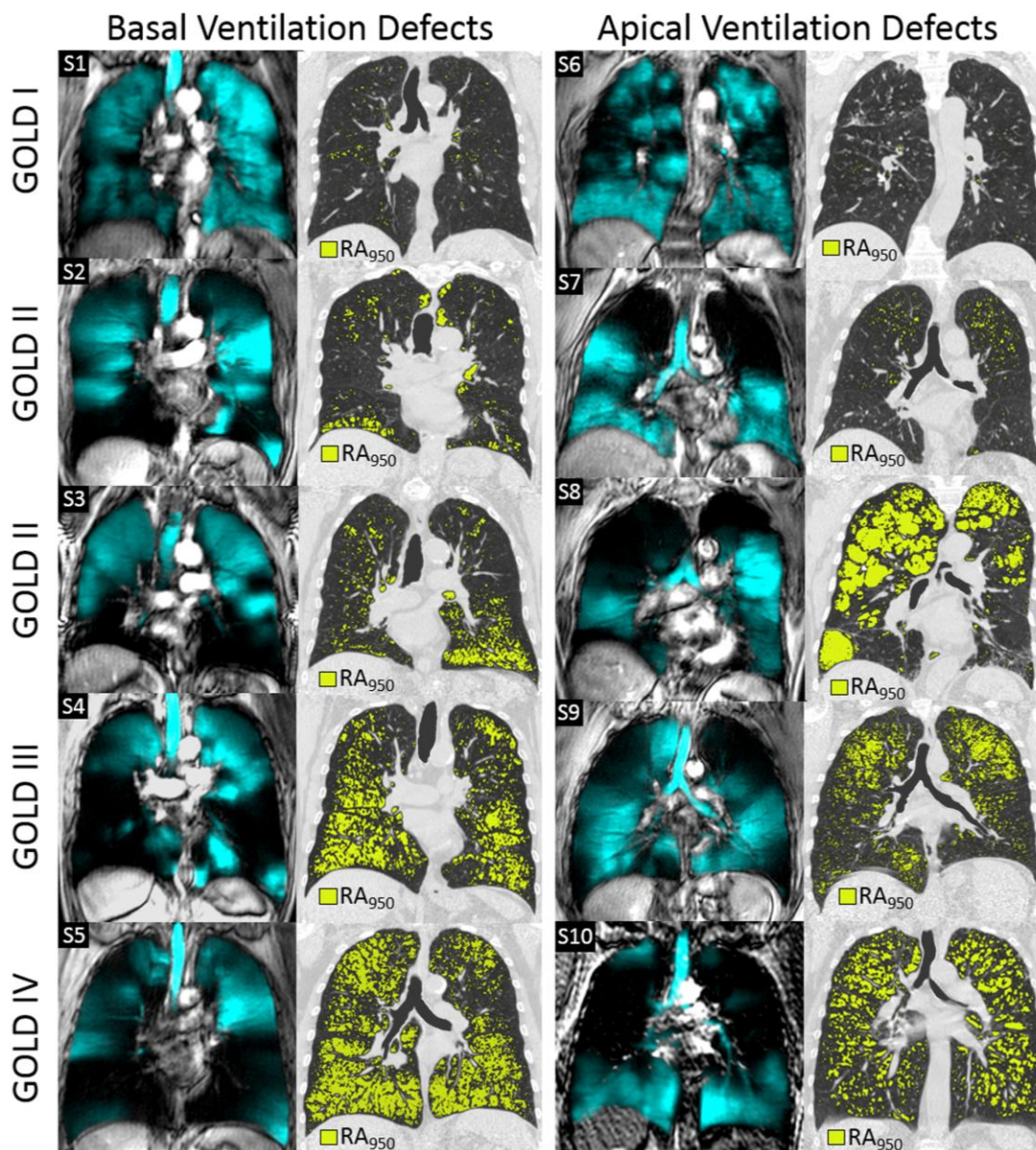


Figure 4-1. Thoracic ^3He MRI and CT of COPD ex-smokers with representative apical- and basal-lung predominant ^3He ventilation defects and corresponding emphysema. Ex-smokers with basal-lung predominant ^3He ventilation defects (S1, S2, S3, S4 and S5) show ventilation heterogeneity localized to the basal-lung while subjects with apical-lung predominant ventilation defects (S6, S7, S8, S9 and S10) show abnormalities localized in the apical lung. Emphysema is shown using a yellow RA_{950} mask. Note that the trachea was excluded from VDP and RA_{950} measurements.

Table 4-3 reports whole-lung and regional imaging measurements for MRI and CT AL- and BL-predominant phenotypes. Based on ^3He MRI VDP, 72 subjects reported BL-

predominant VDP while 28 reported AL-predominant VDP. Subjects with AL-predominant VDP reported significantly greater whole-lung ($p=0.03$) and upper lobe (RUL $p=0.002$, LUL $p=0.01$, RA_{950AL} $p=0.003$) emphysema measured using RA_{950} . Based on CT RA_{950} measurements, 71 subjects reported AL-predominant RA_{950} while 29 subjects reported BL-predominant RA_{950} . Subjects with AL-predominant RA_{950} had significantly diminished VDP in the RLL ($p=0.002$) and basal-lung (VDP_{BL} $p=0.003$).

Figure 4-2 shows the distribution (in percent) for subjects with AL- and BL-predominant MRI and CT phenotypes by GOLD grade. BL-predominant ventilation defects dominated the mild-moderate grades (AL/BL: GOLD I=18%/82%, GOLD II=24%/76%) while there was a more uniform distribution for severe GOLD grades (AL/BL: GOLD III=40%/60%, GOLD IV=43%/57%). The opposite trend was observed for CT emphysema phenotypes whereby the AL-predominant RA_{950} phenotype was more typical in the mild-moderate grade COPD (AL/BL: GOLD I=84%/16%, GOLD II=72%/28%) and in severe grade COPD, the distribution was more equivalent (AL/BL: GOLD III=64%/36%, GOLD IV=43%/57%).

Table 4-4 shows the spatial relationships for whole-lung and regional RA_{950} with VDP. The strongest correlations were observed for VDP and RA_{950} in the apical lobes (RUL: $r=0.77$, $p<0.0001$, LUL: $r=0.65$, $p<0.0001$) with moderate to weak correlations in the basal lobes (RLL: $r=0.48$, $p<0.0001$, LLL: $r=0.37$, $p=0.0001$).

Table 4-2. Imaging measurements

Parameter (\pm SD)	All (n=100)	GOLD I (n=22)	GOLD II (n=46)	GOLD III/IV (n=32)	p*
<i>RA₉₅₀ %</i>					
Whole lung	11 (10)	5 (4)	9 (9)	18 (12)	<0.0001
RUL	12 (14)	6 (8)	10 (13)	19 (15)	<0.0001
RLL	9 (11)	2 (2)	7 (8)	17 (13)	<0.0001
LUL	12 (14)	5 (4)	11 (16)	19 (14)	0.001
LLL	8 (9)	3 (2)	6 (5)	15 (12)	<0.0001
RA _{950AL}	24 (27)	11 (10)	21 (28)	38 (28)	<0.0001
RA _{950BL}	17 (19)	5 (3)	12 (12)	32 (24)	<0.0001
Δ RA ₉₅₀	7 (19)	6 (9)	9 (21)	6 (20)	0.7
<i>Airways</i>					
Pi10 mm	4.2 (0.5)	4.2 (0.2)	4.2 (0.7)	4.3 (0.2)	0.6
WA%	65 (2)	65 (2)	65 (2)	65 (2)	0.5
LA mm ²	13 (5)	13 (3)	13 (6)	13 (3)	1.0
<i>VDP %</i>					
Whole lung	18 (10)	9 (5)	17 (8)	26 (7)	<0.0001
RUL	20 (18)	11 (11)	18 (17)	30 (19)	<0.0001
RLL	29 (20)	17 (10)	28 (20)	38 (22)	0.001
LUL	19 (15)	11 (6)	19 (14)	25 (17)	0.002
LLL	24 (17)	17 (8)	25 (19)	28 (16)	0.05
VDP _{AL}	40 (31)	22 (15)	37 (29)	55 (33)	<0.0001
VDP _{BL}	53 (35)	34 (17)	52 (37)	66 (35)	0.003
Δ VDP	-13 (40)	-12 (15)	-16 (40)	-11 (50)	0.9

RA₉₅₀: Relative area of the lung with attenuation values \leq -950HU, HU: Hounsfield unit, RA_{950AL}=RA_{950RUL}+RA_{950LUL}, RA_{950BL}=RA_{950RLL}+RA_{950LLL}, Δ RA₉₅₀=RA_{950AL}-RA_{950BL}, Pi10: Airway wall thickness of airways with an internal perimeter of 10mm, WA%: Mean fifth generation airway wall area percent, LA: Mean fifth generation airway lumen area, VDP: Ventilation defect percent, VDP_{AL}=VDP_{RUL}+VDP_{LUL}, VDP_{BL}=VDP_{RLL}+VDP_{LLL}, Δ VDP=VDP_{AL}-VDP_{BL}, RUL: Right upper lobe, RLL: Right lower lobe, LUL: Left upper lobe, LLL: Left lower lobe, *ANOVA corrected p-value

Table 4-3. ^3He MRI and CT apical-lung (AL) and basal-lung (BL) phenotype measurements

Parameter (\pm SD)	$^3\text{He MRI}$			CT		
	BL VDP (n=72)	AL VDP (n=28)	p*	BL RA ₉₅₀ (n=29)	AL RA ₉₅₀ (n=71)	p*
RA₉₅₀ %						
Whole lung	9 (8)	16 (13)	0.03	11 (9)	11 (11)	1.0
RUL	9 (11)	20 (17)	0.002	8 (8)	14 (15)	0.3
RLL	8 (10)	11 (11)	1.0	13 (12)	7 (10)	0.3
LUL	9 (12)	20 (16)	0.01	9 (8)	14 (16)	1.0
LLL	7 (9)	9 (11)	0.9	12 (11)	6 (8)	0.07
RA _{950AL}	18 (22)	40 (32)	0.003	17 (15)	28 (30)	0.6
RA _{950BL}	15 (18)	21 (22)	1.0	25 (22)	14 (17)	0.1
Δ RA ₉₅₀	3 (17)	19 (17)	0.001	-8 (8)	14 (18)	<0.0001
Airways						
Pi10 mm	4.3 (0.5)	4.2 (0.2)	0.8	4.1 (0.8)	4.2 (0.2)	0.9
WA%	65 (2)	65 (2)	1.0	66 (2)	65 (2)	1.0
LA mm ²	13 (5)	14 (3)	1.0	13 (4)	13 (5)	2.0
VDP %						
Whole lung	17 (10)	21 (9)	0.4	20 (10)	17 (9)	1.0
RUL	14 (12)	36 (22)	<0.0001	15 (11)	22 (20)	0.8
RLL	32 (21)	21 (14)	0.07	41 (23)	24 (17)	0.002
LUL	15 (11)	31 (17)	<0.0001	16 (12)	21 (15)	1.0
LLL	27 (18)	17 (9)	0.06	32 (22)	21 (13)	0.03
VDP _{AL}	29 (21)	66 (34)	<0.0001	32 (22)	43 (33)	0.8
VDP _{BL}	59 (37)	37 (22)	0.049	73 (42)	45 (28)	0.003
Δ VDP	-30 (28)	29 (34)	<0.0001	-41 (35)	-2 (36)	<0.0001

RA₉₅₀: Relative area of the lung with attenuation values $\leq -950\text{HU}$, HU: Hounsfield unit, RA_{950AL}= RA_{950RUL}+RA_{950LUL}, RA_{950BL}=RA_{950RLL}+RA_{950LLL}, Δ RA₉₅₀= RA_{950AL}-RA_{950BL}, Pi10: Airway wall thickness of airways with an internal perimeter of 10mm, WA%: Mean fifth generation airway wall area percent, LA: Mean fifth generation airway lumen area, VDP: Ventilation defect percent, VDP_{AL}=VDP_{RUL}+VDP_{LUL}, VDP_{BL}=VDP_{RLL}+VDP_{LLL}, Δ VDP=VDP_{AL}-VDP_{BL}, RUL: Right upper lobe, RLL: Right lower lobe, LUL: Left upper lobe, LLL: Left lower lobe, *ANOVA corrected p-value

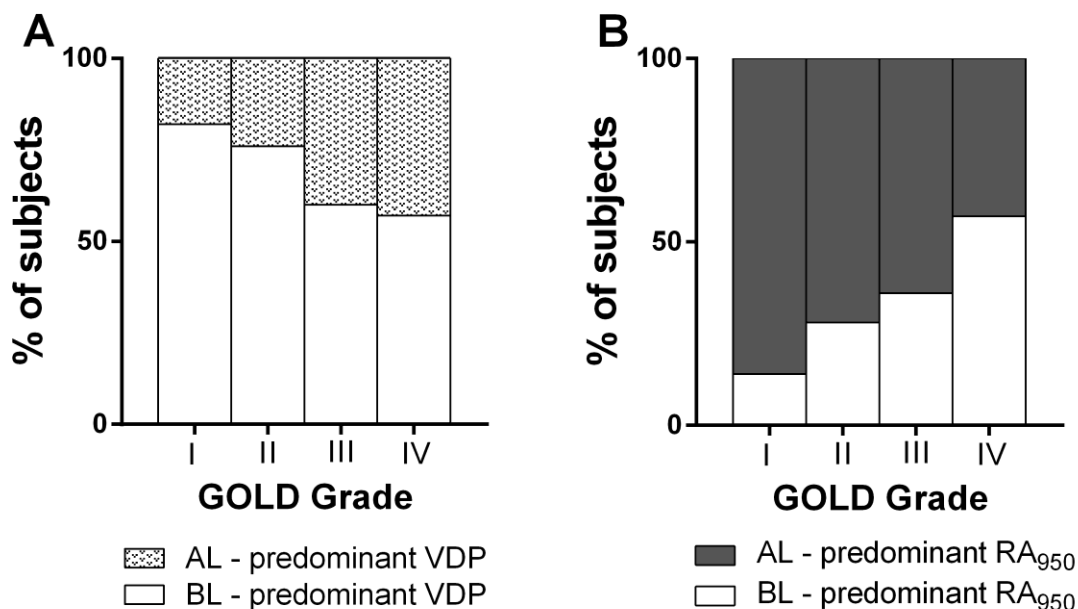


Figure 4-2. GOLD Grade distribution of AL- and BL-predominant VDP and RA₉₅₀ phenotypes. A) Basal-lung ventilation defects predominated in mild-moderate COPD subjects. AL/BL: GOLD I=18%/82%, GOLD II=24%/76%, GOLD III=40%/60% and GOLD IV=43%/57%. **B)** Apical-lung emphysema predominated in mild-moderate COPD subjects. AL/BL: GOLD I=84%/16%, GOLD II=72%/28%, GOLD III=64%/36% and GOLD IV=43%/57%.

Table 4-4. Regional relationships for ventilation defects (VDP) and emphysema (RA₉₅₀) for all subjects and by GOLD Grade

	Pearson Correlation coefficient for VDP and RA ₉₅₀ (p*)			
	All	GOLD I	GOLD II	GOLD III/IV
Whole lung	0.61 (<0.0001)	0.73 (0.0006)	0.47 (0.003)	0.42 (0.06)
RUL	0.77 (<0.0001)	0.72 (0.001)	0.70 (<0.0001)	0.77 (<0.0001)
LUL	0.65 (<0.0001)	0.44 (0.1)	0.62 (<0.0001)	0.59 (0.001)
RLL	0.48 (<0.0001)	0.34 (0.3)	0.34 (0.02)	0.39 (0.05)
LLL	0.37 (0.0001)	0.28 (0.2)	0.38 (0.02)	0.36 (0.04)

RUL: Right upper lobe, LUL: Left upper lobe, RLL: Right lower lobe, LLL: Left lower lobe, GOLD: Global initiative for chronic obstructive lung disease, *p-value corrected for family-wise error

4.4 Discussion

To provide a better understanding of the apical and basal lung regional distribution of emphysema and airways disease phenotypes in COPD, we stratified patients based on functional MRI and parenchymal CT measurements. We observed: 1) patients with mild-moderate COPD reported BL-predominant ventilation defects and AL-predominant emphysema, and, 2) patients with severe COPD reported ventilation defects and emphysema that was homogeneously (or evenly) distributed in the apical and basal lung regions.

Numerous studies have investigated CT measurements of emphysema, their spatial/regional distribution and their relationship with clinical findings. However, there is no consensus about the clinical meaning or physiological outcomes that can be directly related to the distribution of emphysema (10, 14, 17, 20, 41) or airways disease (21, 22). For example, some studies (12, 14, 16) reported that apical-predominant emphysema was associated with diminished pulmonary function, while other studies (13, 17, 20, 41, 42) showed that homogeneous or basal-lung emphysema was related to poorer lung function in patients. Others have reported that (10) the regional location of emphysema may not be clinically important. Unlike CT-based measurements of emphysema, MRI ventilation defects are resultant from both airways disease and emphysema in COPD patients (29). Similar to previous studies (11, 42-44), we observed that smoking-related emphysema was more severe in apical lung regions, especially in the milder grade subgroups. However, we also observed that ventilation abnormalities were predominantly present in the lung bases in the mild COPD stages. For both emphysema and ventilation abnormalities, the apical-basal gradients lessen in more severe disease. The fact that VDP and RA₉₅₀ were quantitatively and strongly correlated appears paradoxical, given their regional differences. However, this may be related to the fact that in COPD patients, the temporal onset of ventilation abnormalities and emphysema is similar, but this study showed that their presence and site of initiation are likely regionally different. Previous MRI studies have shown that in more severe COPD, ventilation defects may reflect both emphysema and airways disease or collapse (45), and this may explain some

of the differences in the regional distribution of ventilation abnormalities in severe COPD.

Patients with mild-moderate and severe disease also showed different distributions of AL- and BL-predominant phenotypes. Similar to a previous report (12), we observed that the relationship between basal-lung emphysema and impaired airflow was stronger than the relationship with apical-lung emphysema. Since ventilation is greater at the lung bases it would follow that increased emphysema at the bases would have a greater impact on FEV₁ than emphysema at the apices. To our knowledge, the spatial relationship between ventilation defects and FEV₁ has not yet been reported. This finding will be investigated further in the future as phenotyping COPD patients based on the distribution of ventilation abnormalities may help explain symptoms or disease progression.

We also wanted to better understand how ventilation abnormalities and emphysema might be related to one another in the apical and basal lung regions. VDP and RA₉₅₀ were significantly correlated in all lung regions but showed the strongest correlations in the apical-lung. Basal-lung ventilation defects predominated in mild-moderate GOLD grades, and a more homogeneous distribution of ventilation defects was observed in more advanced grade COPD; these differences suggest that over time, regional ventilation abnormalities become more homogeneously distributed during disease progression. This is in agreement with previous micro-CT analyses (1) that showed that in early stages, there was evidence of mainly terminal airway obliteration and not emphysematous destruction. In the future, longitudinal studies of ex- and current-smokers who are at risk of developing COPD may provide a deeper understanding of the regional initiation and progression of airways disease and emphysema.

Finally, we must also acknowledge a number of study limitations. First, hyperpolarized ³He MRI is not widely used and likely never will be, because of the high cost and limited global supply of ³He gas, and this limits the applicability of the results presented here. However, our team and others (46, 47) are transitioning to pulmonary MRI using ¹²⁹Xe gas which is much more readily available (24, 48), less expensive and poised on the threshold of regulatory approval and clinical translation. We should also note that the

phenotyping approach used here was adapted from previous work (10) and was based on the binary classification of AL- and BL-predominant phenotypes. Binary classification methods based on a threshold do not stratify subjects based on ΔVDP and ΔRA_{950} so all subjects with a positive ΔVDP and ΔRA_{950} were classified as AL-predominant and those with a negative ΔVDP and ΔRA_{950} were classified as BL-predominant. This straightforward method can certainly be improved by using three- or multi-dimensional indices and thresholds. In addition, we did not take into account emphysema or ventilation heterogeneity distributions between the lung core and rind regions as previously described (12-14, 49). CT images were acquired at the same inhalation volume as MRI (FRC+1L) rather than full inspiration in order to enable the direct comparison of MRI and CT phenotypes at the same lung volume. For this reason, the estimates of emphysema generated here based on CT cannot be directly compared with other quantitative CT emphysema estimates acquired at full inspiration. We note, however that in gas-trapped COPD patients, the differences between full inspiration and FRC+1L is approximately 1L and that the whole-lung RA_{950} values reported here derived at a smaller lung volume are similar to those reported in the COPDGene study (18, 50). Expiratory CT scans were not performed and in future studies, paired inspiratory-expiratory CT scans and phenotyping ex-smokers using novel parametric response mapping (PRM) techniques (21) might provide a better understanding of apical- and basal-predominant phenotypes. Furthermore, although acquired, ADC-based measures of emphysema from ^3He MRI were not used to quantify emphysema here because of the bias that results from the fact that only well-ventilation regions report ADC. Future studies comparing regional ADCs with CT RA_{90} may be useful to further verify the apical to basal pattern observed here. We must also point out that some of the patients classified with GOLD I COPD (ie. Subject 1 in Figure 4-1: 69 year-old female, $FEV_1=84\%_{\text{pred}}$, $FVC=94\%_{\text{pred}}$, $FEV_1/FVC=69\%$) were within the lower limit of normal (LLN) spirometry values for the mean age of this subgroup (75 ± 7 years). The mean values of $95\pm 12\%_{\text{pred}}$ and $109\pm 12\%_{\text{pred}}$ for FEV_1 and FVC respectively for the GOLD I subgroup (as show in Table 4-1) were also greater than the LLN as previously described (51). It is worth noting, however, that for this study, the diagnosis and classification of COPD included clinical symptoms over a 3 month period, a smoking history of >10 pack

years as well as the GOLD thresholds. We also acknowledge that this study focused on COPD patients with mainly mild-moderate disease (grade I COPD=22 subjects and grade II COPD=46 subjects) and that there was a small number of GOLD III (n=25) and GOLD IV (n=7) subjects and therefore our findings must be interpreted in this context.

In conclusion, we phenotyped ex-smokers with COPD based on the apical-basal distribution of emphysema and ventilation defects. We observed that a BL-predominant distribution of ventilation defects and AL-predominant distribution of emphysema was present in subjects with mild–moderate airflow obstruction. With increasing disease severity, there may be a basal-to-apical progression of ventilation abnormalities and an apical-to-basal progression of emphysema.

4.5 References

1. McDonough JE, Yuan R, Suzuki M, Seyednejad N, Elliott WM, Sanchez PG, et al. Small-airway obstruction and emphysema in chronic obstructive pulmonary disease. *N Engl J Med*. 2011;365(17):1567-75.
2. Han MK. Clinical correlations of computed tomography imaging in chronic obstructive pulmonary disease. *Ann Am Thorac Soc*. 2013;10 Suppl:S131-7.
3. Han MK, Kazerooni EA, Lynch DA, Liu LX, Murray S, Curtis JL, et al. Chronic obstructive pulmonary disease exacerbations in the COPDGene study: associated radiologic phenotypes. *Radiology*. 2011;261(1):274-82.
4. Burrows B, Bloom JW, Traver GA, Cline MG. The Course and Prognosis of Different Forms of Chronic Airways Obstruction in a Sample from the General Population. *New England Journal of Medicine*. 1987;317(21):1309-14.
5. Coxson HO, Dirksen A, Edwards LD, Yates JC, Agusti A, Bakke P, et al. The presence and progression of emphysema in COPD as determined by CT scanning and biomarker expression: a prospective analysis from the ECLIPSE study. *Lancet Respir Med*. 2013;1(2):129-36.
6. Smith BM, Austin JH, Newell JD, Jr., D'Souza BM, Rozenshtein A, Hoffman EA, et al. Pulmonary emphysema subtypes on computed tomography: the MESA COPD study. *Am J Med*. 2014;127(1):94 e7-23.
7. Kim SS, Seo JB, Lee HY, Nevrekar DV, Forssen AV, Crapo JD, et al. Chronic Obstructive Pulmonary Disease: Lobe-based Visual Assessment of Volumetric CT by Using Standard Images??? Comparison with Quantitative CT and Pulmonary Function Test in the COPDGene Study. *Radiology*. 2013;266(2):626-35.
8. Vestbo J, Hurd SS, Agusti AG, Jones PW, Vogelmeier C, Anzueto A, et al. Global strategy for the diagnosis, management, and prevention of chronic obstructive pulmonary disease: GOLD executive summary. *American journal of respiratory and critical care medicine*. 2013;187(4):347-65.
9. Agusti A, Calverley P, Celli B, Coxson HO, Edwards LD, Lomas DA, et al. Characterisation of COPD heterogeneity in the ECLIPSE cohort. *Respir Res*. 2010;11(1):122-36.
10. Gietema HA, Zanen P, Schilham A, van Ginneken B, van Klaveren RJ, Prokop M, et al. Distribution of emphysema in heavy smokers: impact on pulmonary function. *Respir Med*. 2010;104(1):76-82.

11. Gurney JW, Jones KK, Robbins RA, Gossman GL, Nelson KJ, Daughton D, et al. Regional distribution of emphysema: correlation of high-resolution CT with pulmonary function tests in unselected smokers. *Radiology*. 1992;183(2):457-63.
12. Nakano Y, Sakai H, Muro S, Hirai T, Oku Y, Nishimura K, et al. Comparison of low attenuation areas on computed tomographic scans between inner and outer segments of the lung in patients with chronic obstructive pulmonary disease: incidence and contribution to lung function. *Thorax*. 1999;54(5):384-9.
13. Haraguchi M, Shimura S, Hida W, Shirato K. Pulmonary function and regional distribution of emphysema as determined by high-resolution computed tomography. *Respiration*. 1998;65(2):125-9.
14. Mair G, Miller JJ, McAllister D, Maclay J, Connell M, Murchison JT, et al. Computed tomographic emphysema distribution: relationship to clinical features in a cohort of smokers. *Eur Respir J*. 2009;33(3):536-42.
15. Mohamed Hoesein FA, Schmidt M, Mets OM, Gietema HA, Lammers JW, Zanen P, et al. Discriminating dominant computed tomography phenotypes in smokers without or with mild COPD. *Respir Med*. 2014;108(1):136-43.
16. Mohamed Hoesein FA, van Rikxoort E, van Ginneken B, de Jong PA, Prokop M, Lammers JW, et al. Computed tomography-quantified emphysema distribution is associated with lung function decline. *Eur Respir J*. 2012;40(4):844-50.
17. Ju J, Li R, Gu S, Leader JK, Wang X, Chen Y, et al. Impact of emphysema heterogeneity on pulmonary function. *PLoS One*. 2014;9(11):e113320.
18. Castaldi PJ, San Jose Estepar R, Mendoza CS, Hersh CP, Laird N, Crapo JD, et al. Distinct quantitative computed tomography emphysema patterns are associated with physiology and function in smokers. *Am J Respir Crit Care Med*. 2013;188(9):1083-90.
19. Owsijewitsch M, Ley-Zaporozhan J, Kuhnigk J-M, Kopp-Schneider A, Eberhardt R, Eichinger M, et al. Quantitative Emphysema Distribution in Anatomic and Non-anatomic Lung Regions. *COPD: Journal of Chronic Obstructive Pulmonary Disease*. 0(0):null.
20. Fishman A. A randomized trial comparing lung-volume-reduction surgery with medical therapy for severe emphysema. *N Engl J Med*. 2003;348(21):2059-73.
21. Galban CJ, Han MK, Boes JL, Chughtai KA, Meyer CR, Johnson TD, et al. Computed tomography-based biomarker provides unique signature for diagnosis of COPD phenotypes and disease progression. *Nat Med*. 2012;18(11):1711-5.
22. Diaz AA, Han MK, Come CE, San Jose Estepar R, Ross JC, Kim V, et al. Effect of emphysema on CT scan measures of airway dimensions in smokers. *Chest*. 2013;143(3):687-93.

23. Fain SB, Panth SR, Evans MD, Wentland AL, Holmes JH, Korosec FR, et al. Early emphysematous changes in asymptomatic smokers: detection with ^3He MR imaging. *Radiology*. 2006;239(3):875-83.
24. Kirby M, Svenningsen S, Owringi A, Wheatley A, Farag A, Ouriadov A, et al. Hyperpolarized ^3He and ^{129}Xe MR imaging in healthy volunteers and patients with chronic obstructive pulmonary disease. *Radiology*. 2012;265(2):600-10.
25. Swift AJ, Wild JM, FICHELE S, Woodhouse N, Fleming S, Waterhouse J, et al. Emphysematous changes and normal variation in smokers and COPD patients using diffusion ^3He MRI. *Eur J Radiol*. 2005;54(3):352-8.
26. Woodhouse N, Wild JM, Paley MN, FICHELE S, Said Z, Swift AJ, et al. Combined helium-3/proton magnetic resonance imaging measurement of ventilated lung volumes in smokers compared to never-smokers. *J Magn Reson Imaging*. 2005;21(4):365-9.
27. Kirby M, Heydarian M, Wheatley A, McCormack DG, Parraga G. Evaluating bronchodilator effects in chronic obstructive pulmonary disease using diffusion-weighted hyperpolarized helium-3 magnetic resonance imaging. *J Appl Physiol*. 2012;112(4):651-7.
28. Mathew L, Evans A, Ouriadov A, Etemad-Rezai R, Fogel R, Santyr G, et al. Hyperpolarized ^3He magnetic resonance imaging of chronic obstructive pulmonary disease: reproducibility at 3.0 tesla. *Acad Radiol*. 2008;15(10):1298-311.
29. Kirby M, Pike D, Coxson HO, McCormack DG, Parraga G. Hyperpolarized ^3He Ventilation Defects Used to Predict Pulmonary Exacerbations in Mild to Moderate Chronic Obstructive Pulmonary Disease. *Radiology*. 2014:140161.
30. Kirby M, Mathew L, Heydarian M, Etemad-Rezai R, McCormack DG, Parraga G. Chronic obstructive pulmonary disease: quantification of bronchodilator effects by using hyperpolarized (^3He) MR imaging. *Radiology*. 2011;261(1):283-92. Epub 2011/08/05.
31. Mathew L, Kirby M, Farquhar D, Licskai C, Santyr G, Etemad-Rezai R, et al. Hyperpolarized ^3He functional magnetic resonance imaging of bronchoscopic airway bypass in chronic obstructive pulmonary disease. *Can Respir J*. 2012;19(1):41-3.
32. Svenningsen S, Kirby M, Starr D, Coxson HO, Paterson NA, McCormack DG, et al. What are ventilation defects in asthma? *Thorax*. 2014;69(1):63-71.
33. GOLD. Global Initiative for Chronic Obstructive Lung Disease: Global Strategy for the Diagnosis, Management and Prevention of Chronic Obstructive Pulmonary Disease (Updated 2015). 2015.
34. Miller MR, Hankinson J, Brusasco V, Burgos F, Casaburi R, Coates A, et al. Standardisation of spirometry. *The European respiratory journal*. 2005;26(2):319-38.

35. Parraga G, Ouriadov A, Evans A, McKay S, Lam WW, Fenster A, et al. Hyperpolarized ³He ventilation defects and apparent diffusion coefficients in chronic obstructive pulmonary disease: preliminary results at 3.0 Tesla. *Invest Radiol*. 2007;42(6):384-91.
36. Owrangi AM, Etemad-Rezai R, McCormack DG, Cunningham IA, Parraga G. Computed tomography density histogram analysis to evaluate pulmonary emphysema in ex-smokers. *Acad Radiol*. 2013;20(5):537-45.
37. Kirby M, Heydarian M, Svenningsen S, Wheatley A, McCormack DG, Etemad-Rezai R, et al. Hyperpolarized ³He magnetic resonance functional imaging semiautomated segmentation. *Acad Radiol*. 2012;19(2):141-52.
38. Nakano Y, Wong JC, de Jong PA, Buzatu L, Nagao T, Coxson HO, et al. The prediction of small airway dimensions using computed tomography. *American journal of respiratory and critical care medicine*. 2005;171(2):142-6.
39. Guo F, Svenningsen S, Bluemke E, Rajchl M, Yuan J, Fenster A, et al., editors. Automated pulmonary lobar ventilation measurements using volume-matched thoracic CT and MRI 2015.
40. Bhatt SP, Sieren JC, Newell JD, Jr., Comellas AP, Hoffman EA. Disproportionate contribution of right middle lobe to emphysema and gas trapping on computed tomography. *PLoS One*. 2014;9(7):e102807.
41. Tanabe N, Muro S, Tanaka S, Sato S, Oguma T, Kiyokawa H, et al. Emphysema distribution and annual changes in pulmonary function in male patients with chronic obstructive pulmonary disease. 2012.
42. Martinez FJ, Foster G, Curtis JL, Criner G, Weinmann G, Fishman A, et al. Predictors of mortality in patients with emphysema and severe airflow obstruction. *Am J Respir Crit Care Med*. 2006;173(12):1326-34.
43. Martelli NA, Hutchison DCS, Barter CE. Radiological distribution of pulmonary emphysema: Clinical and physiological features of patients with emphysema of upper or lower zones of lungs. *Thorax*. 1974;29(1):81-9.
44. Thurlbeck WM, Müller N. Emphysema: definition, imaging, and quantification. *AJR American journal of roentgenology*. 1994;163(5):1017-25.
45. Kirby M, Svenningsen S, Kanhere N, Owrangi A, Wheatley A, Coxson HO, et al. Pulmonary ventilation visualized using hyperpolarized helium-3 and xenon-129 magnetic resonance imaging: differences in COPD and relationship to emphysema. *J Appl Physiol*. 2013;114(6):707-15.

46. Mugler JP, Altes TA. Hyperpolarized ^{129}Xe MRI of the human lung. *Journal of Magnetic Resonance Imaging*. 2013;37(2):313-31.
47. Kaushik SS, Cleveland ZI, Cofer GP, Metz G, Beaver D, Nouls J, et al. Diffusion-weighted hyperpolarized ^{129}Xe MRI in healthy volunteers and subjects with chronic obstructive pulmonary disease. *Magnetic Resonance in Medicine*. 2011;65(4):1154-65.
48. Svenningsen S, Kirby M, Starr D, Leary D, Wheatley A, Maksym GN, et al. Hyperpolarized (^3He and (^{129}Xe) MRI: differences in asthma before bronchodilation. *J Magn Reson Imaging*. 2013;38(6):1521-30.
49. Aziz ZA, Wells AU, Desai SR, Ellis SM, Walker AE, MacDonald S, et al. Functional impairment in emphysema: contribution of airway abnormalities and distribution of parenchymal disease. *American Journal of Roentgenology*. 2005;185(6):1509-15.
50. Rambod M, Porszasz J, Make BJ, Crapo JD, Casaburi R. Six-minute walk distance predictors, including CT scan measures, in the COPDGene cohort. *CHEST Journal*. 2012;141(4):867-75.
51. Quanjer PH, Stanojevic S, Cole TJ, Baur X, Hall GL, Culver BH, et al. Multi-ethnic reference values for spirometry for the 3–95-yr age range: the global lung function 2012 equations. *European Respiratory Journal*. 2012;40(6):1324-43.

CHAPTER 5

5 Conclusions and Future Directions

This last chapter will provide a summary of the research findings in Chapters 2 – 4 and address important research questions that remain unanswered. I will also discuss limitations to the research work presented throughout the thesis and outline future directions that have been motivated by the work presented in Chapters 2 – 4.

5.1 Overview and Research Questions

COPD is the only one of the leading causes of morbidity and mortality that has a steadily increasing mortality rate (1). This increasing mortality rate is suspected to be attributable to poor performance of conventional pulmonary function tests to: 1) characterize early or subclinical lung disease, 2) to identify susceptible individuals and 3) to diagnose individuals in the mild stages. It has become clear over the last few decades that spirometry alone is unable to fully characterize the extreme heterogeneity of the disease (2, 3). In this regard, advances in pulmonary imaging with CT and MRI have become more sophisticated, now able to provide whole-lung and regional quantitative measures of emphysema and airways disease in vivo. The major goal of this thesis was to exploit regional and direct measurements of pulmonary ventilation from hyperpolarized ^3He MRI to tease out clinically relevant pre- and subclinical lung disease phenotypes in ex-smokers with and without airflow limitation. The specific research questions addressed here were: 1) is there a mechanistic link between pre- or subclinical airflow limitation and vascular disease (**Chapter 2**)? 2) What is the underlying, pathophysiological phenotype of disease causing ^3He ventilation abnormalities in ex-smokers without airflow limitation (**Chapter 3**)? 3) Can the apical-to-basal distribution of MRI ventilation abnormalities and CT emphysema be used to identify clinically relevant COPD phenotypes (**Chapter 4**)? Does the apical – basal phenotype change with COPD progression (**Chapter 4**)?

5.2 Summary and Conclusions

In **Chapter 2** we collected carotid three-dimensional ultrasound and hyperpolarized ^3He MRI from ex- and never-smokers without airflow limitation or a diagnosis of

cardiovascular disease to better understand the mechanistic link between pre- or subclinical lung and vascular disease. First, we observed that ex-smokers showed significantly more carotid plaque, indicative of carotid atherosclerosis, and more ^3He ventilation heterogeneity, a sign of subclinical lung disease, compared to never-smokers. Second, carotid ultrasound measurements of plaque, wall thickness and vessel wall volume correlated with ^3He ventilation heterogeneity for all subjects. Together these results suggest that there is a subclinical phenotype in ex-smokers without airflow limitation characterized by mild carotid atherosclerosis and airflow limitation that is not obvious on spirometry.

In **Chapter 3** we aimed to better characterize the underlying pathophysiology of ^3He ventilation defects in ex-smokers without airflow limitation using regional ^3He MRI and CT measurements of emphysema and airways disease. In 60 ex-smokers without airflow limitation, 42 subjects had abnormal ^3He ventilation heterogeneity while 18 had normal ventilation. Those ex-smokers with abnormal ^3He ventilation exhibited worse whole-lung and apical-lung ^3He ADC and we also observed that ventilation defects were spatially related to abnormal airway morphology and microstructural emphysema (ADC) in all subjects. These results suggested that there is a phenotype of ex-smokers with airflow limitation characterized by abnormal ^3He ventilation, abnormal airway morphology and very mild emphysema.

In **Chapter 4** our objectives were: 1) to phenotype COPD ex-smokers based on the apical-to-basal distribution of ^3He ventilation defects and CT emphysema and 2) to evaluate how apical-basal disease phenotypes change with COPD progression. Out of 100 COPD patients, seventy-two reported basal-lung (BL) -predominant MRI ventilation defects and 71 reported apical-lung (AL) -predominant CT emphysema. BL-predominant ventilation defects and AL-predominant emphysema were the major phenotypes in mild-moderate COPD. In severe COPD there was a more uniform distribution for ventilation defects and emphysema. Together these results suggest that with increasing disease severity (worse airflow obstruction) there is a basal-to-apical progression of ventilation abnormalities and an apical-to-basal progression of emphysema.

5.3 Limitations

This section will provide an overview of the major limitations of each study presented in this thesis and how they can be overcome in future work.

5.3.1 Study Specific Limitations

The study in **Chapter 2** was dependent on the collection of carotid three-dimensional ultrasound scans from every subject. The quality of carotid ultrasound scans is highly dependent on; 1) the anatomy of the patient being imaged and 2) having a highly trained technician perform the ultrasound scan (4). In our study, all ultrasound data acquired was sufficient quality for analysis but the scans had to be repeated several times for many individuals. This increased the overall time for ultrasound acquisition and time of each patient visit at our centre. This led us to believe that such a study might not be feasible in large cohorts of subjects, especially in patients with disease who are not as mobile and require careful monitoring even for short study visits. This is an issue because the relatively small sample size in our study may have limited our power to detect clinically meaningful differences in pulmonary function or ultrasound measurements of atherosclerosis. A large-scale cohort study exploiting pulmonary imaging and carotid ultrasound may provide more useful information on the comorbidity between atherosclerosis and airflow limitation, however a challenge would be collecting high-quality ultrasound data in a feasible timeframe. A second limitation to this study was the vessel-wall-volume (VWV) measurement (5) that was used to measure carotid atherosclerosis in the study subjects. We were not surprised that the one-dimensional measurement of carotid intima-media thickness (IMT) was not significantly different between ex- and never-smokers as the dynamic range for this parameter is extremely small which is known to reduce its sensitivity to small changes (6). However, the three-dimensional measurement of total plaque volume (TPV) revealed that ex-smokers had more carotid plaque than never-smokers while VWV, the second three-dimensional measurement, showed no difference between the two subgroups. This was an unexpected result because the VWV is the sum of plaque and carotid wall volume and we observed quantitatively more plaque in the ex-smokers. However, several carotid ultrasound studies (7, 8) have established that the VWV measurement is truly dependent on the

anatomy of the carotid artery and two subjects with a different amount of carotid plaque may have the same vessel-wall-volume. With this in mind, the refined vessel-wall measurement, termed the ‘vessel-wall-plus-plaque thickness’ (VWT) (9) which overcomes the size dependence of vessel wall volume, might provide clinically meaningful three-dimensional ultrasound findings in these ex- and never-smokers.

In **Chapter 3** we endeavored to provide a better understanding of the underlying etiology of ^3He ventilation defects in ex-smokers without airflow limitation using regional MRI and CT measurements. One major limitation to this study was that for regional airway measurements we measured only one individual subsegmental airway that feeds into each lung lobe and not all airways associated with each lobe. We observed significant spatial relationships between ventilation defects in the right lung lobes and subsegmental airway morphology feeding into those lobes but did not observe these significant relationships in the left lung. The lobes of the left lung are larger than those in the right lung (10) and therefore lobar ventilation in the left lung is spread across more airways. By measuring only one subsegmental airway in each lobe we may have potentially missed abnormal airway morphology of other airways in each lobe. Furthermore, the subsegmental airways we measured were 3rd – 6th generation airways which are cartilaginous airways of the conducting zone. We chose to measure these airways in particular because they were consistently measurable in cross-section and clearly visible on thoracic CT for each and every subject, whereas higher generation airways were not always visible and measureable in every subject. Previous work (11) suggested that subsegmental airway morphology measured on CT reflects that of the small airways, however there is also evidence (12) that this may not always be the case. We must also acknowledge that the ability to measure up to a maximum airway generation is an inherent limitation of CT due to the achievable resolution on these scans (13). A second major limitation to this study was that we used a threshold cut off to subdivide ex-smokers into abnormally elevated ventilation defect percent (VDP) and those within the normal range for VDP and therefore our results are dependent on this threshold value. This threshold was based on the upper-limit of normal (95% confidence interval) of VDP in a well characterized group of never-smokers from a previous study (14). We are unsure how our findings would have changed if a different threshold value (ie. 90% confidence interval) was used.

Although it is likely we would have observed slightly different results with a more conservative VDP threshold.

In **Chapter 4** our goal was to phenotype COPD ex-smokers based on the apical-to-basal distribution of ventilation abnormalities and emphysema and to determine if apical-basal phenotype changes with disease progression. We divided subjects into apical- and basal-lung predominant phenotypes based on a method previously described by Gietema (15). In our study phenotypes were defined as follows (where RA_{950} is the relative area with attenuation ≤ -950 HU): RA_{950} in the basal-lung ($RA_{950BL} = RA_{950RLL} + RA_{950LLL}$) and RA_{950} in the apical-lung ($RA_{950AL} = RA_{950RUL} + RA_{950LUL}$) were used to generate the difference between apical- and basal-lung RA_{950} (ΔRA_{950}) where $\Delta RA_{950} = RA_{950AL} - RA_{950BL}$. A positive ΔRA_{950} was indicative of apical-lung-predominant emphysema, and a negative ΔRA_{950} indicated basal-lung-predominant emphysema. Similarly, regional ^3He VDP was used to specify apical-lung- and basal-lung-predominant ^3He ventilation defect phenotypes where the ventilation defect percent in the basal-lung ($VDP_{BL} = VDP_{RLL} + VDP_{LLL}$) was subtracted from the ventilation defect percent in the apical-lung ($VDP_{AL} = VDP_{RUL} + VDP_{LUL}$) to generate the VDP difference between the apical- and basal-lung (ΔVDP). A positive ΔVDP indicated an apical-lung-predominant ventilation defects and a negative ΔVDP indicated basal-lung predominant ventilation defects. Therefore the method we used to phenotype COPD subjects was very specific and it is entirely possible that our findings may have been different if we chose to use a different apical- basal-phenotyping strategy/equation as several others have been described (16-19). At the same time, the binary classification method we used to phenotype subjects might be oversimplistic for characterizing such a heterogeneous and multi-component disease such as COPD. Other strategies that phenotype COPD subjects based on the spatial location of disease using three- or multi-dimensional thresholds may offer more information on how the spatial location of disease impacts lung function. In addition, we did not explore the distribution of ventilation abnormalities and emphysema between the lung core and rind regions to phenotype COPD subjects as previous studies have done (16-18, 20). Phenotyping based on lung core – rind distribution may offer another useful method to identify clinically meaningful COPD subgroups.

5.3.2 General Limitations

The studies present in Chapters 2 – 4 all focus on using ^3He MRI to phenotype ex-smokers. ^3He MRI is an extremely costly research technique and is only used in a handful of research centres worldwide. It requires expensive spin-exchange optical pumping polarization equipment, specialized transmit – receive radiofrequency coils and highly trained physicists and technicians to operate polarization equipment and the MRI scanner. Therefore, just being able to construct and operate a hyperpolarized noble gas research centre alone is a large endeavor (21). At the same time, while we predominantly focused on the use of ^3He noble gas, the global supply of this gas is declining and its price is increasing quickly. Currently, 1 litre of ^3He costs in excess of \$1K. Therefore given the limited supply of ^3He along with the expense and resources required to operate a hyperpolarized noble gas MRI research centre, the transition of this imaging method into clinical setting does not seem likely. Concomitantly, the expense of ^3He MRI ties in with the general limitation common in each study presented in this thesis of small sample sizes. While we believe our results are clinically relevant, we acknowledge that the number of subjects used in each study was much smaller than those in other large-scale lung imaging studies that used CT such as ECLIPSE (22), COPDGene (23) and MESA (24). Future hyperpolarized noble gas studies may benefit from multi-centre trials where more subjects can be recruited for imaging as was previously done in the Polarized Helium to Image the Lung (PHIL) trial (25).

Despite the limitations imposed by the declining levels of ^3He , it is important to note that noble gas MR images of ventilation were first proposed (26) with ^{129}Xe gas which is substantially more abundant and cost effective than ^3He . Furthermore, recent improvements in commercialization of ^{129}Xe polarization equipment and software have made global exploitation of ^{129}Xe MRI a possibility.

Along with general limitations imposed by ^3He MRI in our studies, there may also be inherent limitations in our CT measurements. We aimed to provide an understanding on the structure-function relationships of ^3He ventilation abnormalities and airway and parenchymal disease but it is established that CT is not sensitive to very mild or subclinical changes to the airways and parenchyma (27). First, due to CT resolution

limits, even among the most compliant subjects and highest quality scans, airways can only be counted and measured with confidence up to about the 10th generation (13). And often there will be extreme heterogeneity among the airway generations that can be measured in COPD cohorts making the most commonly reported measurements from the large and central airways of the conducting zone. The highest generation airways we reported were from the 6th generation airways in Chapter 3 and these were ex-smokers with normal spirometry and without severe disease. Therefore the resolution limits imposed by CT may have limited our power to find significant results using these airway measurements, since the airways being measured were more central than the small airways < 2mm which are the origin of airflow limitation in smoking related COPD. At the same time, it has also been shown (27) that CT measurements of emphysema cannot detect small emphysematous lesions, such as those that may occur in early or mild forms of COPD. Therefore another limitation inherent in the studies in Chapters 2 – 4 is related to the ability of CT to measure mild or microstructural emphysema. In this regard, we found that ³He MRI ADC measurements showed much higher sensitivity to early and mild emphysema as these measurements predominantly measure microstructural emphysema.

5.4 Future Directions

5.4.1 Longitudinal Hyperpolarized ³He MRI of Ex-smokers With and Without Airflow Limitation

Longitudinal imaging studies monitoring pulmonary pathophysiology in susceptible groups of ex- and current smokers are essential to improve our understanding of COPD progression and treatment outcomes. The Thoracic Imaging Network of Canada (TINCan) is a three-year follow-up pulmonary imaging study of ³He MRI and CT in ex-smokers with and without airflow limitation (28). Previous research has established that that ³He MRI ventilation measurements are reproducible (29), reflect response to therapy (30) and predict COPD exacerbation episodes (31) and therefore we believe it is valuable to investigate how and if pulmonary MRI ventilation measurements change over time.

Thus far, 82 ex-smokers (33 ex-smokers without airflow limitation, 48 ex-smokers with COPD ($FEV_1/FVC < 70\%$)) have undergone ^3He MRI, inspiratory CT, pulmonary function testing and the six-minute walk test and completed the St. George's Respiratory Questionnaire at baseline and follow-up at approximately three-years. **Figure 5-1** shows ^3He ventilation images at baseline and follow-up and the unventilated lung regions at follow-up for representative subjects (The change in ventilation heterogeneity, or change in ventilation defect percent (ΔVDP) is calculated as $\Delta\text{VDP} = \text{VDP}_{\text{Follow-up}} - \text{VDP}_{\text{Baseline}}$).

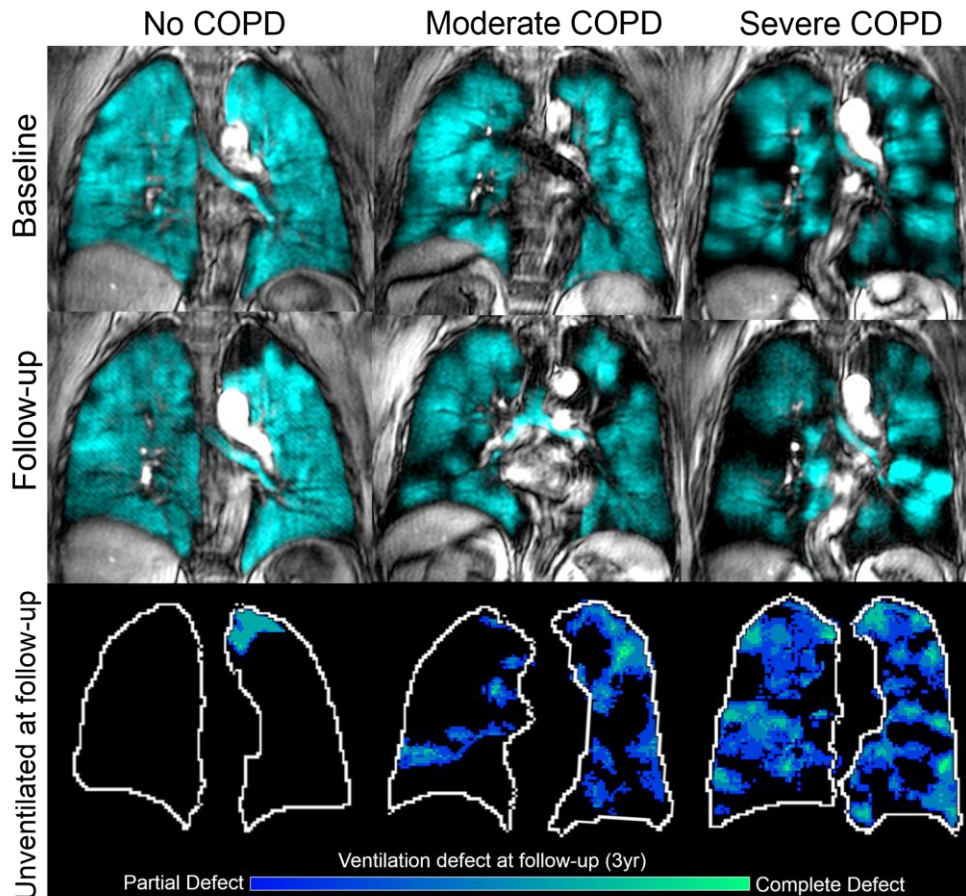


Figure 5-1. ^3He ventilation images in ex-smokers at baseline and follow-up (3yr). Visually and quantitatively ex-smokers with COPD had a greater change and annual rate of change (ROC) in ^3He ventilation over the three-years. S1 is a 65yr male ex-smoker without COPD $\Delta\text{VDP} = +3\%$ (ROC=+1%/yr), S2 is a 76yr male ex-smoker with moderate COPD $\Delta\text{VDP} = +6\%$ (ROC=+2%/yr) and S3 is a 72yr female ex-smoker with severe COPD $\Delta\text{VDP} = +10\%$ (ROC=3%/yr).

This longitudinal pulmonary study will address several compelling questions including:

- 1) *Are there regional and/or whole-lung changes in ^3He ventilation heterogeneity from baseline to follow-up in ex-smokers with and without airflow limitation?*
- 2) *Are there differences in ΔVDP and annual rate of change (ROC) in VDP between ex-smokers with mild, moderate and severe COPD?*
- 3) *How do longitudinal pulmonary imaging measurements compare to longitudinal conventional pulmonary function test and exercise capacity measurements?*
- 4) *How do CT measurements of emphysema and airways disease relate to longitudinal pulmonary MRI measurements?*
- 5) *Do baseline and follow-up MRI measurements predict mortality in ex-smokers with and without airflow limitation?*

5.4.2 Hyperpolarized ^3He MRI Apparent Diffusion Coefficients: A Potential Tool to Evaluate Alpha-1 Antitrypsin Augmentation Therapy

Alpha-1 antitrypsin deficiency (AATD) results in an imbalance of neutrophil elastase and alpha-1 antitrypsin (AAT) causing panlobular emphysema and airflow limitation. AAT augmentation therapy is approved for the treatment of AATD-related lung disease and influences lung function decline in some AATD patients (32). Since ^3He MRI ADC measurements are highly reproducible measurements of alveolar microstructure that are sensitive to emphysematous changes in the lungs, we believe that acquiring longitudinal ^3He MRI ADC measurements in AATD patients might serve as a sensitive and direct method to evaluate disease progression and response to AAT augmentation therapy. **Figure 5-2** shows ^3He ADC maps in three AATD patients and three ex-smokers with centrilobular emphysema at baseline and 3-year follow-up. AATD patients reported elevated ^3He ADC in the basal-lung while COPD ex-smokers reported elevated ADC in the apical-lung. At the same time, AATD patients reported increased whole-lung ADC at 3 year follow-up compared to COPD ex-smokers who reported the same ADC at baseline and follow-up. The AATD subject receiving weekly augmentation therapy had a smaller increase in whole-lung ADC (+0.01 cm^2/s) compared to subjects not receiving

augmentation therapy (S2 and S3, $+0.02 \text{ cm}^2/\text{s}$). Similarly, the basal-lung ADC did not change in the AATD subject on augmentation therapy but increased in both AATD subjects not receiving therapy.

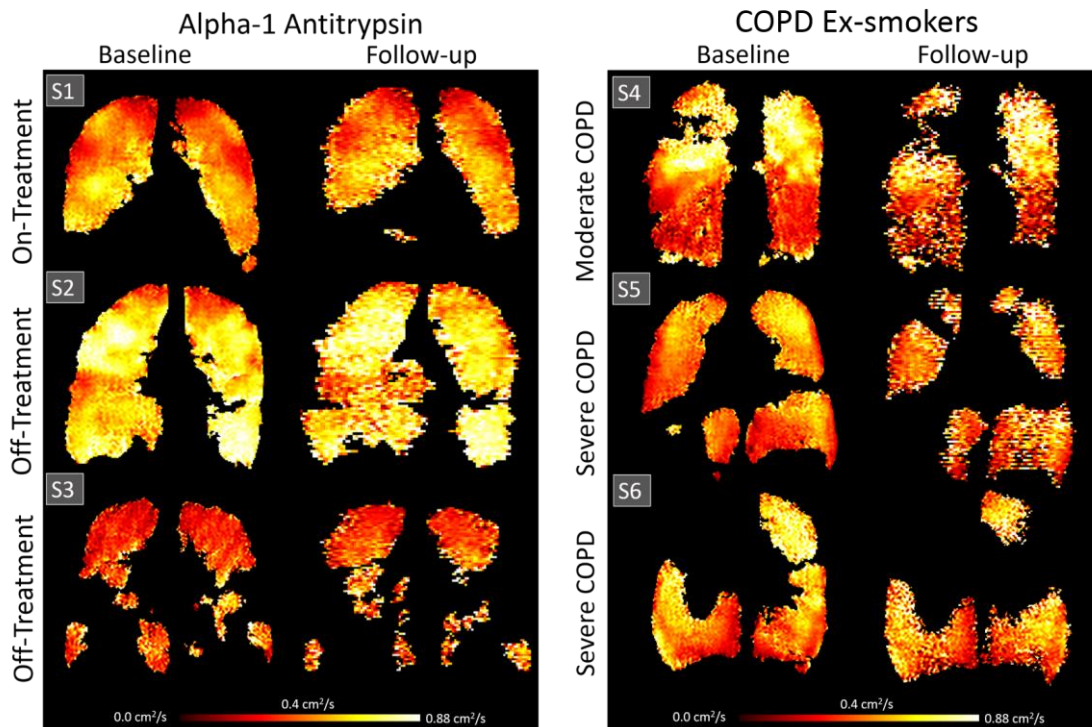


Figure 5-2. ^3He ADC in alpha-1 antitrypsin patients & ex-smokers with emphysema at baseline and three-year follow-up. S1, 66yr male never-smoker undergoing augmentation therapy once/week. S2, 62yr female ex-smoker (44pck yr) and S3, 52yr male never-smoker not receiving augmentation therapy. S4, S5 and S6 are ex-smokers (>20 pack yr) with moderate (GOLD II) and severe (GOLD III) COPD.

Future work on this proof-of-concept longitudinal study of ^3He MRI ADC measurements in AATD will provide answers to the following questions:

- 1) *Do ^3He MRI ADC measurements change regionally and throughout the whole lung in AATD patients over time?*
- 2) *Are changes in ADC measurements different between AATD patients and COPD patients with centrilobular emphysema?*
- 3) *How do ADC measurements change longitudinally in AATD patients receiving augmentation therapy compared to those who are not?*

5.4.3 Second-Order Texture Analysis of Hyperpolarized ^3He MR Images: Beyond the Ventilation Defect

Current image processing methods for evaluating ventilation heterogeneity on ^3He MR images focus on quantifying the volume of ventilation defects throughout the lung as the ventilation defect percent (VDP). Unfortunately, these measurements do not exploit the valuable information inherent in the ventilation signal itself. We and other groups have observed that patients with the same VDP can have different local and regional ventilation patterns as depicted on MRI and different respiratory diseases, suggesting that there are measureable differences in ventilation heterogeneity that are not reflected by the VDP measurement alone. **Figure 5-3** shows an example of this where the ^3He ventilation images from an ex-smoker without COPD, a COPD ex-smoker and an asthmatic subject have the same VDP but each subject has different regions of ventilation heterogeneity and second-order texture measurements of ventilation signal. Therefore we believe that a texture analysis approach of analyzing the ^3He ventilation signal may provide physiologically-relevant information on underlying disease processes.

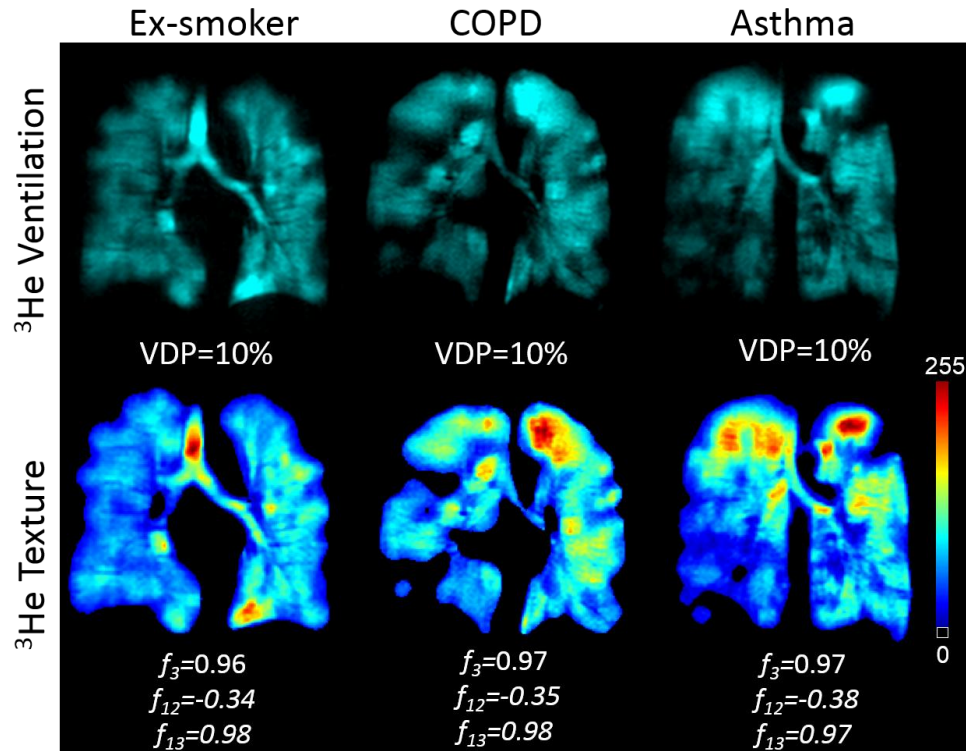


Figure 5-3. ^3He static-ventilation and ^3He texture maps and measurements for a representative ex-smoker without airflow limitation, COPD subject and asthmatic subject.

The Ex-smoker is a 79 year-old female with $\text{FEV}_1=88\%$, $\text{VDP}=10\%$, $f_3=0.96$, $f_{12}=-0.34$ and $f_{13}=0.98$, the COPD subject is a 57 year-old female with $\text{FEV}_1=93\%$, $\text{VDP}=10\%$, $f_3=0.97$, $f_{12}=-0.35$ and $f_{13}=0.98$ and the Asthmatic is a 49 year-old female with $\text{FEV}_1=69\%$, $\text{VDP}=10\%$, $f_3=0.97$, $f_{12}=-0.35$ and $f_{13}=0.97$.

The preliminary work for this research was focused on 1) developing a second-order texture analysis algorithm that measures sixteen ($f_1 - f_{16}$) texture features through statistical evaluation of a grey level co-occurrence matrix (GLCM) (33), 2) using the algorithm to collect texture measurements from ex-smokers without COPD, ex-smokers with COPD and asthmatics with similar VDP and 3) performing statistical analyses on texture measurements to investigate any differences between lung disease phenotypes and testing the sensitivity and specificity of texture measurements for predicting lung disease phenotype. A semi-automated second-order texture analysis algorithm was created in MATLAB and is shown in **Figure 5-4**.

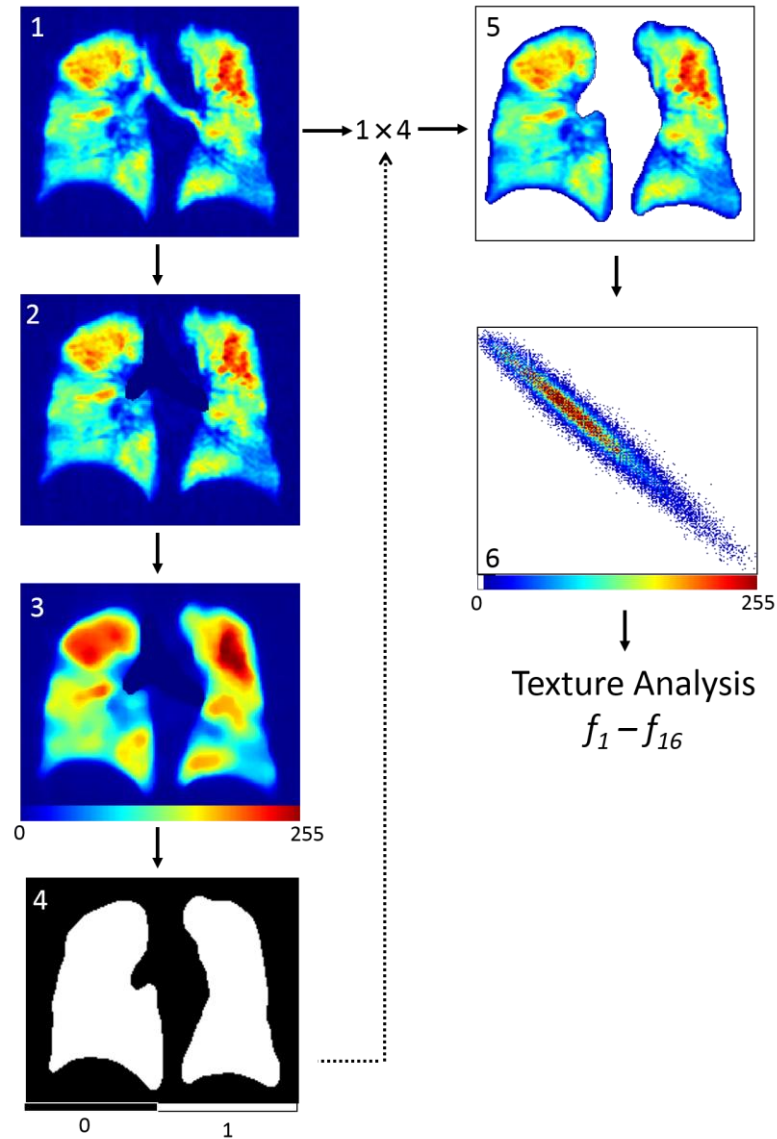


Figure 5-4. Second-order texture analysis algorithm for hyperpolarized ^3He MR images

Texture information was only of interest in the ^3He ventilation signal and not from the regions surrounding it. Therefore we constructed an algorithm that could semi-automatically extract the ^3He ventilation signal without the surrounding signal void and then calculate texture parameters of the signal. 1, is the raw data ^3He static-ventilation MR image coronal centre slice. 2 is the ^3He static-ventilation MR image coronal centre slice with the trachea is removed. 3 is the filtered ^3He image (filtered with a 10×10 median filter) which is used to extract 4, the maximum entropy threshold mask. 4 is then multiplied by 1 to generate 5 which is the ^3He ventilation signal with no surrounding noise. Four gray-level co-occurrence matrices (6, one for each direction of interest; (-1,0), (-1,-1), (0,-1) and (1,-1)) are generated from 5 and are subsequently used to extract the sixteen texture features used in this study (f_1-f_{16}).

The sixteen second-order texture parameters measured by the semi-automated algorithm from are listed in **Table 5-1** (33).

Table 5-1. Second-order texture measurements

f_1 :	Angular Second Moment
f_2 :	Contrast
f_3 :	Correlation
f_4 :	Variance
f_5 :	Homogeneity
f_6 :	Sum Average
f_7 :	Sum Variance
f_8 :	Sum Entropy
f_9 :	Entropy
f_{10} :	Difference Variance
f_{11} :	Difference Entropy
f_{12} :	Information Measures of Correlation 1
f_{13} :	Information Measures of Correlation 2
f_{14} :	Cluster Shade
f_{15} :	Cluster Prominence
f_{16} :	Autocorrelation

Sixty subjects consisting of 20 ex-smokers without COPD, 20 ex-smokers with COPD and 20 asthmatics with VDP < 20% were included in a preliminary analysis which found that f_3 , f_{12} and f_{13} were significantly different on one-way analysis of variance (ANOVA) analysis (**Table 5-2**).

This early work with second-order texture analysis in ^3He MRI provided compelling data and motivated subsequent research from our group using texture analysis in asthmatics.

Table 5-2. Second-order texture measurements for all study subjects

	Ex-smokers (n=20)	Mild COPD (n=20)	Asthma (n=20)	ANOVA p-value*
$f_1 (\times 10^{-4})$	100 (10)	80 (80)	100 (8)	0.70
f_2	70 (62)	63 (44)	63 (48)	0.88
f_3	0.95 (0.01)	0.96 (0.01)	0.96 (0.01)	0.003
f_4	4610 (3420)	5080 (3210)	6350 (4830)	0.36
f_5	0.29 (0.07)	0.29 (0.06)	0.30 (0.07)	0.84
f_6	120 (42)	120 (39)	140 (60)	0.47
$f_7 (\times 10^3)$	17 (13)	19 (12)	23 (19)	0.35
f_8	5 (0.4)	5 (0.4)	5 (0.4)	0.44
f_9	8 (0.7)	8 (0.6)	8 (0.7)	0.76
f_{10}	70 (62)	63 (44)	63 (48)	0.88
f_{11}	2.7 (0.4)	2.7 (0.3)	2.6 (0.4)	0.89
f_{12}	-0.31 (0.03)	-0.34 (0.03)	-0.34 (0.03)	0.009
f_{13}	0.97 (0.01)	0.98 (0.01)	0.98 (0.01)	0.02
$f_{14} (\times 10^3)$	38 (159)	118 (160)	41 (154)	0.21
$f_{15} (\times 10^4)$	3630 (6070)	5080 (5760)	4950 (6180)	0.71
f_{16}	4570 (3390)	5050 (3190)	6310 (4810)	0.35

f_1 : Angular second moment, f_2 : Contrast, f_3 : Correlation, f_4 : Variance, f_5 : Homogeneity, f_6 : Sum Average, f_7 : Sum Variance, f_8 : Sum Entropy, f_9 : Entropy, f_{10} : Difference Variance, f_{11} : Difference Entropy, f_{12} : Information Measures of Correlation 1, f_{13} : Information Measures of Correlation 2, f_{14} : Cluster Shade, f_{15} : Cluster Prominence, f_{16} : Autocorrelation

The Future of Texture Analysis in Pulmonary MRI: Applications in ^{129}Xe and ^{19}F MRI

The theory and data presented in this subsection laid the groundwork for the manuscript titled ‘Second-Order Texture Measurements of ^3He Ventilation MRI: Proof-of-Concept Evaluation of Asthma Bronchodilator Response’ published in Academic Radiology (DOI: 10.1016/j.acra.2015.10.010). The manuscript was co-authored by Nanxi Zha, Damien Pike, Sarah Svenningsen, Dante PI Capaldi, David G McCormack and Grace Parraga.

This manuscript confirmed that texture analysis methods can be applied to ^3He ventilation MR images and used to extract measurements that quantify ventilation heterogeneity and change in response to therapy (34, 35). However, in the future it is likely that pulmonary MRI studies using inhaled gases may transition from the use of ^3He

to ^{129}Xe and fluorinated (^{19}F) gases. Therefore, owing to this previous research that has revealed clinically meaningful results in ^3He , scientists and clinicians should start investigating and implementing texture analysis algorithms (first, second, third and/or higher order) in ^{129}Xe and ^{19}F MR images. Texture analysis algorithms and texture measurements, unlike quantitative measurements of ventilation defects, take advantage of ventilation signal present within the lung. Early work with ^{129}Xe has shown that ventilation defects are larger in ^{129}Xe MR images compared to ^3He MR images (36). This means that ^{129}Xe MR images have less ventilation signal from which to extract texture measurements from compared to ^3He MR images. This may cause the texture measurements to be different between ^{129}Xe to ^3He MR images and importantly, the clinically important change in response to therapy previously observed in ^3He MR images may also change or not be detected using texture measurements from ^{129}Xe or ^{19}F images. Future work using ^{129}Xe and ^{19}F MRI should focus on providing a better understanding of how/if texture measurements show clinically relevant changes in response to therapy in these images analogous to those observed with ^3He MRI. Since most previous work with pulmonary MRI and pulmonary ventilation has focused on ventilation defects (regions of signal void), a deeper understanding of pulmonary ventilation signal present in the lung through texture measurements could provide scientists and clinicians with novel findings related to ventilation heterogeneity and lung disease phenotypes.

5.5 Significance and Impact

Spirometry measurements are continuously used as the gold-standard for assessing pulmonary function and airflow limitation in COPD patients. Although expiratory airflow measurements are globally used as diagnostic criteria for COPD, it is now widely known that these measurements alone do not adequately characterize the heterogeneity of COPD with regards to lung function and structure. In light of this, imaging phenotypes of COPD have emerged as a solution to identify and characterize clinically relevant components of pulmonary structure and function in patients beyond conventional pulmonary function testing. In this thesis we demonstrated that ^3He MRI measurements of pulmonary structure and function provide a way to phenotype ex-smokers without

airflow limitation and COPD patients. In this regard, in ex-smokers with normal spirometry there was ^3He MRI evidence of pulmonary structural and functional abnormalities that were concordant with carotid atherosclerosis and mild microstructural emphysematous destruction or gas trapping. In COPD patients, ^3He MRI provided a way to identify distinct apical- and basal-lung predominant disease phenotypes and we observed that these phenotypes were different according to disease severity.

Taken together, these results show how hyperpolarized noble gas MRI can be used as a tool to identify and characterize clinically relevant structural and functional changes that occur in COPD. As advances in pulmonary imaging continue, and novel quantitative measurements emerge to evaluate lung disease, the important findings from this thesis will serve as a foundation for knowledge for understanding COPD phenotypes.

5.6 References

1. Organization WH. The Global Burden of Disease: 2004 Update. Switzerland: WHO Press; 2008.
2. Vestbo J, Hurd SS, Agusti AG, Jones PW, Vogelmeier C, Anzueto A, et al. Global strategy for the diagnosis, management, and prevention of chronic obstructive pulmonary disease: GOLD executive summary. *American journal of respiratory and critical care medicine*. 2013;187(4):347-65.
3. Agusti A, Calverley P, Celli B, Coxson HO, Edwards LD, Lomas DA, et al. Characterisation of COPD heterogeneity in the ECLIPSE cohort. *Respir Res*. 2010;11(1):122-36.
4. Buchanan D, Gyacskov I, Ukwatta E, Lindenmaier T, Fenster A, Parraga G, editor *Semi-automated Segmentation of Carotid Artery Plaque Volume from Three-dimensional Ultrasound Imaging Society of Photographic Instrumentation Engineers Proceedings 2012*.
5. Egger M, Spence JD, Fenster A, Parraga G. Validation of 3D ultrasound vessel wall volume: an imaging phenotype of carotid atherosclerosis. *Ultrasound Med Biol*. 2007;33(6):905-14.
6. Spence JD. Measurement of intima-media thickness vs. carotid plaque: uses in patient care, genetic research and evaluation of new therapies. *International Journal of Stroke*. 2006;1(4):216-21.
7. Chiu B, Beletsky V, Spence JD, Parraga G, Fenster A. Analysis of carotid lumen surface morphology using three-dimensional ultrasound imaging. *Physics in medicine and biology*. 2009;54(5):1149.
8. Chiu B, Egger M, Spence DJ, Parraga G, Fenster A. Area-preserving flattening maps of 3D ultrasound carotid arteries images. *Medical image analysis*. 2008;12(6):676-88.
9. Chiu B, Egger M, Spence JD, Parraga G, Fenster A. Quantification of carotid vessel wall and plaque thickness change using 3D ultrasound images. *Medical physics*. 2008;35(8):3691-710.
10. West JB. *Respiratory Physiology: The Essentials (8th Edition)*: Lippincott Williams and Wilkins; 2008.
11. Nakano Y, Wong JC, de Jong PA, Buzatu L, Nagao T, Coxson HO, et al. The prediction of small airway dimensions using computed tomography. *American journal of respiratory and critical care medicine*. 2005;171(2):142-6.
12. McDonough JE, Yuan R, Suzuki M, Seyednejad N, Elliott WM, Sanchez PG, et al. Small-airway obstruction and emphysema in chronic obstructive pulmonary disease. *N Engl J Med*. 2011;365(17):1567-75.

13. Coxson HO, Lam S. Quantitative assessment of the airway wall using computed tomography and optical coherence tomography. *Proc Am Thorac Soc.* 2009;6(5):439-43.
14. Sheikh K, Paulin GA, Svenningsen S, Kirby M, Paterson NA, McCormack DG, et al. Pulmonary ventilation defects in older never-smokers. *J Appl Physiol* (1985). 2014;117(3):297-306.
15. Gietema HA, Zanen P, Schilham A, van Ginneken B, van Klaveren RJ, Prokop M, et al. Distribution of emphysema in heavy smokers: impact on pulmonary function. *Respir Med.* 2010;104(1):76-82.
16. Haraguchi M, Shimura S, Hida W, Shirato K. Pulmonary function and regional distribution of emphysema as determined by high-resolution computed tomography. *Respiration.* 1998;65(2):125-9.
17. Mair G, Miller JJ, McAllister D, Maclay J, Connell M, Murchison JT, et al. Computed tomographic emphysema distribution: relationship to clinical features in a cohort of smokers. *Eur Respir J.* 2009;33(3):536-42.
18. Nakano Y, Sakai H, Muro S, Hirai T, Oku Y, Nishimura K, et al. Comparison of low attenuation areas on computed tomographic scans between inner and outer segments of the lung in patients with chronic obstructive pulmonary disease: incidence and contribution to lung function. *Thorax.* 1999;54(5):384-9.
19. Mohamed Hoesein FA, van Rikxoort E, van Ginneken B, de Jong PA, Prokop M, Lammers JW, et al. Computed tomography-quantified emphysema distribution is associated with lung function decline. *Eur Respir J.* 2012;40(4):844-50.
20. Aziz ZA, Wells AU, Desai SR, Ellis SM, Walker AE, MacDonald S, et al. Functional impairment in emphysema: contribution of airway abnormalities and distribution of parenchymal disease. *American Journal of Roentgenology.* 2005;185(6):1509-15.
21. Kirby M, Parraga G. Pulmonary functional imaging using hyperpolarized noble gas MRI: six years of start-up experience at a single site. *Academic radiology.* 2013;20(11):1344-56.
22. Vestbo J, Anderson W, Coxson HO, Crim C, Dawber F, Edwards L, et al. Evaluation of COPD Longitudinally to Identify Predictive Surrogate End-points (ECLIPSE). *The European respiratory journal.* 2008;31(4):869-73.
23. Regan EA, Hokanson JE, Murphy JR, Make B, Lynch DA, Beaty TH, et al. Genetic epidemiology of COPD (COPDGene) study design. *COPD.* 2010;7(1):32-43.
24. Smith BM, Austin JH, Newell JD, Jr., D'Souza BM, Rozenshtein A, Hoffman EA, et al. Pulmonary emphysema subtypes on computed tomography: the MESA COPD study. *Am J Med.* 2014;127(1):94 e7-23.

25. van Beek EJ, Dahmen AM, Stavngaard T, Gast KK, Heussel CP, Krummenauer F, et al. Hyperpolarised ³He MRI versus HRCT in COPD and normal volunteers: PHIL trial. *The European respiratory journal*. 2009;34(6):1311-21.
26. Albert MS, Cates GD, Driehuys B, Happer W, Saam B, Springer CS, Jr., et al. Biological magnetic resonance imaging using laser-polarized ¹²⁹Xe. *Nature*. 1994;370(6486):199-201.
27. Miller RR, Muller NL, Vedal S, Morrison NJ, Staples CA. Limitations of computed tomography in the assessment of emphysema. *Am Rev Respir Dis*. 1989;139(4):980-3.
28. Kirby M, Pike D, McCormack DG, Lam S, Sin DD, Coxson HO, et al. Longitudinal Computed Tomography and Magnetic Resonance Imaging of COPD: Thoracic Imaging Network of Canada (TINCan) Study Objectives. *Chronic Obstructive Pulmonary Diseases: Journal of the COPD Foundation*.1(2):200-11.
29. Mathew L, Evans A, Ouriadov A, Etemad-Rezai R, Fogel R, Santyr G, et al. Hyperpolarized ³He magnetic resonance imaging of chronic obstructive pulmonary disease: reproducibility at 3.0 tesla. *Acad Radiol*. 2008;15(10):1298-311.
30. Kirby M, Mathew L, Heydarian M, Etemad-Rezai R, McCormack DG, Parraga G. Chronic obstructive pulmonary disease: quantification of bronchodilator effects by using hyperpolarized (³)He MR imaging. *Radiology*. 2011;261(1):283-92. Epub 2011/08/05.
31. Kirby M, Pike D, Coxson HO, McCormack DG, Parraga G. Hyperpolarized ³He Ventilation Defects Used to Predict Pulmonary Exacerbations in Mild to Moderate Chronic Obstructive Pulmonary Disease. *Radiology*. 2014:140161.
32. Seersholm N, Wencker M, Banik N, Viskum K, Dirksen A, Kok-Jensen A, et al. Does alpha1-antitrypsin augmentation therapy slow the annual decline in FEV1 in patients with severe hereditary alpha1-antitrypsin deficiency? Wissenschaftliche Arbeitsgemeinschaft zur Therapie von Lungenerkrankungen (WATL) alpha1-AT study group. *European Respiratory Journal*. 1997;10(10):2260-3.
33. Haralick RM, Shanmugam K, Dinstein IH. Textural Features for Image Classification. *Systems, Man and Cybernetics, IEEE Transactions on*. 1973;SMC-3(6):610-21.
34. Risse F, Pesic J, Young S, Olsson LE. A texture analysis approach to quantify ventilation changes in hyperpolarised ³He MRI of the rat lung in an asthma model. *NMR in Biomedicine*. 2012;25(1):131-41.
35. Zha N, Pike D, Svenningsen S, Capaldi DPI, McCormack DG, Parraga G. Second-order Texture Measurements of ³He Ventilation MRI. *Academic Radiology*.23(2):176-85.
36. Kirby M, Svenningsen S, Kanhere N, Owrangi A, Wheatley A, Coxson HO, et al. Pulmonary ventilation visualized using hyperpolarized helium-3 and xenon-129 magnetic

resonance imaging: differences in COPD and relationship to emphysema. *J Appl Physiol.* 2013;114(6):707-15.

APPENDIX

APPENDIX A – Imaging Evidence of the Relationship Between Carotid Atherosclerosis and Chronic Obstructive Pulmonary Disease

As the focus of this thesis is on pulmonary imaging phenotypes of COPD, and given that the study in Chapter 1 provides an overview and understanding on the relationships between MR imaging measurements of airflow limitation and 3DUS measurements of carotid atherosclerosis, In Appendix A we have provided the review article titled 'Imaging Evidence of the Relationship between Atherosclerosis and Chronic Obstructive Pulmonary Disease' which is published in Imaging in Medicine (DOI: 10.2217/iim.13.70, 2013). Permission to reproduce the chosen section(s) of this article was granted by Future Medicine® and is provided in Appendix D.

D Pike, TJ Lindenmaier, DD Sin and G Parraga. Imaging Evidence of the Relationship between Atherosclerosis and Chronic Obstructive Pulmonary Disease. Imaging in Medicine; DOI: 10.2217/iim.13.70, 2013

REVIEW ARTICLE:

Imaging Evidence of the Relationship between Atherosclerosis and Chronic Obstructive Pulmonary Disease

D Pike, TJ Lindenmaier, DD Sin and G Parraga

ABSTRACT

Tobacco smoking is a risk factor for both pulmonary disease and atherosclerosis and a number of studies have provided experimental and epidemiological evidence about the potential links between chronic obstructive pulmonary disease (COPD) and atherosclerosis that is not explained by tobacco smoking alone. While this evidence is very compelling, the direct mechanisms that potentially accelerate atherosclerosis development in patients with COPD have not been established. At the same time, major

advances in quantitative pulmonary and vascular non-invasive imaging tools have advanced the development and validation of surrogate or intermediate endpoints of these chronic disorders. This article provides a review of emerging and established imaging methods that have the potential to quantify pulmonary disease and atherosclerosis non-invasively and robustly, in the same patients over time; we summarize studies that endeavored to evaluate lung structure-function and atherosclerosis in order to provide novel insights on disease pathogenesis and progression.

INTRODUCTION AND OVERVIEW: *Is there a relationship between chronic lung and vascular disease that is not explained by smoking history?*

There is increasing evidence that chronic obstructive pulmonary disease (COPD) and atherosclerosis may be directly and mechanistically related beyond shared risk factors of cigarette smoking and exposure to environmental pollutants. Large scale investigations such as the Lung Health Study (1), the Multi-ethnic Study of Atherosclerosis (MESA) Lung Study (2) and the Atherosclerosis Risk in Communities (ARIC) study (3), along with population based studies on COPD mortality and morbidity (4-6) have established that impaired lung function is a risk factor for vascular disease, independent of cigarette smoking. While atherosclerosis and chronic pulmonary disease share common risk factors such as cigarette smoke, air pollution, biomass exposure, poor nutrition and in much of the developed world, low socio-economic status (7), the relationship between COPD and atherosclerosis-related morbidities such as ischemic heart disease and stroke extend beyond these shared risk factors. However, the exact mechanisms underlying this relationship are not well understood (8).

As shown in Figure 1, recently, van Eeden and others have proposed the “lung permeability” theory as an important mechanism behind the relationship between COPD and atherosclerosis (8). These authors and others suggest that inhalation of the environmental irritant (e.g. cigarette smoke, air pollution particles, respiratory viral or bacterial microbes) is the inciting event. In response, the host mounts a robust inflammatory reaction to control and eliminate these environmental irritants, preventing

the direct translocation of toxic chemicals, respiratory pathogens and air pollution particles into the systemic circulation and enabling the host defenses to remove these unwanted visitors. To promote this process, airway epithelial cells, alveolar macrophages and various circulating hematopoietic cells (eg. neutrophils) synthesize cytokines, chemokines and reactive oxygen and nitrogen species in the lungs. Because the lungs are highly vascularized, it is possible although not proven, that during periods of inflammatory and oxidant stress, the alveolar-capillary interface may become highly permeable and allow inflammatory mediators to migrate into the systemic circulation. Some of these inflammatory mediators (e.g. interleukin-6 (IL-6) and interleukin 1-beta) can coax the liver to increase production of secondary mediators of inflammation such as C-reactive protein, fibrinogen, serum amyloid protein and pro-coagulant factors, and the bone marrow to increase the synthesis and release of leukocytes into the systemic circulation, causing an amplification of the inflammatory signal. With chronic lung insult (as in the case of cigarette smoking or living in highly polluted areas), the alveolar-capillary interface may “re-model” and become persistently “leaky”, leading to a state of chronic (low-grade) systemic inflammation even after the environmental exposure is removed (as in the case of smoking cessation). The constantly elevated level of inflammatory markers may contribute to the genesis and progression of atherosclerosis. However recent work in this area (9, 10) has shown that systemic inflammation is not the only factor contributing to atherogenesis in COPD. In fact, systemic inflammation is common to several COPD comorbidities (9) and it was recently shown that COPD patients with cardiovascular disease differ only in levels of IL-6 (10). This suggests there must be other drivers of cardiovascular disease in COPD. Potential mediators such as nutrition, inactivity, genetic factors or medication may promote vascular dysfunction in COPD patients.

To date, the large majority of studies evaluating links between pulmonary and vascular disease have focused on pulmonary function tests to assess lung function and mainly carotid atherosclerosis intermediate endpoints such as intima media thickness. One major limitation of “global” pulmonary function tests is that they provide no anatomical or regional information of the lungs (11). This limitation has been surmounted by the advent of non-invasive pulmonary imaging techniques that can directly quantify

pulmonary structure-function correlates and enable accurate phenotyping of disease (12-14).

The risk of atherosclerosis can be monitored with or without vascular imaging techniques. Commonly, blood level measurements of lipids such as low density lipoprotein (LDL), high density lipoprotein (HDL) and triglycerides and less frequently, inflammatory mediators such as C-reactive protein and myeloperoxidase are used to provide surrogate measures of lipid profile and systemic inflammation which may play a role in atherogenesis. In addition to blood sampling, the ankle brachial index (ABI) -the ratio of the systolic pressure of the ankle to the arm, is also widely used as another “non-imaging” surrogate measure of atherosclerosis (15, 16). Although these non-imaging methods have been used in pulmonary-vascular disease studies, they are limited in the fact that they provide measurements of “generalized” atherosclerosis or vascular disease (15). From a direct imaging perspective, carotid ultrasound (US) measurements have emerged as reliable tools for evaluating atherosclerosis burden because they correlate well with future cardiovascular events (17, 18) and importantly, the method is relatively rapid, inexpensive and uncomplicated to acquire and quantify. Although there is still some controversy as to which ultrasound measurement best estimates risk of outcomes such as stroke (19), there is no disagreement that extensive development of non-invasive imaging methods to directly quantify atherosclerosis (20-24) has stimulated the development of improved medical treatment options and improved outcomes (25).

As several excellent reviews are available on chronic respiratory disease (26) and cardiovascular risk (7, 27-29), and owing to the limited use of angiography (30-33) and intravascular ultrasound (IVUS) (34, 35) for research purposes outside of coronary artery disease, here we focus on emerging pulmonary and atherosclerosis imaging techniques. There are few studies published that use imaging to interrogate pulmonary and vascular disease in the same patients. As summarized in Table 1, a number of key studies have primarily used imaging to investigate the relationship between carotid atherosclerosis and pulmonary function in COPD. Collectively, these studies provide a strong foundation for future studies that may incorporate novel imaging methods of both pulmonary and vascular disease in smokers and ex-smokers.

Table 1. Summary of studies investigating lung and heart disease using imaging

Reference	Sample (n)	age yrs	Sex M/F	Location	Cardiovascular measurements	Pulmonary measurements	Study Results
Ebrahim [55]	800	56-77	53/47	Britain	-Carotid US	- FEV ₁	-Cross-sectional association with FEV ₁ and IMT
Engström [117]	207	55	100/0	Sweden	-Calf plethysmography -ABI, Doppler US	- FEV ₁ , VC	- lower FEV ₁ and VC in men with atherosclerosis
Zureik [116]	656	59-71	38/62	France	-Carotid US	-PEF	-Subjects within lowest quintile of PEF > IMT
van den Hout [114]	19	21-73	79/21	Netherlands	-Real time MRI flow	-Breathing maneuvers	-Decreased stroke volume in COPD
Schroeder [3]	14480	45-64	43/57	ARIC (USA)	-ABI	- FEV ₁ , FVC, FEV ₁ /FVC	-Decreased FEV ₁ associated with <ABI and >IMT
Iwamoto [105]	305	45-60	100/0	Japan	-Carotid US	- FEV ₁ , FVC, FEV ₁ /FVC	-IMT and plaque highest in smokers with COPD - negative correlation between FEV ₁ and IMT
van Gestel [107]	585	69	78/22	Netherlands	-Carotid US	-COPD based on GOLD	-IMT associated with COPD severity -Increased IMT associated with increased risk of total mortality in COPD patients
Draaisfield [124]	240	55-74	154/86	NLST (USA)	-CT aortic calcification	-CT percent emphysema	-COPD subjects had greater aortic calcification -Aortic calcification correlated with percent emphysema
Kim [106]	116	60	98/2	Korea	-Carotid US	- FEV ₁ , FVC and FEV ₁ /FVC	-IMT higher in COPD subjects -MT negatively correlated with FEV ₁ , FVC and FEV ₁ /FVC
McAllister [113]	1312	45-84	52/48	MESA (USA)	-CT coronary calcification -MRI aortic distensibility	- FEV ₁ , FVC and FEV ₁ /FVC -CT percent emphysema	-Lower FEV ₁ and FEV ₁ /FVC associated with aortic calcification
Matsuoka [112]	51	47-82	57/43	LTRC (USA)	-CT aortic calcification	-CT of pulmonary vessels, LAA - FEV ₁ , FVC, FEV ₁ /FVC, DL _{CO}	-Aortic calcification related to %CSA<5mm ² but not with LAA or FEV ₁
Franz [118]	448	46-78	41/59	Sweden	-Carotid US	- FEV ₁ , FVC, FEV ₁ /FVC - TLC, RV, DL _{CO}	-More subjects with a COPD diagnosis had plaques -FEV ₁ , VC and DL _{CO} lower and RV higher in subjects with ICA plaques
Barr [2]	3642	45-84	49/51	MESA (USA)	-Carotid US -ABI -CT coronary calcification	- FEV ₁ , FVC, FEV ₁ /FVC -CT for LAA	-FEV ₁ , FVC and FEV ₁ /FVC associated with ABI -Upper-lobe emphysema associated with ABI and IMT
Lahousse [57]	1173	55	43/57	Rotterdam (Netherlands)	-Carotid US, MRI	- FEV ₁ , FVC, FEV ₁ /FVC -COPD based on GOLD	-Carotid wall thickening higher in subjects with COPD -Carotid artery plaques with a lipid core more prevalent in COPD
Rasmussen [111]	1535	57-65	55/45	Danish LCST (Denmark)	-CT coronary calcification	- FEV ₁ , FVC, FEV ₁ /FVC	-Correlation between coronary artery calcification and FEV ₁ -COPD severity related to calcification risk score
Chae [123]	134	52	87/14	Korea	-CT coronary calcification	-CT percent emphysema - FEV ₁ , FVC, FEV ₁ /FVC, DL _{CO}	-Correlation between coronary artery calcification and FEV ₁ -COPD severity related to calcification risk score

ARIC: Atherosclerosis Risk in Communities Study, NLST: National Lung Screening Trial, MESA: Multi-Ethnic Study of Atherosclerosis, LTRC: Lung Tissue Research Consortium, LCST: Danish Lung Cancer Screening Trial IMT: Intima media thickness, CT: Computed tomography, MRI: Magnetic Resonance imaging, US: Ultrasound, ABI: Ankle-brachial index, FEV₁: Forced expiratory volume in one second, FVC: Forced vital capacity, DL_{CO}: Diffusing capacity of the lung for carbon monoxide, PEF: Peak expiratory flow, GOLD: Global initiative for Chronic Obstructive Lung Disease, PA: Pulmonary artery, A: Aorta, LAA: Low attenuation area, CSA: Cross sectional area

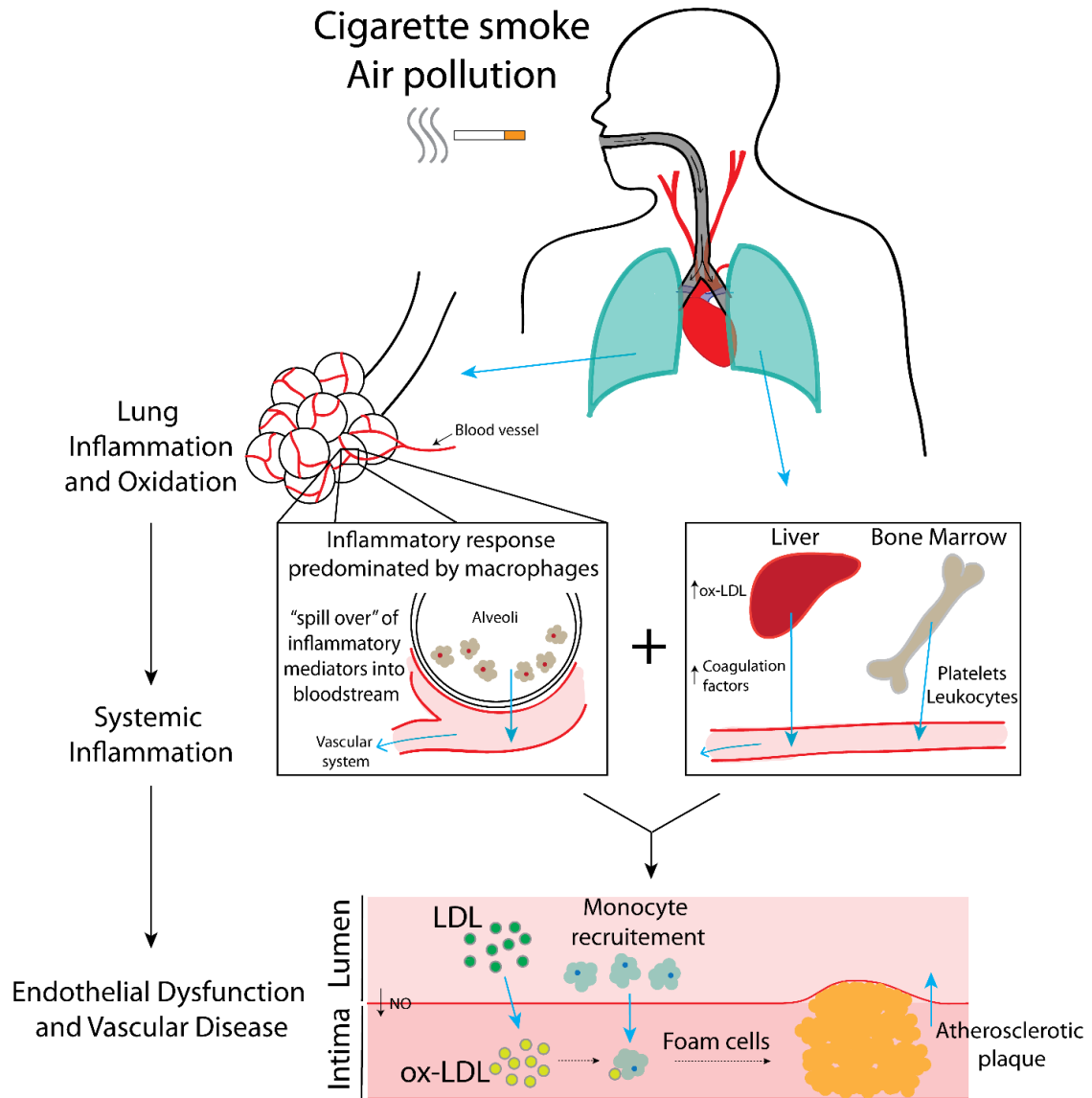


Figure 1: Schematic for proposed mechanism explaining atherosclerosis burden in patients with chronic lung disease related to smoking or environmental toxins.

Chronic exposure to toxins, mainly cigarette smoke and/or air pollution triggers an inflammatory response within the lung airspaces that is dominated by alveolar macrophages. The inflammatory markers within the alveoli spill [8] into the vascular system where they stimulate the liver and bone marrow to release various inflammatory and coagulation mediators such as; C-reactive protein (CRP), fibrinogen, platelets and leukocytes. The systemic inflammatory response that follows promotes atherogenesis in combination with high levels of circulating cholesterol, coagulation factors and inflammatory mediators.

IMAGING ATHEROSCLEROSIS:

Carotid Arteries

Carotid atherosclerosis is the main cause of transient ischemic attack and ischemic stroke, and is believed to be closely linked to atherosclerosis in the coronary and peripheral vascular beds that cause myocardial infarction, and leg claudication, respectively (36). As shown in Figure 1 and in more detail in Figure 2, the carotid artery bifurcates within the neck and in most subjects, this allows for direct and non-invasive imaging through the neck tissues using ultrasound methods. In the longitudinal or transverse view, atherosclerotic plaque is typically observed near the bifurcation and in the internal carotid artery and in the axial view, wall thickening and lumen stenosis can be visualized.

Several imaging techniques have evolved to better understand the morphology of atherosclerosis and monitor its progression over time. B-mode carotid ultrasound is a non-invasive, relatively inexpensive imaging technique that provides direct morphological measurements at the site of future cardiovascular events (18, 37). Doppler ultrasound is commonly used for evaluating carotid stenosis (38). For research purposes, three-dimensional US (3DUS) and carotid magnetic resonance imaging (MRI) are unique among carotid imaging methods in their ability to readily distinguish between different atherosclerotic tissue components and plaque. This provides a way to potentially assess carotid plaque vulnerability (20). Distinct from carotid atherosclerosis imaging, imaging the heart using thoracic computed tomography (CT) for the detection and quantification of coronary artery calcifications has also emerged as a means to non-invasively evaluate atherosclerosis risk (33).

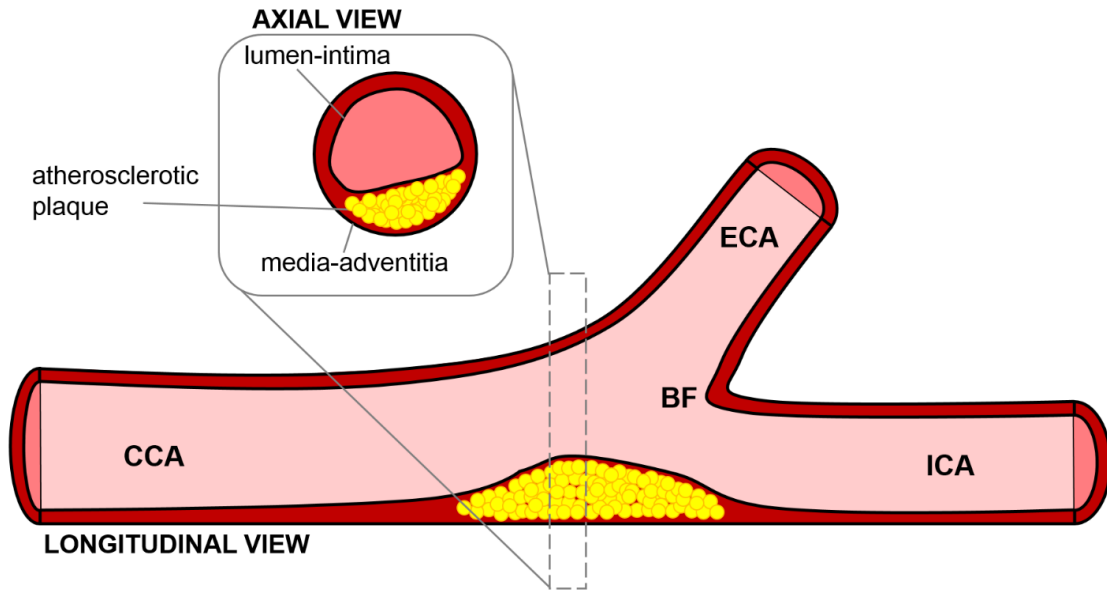


Figure 2: Schematic for Carotid Artery Atherosclerosis.

Axial or Cross-sectional view: The common carotid artery (CCA) is shown with atherosclerotic plaque in yellow under a thin fibrous cap within the intima layer and modest lumen narrowing or arterial stenosis.

Longitudinal or Transverse view: The CCA bifurcates approximately at the jaw line into the internal carotid artery (ICA) and the external carotid artery (ECA), at the bifurcation (BF) point. The lumen-intima, and media-adventitia boundaries and calcified atherosclerotic plaque are readily visible in both the axial and longitudinal views of the artery.

B-mode ultrasound

Brightness-mode (B-mode) ultrasound (US) is typically used to image carotid arteries for atherosclerotic burden principally because it is non-invasive, it is relatively inexpensive and it is widely available in most clinical facilities. To obtain a two-dimensional (2D) grey-scale image, high frequency ultrasound pulses are transmitted to internal tissues and their reflections (which themselves are dependent on the different acoustic impedances of the tissues) are converted to different pixel intensities (39, 40). A good example of this is provided in Figure 3 and shows the IMT measurement that is now recognized as robust and reliable for evaluating atherosclerotic burden (41). It provides a 1D measurement of

the mean distance between the lumen-intima and media-adventitia boundaries of the common carotid artery (CCA) (40). To standardize IMT measurements, guidelines were established by the Mannheim Intima-Media Thickness Consensus (42, 43). The 2D ultrasound images used to segment IMT are either generated by navigating a reconstructed 3D volume to visualize the desired plane (44), or by directly acquiring a 2D image using the ultrasound probe (23). Importantly, IMT measurements do not incorporate a measure of carotid plaque, as users are encouraged to perform IMT segmentation only in regions of the CCA that are void of plaque to ensure they capture an accurate representation of the intima-media layer(42, 43).

Doppler ultrasound

Carotid Doppler ultrasound incorporates B-mode and Doppler ultrasound imaging (45). The recorded B-mode 2D image provides structural and anatomical information about the vessel and surrounding tissues, while the Doppler component provides useful information about the blood flow in the vessel (46). This offers a way to determine the velocity of blood in a vessel and provides information regarding the degree of stenosis in the artery (46). Atherosclerotic stenosis and blood flow velocity are directly proportional; therefore arteries with larger plaques present with a greater blood velocity (46). Even though carotid disease is still diagnosed using conventional angiography, carotid Doppler US is suggested to be the most accurate non-invasive imaging modality in screening individuals for carotid artery stenosis (38, 46).

Three-dimensional ultrasound

Figure 4 shows a schematic for the methodology of three dimensional (3D) ultrasound (US) volume acquisition. These scans differ slightly from 2D acquisition because the US probe is translated along the neck of the individual. This “linear translation” (21) along the neck acquires a series of 2D images that are co-registered spatially into a 3D volume (40). As shown in Figure 3, several measurements have been developed to date that utilize reconstructed 3DUS volumes in order to monitor atherosclerotic disease progression. These measurements include 2D total plaque area (TPA) measurement, and the 3D total plaque volume (TPV) and vessel wall volume (VWV) measurement (47-50).

The TPA ultrasound measurement provides a 2D measurement that quantifies the area of a plaque along the longitudinal view of the artery. The user is required to outline the plaque as it appears in its largest dimension which can be somewhat subjective. The segmentation can be performed on the US scanner by finding the plane of interest and freezing and magnifying the image (47) and the cursor is used to trace around the selected plaque (47). The reconstructed 3D volume can also be used to isolate the longitudinal view of interest and perform the measurement by tracing the perimeter of the plaque using computer software. Previous research (47, 51) has demonstrated that TPA is associated with serum cholesterol levels, hypertension myocardial infarction, risk of stroke and risk of death.

Three-dimensional TPV and VWV measurements have been developed to monitor atherosclerotic disease progression, while providing useful information about the development of atherosclerotic plaques. The first technical development of TPV (48) used a manual segmentation approach where the volume of the plaque was generated from the area of a series of axial slices. However, more recently, TPV has been generated using a semi-automated approach (52) and this has helped to improve speed and reproducibility of the measurements.

A 3D IMT measurement that includes plaque can be generated from 3DUS – the 3DUS vessel wall volume (VWV) (41). 3DUS VWV provides a circumferential wall thickness measurement, including plaque (41, 53) and can be used to track changes over short time scales (54) and recent research has shown that these measurements correlate well with age and sex (40). Ultrasound imaging measurements have been widely used to understand cardiovascular disease and patient outcomes (47, 55), although it is difficult to distinguish between atherosclerotic plaque components.

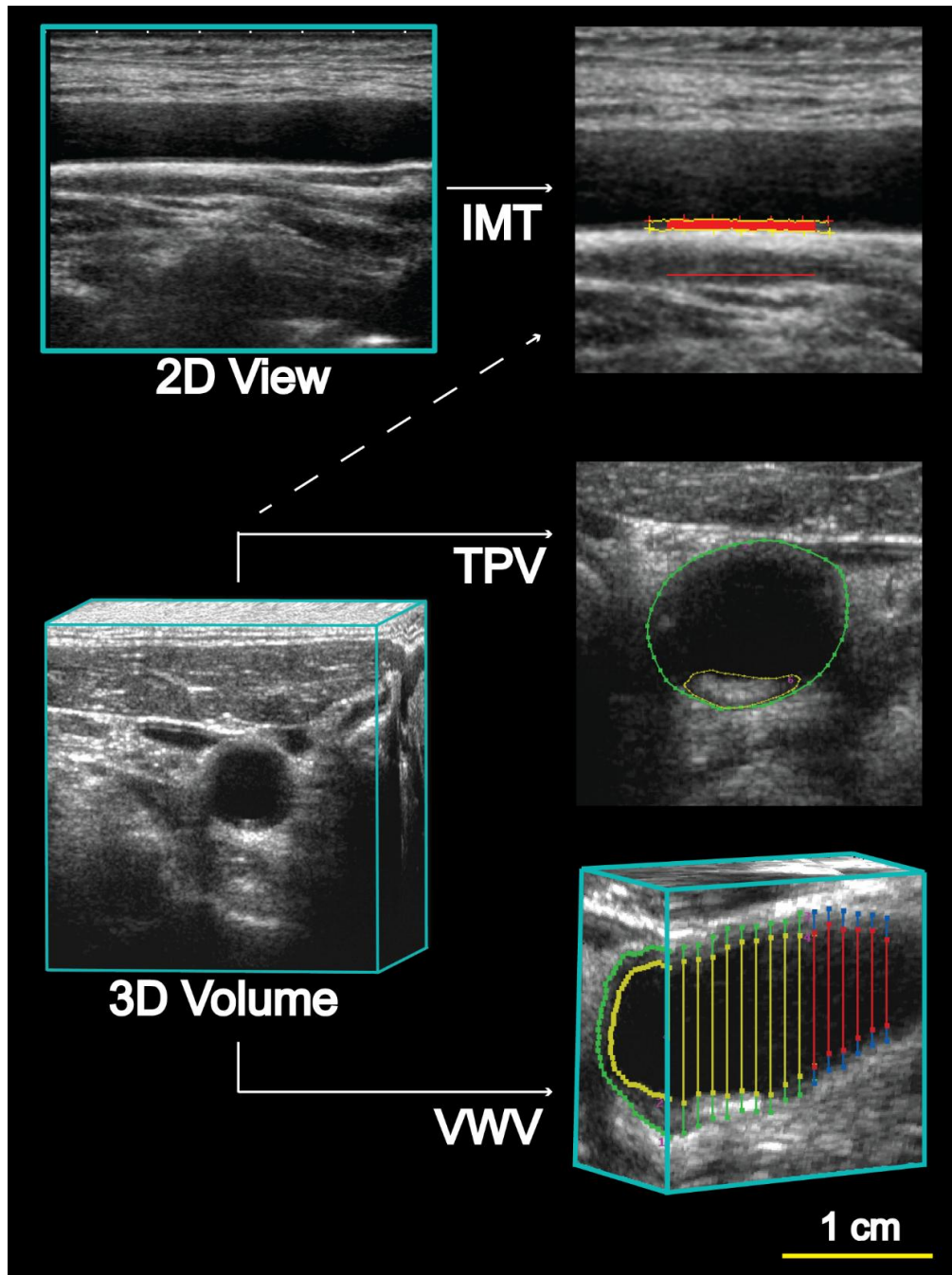


Figure 3: B-mode and 3DUS of the Common Carotid Artery.

Top panel: Conventional B-mode ultrasound common carotid artery image in the transverse plane and the generation of intima-media thickness (IMT) measurement. Bottom panel: 3DUS common carotid artery in the axial or cross-sectional plane with the generation of total plaque volume (TPV), and vessel wall volume (VWV) ultrasound measurements.

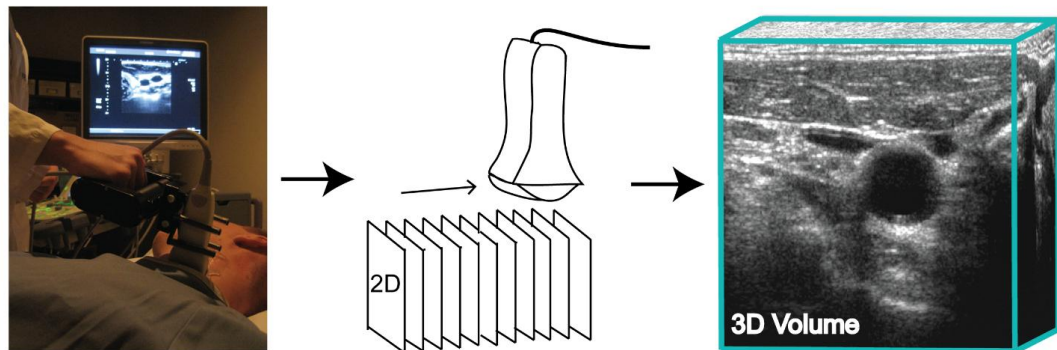


Figure 4: Three-Dimensional Ultrasound Image Acquisition.

Left panel: Typical 3DUS scanning procedure. The subject is supine with head turned to enable access to R or L carotid artery. The mechanical mover shown in the left panel holds the transducer in place and translates it up the neck. Middle panel: Schematic for transducer acquiring a series of two-dimensional images that are co-registered to generate a three-dimensional (3D) volume. Right panel: 3D volume for the common carotid artery in the axial or transverse plane.

Carotid magnetic resonance imaging

Magnetic resonance imaging (MRI) provides a way to distinguish between soft tissues, allowing for the evaluation of plaque composition and potentially, plaque vulnerability to rupture and thrombosis (56). Plaque vulnerability is typically assessed by examining different characteristics such as the fibrous cap, lipid core and localized calcifications in the carotid arteries (20, 57). In particular, the thickness of the fibrous cap is of great interest, since rupturing of this component would expose the necrotic lipid core to the blood flow which is believed to cause thromboembolic events; recent studies (58) have shown that carotid MRI findings correlate with histology and are sensitive in detecting thin and ruptured fibrous layers (59). Other studies (60, 61) have reported the use of a gadolinium-based contrast agent to obtain a higher contrast between atherosclerotic plaque characteristics and have found that the contrast between plaque structures can be enhanced even more.

Thoracic computed tomography

As shown in Figure 5, thoracic CT can be used to reveal and quantify calcifications within the coronary arteries as a surrogate measurement of advanced coronary artery disease and atherosclerosis (33). Such calcified lesions within the arterial wall are much denser than surrounding cardiovascular tissue and are visualized as regions of greater x-ray attenuation on thoracic CT scans. Commonly, a threshold of $\geq 130\text{HU}$ is used to identify calcified lesions on thoracic CT based on the scoring method previously described by Agatston (62). This approach has been the most widely-used quantification method for coronary calcifications and studies have shown that Agatston scores correlate with future cardiovascular events (63, 64). The use of coronary artery calcifications has not been widely-used however to evaluate the relationship between vascular and pulmonary disease.

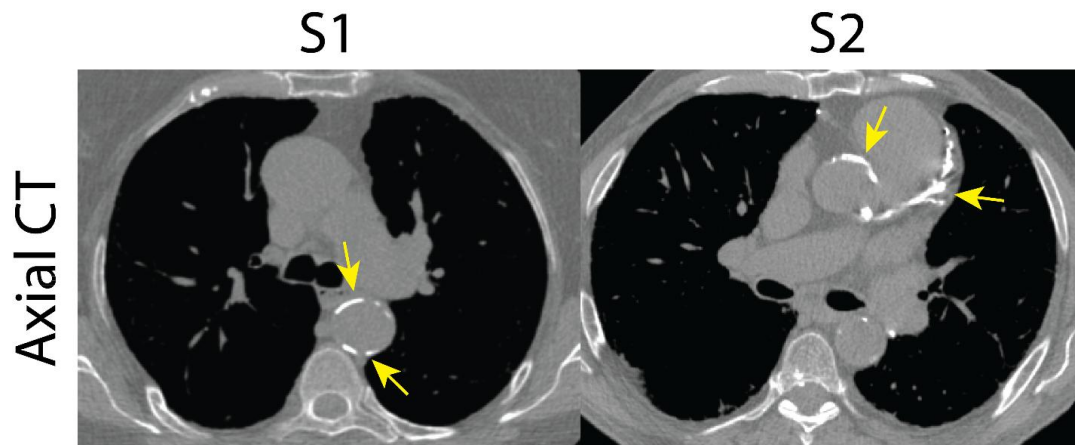


Figure 5: Axial CT view of Chronic Obstructive Pulmonary Disease Patients with Coronary Calcifications.

Yellow arrows point to coronary calcifications which are easily visible by increased x-ray attenuation within cardiovascular tissues.

IMAGING CHRONIC OBSTRUCTIVE PULMONARY DISEASE

COPD is characterized by chronic airflow limitation and systemic inflammation and is currently the fourth leading cause of death worldwide, affecting approximately 10% of the population over 40 years of age (65). COPD is a heterogeneous disease comprised of airway inflammation, alveolar destruction (emphysema), mucociliary dysfunction, pulmonary hypertension, and small airway remodeling (11, 66). Traditionally, COPD is diagnosed using the spirometry threshold of the forced expiratory volume in one second (FEV_1) $<70\%$ of the forced vital capacity (FVC). However, it has been suggested that FEV_1 and FVC are relatively insensitive to the pathophysiological changes that occur well before lung function declines (66). Consequently, FEV_1 and FVC alone do not sufficiently characterize lung disease onset, progression or response to treatment, especially early in the disease (67, 68). Moreover, spirometry provides only a global measurement of overall lung disease with no regional structural or functional information to identify the diseased area or the underlying pathology. These drawbacks have provided the major motivation behind the development and optimization of sensitive and non-invasive pulmonary imaging modalities that can locate, characterize and quantify pathophysiological changes that cause lung function decline.

Pulmonary imaging offers several advantages for characterization of COPD: 1) it is sensitive to early structural and functional changes in the lungs (69-73), 2) it allows visualization of the pathophysiological processes contributing to airflow limitation (14, 74), 3) it provides regional information of which anatomical locations of the lung are affected by disease (14, 75), and, 4) patients can potentially be stratified for treatment based on lung disease phenotype identified using pulmonary imaging (74, 76-78).

Thoracic X-ray computed tomography of COPD

The development of quantitative tools to measure airway dimensions and parenchyma structure using high-resolution computed tomography (CT) have made it the pulmonary imaging modality of choice (13, 14, 78, 79). As previously mentioned, pulmonary function tests do not correlate well with morphological changes in the lung (11, 67, 68). CT however, is well suited to distinguish whether lung function decline is attributable to

emphysema or airways disease. Thoracic CT images of pulmonary structure are based on tissue attenuation of x-rays in the lung parenchyma and surrounding vasculature. Therefore, high-resolution images of pulmonary structure can be acquired without the use of contrast agents.

Smoking-related emphysema is characterized by alveolar destruction which leads to increased lung volume, decreased surface area for gas exchange and either localized or uniform emphysematous lesions to the lung parenchyma (66). The emphysematous lesions have markedly reduced density which can be identified by regions of lower x-ray attenuation values in Hounsfield units from the density frequency histogram taken from CT images (78). One approach for quantifying the extent of emphysema has employed a threshold cutoff for voxels with attenuation values below a predetermined Hounsfield unit as emphysematous tissue (78). CT attenuation thresholds have been used to identify emphysema at -910HU (80), -950HU (81), -960HU and -970HU (82). However, -950HU has emerged as the most common cutoff to distinguish between emphysematous and healthy lung tissue (81). Another widely-used method for determining emphysema severity is with a “percentile cutoff” (eg. the lowest 15th percentile) that identified the percent of emphysematous tissue based on the frequency distribution of attenuation values across a group of subjects (78, 82, 83). Both techniques are considered acceptable for cross-sectional COPD studies. However, the Alpha-1 Foundation workshop committee recommended (84) that only the percentile cutoff approach be used for longitudinal studies since technical variations have less influence on these measurements (84). Another technique for quantifying emphysema also incorporated attenuation cutoff values, but used a statistical approach to identify low attenuation clusters (LAC) (85, 86). Briefly, the size of an emphysematous lesion (connected voxels below a certain attenuation value) is plotted against the total number of “clusters” of connected voxels on a log-log plot (cluster size on x axis, number of clusters on y-axis). The slope of this relationship, which follows a power law, represents the size of the emphysematous lesion (87). Typically flatter curves with lower slope values represent larger emphysematous lesions.

Airways disease can be assessed using CT-derived measurements of airways dimensions. Airway remodeling in COPD is prominently caused by inflammation within the airway wall epithelium and mucous plugs in the airway lumen (66). Therefore, CT measurements of airway wall area (WA) and lumen area (LA) are of interest for evaluating the severity of airways disease. The primary limitation of CT airway analysis lies within the limits of x-ray resolution and dose (78). Previous work (88) has established that the major site of airflow limitation in COPD is in airways <2 mm in diameter. These airways, however, are difficult to visualize on CT (89). Many different computational algorithms have been used to measure airways (90-93) however, it remains unknown which algorithm provides the most useful airway data (84). Figure 6 shows representative coronal CT images and CT-derived airway trees and LAC maps for two healthy ($FEV_1/FVC \geq .70$) and two COPD subjects ($FEV_1/FVC < .70$). Compared to the healthy subjects, the COPD patients have larger and greater heterogeneity of attenuation values which are reflected in the large LAC clusters corresponding to these low attenuation regions. These images are a good representation of how CT along with quantification software can be used to evaluate disease severity.

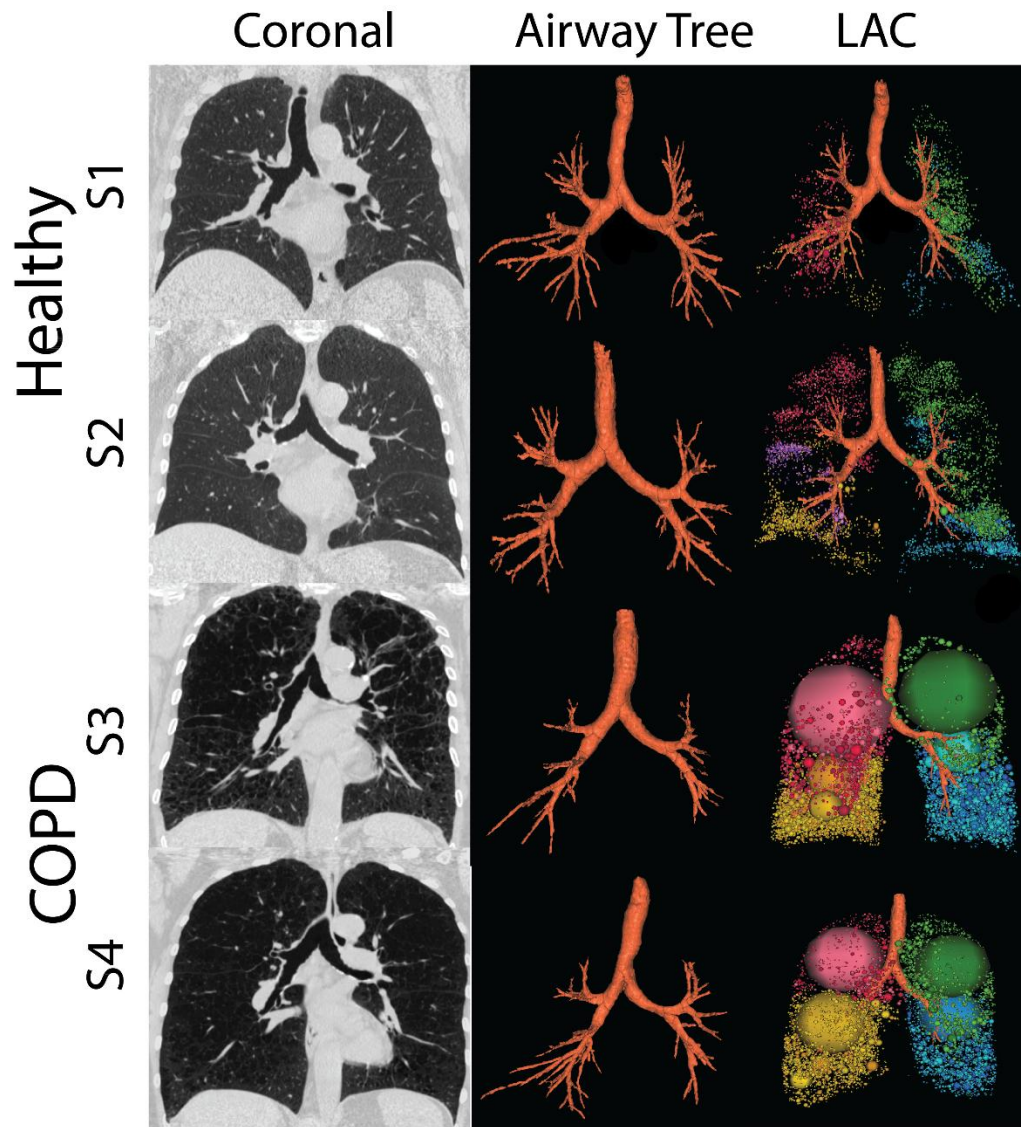


Figure 6: Thoracic x-ray Computed tomography (CT) in Healthy older subjects and patients with Chronic Obstructive Pulmonary Disease.

Left panels: CT coronal and axial centre slice scans Right panels: Corresponding CT-derived volume rendered airway tree next to co-registered airway tree with low attenuation cluster (LAC) map for two healthy subjects (S1 and S2) and two COPD subjects (S3 and S4).

Magnetic Resonance Imaging of COPD

Until recently, pulmonary magnetic resonance imaging (MRI) has been challenging owing to the low proton (^1H) density (and in contrast high air density) within the lungs. Conventional MRI generates signal and tissue contrast based on the perturbation of ^1H which is bound to both water and fat in most tissues of the body. Distinct from other organs, the lungs have very low proton density which results in low contrast and little to no morphological information on pulmonary ^1H MR images (25). This has motivated the development and optimization of MRI techniques that are able to visualize lung structure and function. Namely, hyperpolarized noble gas MRI and ultra-short echo time (UTE) ^1H MRI have emerged as promising methods to non-invasively image the lungs and have been used to study COPD.

Hyperpolarized noble-gas MRI provides a way to visualize lung function by imaging ventilation within the lung. As shown in Figure 7, this breath-hold technique can be performed using hyperpolarized ^3He or ^{129}Xe gases (94) to generate images of ventilation within the lungs. These “static-ventilation” (SV) images provide functional information by visualizing gas distribution, and as shown in Figure 8, ventilation distribution in healthy subjects is homogeneous, with gas filling all regions within the lung (95). In contrast, COPD patients have regions of signal void, or ventilation defects, which represent areas of the lung that do not participate in ventilation (25). To quantify hyperpolarized ^3He and ^{129}Xe MRI data the volume of gas visualized in the images can be normalized to patient’s thoracic cavity volume to generate a ventilation defect volume (VDV) (96), a ventilation defect percent (VDP) (97) and percent ventilation volume (PVV) (71). Although it is likely that ventilation defects represent disease, the exact etiology underlying them is not entirely clear. In COPD, these ventilation abnormalities may be due to airway disease, emphysema or a combination of both diseases. Another possibility is that these areas may be slow filling and are not ventilated during the breath-hold scan. In the future, uncovering the pathophysiology of noble gas ventilation defects in COPD will require the accurate registration of structural CT images with functional MR images, integrating other lung structural modalities such as optical coherence tomography (98) and comparing MRI data with histology (99). Beyond functional

imaging, noble gas MRI can also be used to probe lung microstructure by using diffusion-weighted MRI which can characterize the dimensions of acinar ducts and alveoli, the main structures involved in gas exchange (12, 100, 101). By sensitizing the MRI system to diffusion of the noble gas atoms, apparent diffusion coefficient (ADC) maps can be generated and quantified to assess lung microstructure (100). In COPD, emphysema is associated with acinar duct enlargement and alveolar destruction (66). These larger alveolar spaces in diseased subjects will generate higher ADC values on diffusion-weighted MRI scans compared to small, intact alveoli of a healthy volunteer (75, 99) because the gas atoms have a larger distance per unit time to travel. This is represented in Figure 8 where the ADC maps display brighter colors as COPD/emphysema severity increases, representing an increase in ADC values and larger airspaces in these subjects. A limitation to diffusion-weighted MRI in noble gas imaging of the lungs is related to the ventilation patterns mentioned previously. ADC values can be extracted only for regions of the lung that participate in ventilation, therefore in patients with high VDP the structure of the VDV cannot be probed.

Independent of MRI methods that employ tracer gases to visualize lung structure and function, conventional ^1H MRI using short echo times can be used to visualize pulmonary structure (12). Such methods have been employed to try to reduce air-tissue interface artifacts (102) which are typically abundant on pulmonary MRI, allowing acquisition of images that can provide structural information by differentiating between regions of low and high proton density (103). This has potentially useful applications to COPD because low proton-density regions may represent emphysematous lesions whereas regions of high proton density could represent areas of other diseases or lung injuries such as edema (25, 103).

Imaging Relationships Between Lung Disease and Atherosclerosis

While cardiovascular and respiratory diseases are the first and third leading causes of death in the United States (104), both diseases are typically evaluated as separate conditions. However, the last two decades have seen numerous studies providing imaging evidence that both diseases are related (1, 2, 5, 6, 57, 105-115). These studies,

summarized in Table 1, have established two important clinical findings: 1) COPD patients have an increased burden of atherosclerosis in the form of carotid atherosclerosis and coronary artery plaque, and, 2) the relationship linking lung and heart diseases is complex and involves both structural and functional abnormalities to the lungs and vascular system.

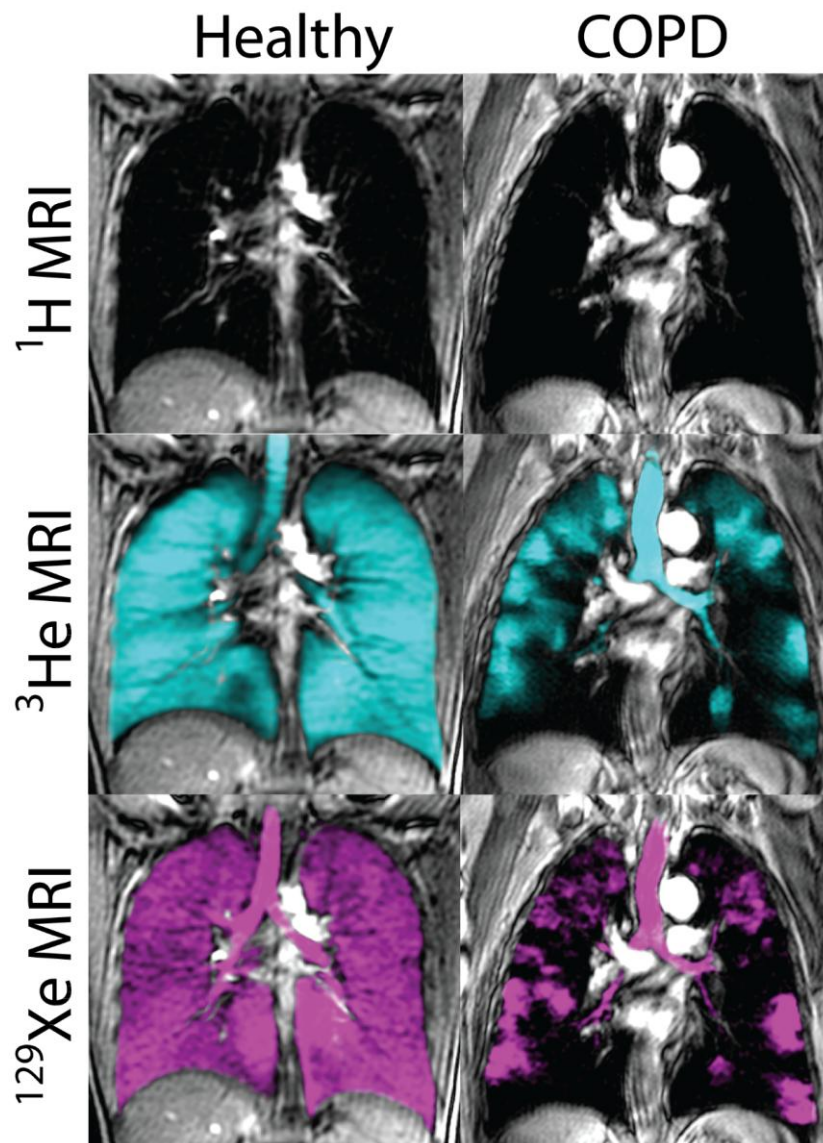


Figure 7: Conventional anatomical ^1H MR and functional ^3He and ^{129}Xe MR images.

Top panel: Anatomical ^1H MRI, and, Bottom panels: corresponding ^3He (aqua-blue) and ^{129}Xe (purple) MRI co-registered to anatomical MRI (grey-scale) for a healthy and COPD subject.

Application of Carotid Ultrasound to Lung and Atherosclerosis Studies

Carotid ultrasound semi-automated measurements of IMT make it well-suited to be used in large-scale studies investigating atherosclerosis and lung disease. Studies using carotid ultrasound to investigate a relationship between atherosclerosis and lung disease started to emerge over a decade ago (55, 116, 117). In one study (55), subjects from the British Regional Heart Study were evaluated and the investigators observed a cross-sectional relationship between carotid IMT and spirometry. Shortly after, a significant association between spirometry and Doppler ultrasound measurements of stenosis in an elderly population of Swedish men was reported (117). Another study (116) used carotid ultrasound to examine carotid IMT and the development of carotid plaques in relation to peak expiratory flow (PEF) in an elderly cohort from France. Consistent with the two other studies, they found that reduced lung function (reduced PEF) was associated with increased atherosclerotic burden through elevated IMT and increased carotid plaque occurrence. Four years later this area of research was revisited (3) in a large cohort recruited from the Atherosclerosis Risk in Communities (ARIC) study. Using carotid ultrasound IMT and the ankle-brachial index (ABI) or the ratio of ankle to arm systolic blood pressure in tandem with spirometry measurements, a cross-sectional association was observed between spirometry and IMT and ABI. This study invited future research on the coincident findings of lung disease and atherosclerosis using a number of imaging techniques. Subsequent work focused on the relationship of carotid ultrasound measurements of atherosclerosis and spirometry measurements of pulmonary function.

Several years later, a study (105) in 305 Japanese volunteers showed that COPD smokers had significantly greater IMT and plaque compared to smokers and non-smokers without airflow limitation. Furthermore it was observed that FEV_1 was independently associated with IMT after adjustment for age, BMI and blood pressure. The finding that IMT was elevated in patients with airflow limitation was replicated two years later (106) in a

Korean study that showed greater IMT in COPD patients compared to non-COPD subjects. This group also observed a significant correlation between IMT and spirometry (FEV_1 , FEV_1/FVC and FVC). There is evidence that this relationship may work in both directions, meaning that cardiovascular disease patients may have equally high risk of developing respiratory diseases as COPD patients are of developing cardiovascular conditions. Another research team obtained pre-operative spirometry and carotid ultrasound measurements in a group of vascular surgery patients undergoing aortic or carotid artery surgeries and classified the patients based on severity of COPD (107). They observed that subjects with spirometry evidence of airflow limitation had significantly greater IMT than non-COPD vascular surgery patients. In the five-year follow-up period nearly 30% of vascular surgery patients died, and after adjusting for confounders, elevated IMT was associated with increased total mortality. This work was in agreement with another investigation that evaluated (118) relationships between carotid plaque, FEV_1 and VC along with total lung capacity (TLC), residual volume (RV) and diffusion capacity of the lung for carbon monoxide (DL_{CO}). The researchers observed that subjects with plaque had statistically significantly lower FEV_1 , VC and DL_{CO} and higher RV but no significant difference in TLC. This was the first study to probe pulmonary measurements beyond spirometry and PEF, and showed that these relationships were complex, with lung structure-function implications (118).

Application of Carotid Magnetic Resonance Imaging to Lung and Atherosclerosis Studies

Few studies have utilized carotid MRI to study lung and heart disease that is coincident in patients. One recent study (57) evaluated a subgroup from the Rotterdam cohort (119) using carotid MRI, carotid ultrasound and pulmonary function tests. The results were consistent with other studies, showing elevated carotid wall thickening in subjects with airflow limitation. However the carotid MRI data added valuable information about carotid plaque characteristics in COPD subjects that had not previously been reported. They showed that: 1) the severity of stenosis measured using carotid MRI was greater in COPD patients, 2) subjects without COPD had higher incidence of plaque calcification than subjects with COPD, and, 3) carotid plaque in COPD patients were more likely to

have a large lipid core, a recognized plaque component that is associated with cerebrovascular events (120). These results were the first to associate carotid plaque characteristics with COPD cases and increased awareness that COPD is a risk factor for cardiovascular disease and importantly for debilitating ischemic events such as stroke.

Application of Pulmonary Imaging to Lung and Atherosclerosis Studies

Thus far, pulmonary imaging has not played a large role in studies focused on the relationship between lung and heart disease in smokers. In Figure 9, we show the direct comparison of carotid 3DUS total plaque volume and intima media thickness with hyperpolarized ^3He MRI ventilation defect percent in a never- and 2 ex-smokers with normal pulmonary function and without airflow limitation from our own centre. In a similar approach, a study from the Emphysema and Cancer Action Project (EMCAP) (121) incorporated the use of thoracic CT to evaluate flow-mediated dilation (FMD) of the brachial artery in a group of ex-smokers with early or very mild COPD. The results showed that low FEV₁ and greater indices of emphysema was associated with attenuated FMD, suggesting that vascular endothelial function is influenced by lung function and structure. Other findings from the Multi-Ethnic Study of Atherosclerosis (MESA) Lung Study (2, 122) also used thoracic CT to measure emphysema in subjects without cardiovascular disease, and evaluated subclinical atherosclerosis with carotid ultrasound and cardiac CT to determine vascular phenotypes. Inverse associations were observed between spirometry and IMT, similar to previously described (3, 55, 105-107), but novel insights with respect to the relationship between emphysema and vascular disease were also provided. Although whole lung emphysema percent was not related to IMT, upper-lobe emphysema was significantly related with internal carotid IMT. Other studies (123, 124), have furthered our understanding of this relationship between emphysema and vascular disease by showing that emphysema percentage is related not only to carotid atherosclerosis, but also to calcification scores in the aorta, coronary arteries, as well as aortic and mitral annuli. Collectively, these studies provide strong evidence of a relationship between atherosclerosis and emphysema and support the notion of complex, heterogeneous vascular and lung disease in ex-smokers.

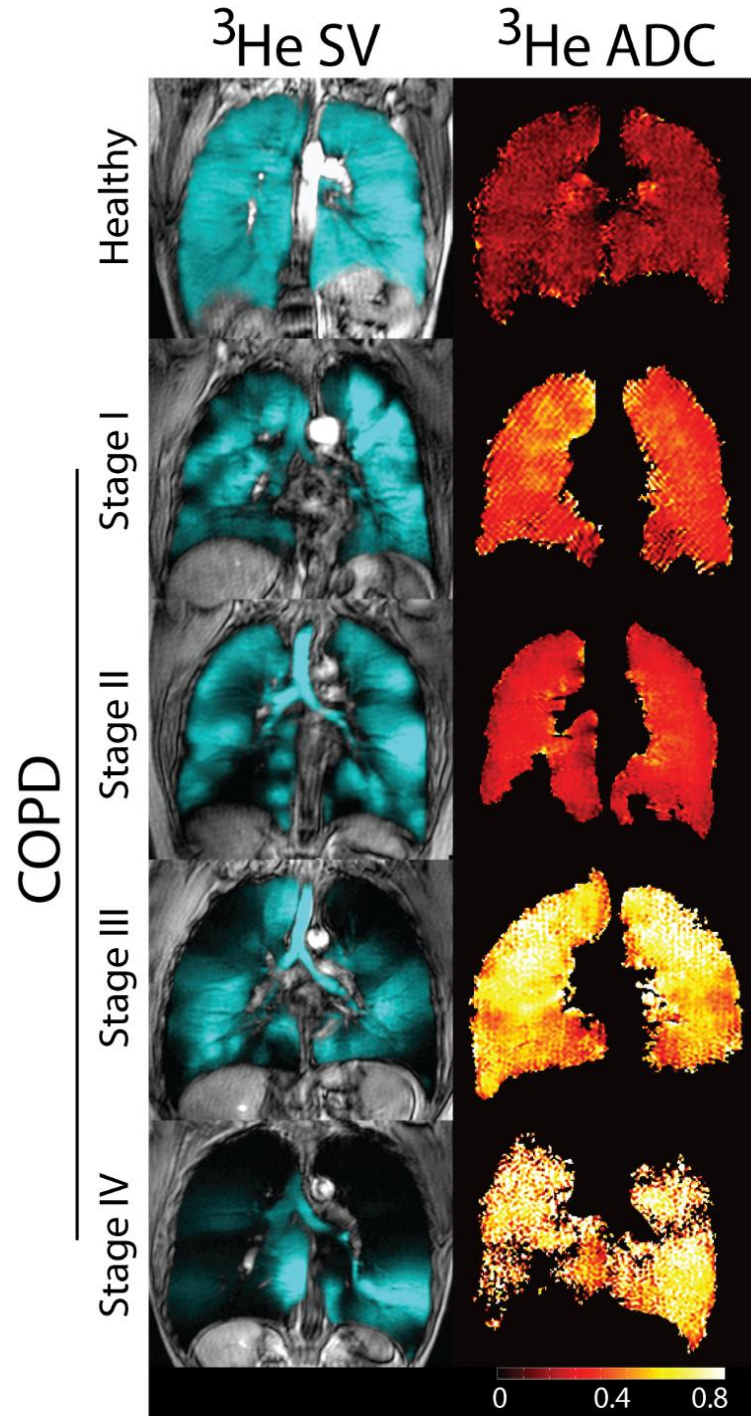


Figure 8: ^3He MRI ventilation and ADC maps.

Top Row: Healthy older never-smoker. Bottom Rows: Four representative COPD subjects with GOLD stages I–IV. Greyscale ^1H anatomical MRI is co-registered to aqua-blue ventilation pattern from ^3He MRI. Corresponding apparent diffusion coefficient (ADC) maps generated from diffusion-weighted MRI using $b=1.6 \text{ s/cm}^2$.

Application of Thoracic and Vascular Imaging to Evaluate Pulmonary and Cardiovascular Disease

The development of cardiovascular imaging modalities that can provide surrogate measurements of vascular disease has played an important role in characterizing lung-vascular disease phenotypes. In 2003, real-time MRI of aortic flow (125) was used to quantify left ventricle stroke volume and cardiac performance in healthy control and COPD subjects (114). The investigators observed that the COPD subjects had decreased cardiac performance compared to healthy volunteers and that the non-uniform breathing patterns in the COPD patients resulted in decreased stroke-volume. Taken together these results provided evidence that the abnormal breathing patterns and shallow respiration that may accompany COPD may be related to cardiovascular complications. Thoracic CT has also been used to provide a way to measure vascular changes and coronary artery calcification in patients with lung disease. Three studies in particular (111-113), have used thoracic CT to investigate the relationship between aortic calcification and pulmonary physiology using pulmonary function tests. Importantly, associations between the severity of aortic calcification were reported with lung function and morphologic parameters. Interestingly, (112) this work showed that pulmonary vascular alterations were correlated with aortic calcification, whereas other studies (111, 113) showed associations between aortic calcifications and FEV₁. A number of studies (126-128) have also investigated vascular dysfunction and arterial stiffness in COPD patients using pulse wave velocity (PWV), a functional measurement of vascular tone. These findings showed that COPD patients exhibit increased arterial stiffness (126) and furthermore, that the degree of arterial stiffness was related to the severity of airflow limitation (127, 128).

FUTURE PERSPECTIVE

A number of recent studies have demonstrated the value of emerging and well-established vascular and pulmonary imaging approaches for furthering our understanding on the direct relationship between advanced lung and vascular disease in smokers and ex-

smokers that cannot be explained on the basis of tobacco-smoking alone. In particular, carotid ultrasound measurements are valuable tools for the evaluation of cardio- and cerebrovascular risk.

Beyond the evaluation and screening for inflammatory markers, the incorporation of carotid ultrasound and perhaps other atherosclerosis imaging methods into the clinical workflow and treatment plan for COPD may help identify significant peripheral, cardiovascular or cerebrovascular atherosclerosis. Similarly, the acquisition of spirometry and other pulmonary function measurements in ex-smokers with cardiovascular disease or vascular risk factors would help detect airflow limitation that might otherwise go undiagnosed (8, 106). In mild COPD especially, cardiovascular events are a major source of morbidity and mortality (8), so it is possible that advanced imaging of both diseases may help treatment decisions that improve outcomes overall and cardiovascular events in particular. Regardless, it is important to keep in mind that the underlying mechanisms linking COPD and atherosclerosis are still not clear, and as recently described (9, 10) systemic inflammation may only provide a partial explanation for the links between COPD and advanced progressive atherosclerosis.

The incorporation of pulmonary functional imaging into vascular disease studies will provide new insight on the role of pulmonary morphological changes in the pathophysiology of vascular disease. Such studies will build on previous findings of emphysema in subjects with subclinical atherosclerosis (2, 123, 124). In addition, the notion of different vascular and lung disease phenotypes (74, 76, 77, 129-132) also holds promise for this area of research. In the future, a large-scale prospective study should be executed to monitor longitudinal changes in vascular and pulmonary conditions using sophisticated imaging techniques. Longitudinal monitoring of vascular and pulmonary disease in ex-smokers will provide more insight onto the genesis and progression of vascular disease changes in COPD patients and using imaging, there is potential to monitor treatment effects and phenotype relationships. At present, there is some evidence supporting a mechanistic link between pulmonary and vascular disease that is not explained by tobacco smoking alone, however the direct mechanisms that potentially accelerate atherosclerosis in ex-smokers with COPD have not been firmly established.

At the same time, major advances in quantitative pulmonary and vascular non-invasive imaging tools have advanced the development and validation of surrogate or intermediate endpoints of these chronic disorders. Based on this foundation of previous research, there is a clear role for novel vascular and pulmonary imaging methods to identify the direct potential links in future studies.

REFERENCES

1. Anthonisen NR, Skeans MA, Wise RA, Manfreda J, Kanner RE, Connett JE, et al. The effects of a smoking cessation intervention on 14.5-year mortality: a randomized clinical trial. *Ann Intern Med.* 2005;142(4):233-9.
2. Barr RG, Ahmed FS, Carr JJ, Hoffman EA, Jiang R, Kawut SM, et al. Subclinical atherosclerosis, airflow obstruction and emphysema: the MESA Lung Study. *The European respiratory journal.* 2012;39(4):846-54.
3. Schroeder EB, Welch VL, Evans GW, Heiss G. Impaired lung function and subclinical atherosclerosis. The ARIC Study. *Atherosclerosis.* 2005;180(2):367-73.
4. Sin DD, Man SF. Chronic obstructive pulmonary disease as a risk factor for cardiovascular morbidity and mortality. *Proc Am Thorac Soc.* 2005;2(1):8-11.
5. Hansell AL, Walk JA, Soriano JB. What do chronic obstructive pulmonary disease patients die from? A multiple cause coding analysis. *The European respiratory journal.* 2003;22(5):809-14.
6. Soriano JB, Visick GT, Muellerova H, Payvandi N, Hansell AL. Patterns of comorbidities in newly diagnosed COPD and asthma in primary care. *Chest.* 2005;128(4):2099-107.
7. Ghoorah K, De Soyza A, Kunadian V. Increased cardiovascular risk in patients with chronic obstructive pulmonary disease and the potential mechanisms linking the two conditions: a review. *Cardiol Rev.* 2013;21(4):196-202.
8. Van Eeden S, Leipsic J, Paul Man SF, Sin DD. The relationship between lung inflammation and cardiovascular disease. *American journal of respiratory and critical care medicine.* 2012;186(1):11-6.
9. Agusti A, Edwards LD, Rennard SI, MacNee W, Tal-Singer R, Miller BE, et al. Persistent systemic inflammation is associated with poor clinical outcomes in COPD: a novel phenotype. *PLoS One.* 2012;7(5):e37483.
10. Vanfleteren LE, Spruit MA, Groenen M, Gaffron S, van Empel VP, Bruijnzeel PL, et al. Clusters of comorbidities based on validated objective measurements and systemic inflammation in patients with chronic obstructive pulmonary disease. *American journal of respiratory and critical care medicine.* 2013;187(7):728-35.
11. Vestbo J, Anderson W, Coxson HO, Crim C, Dawber F, Edwards L, et al. Evaluation of COPD Longitudinally to Identify Predictive Surrogate End-points (ECLIPSE). *The European respiratory journal.* 2008;31(4):869-73.
12. Fain S, Schiebler ML, McCormack DG, Parraga G. Imaging of lung function using hyperpolarized helium-3 magnetic resonance imaging: Review of current and emerging translational methods and applications. *J Magn Reson Imaging.* 2010;32(6):1398-408.

13. Coxson HO, Rogers RM. Quantitative computed tomography of chronic obstructive pulmonary disease. *Acad Radiol.* 2005;12(11):1457-63.
14. Mets OM, de Jong PA, van Ginneken B, Gietema HA, Lammers JW. Quantitative computed tomography in COPD: possibilities and limitations. *Lung.* 2012;190(2):133-45.
15. Collaboration ABI, Fowkes F, Murray G, Butcher I, Heald C, Lee R, et al. Ankle brachial index combined with Framingham risk score to predict cardiovascular events and mortality. *JAMA: the journal of the American Medical Association.* 2008;300(2):197-208.
16. Khan TH, Farooqui FA, Niazi K. Critical review of the ankle brachial index. *Curr Cardiol Rev.* 2008;4(2):101-6.
17. Polak JF, Pencina MJ, Pencina KM, O'Donnell CJ, Wolf PA, D'Agostino RB, Sr. Carotid-wall intima-media thickness and cardiovascular events. *N Engl J Med.* 2011;365(3):213-21.
18. Stein JH, Korcarz CE, Hurst RT, Lonn E, Kendall CB, Mohler ER, et al. Use of carotid ultrasound to identify subclinical vascular disease and evaluate cardiovascular disease risk: a consensus statement from the American Society of Echocardiography Carotid Intima-Media Thickness Task Force. Endorsed by the Society for Vascular Medicine. *J Am Soc Echocardiogr.* 2008;21(2):93-111; quiz 89-90.
19. Wannarong T, Parraga G, Buchanan D, Fenster A, House AA, Hackam DG, et al. Progression of carotid plaque volume predicts cardiovascular events. *Stroke.* 2013;44(7):1859-65.
20. Toussaint JF, LaMuraglia GM, Southern JF, Fuster V, Kantor HL. Magnetic resonance images lipid, fibrous, calcified, hemorrhagic, and thrombotic components of human atherosclerosis in vivo. *Circulation.* 1996;94(5):932-8.
21. Fenster A, Parraga G, Bax J. Three-dimensional ultrasound scanning. *Interface Focus.* 2011;1(4):503-19.
22. Fenster A, Landry A, Downey DB, Hegele RA, Spence JD. 3D ultrasound imaging of the carotid arteries. *Curr Drug Targets Cardiovasc Haematol Disord.* 2004;4(2):161-75.
23. Mallett C, House AA, Spence JD, Fenster A, Parraga G. Longitudinal ultrasound evaluation of carotid atherosclerosis in one, two and three dimensions. *Ultrasound Med Biol.* 2009;35(3):367-75.
24. Grant EG, Benson CB, Moneta GL, Alexandrov AV, Baker JD, Bluth EI, et al. Carotid artery stenosis: gray-scale and Doppler US diagnosis--Society of Radiologists in Ultrasound Consensus Conference. *Radiology.* 2003;229(2):340-6.

25. Simon BA, Kaczka DW, Bankier AA, Parraga G. What can computed tomography and magnetic resonance imaging tell us about ventilation? *J Appl Physiol.* 2012;113(4):647-57.
26. Sin DD, Anthonisen NR, Soriano JB, Agusti AG. Mortality in COPD: Role of comorbidities. *The European respiratory journal.* 2006;28(6):1245-57.
27. Man SF, Van Eeden S, Sin DD. Vascular risk in chronic obstructive pulmonary disease: role of inflammation and other mediators. *Can J Cardiol.* 2012;28(6):653-61.
28. Sin DD, Wu L, Man SF. The relationship between reduced lung function and cardiovascular mortality: a population-based study and a systematic review of the literature. *Chest.* 2005;127(6):1952-9.
29. Maclay JD, McAllister DA, Macnee W. Cardiovascular risk in chronic obstructive pulmonary disease. *Respirology.* 2007;12(5):634-41.
30. Hartung MP, Grist TM, Francois CJ. Magnetic resonance angiography: current status and future directions. *J Cardiovasc Magn Reson.* 2011;13:19.
31. Miller JM, Rochitte CE, Dewey M, Arbab-Zadeh A, Niinuma H, Gottlieb I, et al. Diagnostic performance of coronary angiography by 64-row CT. *N Engl J Med.* 2008;359(22):2324-36.
32. Schuleri KH, George RT, Lardo AC. Applications of cardiac multidetector CT beyond coronary angiography. *Nat Rev Cardiol.* 2009;6(11):699-710.
33. Schoepf UJ, Becker CR, Ohnesorge BM, Yucel EK. CT of coronary artery disease. *Radiology.* 2004;232(1):18-37.
34. Berry C, L'Allier PL, Gregoire J, Lesperance J, Levesque S, Ibrahim R, et al. Comparison of intravascular ultrasound and quantitative coronary angiography for the assessment of coronary artery disease progression. *Circulation.* 2007;115(14):1851-7.
35. Kaneda H, Ako J, Terashima M. Intravascular ultrasound imaging for assessing regression and progression in coronary artery disease. *Am J Cardiol.* 2010;106(12):1735-46.
36. Ross R. The pathogenesis of atherosclerosis: a perspective for the 1990s. *Nature.* 1993;362(6423):801-9.
37. Bots ML, Hoes AW, Hofman A, Witteman JC, Grobbee DE. Cross-sectionally assessed carotid intima-media thickness relates to long-term risk of stroke, coronary heart disease and death as estimated by available risk functions. *J Intern Med.* 1999;245(3):269-76.

38. Carpenter JP, Lexa FJ, Davis JT. Determination of sixty percent or greater carotid artery stenosis by duplex Doppler ultrasonography. *J Vasc Surg.* 1995;22(6):697-703; discussion -5.
39. Chan V, Perlas A. Basics of ultrasound imaging. *Atlas of Ultrasound-Guided Procedures in Interventional Pain Management*: Springer; 2011. p. 13-9.
40. Buchanan DN, Lindenmaier T, McKay S, Bureau Y, Hackam DG, Fenster A, et al. The relationship of carotid three-dimensional ultrasound vessel wall volume with age and sex: comparison to carotid intima-media thickness. *Ultrasound Med Biol.* 2012;38(7):1145-53.
41. Egger M, Spence JD, Fenster A, Parraga G. Validation of 3D ultrasound vessel wall volume: an imaging phenotype of carotid atherosclerosis. *Ultrasound Med Biol.* 2007;33(6):905-14.
42. Touboul PJ, Hennerici MG, Meairs S, Adams H, Amarenco P, Desvarieux M, et al. Mannheim intima-media thickness consensus. *Cerebrovasc Dis.* 2004;18(4):346-9.
43. Touboul PJ, Hennerici MG, Meairs S, Adams H, Amarenco P, Bornstein N, et al. Mannheim carotid intima-media thickness consensus (2004-2006). An update on behalf of the Advisory Board of the 3rd and 4th Watching the Risk Symposium, 13th and 15th European Stroke Conferences, Mannheim, Germany, 2004, and Brussels, Belgium, 2006. *Cerebrovasc Dis.* 2007;23(1):75-80.
44. Shai I, Spence JD, Schwarzfuchs D, Henkin Y, Parraga G, Rudich A, et al. Dietary intervention to reverse carotid atherosclerosis. *Circulation.* 2010;121(10):1200-8.
45. Schäberle W. *Ultrasonography in Vascular Diagnosis: A Therapy-Oriented Textbook and Atlas*: Springer; 2010.
46. Byrnes KR, Ross CB. The Current Role of Carotid Duplex Ultrasonography in the Management of Carotid Atherosclerosis: Foundations and Advances. *International journal of vascular medicine.* 2012;2012.
47. Spence JD, Eliasziw M, DiCicco M, Hackam DG, Galil R, Lohmann T. Carotid plaque area: a tool for targeting and evaluating vascular preventive therapy. *Stroke.* 2002;33(12):2916-22.
48. Landry A, Spence JD, Fenster A. Measurement of carotid plaque volume by 3-dimensional ultrasound. *Stroke.* 2004;35(4):864-9.
49. Landry A, Spence JD, Fenster A. Quantification of carotid plaque volume measurements using 3D ultrasound imaging. *Ultrasound Med Biol.* 2005;31(6):751-62.
50. Landry A, Fenster A. Theoretical and experimental quantification of carotid plaque volume measurements made by three-dimensional ultrasound using test phantoms. *Med Phys.* 2002;29(10):2319-27.

51. Barnett PA, Spence JD, Manuck SB, Jennings JR. Psychological stress and the progression of carotid artery disease. *Journal of hypertension*. 1997;15(1):49-55.
52. Buchanan D, Gyacskov I, Ukwatta E, Lindenmaier T, Fenster A, Parraga G, editors. *Semi-automated segmentation of carotid artery total plaque volume from three dimensional ultrasound carotid imaging*2012.
53. Ukwatta E, Awad J, Ward A, Buchanan D, Samarabandu J, Parraga G, et al. Three-dimensional ultrasound of carotid atherosclerosis: Semiautomated segmentation using a level set-based method. *Medical Physics*. 2011;38:2479.
54. Krasinski A, Chiu B, Spence JD, Fenster A, Parraga G. Three-dimensional ultrasound quantification of intensive statin treatment of carotid atherosclerosis. *Ultrasound in medicine & biology*. 2009;35(11):1763-72.
55. Ebrahim S, Papacosta O, Whincup P, Wannamethee G, Walker M, Nicolaides AN, et al. Carotid plaque, intima media thickness, cardiovascular risk factors, and prevalent cardiovascular disease in men and women: the British Regional Heart Study. *Stroke*. 1999;30(4):841-50.
56. Yuan C, Oikawa M, Miller Z, Hatsukami T. MRI of carotid atherosclerosis. *Journal of nuclear cardiology*. 2008;15(2):266-75.
57. Lahousse L, van den Bouwhuijsen QJ, Loth DW, Joos GF, Hofman A, Wittteman JC, et al. Chronic obstructive pulmonary disease and lipid core carotid artery plaques in the elderly: the Rotterdam Study. *American journal of respiratory and critical care medicine*. 2013;187(1):58-64.
58. Hatsukami TS, Ross R, Polissar NL, Yuan C. Visualization of fibrous cap thickness and rupture in human atherosclerotic carotid plaque in vivo with high-resolution magnetic resonance imaging. *Circulation*. 2000;102(9):959-64.
59. Mitsumori LM, Hatsukami TS, Ferguson MS, Kerwin WS, Cai J, Yuan C. In vivo accuracy of multisequence MR imaging for identifying unstable fibrous caps in advanced human carotid plaques. *Journal of magnetic resonance imaging*. 2003;17(4):410-20.
60. Yuan C, Kerwin WS, Ferguson MS, Polissar N, Zhang S, Cai J, et al. Contrast-enhanced high resolution MRI for atherosclerotic carotid artery tissue characterization. *Journal of magnetic resonance imaging : JMRI*. 2002;15(1):62-7.
61. Wasserman BA, Smith WI, Trout HH, Cannon RO, Balaban RS, Arai AE. Carotid Artery Atherosclerosis: In Vivo Morphologic Characterization with Gadolinium-enhanced Double-oblique MR Imaging—Initial Results1. *Radiology*. 2002;223(2):566-73.
62. Agatston AS, Janowitz WR, Hildner FJ, Zusmer NR, Viamonte M, Jr., Detrano R. Quantification of coronary artery calcium using ultrafast computed tomography. *J Am Coll Cardiol*. 1990;15(4):827-32.

63. Folsom AR, Kronmal RA, Detrano RC, O'Leary DH, Bild DE, Bluemke DA, et al. Coronary artery calcification compared with carotid intima-media thickness in prediction of cardiovascular disease incidence: the Multi-Ethnic Study of Atherosclerosis (MESA). *Archives of Internal Medicine*. 2008;168(12):1333.
64. Becker A, Leber AW, Becker C, von Ziegler F, Tittus J, Schroeder I, et al. Predictive value of coronary calcifications for future cardiac events in asymptomatic patients with diabetes mellitus: a prospective study in 716 patients over 8 years. *BMC Cardiovasc Disord*. 2008;8:27.
65. Buist AS, McBurnie MA, Vollmer WM, Gillespie S, Burney P, Mannino DM, et al. International variation in the prevalence of COPD (the BOLD Study): a population-based prevalence study. *Lancet*. 2007;370(9589):741-50.
66. Hogg JC. Pathophysiology of airflow limitation in chronic obstructive pulmonary disease. *Lancet*. 2004;364(9435):709-21.
67. Franciosi LG, Page CP, Celli BR, Cazzola M, Walker MJ, Danhof M, et al. Markers of disease severity in chronic obstructive pulmonary disease. *Pulm Pharmacol Ther*. 2006;19(3):189-99.
68. Gelb AF, Hogg JC, Muller NL, Schein MJ, Kuei J, Tashkin DP, et al. Contribution of emphysema and small airways in COPD. *Chest*. 1996;109(2):353-9.
69. Wang C MJPI, de Lange E and Altes T A, editor Elevated short-time-scale hyperpolarized helium-3 diffusion in secondhand smokers. *International Society of Magnetic Resonance in Medicine Proceedings 2012*; 2012.
70. Fain SB, Panth SR, Evans MD, Wentland AL, Holmes JH, Korosec FR, et al. Early emphysematous changes in asymptomatic smokers: detection with ³He MR imaging. *Radiology*. 2006;239(3):875-83.
71. Woodhouse N, Wild JM, Paley MN, FICHELE S, Said Z, Swift AJ, et al. Combined helium-3/proton magnetic resonance imaging measurement of ventilated lung volumes in smokers compared to never-smokers. *J Magn Reson Imaging*. 2005;21(4):365-9.
72. Swift AJ, Wild JM, FICHELE S, Woodhouse N, Fleming S, Waterhouse J, et al. Emphysematous changes and normal variation in smokers and COPD patients using diffusion ³He MRI. *Eur J Radiol*. 2005;54(3):352-8.
73. Irion KL, Marchiori E, Hochegger B, Porto Nda S, Moreira Jda S, Anselmi CE, et al. CT quantification of emphysema in young subjects with no recognizable chest disease. *AJR Am J Roentgenol*. 2009;192(3):W90-6.
74. Galban CJ, Han MK, Boes JL, Chughtai KA, Meyer CR, Johnson TD, et al. Computed tomography-based biomarker provides unique signature for diagnosis of COPD phenotypes and disease progression. *Nat Med*. 2012;18(11):1711-5.

75. Kirby M, Heydarian M, Wheatley A, McCormack DG, Parraga G. Evaluating bronchodilator effects in chronic obstructive pulmonary disease using diffusion-weighted hyperpolarized helium-3 magnetic resonance imaging. *J Appl Physiol*. 2012;112(4):651-7.
76. Tulek B, Kivrak AS, Ozbek S, Kanat F, Suerdem M. Phenotyping of chronic obstructive pulmonary disease using the modified Bhalla scoring system for high-resolution computed tomography. *Can Respir J*. 2013;20(2):91-6.
77. Coxson HO, Eastwood PR, Williamson JP, Sin DD. Phenotyping airway disease with optical coherence tomography. *Respirology*. 2011;16(1):34-43.
78. Coxson HO, Mayo J, Lam S, Santyr G, Parraga G, Sin DD. New and current clinical imaging techniques to study chronic obstructive pulmonary disease. *American journal of respiratory and critical care medicine*. 2009;180(7):588-97.
79. Matsuoka S, Yamashiro T, Washko GR, Kurihara Y, Nakajima Y, Hatabu H. Quantitative CT assessment of chronic obstructive pulmonary disease. *Radiographics*. 2010;30(1):55-66.
80. Muller NL, Staples CA, Miller RR, Abboud RT. "Density mask". An objective method to quantitate emphysema using computed tomography. *Chest*. 1988;94(4):782-7.
81. Gevenois PA, De Vuyst P, de Maertelaer V, Zanen J, Jacobovitz D, Cosio MG, et al. Comparison of computed density and microscopic morphometry in pulmonary emphysema. *American journal of respiratory and critical care medicine*. 1996;154(1):187-92.
82. Madani A, Zanen J, de Maertelaer V, Gevenois PA. Pulmonary emphysema: objective quantification at multi-detector row CT--comparison with macroscopic and microscopic morphometry. *Radiology*. 2006;238(3):1036-43.
83. Dirksen A, Piitulainen E, Parr DG, Deng C, Wencker M, Shaker SB, et al. Exploring the role of CT densitometry: a randomised study of augmentation therapy in alpha1-antitrypsin deficiency. *The European respiratory journal*. 2009;33(6):1345-53.
84. Coxson HO. Quantitative chest tomography in COPD research: chairman's summary. *Proc Am Thorac Soc*. 2008;5(9):874-7.
85. Mishima M, Hirai T, Itoh H, Nakano Y, Sakai H, Muro S, et al. Complexity of terminal airspace geometry assessed by lung computed tomography in normal subjects and patients with chronic obstructive pulmonary disease. *Proc Natl Acad Sci U S A*. 1999;96(16):8829-34.
86. Coxson HO, Whittall KP, Nakano Y, Rogers RM, Sciruba FC, Keenan RJ, et al. Selection of patients for lung volume reduction surgery using a power law analysis of the computed tomographic scan. *Thorax*. 2003;58(6):510-4.

87. Gietema HA, Muller NL, Fauerbach PV, Sharma S, Edwards LD, Camp PG, et al. Quantifying the extent of emphysema: factors associated with radiologists' estimations and quantitative indices of emphysema severity using the ECLIPSE cohort. *Acad Radiol.* 2011;18(6):661-71.
88. Hogg JC, Chu F, Utokaparch S, Woods R, Elliott WM, Buzatu L, et al. The nature of small-airway obstruction in chronic obstructive pulmonary disease. *N Engl J Med.* 2004;350(26):2645-53.
89. Lutey BA, Conradi SH, Atkinson JJ, Zheng J, Schechtman KB, Senior RM, et al. Accurate measurement of small airways on low-dose thoracic CT scans in smokers. *Chest.* 2013;143(5):1321-9.
90. Nakano Y, Muro S, Sakai H, Hirai T, Chin K, Tsukino M, et al. Computed tomographic measurements of airway dimensions and emphysema in smokers. Correlation with lung function. *American journal of respiratory and critical care medicine.* 2000;162(3 Pt 1):1102-8.
91. King GG, Muller NL, Whittall KP, Xiang QS, Pare PD. An analysis algorithm for measuring airway lumen and wall areas from high-resolution computed tomographic data. *American journal of respiratory and critical care medicine.* 2000;161(2 Pt 1):574-80.
92. Reinhardt JM, D'Souza ND, Hoffman EA. Accurate measurement of intrathoracic airways. *IEEE Trans Med Imaging.* 1997;16(6):820-7.
93. Saba OI, Hoffman EA, Reinhardt JM. Maximizing quantitative accuracy of lung airway lumen and wall measures obtained from X-ray CT imaging. *J Appl Physiol.* 2003;95(3):1063-75.
94. Albert MS, Cates GD, Driehuys B, Happer W, Saam B, Springer CS, Jr., et al. Biological magnetic resonance imaging using laser-polarized ^{129}Xe . *Nature.* 1994;370(6486):199-201.
95. Kirby M, Svenningsen S, Owrangi A, Wheatley A, Farag A, Ouriadov A, et al. Hyperpolarized ^3He and ^{129}Xe MR imaging in healthy volunteers and patients with chronic obstructive pulmonary disease. *Radiology.* 2012;265(2):600-10.
96. Parraga G, Mathew L, Etemad-Rezai R, McCormack DG, Santyr GE. Hyperpolarized ^3He magnetic resonance imaging of ventilation defects in healthy elderly volunteers: initial findings at 3.0 Tesla. *Acad Radiol.* 2008;15(6):776-85.
97. Mathew L, Evans A, Ouriadov A, Etemad-Rezai R, Fogel R, Santyr G, et al. Hyperpolarized ^3He magnetic resonance imaging of chronic obstructive pulmonary disease: reproducibility at 3.0 tesla. *Acad Radiol.* 2008;15(10):1298-311.

98. Coxson HO, Quiney B, Sin DD, Xing L, McWilliams AM, Mayo JR, et al. Airway wall thickness assessed using computed tomography and optical coherence tomography. *American journal of respiratory and critical care medicine*. 2008;177(11):1201-6.
99. Woods JC, Choong CK, Yablonskiy DA, Bentley J, Wong J, Pierce JA, et al. Hyperpolarized ³He diffusion MRI and histology in pulmonary emphysema. *Magn Reson Med*. 2006;56(6):1293-300.
100. Yablonskiy DA, Sukstanskii AL, Woods JC, Gierada DS, Quirk JD, Hogg JC, et al. Quantification of lung microstructure with hyperpolarized ³He diffusion MRI. *J Appl Physiol*. 2009;107(4):1258-65.
101. Saam BT, Yablonskiy DA, Kodibagkar VD, Leawoods JC, Gierada DS, Cooper JD, et al. MR imaging of diffusion of (³)He gas in healthy and diseased lungs. *Magn Reson Med*. 2000;44(2):174-9.
102. Edelman RR, Hatabu H, Tadamura E, Li W, Prasad PV. Noninvasive assessment of regional ventilation in the human lung using oxygen-enhanced magnetic resonance imaging. *Nat Med*. 1996;2(11):1236-9.
103. Ohno Y, Koyama H, Nogami M, Takenaka D, Matsumoto S, Obara M, et al. Dynamic oxygen-enhanced MRI versus quantitative CT: pulmonary functional loss assessment and clinical stage classification of smoking-related COPD. *AJR Am J Roentgenol*. 2008;190(2):W93-9.
104. Minino AM, Murphy SL, Xu J, Kochanek KD. Deaths: final data for 2008. *Natl Vital Stat Rep*. 2011;59(10):1-126.
105. Iwamoto H, Yokoyama A, Kitahara Y, Ishikawa N, Haruta Y, Yamane K, et al. Airflow limitation in smokers is associated with subclinical atherosclerosis. *American journal of respiratory and critical care medicine*. 2009;179(1):35-40.
106. Kim SJ, Yoon DW, Lee EJ, Hur GY, Jung KH, Lee SY, et al. Carotid atherosclerosis in patients with untreated chronic obstructive pulmonary disease. *Int J Tuberc Lung Dis*. 2011;15(9):1265-70, i.
107. van Gestel YR, Flu WJ, van Kuijk JP, Hoeks SE, Bax JJ, Sin DD, et al. Association of COPD with carotid wall intima-media thickness in vascular surgery patients. *Respir Med*. 2010;104(5):712-6.
108. Celli BR, Cote CG, Marin JM, Casanova C, Montes de Oca M, Mendez RA, et al. The body-mass index, airflow obstruction, dyspnea, and exercise capacity index in chronic obstructive pulmonary disease. *N Engl J Med*. 2004;350(10):1005-12.
109. Zvezdin B, Milutinov S, Kojicic M, Hadnadjev M, Hromis S, Markovic M, et al. A postmortem analysis of major causes of early death in patients hospitalized with COPD exacerbation. *Chest*. 2009;136(2):376-80.

110. Sidney S, Sorel M, Quesenberry CP, Jr., DeLuise C, Lanes S, Eisner MD. COPD and incident cardiovascular disease hospitalizations and mortality: Kaiser Permanente Medical Care Program. *Chest*. 2005;128(4):2068-75.
111. Rasmussen T, Kober L, Pedersen JH, Dirksen A, Thomsen LH, Stender S, et al. Relationship between chronic obstructive pulmonary disease and subclinical coronary artery disease in long-term smokers. *Eur Heart J Cardiovasc Imaging*. 2013.
112. Matsuoka S, Yamashiro T, Diaz A, Estepar RS, Ross JC, Silverman EK, et al. The relationship between small pulmonary vascular alteration and aortic atherosclerosis in chronic obstructive pulmonary disease: quantitative CT analysis. *Acad Radiol*. 2011;18(1):40-6.
113. McAllister DA, MacNee W, Duprez D, Hoffman EA, Vogel-Claussen J, Criqui MH, et al. Pulmonary function is associated with distal aortic calcium, not proximal aortic distensibility. MESA lung study. *COPD*. 2011;8(2):71-8.
114. van den Hout RJ, Lamb HJ, van den Aardweg JG, Schot R, Steendijk P, van der Wall EE, et al. Real-time MR imaging of aortic flow: influence of breathing on left ventricular stroke volume in chronic obstructive pulmonary disease. *Radiology*. 2003;229(2):513-9.
115. Wells JM, Washko GR, Han MK, Abbas N, Nath H, Marmar AJ, et al. Pulmonary arterial enlargement and acute exacerbations of COPD. *N Engl J Med*. 2012;367(10):913-21.
116. Zureik M, Kauffmann F, Touboul PJ, Courbon D, Ducimetiere P. Association between peak expiratory flow and the development of carotid atherosclerotic plaques. *Arch Intern Med*. 2001;161(13):1669-76.
117. Engstrom G, Hedblad B, Valind S, Janzon L. Asymptomatic leg and carotid atherosclerosis in smokers is related to degree of ventilatory capacity: longitudinal and cross-sectional results from 'Men born in 1914', Sweden. *Atherosclerosis*. 2001;155(1):237-43.
118. Frantz S, Nihlen U, Dencker M, Engstrom G, Lofdahl CG, Wollmer P. Atherosclerotic plaques in the internal carotid artery and associations with lung function assessed by different methods. *Clin Physiol Funct Imaging*. 2012;32(2):120-5.
119. Hofman A, van Duijn CM, Franco OH, Ikram MA, Janssen HL, Klaver CC, et al. The Rotterdam Study: 2012 objectives and design update. *Eur J Epidemiol*. 2011;26(8):657-86.
120. Takaya N, Yuan C, Chu B, Saam T, Underhill H, Cai J, et al. Association between carotid plaque characteristics and subsequent ischemic cerebrovascular events: a prospective assessment with MRI--initial results. *Stroke*. 2006;37(3):818-23.

121. Barr RG, Mesia-Vela S, Austin JH, Basner RC, Keller BM, Reeves AP, et al. Impaired flow-mediated dilation is associated with low pulmonary function and emphysema in ex-smokers: the Emphysema and Cancer Action Project (EMCAP) Study. *American journal of respiratory and critical care medicine*. 2007;176(12):1200-7.
122. Bild DE, Bluemke DA, Burke GL, Detrano R, Diez Roux AV, Folsom AR, et al. Multi-ethnic study of atherosclerosis: objectives and design. *Am J Epidemiol*. 2002;156(9):871-81.
123. Chae EJ, Seo JB, Oh YM, Lee JS, Jung Y, Lee SD. Severity of systemic calcified atherosclerosis is associated with airflow limitation and emphysema. *J Comput Assist Tomogr*. 2013;37(5):743-9.
124. Dransfield MT, Huang F, Nath H, Singh SP, Bailey WC, Washko GR. CT emphysema predicts thoracic aortic calcification in smokers with and without COPD. *COPD*. 2010;7(6):404-10.
125. Eichenberger AC, Schwitter J, McKinnon GC, Debatin JF, von Schulthess GK. Phase-contrast echo-planar MR imaging: real-time quantification of flow and velocity patterns in the thoracic vessels induced by Valsalva's maneuver. *J Magn Reson Imaging*. 1995;5(6):648-55.
126. Maclay JD, McAllister DA, Mills NL, Paterson FP, Ludlam CA, Drost EM, et al. Vascular dysfunction in chronic obstructive pulmonary disease. *American journal of respiratory and critical care medicine*. 2009;180(6):513-20.
127. Cinarka H, Kayhan S, Gumus A, Durakoglugil ME, Erdogan T, Ezberci I, et al. Arterial stiffness measured by carotid femoral pulse wave velocity is associated with disease severity in chronic obstructive pulmonary disease. *Respir Care*. 2013.
128. Sabit R, Bolton CE, Edwards PH, Pettit RJ, Evans WD, McEniery CM, et al. Arterial stiffness and osteoporosis in chronic obstructive pulmonary disease. *American journal of respiratory and critical care medicine*. 2007;175(12):1259-65.
129. Burgel PR, Paillasseur JL, Caillaud D, Tillie-Leblond I, Chanez P, Escamilla R, et al. Clinical COPD phenotypes: a novel approach using principal component and cluster analyses. *The European respiratory journal*. 2010;36(3):531-9.
130. Burgel PR, Paillasseur JL, Peene B, Dusser D, Roche N, Coolen J, et al. Two distinct chronic obstructive pulmonary disease (COPD) phenotypes are associated with high risk of mortality. *PLoS One*. 2012;7(12):e51048.
131. Marsh SE, Travers J, Weatherall M, Williams MV, Aldington S, Shirtcliffe PM, et al. Proportional classifications of COPD phenotypes. *Thorax*. 2008;63(9):761-7.
132. Pike D, Parraga G. Chronic obstructive pulmonary disease: more imaging, more phenotyping...better care? *Can Respir J*. 2013;20(2):90.

APPENDIX B – Pulmonary Imaging Abnormalities in an Adult Case of Congenital Lobar Emphysema

Appendix B reports pulmonary imaging findings in a rare case of congenital lobar emphysema in an adult. While imaging of congenital pulmonary disorders is not the focus of this thesis, data from this Case Report highlights how imaging measurements of airway morphology and emphysema can be used to identify and characterize bullous emphysema which is a phenotype of chronic obstructive pulmonary disease. The contents of Appendix B have been previously published in the Journal of Radiology Case Reports and permission to reproduce the article was granted by Dr. Roland Talanow, MD, PhD (editor-in-chief) and is provided in Appendix D.

D Pike, S Mohan, W Ma, JF Lewis and G Parraga. Pulmonary Imaging Abnormalities in an Adult Case of Congenital Lobar Emphysema. The Journal of Radiology Case Reports; DOI: 10.3941/jrcr.v9i2.2048 2015

Pulmonary Imaging Abnormalities in an Adult Case of Congenital Lobar Emphysema

D Pike, S Mohan, W Ma, JF Lewis and G Parraga

Congenital lobar emphysema (CLE) is a rare pulmonary abnormality that is typically detected in the neonatal period, although rare cases have been reported in early adulthood (1). CLE is commonly associated with bronchial abnormalities/obstruction and vascular dysfunction, resulting in ventilation-perfusion mismatch, hyperinflation and dyspnea (2). Diagnosis is often based on x-ray computed tomography (CT) findings of hyperlucent and/or hyperinflated lung lobes along with malformations of the pulmonary vasculature or mediastinum. Here, we used imaging to quantitatively evaluate the function and morphology of alveolar and airway structures in a young adult with acute breathlessness and chest pain.

A twenty-year-old female with a one-year, five-cigarette/day smoking history and no previous chronic respiratory disease presented with severe chest pain and shortness of breath. Chest x-ray showed localized left upper lobe (LUL) hyperlucency whereupon she provided written informed consent to a Health Canada and local ethics board approved research protocol. The subject underwent two visits, 75 days apart that included spirometry, plethysmography and hyperpolarized ³He magnetic resonance imaging (MRI) to evaluate regional pulmonary ventilation as well as parenchymal morphology using the

^3He apparent diffusion coefficient (ADC) – a surrogate measurement of emphysema (3). MRI was performed in breath-hold after inhalation of a 1L $^3\text{He}/\text{N}_2$ gas mixture from functional residual capacity (FRC) using a fast-gradient-recalled-echo (FGRE) sequence, previously described (4). ^3He MRI ventilation images were quantified to generate ventilation defect percent (VDP) (4) which is the volume of the lung not participating in ventilation, normalized to total lung volume. For the generation of ^3He ADC, diffusion-weighted images were acquired as previously described (4). To evaluate parenchymal microstructure, we adapted a method (3) whereby D_L and D_T were defined as the longitudinal and transverse diffusion coefficients in the acinar ducts respectively with R representing the outer radius and h the depth of the intra-acinar duct.

Thoracic CT was acquired once within twenty minutes of MRI using a 64-slice Lightspeed VCT scanner (GEHC, Milwaukee, WI, USA) as previously described (4). Pulmonary Workstation 2.0 (VIDA Diagnostics, Iowa City, IA, USA) was used to generate emphysema measurements including the relative area of the lung with attenuation values $<-950\text{HU}$ (RA_{950}), low attenuation clusters (LAC), and as well airway measurements including airway wall area percent (WA%) and lumen area (LA).

Spirometry, plethysmography and diffusing capacity of carbon monoxide (DL_{CO}) measurements showed there was modestly abnormal forced expiratory volume in one second (FEV_1 , V1:V2 70%:75%), and highly abnormal residual volume (RV, V1:V2 125%:150%), and airways resistance (R_{aw} , V1:V2 185%:180%), but normal DL_{CO} (V1:V2 100%:115%). Figure 1 shows CT low attenuating area (LAA) and low attenuation clusters (LAC) and ^3He MRI ventilation imaging with a large LUL ventilation defect spatially coincident with the CT- and ^3He MRI-defined emphysematous region. ^3He MRI morphometric maps (higher intensity representing greater acinar duct dimensions) are also shown for the intra-acinar duct outer radius (R), depth (h), and inner radius ($R-h$). Quantitative LUL measurements showed abnormal RA_{950} (LUL: 13%, other lobes: 0%), LAC (LUL: -1.5, other lobes: -2.3 to -1.8) and VDP (LUL: 29%, other lobes: 1%-7%). For the LUL, acinar outer and inner radii were markedly abnormal (490 μm and 310 μm respectively) compared to the other lung lobes (300-310 μm and 130-140 μm respectively). CT airway measurements for the subsegmental bronchus leading to

the LUL were abnormal (WA%: 50%, LA: 19mm²) compared to other airways of the same generation (WA%: 57%-66%, LA: 10mm²- 16mm²).

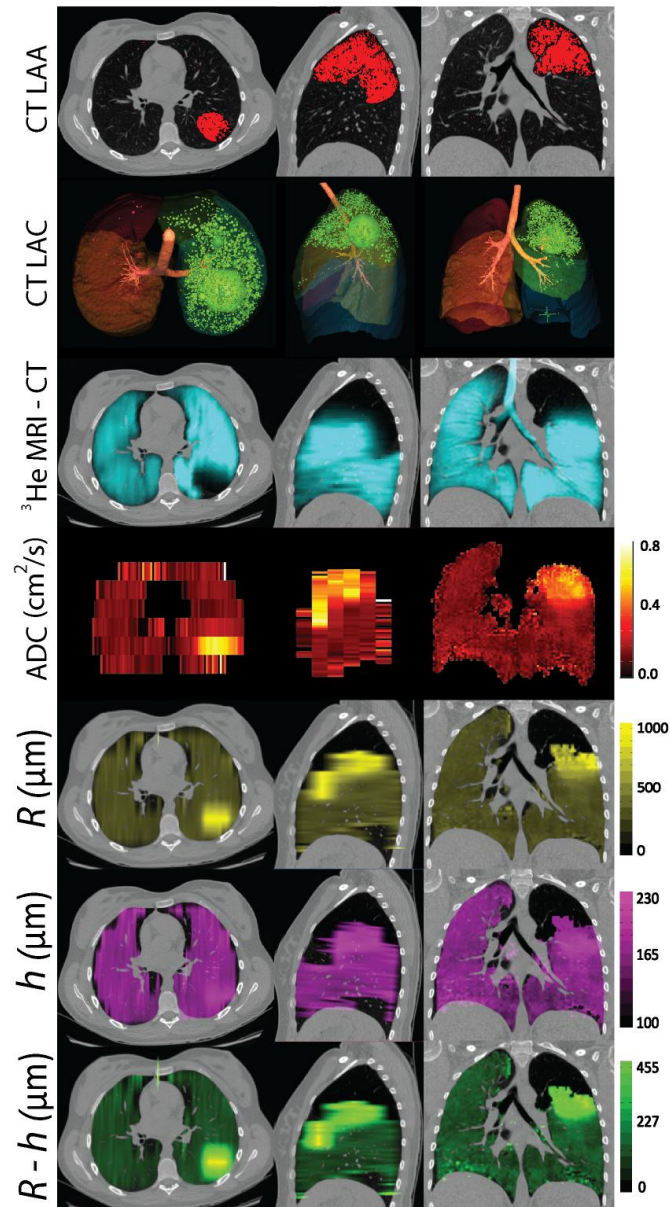


Figure 1: Thoracic CT and ³He MRI measurements, co-registration and analysis in the axial, sagittal and coronal planes for the 20 year-old female with congenital lobar emphysema presented in this case.

CT LAA: CT low attenuation area (LAA, in red, attenuation <-950HU) with the thoracic CT as the background (in grey-scale), CT LAC: 3D low attenuation clusters (LAC) analysis generated using VIDA Pulmonary Workstation 2.0, ³He MRI-CT: ³He MRI static ventilation image (in blue) registered to thoracic CT (in grey-scale), ³He MRI ADC: ³He MRI apparent diffusion coefficient (ADC) maps for $b=1.6\text{cm}^2/\text{s}$, where

brighter yellow-green represents higher ADC values, R :intra-acinar duct outer radius generated from ^3He MRI co-registered with thoracic CT (in grey-scale), h : intra-acinar duct depth generated from ^3He MRI co-registered with thoracic CT (in grey-scale), $R-h$: intra-acinar duct inner radius co-registered with thoracic CT (in grey-scale).

In Figure 2, the CT-derived airway tree is shown in yellow co-registered with the ^3He MRI ventilation image with the hyperlucent region outlined in white and the fissure between the LUL and LLL shown in black. The left upper subsegmental bronchus is abnormally terminated with the proximal end apparently disconnected from the rest of the airway tree. Relative dimensions for this abnormal airway and a similar generation normal airway are shown in schematic along with acinar duct morphological measurements for normal and abnormal LUL parenchyma estimated using ^3He MRI and the Weibel model (5) assumptions.

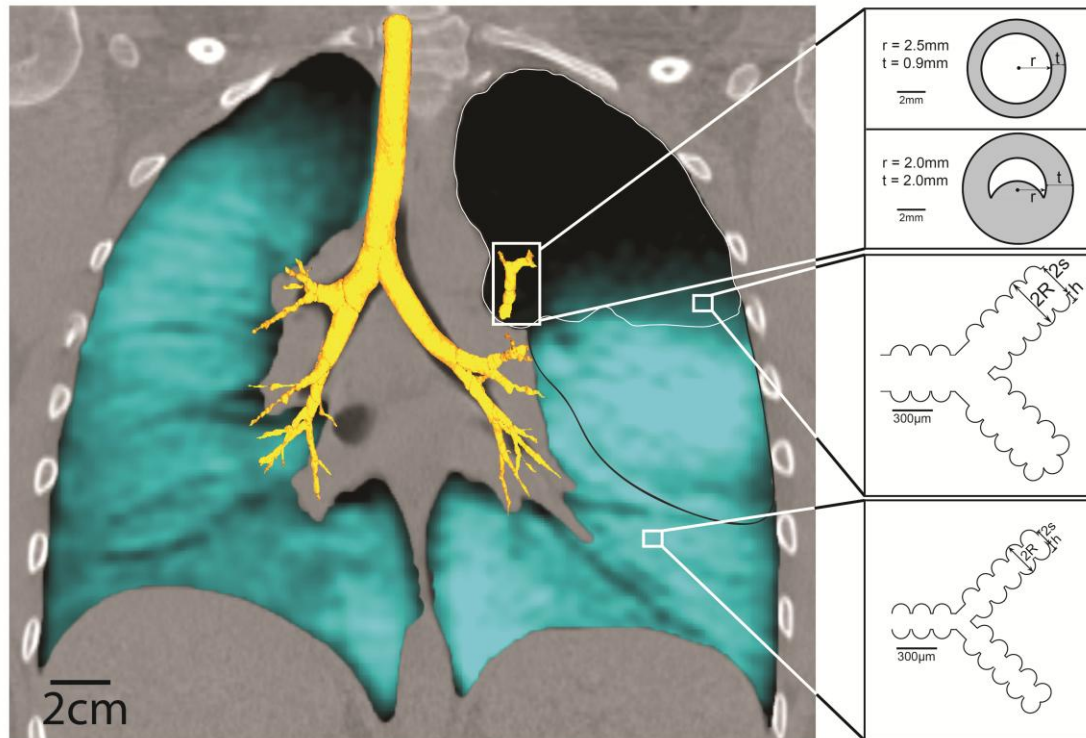


Figure 2: Registered CT airway tree with ^3He MRI and CT for the 20 year-old female with congenital lobar emphysema presented in this case. The white contour outlines the emphysematous region in the left upper lobe (LUL), the black contour outlines the entire LUL. There is a noticeable mediastinal shift onto the contralateral right lung due to hyperinflation in the LUL. The subsegmental bronchus feeding into the LUL was abnormally terminated and not connected to the rest of the airway tree and dimensions of the resulting airway segment were abnormal (top panel). Acinar duct schematics for the

abnormal LUL parenchyma (middle panel) and normal parenchyma (bottom panel) are shown to scale and were estimated using Weibel model assumptions.

DISCUSSION

Albeit a rare diagnosis in adults, CLE is an important differential for unilateral hyperlucent lung. The number of adult diagnoses has recently increased due to incidental radiological findings, but to our knowledge, this is the first report of quantitative, non-invasive regional measurements of airway morphology, parenchymal microstructure and ^3He ventilation. Thoracic CT showed that the hyperlucent region was highly localized, with a mediastinal shift to the contralateral right side likely related to LUL over-inflation - a common finding in CLE. Interestingly, we also observed focal obliteration of the proximal aspect of the tertiary bronchi serving the LUL apico-posterior segment (the LUL-LB1+2 bronchus). This leads to a lack of connection between this segment and the central airways although there was no evidence of localized endobronchial mucus plugging, foreign body or other masses resulting in extra-luminal compression. The distal segment of the apico-posterior bronchus was present but highly abnormal with a thinner wall (decreased WA%) and widening of the lumen (high LA) compared to similar airways in other regions, consistent with an occult atretic bronchus. The precise relationship between bronchial atresia and CLE is unknown although the timing and level of embryofetal airway obstruction may explain the variety of congenital lung lesions.

We also observed a markedly elevated (worse) LUL VDP compared to the other lobes and a heterogeneous pattern of ^3He signal filling inwards from the edges of the emphysematous region of the apico-posterior region. We propose collateral ventilation into the emphysematous area as a potential mechanism for this finding, first described in excised emphysematous lungs (6) and COPD patients (7). In emphysema, there is lower resistance to collateral flow that may involve the 1-2 micrometer pores of Kohn, the 30 micrometer channels described by Lambert, or the 80-150 micrometer interbronchiolar paths described by Martin (8).

In contrast to healthy lung tissue in the unaffected lobes, there was an elevated outer and inner radius of the LUL acinar ducts as previously shown in patients with emphysema.

There was also an elevated acinar duct sleeve depth and this is a novel finding that contrasts with results in emphysema ex-smokers where decreased alveolar duct sleeve depths were reported.

Finally, although we observed significant airway and parenchymal abnormalities, airflow limitation was mild and DL_{CO} was normal in this adult patient. There was evidence of gas trapping and very high airways resistance, both of which may be related to the atretic bronchus and slower time constants for LUL emptying which may have been worsened by collateral ventilation. The increased airways resistance may also be driving collateral ventilation into the emphysematous lobe and hyperinflation— a potential source of severe symptoms in this patient. Other pathologies that should be considered when encountering hyperlucencies on x-ray or CT that resemble CLE (in infants or adults) include; bronchial atresia, congenital pulmonary airway malformations (CPAM) and spontaneous or traumatic pneumothorax.

Bronchial atresia is generally asymptomatic and most commonly diagnosed incidentally using x-ray or CT, similar to CLE. CLE often coexists with bronchial atresia making it difficult to differentiate these pathologies independently. In adult cases, both bronchial atresia and CLE show locally hyperinflated/emphysematous regions however, bronchial atresia patients exhibit mucocoeles (club-like or rounded shape pathologies at the proximal ends of segmental or subsegmental bronchi) which are easily visualized on thoracic CT. Further investigation with bronchoscopy after the location of mucocoeles may then identify blind-ending bronchi characteristic of bronchial atresia.

Congenital pulmonary airway malformations (CPAMs) appear on CT as cysts attached to segmental bronchi and are frequently observed concomitant with other congenital lung lesions such as bronchopulmonary sequestration or bronchial atresia. The diagnoses of CPAM typically occurs in the neonatal period and is sub-categorized into one of five subtypes with “type 3 CPAM” being the most similar to CLE because it affects at least one entire lobe. In prenatal cases, ultrasound most often identifies the presence of CPAM as hyperechoic lesions with microcystic patterns. If these malformations are not detected

until adulthood, recurrent pulmonary infections are the most common finding that subsequently may result in incidental chest x-ray or CT findings.

Finally, CLE may resemble pneumothorax on chest x-ray and/or CT as evidenced by a prominent mediastinal shift opposite the hyperlucent lobe. However, CLE and pneumothorax can be differentiated using conventional chest x-ray where the absence of bronchovascular abnormalities indicates pneumothorax and not CLE. Pneumothorax is more easily differentiated from other diagnoses of localized hyperlucency because these cases most frequently report to urgent care following trauma to the thorax, when the possibility of congenital lesions can be ruled out.

It is important to note that with the increasing use of chest CT, all these pulmonary pathologies may be observed in young adults and frequently, the exact genesis of the malformations may never be determined. In summary, quantitative thoracic imaging provides a way to definitively diagnose and quantify the critical structure-function relationships in an adult case of CLE in whom established measurements of pulmonary function (DL_{CO} , FEV_1) do not.

TEACHING POINT

In a 20 year old with acute, severe chest pain and dyspnea, thoracic CT and ^3He MRI revealed an abnormal atretic bronchus leading to a left upper lobe (LUL) congenital lobar emphysema with acinar duct morphologies that were very different from smoking-related emphysematous bullae. There was also functional imaging evidence of collateral ventilation leaking from the fissure into the LUL, providing an explanation for severe symptoms in this adult in whom pulmonary function (Diffusing capacity of carbon monoxide (DL_{CO}), Forced expiratory volume in one second (FEV_1)) measurements do not.

TABLES

Table 1: Summary Table for Congenital Lobar Emphysema (CLE)

Etiology	<ul style="list-style-type: none"> • Characterized by compression of lung tissue – emphysema, that is usually localized to one but can be several lung lobes • Usually the upper lobes are affected (>50% of cases) • Trapped gas within the localized emphysematous region causes displacement of the mediastinum into the opposite lung
Incidence	<ul style="list-style-type: none"> • Prevalence of 1 in 20,000 to 1 in 30,000
Gender Ratio	<ul style="list-style-type: none"> • Affects males more than females 3:1
Age Predilection	<ul style="list-style-type: none"> • Nearly all cases present within the first year after birth but rare cases have been diagnosed in adulthood
Risk Factors	<ul style="list-style-type: none"> • Prenatal vascular abnormalities • Congenital heart disease (ventricular septal defects, ductus arteriosus)
Treatment	<ul style="list-style-type: none"> • Lobectomy is the accepted treatment for CLE • In older patients conservative management may be effective • In infants and neonates an emergency thoracotomy is sometimes performed
Prognosis	<ul style="list-style-type: none"> • Following surgical intervention, patients generally develop normal lung function without respiratory impairment in follow-up (>1 year)
Findings on Imaging	<ul style="list-style-type: none"> • Localized hyperlucency or regions of reduced density (<- 950HU) on x-ray computed tomography (CT) scans • Mediastinal shift towards the opposite lung from the affected lobe • Tracheo-bronchial and abnormalities • Localized abnormalities to the pulmonary vasculature in the affected lung lobe

Table 2. Differential Diagnosis Table for Congenital Lobar Emphysema				
Disease	Clinical	X-ray	CT	Other Modalities
Pulmonary Causes				
Congenital Lobar Emphysema	<ul style="list-style-type: none"> Dyspnea, tachypnea, wheezing, tachycardia and cyanosis are common symptoms. Fifty percent symptomatic in the neonatal period. 	<ul style="list-style-type: none"> Hyperlucency of involved lobe, most commonly left upper lobe (LUL). Herniation of hyperinflated lobe to opposite side with mediastinal shift and adjacent lobe collapse. Flattening of ipsilateral diaphragm. Scant lung markings are usually present within the radiolucent area. 	<ul style="list-style-type: none"> Localized hyperlucency and loss of parenchymal density in an individual lung lobe. Attenuated sparse vasculature of the emphysematous lobe. Loss of distal airways in localized emphysematous lobe, compressive atelectasis of other lobes. Abnormally narrowed bronchus or bronchial atresia may be present, however many cases do not have any demonstrable airway anomaly. 	<p>MRI: Prominent region of signal void on ³He MRI ventilation images. Elevated apparent diffusion coefficients (ADC) on diffusion-weighted ³He MR images. Abnormal outer and inner radii and acinar duct sleeve depth in localized emphysematous lobe</p>
Bronchial Atresia	<ul style="list-style-type: none"> Usually asymptomatic and diagnosed incidentally on x-ray in an older child or adult. Since no communication exists with the normal tracheobronchial tree, infection is rare. 	<ul style="list-style-type: none"> Hilar-mass like shadows with hyperexpansion, oligemia and hyperlucency of the peripheral lung fields in the affected lobe. 	<ul style="list-style-type: none"> Presence of a mucocoele (club-like or rounded in shape) with focal interruption of a lobar, segmental, or subsegmental bronchus. Hyperinflation of the affected lobe or segment and emphysematous changes of the peripheral lung fields and occlusion of the bronchus central to the mucocoele are diagnostic criteria. 	<p>Bronchoscopy: A blind-ending bronchus may be found in up to 50% of cases, which is pathognomonic. Helpful to exclude acquired causes of bronchial obstruction such as foreign body, strictures and tumors.</p>
Congenital pulmonary airway malformations (CPAM)	<ul style="list-style-type: none"> Rare cystic lung lesions arising from proliferation of tubular bronchial structures. 5 subtypes with 80% diagnosed in the neonatal period. In adulthood, recurrent pulmonary infection is 	<ul style="list-style-type: none"> Localized patchy density representing the cystic mass with an area of hyperinflation and parenchymal oligemia. Type 3 CPAM can involve an entire lobe or several lobes. TCPAMs that present during adulthood most commonly present in the lower lobes. 	<ul style="list-style-type: none"> Over-inflation with malformed multiple air cysts (irregular and thin walled) connected to the segmental bronchus and well demarcated from the normal lung parenchyma. 	<p>Ultrasound: Usually for prenatal diagnosis revealing a homogeneously hyperechoic lesion with microcystic pattern.</p>
<p>Others: Airways obstruction due to bronchial compression from extrinsic factors (cardiomegaly, lymphadenopathy), endobronchial obstruction (tumor, foreign body, mucus plug) and obliterative bronchiolitis, Unilateral bullus/bullae and post-pneumectomy are other differentials.</p>				

Table 2. Differential Diagnosis Table for Congenital Lobar Emphysema Continued

Disease	Clinical	X-ray	CT	Other Modalities
Pleural Space Causes				
Pneumothorax	<ul style="list-style-type: none"> • .Dyspnea, tachypnea, tachycardia, cyanosis, decreased breath sounds, tracheal deviation in tension pneumothorax. • May be spontaneous, traumatic or iatrogenic. 	<ul style="list-style-type: none"> • Visceral pleural line (and lung) is separated from parietal pleural (and chest wall) with hyperlucency of gas in between. • Tracheal deviation and mediastinal shift maybe present.. 	<ul style="list-style-type: none"> • Most sensitive imaging modality to detect pneumothorax. • Can detect small pneumothoraces, hydro-pneumothorax, loculated pneumothorax, bronchopleural fistulas, underlying emphysema/bullous lung diseases. 	<p>Ultrasound: Used in point-of-care situations eg: emergency department/ICU. Absence of 'lung sliding', seen as a shimmering line due to sliding of visceral and parietal pleural relative to each other is suspicious for a pneumothorax.</p>
<p>Others: A contralateral pleural effusion may sometimes appear as a hyperlucent hemithorax</p>				

ABBREVIATIONS

CLE: Congenital lobar emphysema

CPAM: Congenital pulmonary airway malformations

LUL: Left upper lobe

LLL: Left lower lobe

³He MRI: Hyperpolarized helium-3 magnetic resonance imaging

FGRE: Fast gradient recalled echo sequence

CT: Computed tomography

VDP: Ventilation defect percent

ADC: Apparent diffusion coefficient

RA₉₅₀: Relative area of the lung with attenuation values <-950HU

LAA: Low attenuation areas

LAC: Low attenuation clusters

WA: Airway wall area

LA: Airway lumen area

FEV₁: Forced expiratory volume in one second

Raw: Airways resistance

DL_{CO}: Diffusing capacity of the lung for carbon monoxide

FRC: Functional residual capacity

D_L : Longitudinal diffusion coefficient of acinar ducts

D_T : Transverse diffusion coefficient of the acinar ducts

R : Outer radius of the intra-acinar ducts

h : Depth of the intra-acinar ducts

KEYWORDS

Congenital Lobar Emphysema, Bronchial Atresia, Hyperpolarized ³He, Magnetic Resonance Imaging, Computed Tomography, Emphysema, Airways Disease

References

1. Khalid M SS, Khan B. Congenital Lobar Emphysema in Adult: A rare case report. *Respiratory Medicine CME*. 2010;3:150-2.
2. Kennedy CD, Habibi P, Matthew DJ, Gordon I. Lobar emphysema: long-term imaging follow-up. *Radiology*. 1991;180(1):189-93.
3. Yablonskiy DA, Sukstanskii AL, Leawoods JC, Gierada DS, Bretthorst GL, Lefrak SS, et al. Quantitative in vivo assessment of lung microstructure at the alveolar level with hyperpolarized ³He diffusion MRI. *Proc Natl Acad Sci U S A*. 2002;99(5):3111-6.
4. Kirby M, Owrangi A, Svenningsen S, Wheatley A, Coxson HO, Paterson NA, et al. On the role of abnormal DLCO in ex-smokers without airflow limitation: symptoms, exercise capacity and hyperpolarised helium-3 MRI. *Thorax*. 2013.
5. Haefeli-Bleuer B, Weibel ER. Morphometry of the human pulmonary acinus. *Anat Rec*. 1988;220(4):401-14.
6. Hogg JC, Macklem PT, Thurlbeck WM. The resistance of collateral channels in excised human lungs. *J Clin Invest*. 1969;48(3):421-31.
7. Marshall H, Deppe MH, Parra-Robles J, Hillis S, Billings CG, Rajaram S, et al. Direct visualisation of collateral ventilation in COPD with hyperpolarised gas MRI. *Thorax*. 2012;67(7):613-7.
8. Modat M, McClelland J, Ourselin S. Lung registration using the NiftyReg package. *Medical Image Analysis for the Clinic-A Grand Challenge*. 2010;2010:33-42.

APPENDIX C – Permissions for Reproduction of Scientific Articles

Permission to reproduce manuscript in Chapter 1 (**Pulmonary Abnormalities and Carotid Atherosclerosis in Ex-smokers without Airflow Limitation**) granted by Informa Healthcare and Taylor and Francis Publishing Group as shown below:



Permissions

T & F Reference Number: P051316-03

5/13/2016

Damien Pike
University of Western Ontario

Dear Mr. Pike,

We are in receipt of your request to reproduce your forthcoming article

Damien Pike, Miranda Kirby, Tamas J. Lindenmaier, et al (2015)
Pulmonary Abnormalities and Carotid Atherosclerosis in Ex-smokers without Airflow Limitation
COPD: Journal of Chronic Obstructive Pulmonary Disease 12 (1): 62-70.
DOI: 10.3109/15412555.2014.908833

for use in your dissertation

You retain the right as author to post your Accepted Manuscript on your departmental or personal website with the following acknowledgment: "This is an Accepted Manuscript of an article published in the *COPD: Journal of Chronic Obstructive Pulmonary Disease* online on June 12, 2014, available online: <http://www.tandfonline.com/doi/full/10.3109/15412555.2014.908833>

This permission is all for print and electronic editions.

For the posting of the full article it must be in a secure, password-protected intranet site only.

We will be pleased to grant you permission free of charge on the condition that:

This permission is for non-exclusive English world rights. This permission does not cover any third party copyrighted work which may appear in the material requested.

Full acknowledgment must be included showing article title, author, and full Journal title, reprinted by permission of Taylor & Francis LLC (<http://www.tandfonline.com>).

Thank you very much for your interest in Taylor & Francis publications. Should you have any questions or require further assistance, please feel free to contact me directly.

Sincerely,

Mary Ann Muller
Permissions Coordinator

**COPYRIGHT TRANSFER AGREEMENT**

Date: February 21, 2015 Contributor name: Damien Pike (on behalf of Dr. Grace Parraga's Laboratory)
 Contributor address: Western University, 1151 Richmond Street North, London, Ontario, Canada, N6A 5B7
 Manuscript number: 908833

Re: Manuscript entitled: Pulmonary Abnormalities and Carotid Atherosclerosis in Ex-smokers without Airflow Limitation

For publication in _____ (the "Contribution")

Published by **COPD: Journal of Chronic Obstructive Pulmonary** (the Journal)

Published by **Informa Healthcare USA, Inc.** ("Informa")

Dear Contributor(s):

Thank you for submitting your Contribution for publication. In order to expedite the editing and publishing process and enable Informa to disseminate your Contribution to the fullest extent, we need to have this Copyright Transfer Agreement signed and returned as directed in the Journal's instructions for authors as soon as possible. If the Contribution is not accepted for publication, or if the Contribution is subsequently rejected, this Agreement shall be null and void. **Publication cannot proceed without a signed copy of this Agreement.**

A. COPYRIGHT**1. The Contributor EITHER:**

- (a) assigns to Informa, during the full term of copyright and any extensions or renewals, all copyright in and to the Contribution and all rights therein, including but not limited to the right to publish, republish, transmit, sell, distribute and otherwise use the Contribution in whole or in part in electronic and print editions of the Journal and derivative works throughout the world, in all languages and in all media of expression now known or later developed, and to license or permit others to do so; or
- (b) In the case of U.S. Government employees or NIH funded Contributions (as notified to Informa by Contributor at the end of this Agreement) the Contributor provides Informa with a non-exclusive world-wide licence to publish, republish, transmit, sell, distribute and otherwise use the Contribution in whole or in part in electronic and print editions of the Journal and in derivative works throughout the world, in all languages and in all media of expression now known or later developed and to license or permit others to do so.

2. Reproduction, posting, transmission or other distribution or use of the final Contribution in whole or in part in any medium by the Contributor as permitted by this Agreement requires a citation to the Journal and an appropriate credit to Informa as Publisher, and/or the Society if applicable, suitable in form and content as follows: (Title of Article, Author, Journal Title and Volume/Issue, Copyright © [year], copyright owner as specified in the Journal). Links to the final article on Informa's website are encouraged where appropriate.

B. RETAINED RIGHTS

Notwithstanding the above, the Contributor or, if applicable, the Contributor's Employer, retains all proprietary rights other than copyright, such as patent rights, in any process, procedure or article of manufacture described in the Contribution.

C. PERMITTED USES BY CONTRIBUTOR

1. **Submitted Version.** Informa licenses back the following rights to the Contributor, without charge, in the version of the Contribution as originally submitted for publication:

2.
 - a. After publication of the final article, the right to self-archive on the Contributor's personal website or in the Contributor's institution's/employer's institutional repository or archive. This right extends to both intranets and the Internet. The Contributor may not update the submission version or replace it with the published Contribution. The version posted must contain a legend as follows: This is the pre-peer reviewed version of the following article: [Full cite], which has been published in final form at [link to final article].
 - b. The right to transmit, print and share copies with colleagues.

3. **Accepted Version.** Reuse of the accepted and peer-reviewed (but not final) version of the Contribution shall be solely by separate agreement with Informa. Informa has agreements with certain funding agencies governing reuse of this version. The details of those relationships and other offerings allowing open web use can be obtained from your Informa Editor. NIH grantees should check the box at the bottom of this document.

4. **Final Published Version.** Informa hereby licenses back to the Contributor the following rights with respect to the final published version of the Contribution:

- a. Copies for colleagues. The personal right of the Contributor only to send or transmit individual copies of the final published version in any format to colleagues upon their specific request, provided no fee is charged, and that there is no systematic distribution of the Contribution, e.g. posting on a list serve, website or automated delivery.
- b. Reuse in other publications. The right to reuse the final Contribution or parts thereof for any publication authored or edited by the Contributor (excluding journal articles) where such reused material constitutes less than half of the total material in such publication. In such case, any modifications should be accurately noted.
- c. Teaching duties. The right to include the Contribution in teaching or training duties at the Contributor's institution/place of employment including in course packs, e-reserves, presentation at professional conferences, in-house training, or distance learning. The Contribution may not be used in seminars outside of normal teaching obligations (e.g. commercial seminars). Electronic posting of the final published version in connection with teaching/training at the Contributor's institution/place of employment is permitted subject to the implementation of reasonable access control mechanisms, such as username and password. Posting the final published version on the open Internet is not permitted.
- d. Oral presentations. The right to make oral presentations based on the Contribution.

5. **Article Abstracts, Figures, Tables, Data Sets, Artwork and Selected Text (up to 250 words).**

Contributors may reuse figures, tables, data sets, artwork, and selected text up to 250 words from their Contributions as finally published, provided the following conditions are met:

- a) Full and accurate credit must be given to the Contribution.
- b) Modifications to the figures, tables and data must be noted. Otherwise, no changes may be made.
- c) The reuse may not be made for direct commercial purposes, or for financial consideration to the Contributor.
- d) Nothing herein shall permit dual publication in violation of Journal ethical practices.

D. CONTRIBUTIONS OWNED BY EMPLOYER

1. If the Contribution was written by the Contributor in the course of the Contributor's employment (as a "work-made-for-hire" in the course of employment), the Contribution is owned by the company/employer which must sign this Agreement (in addition to the Contributor's signature) in the space provided below. In such case, the company/employer hereby assigns to Informa, during the full term of copyright all copyright in and to the Contribution for the full term of copyright throughout the world as specified in paragraph A above.
2. In addition to the rights specified as retained in paragraph B above and the rights granted back to the Contributor pursuant to paragraph C above, Informa hereby grants back, without charge, to such company/employer, its subsidiaries and divisions, the right to make

LCPD 908833 Pulmonary Abnormalities and Carotid Atherosclerosis in Ex-smokers without A...

copies of and distribute the final published Contribution internally in print format or electronically on the Company's internal network. Copies so used may not be resold or distributed externally. However the company/employer may include information and text from the Contribution as part of an information package included with software or other products offered for sale or license or included in patent applications. Posting of the final published Contribution by the institution on a public access website may only be done with Informa's written permission, and payment of any applicable fee(s). Also, upon payment of Informa's reprint fee, the Institution may distribute print copies of the published Contribution externally.

E. GOVERNMENT CONTRACTS

In the case of a Contribution prepared under U.S. Government contract or grant, the U.S. Government may reproduce, without charge, all or portions of the Contribution and may authorise others to do so, for official U.S. Government purposes only, if the U.S. Government contract or grant so requires. (U.S. Government, U.K. Government, and other government employees: see notes at end).

F. COPYRIGHT NOTICE

The Contributor and the company/employer agree that any and all copies of the final published version of the Contribution or any part thereof distributed or posted by them in print or electronic format as permitted herein will include the notice of copyright as stipulated in the Journal and a full citation to the Journal as published by Informa.

G. CONTRIBUTOR'S REPRESENTATIONS

The Contributor represents that the Contribution is the Contributor's original work, all individuals identified as Contributors actually contributed to the Contribution, and all individuals who contributed are included.

If the Contribution was prepared jointly, the Contributor agrees to inform the co-Contributors of the terms of this Agreement and to obtain their signature to this Agreement or their written permission to sign on their behalf. The Contribution is submitted only to this Journal and has not been published before. (If excerpts from copyrighted works owned by third parties are included, the Contributor will obtain written permission from the copyright owners for all uses as set forth in Informa's permissions form or in the Journal's Instructions for Contributors, and show credit to the sources in the Contribution.) The Contributor also warrants that the Contribution contains no libellous or unlawful statements, does not infringe upon the rights (including without limitation

the copyright, patent or trademark rights) or the privacy of others, or contain material or instructions that might cause harm or injury. The Contributor further warrants that:

- (a) wherever possible and where appropriate any patient, client or participant in any research, experiment or study, who is mentioned in the Contribution has given consent for material pertaining to themselves, to be included in the Contribution and that they have acknowledged to the Contributor that they cannot be identified by the Contribution in any way; and
- (b) they shall include in the Contribution appropriate warnings concerning any particular hazards that may be involved in carrying out experiments or procedures or involved in instructions, materials, or formulae described in the Contribution, and shall mention explicitly relevant safety precautions and give, if an accepted code of practice is relevant, a reference to the relevant standard or code.

The Contributor undertakes to advise the Publisher if any part of the Contribution is affected by technological, commercial or legislative developments which might make it necessary or advisable for the Article to be amended, altered or updated.

H. ASSIGNMENT

Under this Agreement the Publisher may assign its rights or obligations without the consent of the Contributor.

I. NO EMPLOYMENT

Nothing in the Agreement shall constitute or should be construed as constituting a partnership or contract of employment between the parties and the Publisher shall not be responsible for the provision of any benefits, pension, sick pay or national insurance contributions. In addition, the Contributor shall be responsible for all taxes relating to the Contributor's services under this Agreement and shall keep the Publisher indemnified against any claim against the Publisher in respect of the same.

J. GOVERNING LAW

Each Party to this Agreement irrevocably agrees that this Agreement is construed under English law and submits to the non-exclusive jurisdiction of the English courts to settle any disputes arising out of or in connection with this Agreement or its formation.

CHECK ONE BOX:

Contributor-owned work

Company/Institution-owned work (made-for-hire in the course of employment)

Company or institution (Employer-for-Hire) _____

Authorised signature of employer _____

Date: _____

U.S. Government work

Note to U.S. Government Employees

A contribution prepared by a U.S. federal government employee as part of the employee's official duties, or which is an official U.S. Government publication is called "U.S. Government Work," and is in the public domain in the United States. In such use, the employee may cross out Paragraph A1(a) but must sign (in the Contributor's signature line) and return this Agreement. If the Contribution was not prepared as part of the employee's duties or is not an official U.S. Government publication, it is not a U.S. Government Work.

U.K. Government work
(Crown Copyright)

Note to U.K. Government Employees

The rights in a Contribution prepared by an employee of a U.K. government department, agency or other Crown body as part of his/her official duties, or which is an official government publication, belong to the Crown. U.K. government authors should submit a signed declaration form together with this Agreement. The form can be obtained via <http://www.opsi.gov.uk/advice/crown-copyright/copyright-guidance/publication-of-articles-written-by-ministers-and-civil-servants.htm>

Other Government work

Note to Non-U.S., Non U.K. Government Employees

If your status as a government employee legally prevents you from signing this Agreement please contact the editorial office.

NIH Grantees
(Also check another box)

Note to NIH Grantees

Pursuant to NIH mandate, Authors may post the accepted version of Contributions authorised by NIH grant-holders to PubMed Central upon acceptance. This accepted version will be made publicly available 12 months after publication. For further information see http://publicaccess.nih.gov/address_copyright.htm

ALL CLASSES OF CONTRIBUTOR MUST SIGN HERE:

Contributor's signature _____

Date: Feb. 21, 2015

Type or print name and title Damien Pike

Permission to reproduce the manuscript in Chapter 2 (**Ventilation Heterogeneity in Ex-smokers without Airflow Limitation**) granted by Elsevier Publishing in the following correspondence:

**ELSEVIER LICENSE
TERMS AND CONDITIONS**

Jun 01, 2016

This is a License Agreement between Damien Pike ("You") and Elsevier ("Elsevier") provided by Copyright Clearance Center ("CCC"). The license consists of your order details, the terms and conditions provided by Elsevier, and the payment terms and conditions.

All payments must be made in full to CCC. For payment instructions, please see information listed at the bottom of this form.

Supplier	Elsevier Limited
Registered Company Number	1962084
Customer name	Damien Pike
Customer address	
License number	3784150333090
License date	Jan 06, 2016
Licensed content publisher	Elsevier
Licensed content publication	Academic Radiology
Licensed content title	Ventilation Heterogeneity in Ex-smokers without Airflow Limitation
Licensed content author	Damien Pike, Miranda Kirby, Fumin Guo, David G. McCormack, Grace Parraga
Licensed content date	August 2015
Licensed content volume number	22
Licensed content issue number	8
Number of pages	11
Start Page	1068
End Page	1078
Type of Use	reuse in a thesis/dissertation
Portion	full article
Format	both print and electronic
Are you the author of this Elsevier article?	Yes
Will you be translating?	No
Title of your thesis/dissertation	Magnetic Resonance Imaging Biomarkers of Chronic Obstructive Pulmonary Disease
Expected completion date	Jul 2016
Estimated size (number of pages)	
Elsevier VAT number	GB 494 6272 12
Permissions price	0.00 CAD
VAT/Local Sales Tax	0.00 CAD / 0.00 GBP
Total	0.00 CAD

Permission to reproduce the manuscript in in Chapter 3 (**Regional Heterogeneity of Chronic Obstructive Pulmonary Disease Phenotypes: Pulmonary ^3He Magnetic Resonance Imaging and Computed Tomography**) granted by Taylor and Francis Publishing Group as shown below:



Permissions

T & F Reference Number: P010516-01

1/5/2016

Damien Pike
University of Western Ontario

Dear Mr. Pike,

We are in receipt of your request to reproduce your forthcoming article

Damien Pike
Regional Heterogeneity of Chronic Obstructive Pulmonary Disease Phenotypes: Pulmonary ^3He Magnetic Resonance Imaging and Computed Tomography
Manuscript ID: COPD-2015-0164.R1
COPD: Journal of Chronic Obstructive Pulmonary Disease (in press)

for use in your dissertation

You retain the right as author to post your Accepted Manuscript on your departmental or personal website with the following acknowledgment: "This is an Accepted Manuscript of an article published in the *COPD: Journal of Chronic Obstructive Pulmonary Disease* online [Date of Online Publication], available online: <http://www.tandfonline.com> [Article DOI]"

This permission is all for print and electronic editions.

For the posting of the full article it must be in a secure, password-protected intranet site only.

An embargo period of twelve months applies for the Accepted Manuscript to be posted to an institutional or subject repository.

We will be pleased to grant you permission free of charge **with the understanding that Taylor & Francis is the first to publish the full article** on the condition that:

This permission is for non-exclusive English world rights. This permission does not cover any third party copyrighted work which may appear in the material requested.


Full acknowledgment must be included showing article title, author, and full Journal title, reprinted by permission of Taylor & Francis LLC (<http://www.tandfonline.com>).

Thank you very much for your interest in Taylor & Francis publications. Should you have any questions or require further assistance, please feel free to contact me directly.


Sincerely,

Mary Ann Muller
Permissions Coordinator

Permission to reproduce review article manuscript in Appendix A (**Imaging Evidence of the Relationship between Carotid Atherosclerosis and Chronic Obstructive Pulmonary Disease**) granted by Future Medicine on behalf of Future Science Group as shown below:



an imprint of



Welcome University of Western Ontario | Login via [Athens](#) or your [home institution](#)

Home	Browse Journals	Browse eBooks	Advanced Search	Contact Us	About Us	My Profile			
<div style="background-color: #2c3e50; color: white; padding: 2px;">Titles</div> Future Medicine eBooks Future Medicine Journals Future Science eBooks Future Science Journals	<h2 style="margin: 0;">Permissions</h2> <p>Welcome to Future Medicine Ltd permissions page. Written permission is required from the publisher if you wish to reproduce any of our material.</p> <h3 style="margin: 0;">Are you a Future Medicine author seeking to reuse your own material?</h3> <p>Once a manuscript has been accepted for publication, authors may contact Future Medicine Ltd for permission to use all or part of an article in other publications for non-commercial purposes. In these cases, permission should be granted free of charge.</p> <p>Authors can find out more information on our For Authors page</p> <h3 style="margin: 0;">Do you intend to reuse material from Future Medicine publications in other print and/or online journal or book publications?</h3> <p>Reuse of material such as figures, tables, boxes or text blocks attracts a permission fee (unless the publisher is a co-signatory to the STM permission guidelines). Please contact permissions@futuremedicine.com explaining which material you intend to use, the name of the publisher, in which publication and in what format.</p> <p>Future Medicine Ltd is a signatory to the STM Permissions Guidelines produced by the International Association of Scientific, Medical and Technical Publishers (http://www.stm-assoc.org/). Future Medicine requires express permission requests to be made irrespective of whether charges apply.</p> <p>If the reused material is to appear in a conventional print or electronic book or journal (only) produced by a <i>publisher that is a co-signatory to the STM agreement</i>, you may make the following use of the material without charge:</p> <ul style="list-style-type: none"> • Use up to three figures (including tables) from a journal article or book chapter, but: <ul style="list-style-type: none"> ◦ Not more than five figures from a whole book or journal issue/edition; ◦ Not more than six figures from an annual journal volume; and ◦ Not more than three figures from works published by a single publisher for an article, and not more than three figures from works published by a single publisher for a book chapter (and in total not more than thirty figures from a single publisher for re-publication in a book, including a multi-volume book with different authors per chapter) • Use single text extracts of less than 400 words from a journal article or book chapter, but not more than a total of 800 words from a whole book or journal issue/edition. <h3 style="margin: 0;">Do you intend to reuse material in other media intended for commercial use, such as promotional packs or pamphlets?</h3> <p>If the intended publication vehicle is not a conventional print or electronic book or journal (e.g. educational information attracting commercial sponsorship) fees will apply. Please contact permissions@futuremedicine.com in such instances or to establish whether charges apply.</p> <div style="border: 2px solid red; padding: 5px;"> <h3 style="margin: 0;">Are you planning on using our material in a Thesis/dissertation?</h3> <p>If you are using figure(s)/table(s), permission is granted for use in print and electronic versions of your thesis/dissertation</p> <p>A full text article may be used only in print versions of a dissertation/thesis. Future Medicine Ltd does not permit the reproduction of full text articles in electronic versions of theses or dissertations.</p> </div>						<div style="background-color: #2c3e50; color: white; padding: 2px;">Resources</div> Register For Authors For Librarians For Advertisers Submitting an article	<div style="background-color: #2c3e50; color: white; padding: 2px;">Services</div> Alerts Subscriptions/Pricing Institutional Trials Reprints/ Publication Solutions Supplements Advertising Permission Requests Press Releases/News	<div style="background-color: #2c3e50; color: white; padding: 2px;">Downloads/Links</div> Online Submission 2015 Catalogue Library Recommendation Future Science Group

Permission to reproduce Case Report in Appendix B (**Pulmonary Imaging Abnormalities in an Adult Case of Congenital Lobar Emphsema**) granted by Dr. Roland Talanow (Editor in chief of the Journal of Radiology Case Reports) as shown:




Sun 22/02/2015 8:16 PM

Roland Talanow, M.D., Ph.D.

RE: Permission to Use Copyrighted Material in a Doctoral/Master's Thesis

To Damien Pike

 Click here to download pictures. To help protect your privacy, Outlook prevented automatic download of some pictures in this message.

Dr. Pike,

If you are properly referencing the article (including the journal URL), that should be fine with us.
Good luck and best of success with your thesis!

Sincerely,

Roland Talanow M.D., Ph.D.

Editor-in-Chief

Journal of Radiology Case Reports

Indexed - open access - interactive

<http://www.RadiologyCases.com>

APPENDIX D – Research Ethics Board Approval Notices



Office of Research Ethics

The University of Western Ontario

Use of Human Subjects - Ethics Approval Notice

Principal Investigator: Dr. G. Parraga

Review Number: 15930

Review Level: Full Board

Review Date: February 10, 2009

Protocol Title: Longitudinal Study of Helium-3 Magnetic Resonance Imaging of COPD

Department and Institution: Diagnostic Radiology & Nuclear Medicine, Robarts Research Institute

Sponsor: INTERNAL RESEARCH FUND-UWO

Ethics Approval Date: May 25, 2009

Expiry Date: November 30, 2013

Documents Reviewed and Approved: UWO Protocol, Letter of information & consent form for Patients dated March 26/09 & Letter of information & consent form for Healthy Volunteers dated March 26/09

Documents Received for Information: Protocol, January 27, 2009; IB, ed 6, 09 Sep. 05

This is to notify you that The University of Western Ontario Research Ethics Board for Health Sciences Research Involving Human Subjects (HSREB) which is organized and operates according to the Tri-Council Policy Statement: Ethical Conduct of Research Involving Humans and the Health Canada/ICH Good Clinical Practice Practices: Consolidated Guidelines; and the applicable laws and regulations of Ontario has reviewed and granted approval to the above referenced study on the approval date noted above. The membership of this REB also complies with the membership requirements for REB's as defined in Division 5 of the Food and Drug Regulations.

The ethics approval for this study shall remain valid until the expiry date noted above assuming timely and acceptable responses to the HSREB's periodic requests for surveillance and monitoring information. If you require an updated approval notice prior to that time you must request it using the UWO Updated Approval Request Form.

During the course of the research, no deviations from, or changes to, the protocol or consent form may be initiated without prior written approval from the HSREB except when necessary to eliminate immediate hazards to the subject or when the change(s) involve only logistical or administrative aspects of the study (e.g. change of monitor, telephone number). Expedited review of minor change(s) in ongoing studies will be considered. Subjects must receive a copy of the signed information/consent documentation.

Investigators must promptly also report to the HSREB:

- changes increasing the risk to the participant(s) and/or affecting significantly the conduct of the study;
- all adverse and unexpected experiences or events that are both serious and unexpected;
- new information that may adversely affect the safety of the subjects or the conduct of the study.

If these changes/adverse events require a change to the information/consent documentation, and/or recruitment advertisement, the newly revised information/consent documentation, and/or advertisement, must be submitted to this office for approval.

Members of the HSREB who are named as investigators in research studies, or declare a conflict of interest, do not participate in discussion related to, nor vote on, such studies when they are presented to the HSREB.

Chair of HSREB: Dr. Joseph Gilbert

Ethics Officer to Contact for Further Information

<input checked="" type="checkbox"/> Janice Sutherland (jsuther@uwo.ca)	<input type="checkbox"/> Elizabeth Wambolt (ewambolt@uwo.ca)	<input type="checkbox"/> Grace Kelly (grace.kelly@uwo.ca)	<input type="checkbox"/> Denise Grafton (dgrafton@uwo.ca)
---	---	--	--

This is an official document. Please retain the original in your files.

cc: ORE File
LHRI



Office of Research Ethics

The University of Western Ontario

Use of Human Subjects - Ethics Approval Notice

Principal Investigator: Dr. G. Parraga	Review Level:
Review Number: 12433E	Revision Number: 5
Review Date: February 4, 2011	Approved Local # of Participants: 100
Protocol Title: 3-dimensional Ultrasound Software and Hardware Development	
Department and Institution: Diagnostic Radiology & Nuclear Medicine, Robarts Research Institute	
Sponsor: CIHR-CANADIAN INSTITUTE OF HEALTH RESEARCH	
Ethics Approval Date: February 4, 2011	Expiry Date: December 31, 2015
Documents Reviewed and Approved: Revised Study End Date	
Documents Received for Information:	

This is to notify you that The University of Western Ontario Research Ethics Board for Health Sciences Research Involving Human Subjects (HSREB) which is organized and operates according to the Tri-Council Policy Statement: Ethical Conduct of Research Involving Humans and the Health Canada/ICH Good Clinical Practice Practices: Consolidated Guidelines; and the applicable laws and regulations of Ontario has reviewed and granted approval to the above referenced revision(s) or amendment(s) on the approval date noted above. The membership of this REB also complies with the membership requirements for REB's as defined in Division 5 of the Food and Drug Regulations.

The ethics approval for this study shall remain valid until the expiry date noted above assuming timely and acceptable responses to the HSREB's periodic requests for surveillance and monitoring information. If you require an updated approval notice prior to that time you must request it using the UWO Updated Approval Request Form.

During the course of the research, no deviations from, or changes to, the protocol or consent form may be initiated without prior written approval from the HSREB except when necessary to eliminate immediate hazards to the subject or when the change(s) involve only logistical or administrative aspects of the study (e.g. change of monitor, telephone number). Expedited review of minor change(s) in ongoing studies will be considered. Subjects must receive a copy of the signed information/consent documentation.

Investigators must promptly also report to the HSREB:

- changes increasing the risk to the participant(s) and/or affecting significantly the conduct of the study;
- all adverse and unexpected experiences or events that are both serious and unexpected;
- new information that may adversely affect the safety of the subjects or the conduct of the study.

If these changes/adverse events require a change to the information/consent documentation, and/or recruitment advertisement, the newly revised information/consent documentation, and/or advertisement, must be submitted to this office for approval.

Members of the HSREB who are named as investigators in research studies, or declare a conflict of interest, do not participate in discussion related to, nor vote on, such studies when they are presented to the HSREB.

Chair of HSREB: Dr. Joseph Gilbert
FDA Ref. #: IRB 00000940

Ethics Officer to Contact for Further Information		
<input type="checkbox"/> Janice Sutherland	<input type="checkbox"/> Elizabeth Wambolt	<input checked="" type="checkbox"/> Grace Kelly

This is an official document. Please retain the original in your files.

cc: ORE File



Office of Research Ethics

The University of Western Ontario

Use of Human Subjects - Ethics Approval Notice

Principal Investigator: Dr. G. Parraga
Review Number: 17396
Review Date: September 14, 2010
Protocol Title: Longitudinal 3He Magnetic Resonance Imaging of Health Lung
Department and Institution: Imaging, Robarts Research Institute
Sponsor: CIHR-CANADIAN INSTITUTE OF HEALTH RESEARCH
Ethics Approval Date: November 09, 2010
Expiry Date: September 30, 2014
Documents Reviewed and Approved: UWO Protocol (including instruments noted in Section 8.1), Letter of Information and Consent Form dated Sept. 27, 2010 version 2, and Advertisement.
Documents Received for Information: Clinical Study Protocol Version #1 27 August 2010; IB NC100182-Inhalation (Hyperpolarised 3HE) 6th edition 09 Sep 05; NC1000182 IB April 7, 2009; Product Monograph Ventolin HFA

This is to notify you that The University of Western Ontario Research Ethics Board for Health Sciences Research Involving Human Subjects (HSREB) which is organized and operates according to the Tri-Council Policy Statement: Ethical Conduct of Research Involving Humans and the Health Canada/ICH Good Clinical Practice Practices: Consolidated Guidelines; and the applicable laws and regulations of Ontario has reviewed and granted approval to the above referenced study on the approval date noted above. The membership of this REB also complies with the membership requirements for REB's as defined in Division 5 of the Food and Drug Regulations.

The ethics approval for this study shall remain valid until the expiry date noted above assuming timely and acceptable responses to the HSREB's periodic requests for surveillance and monitoring information. If you require an updated approval notice prior to that time you must request it using the UWO Updated Approval Request Form.

During the course of the research, no deviations from, or changes to, the protocol or consent form may be initiated without prior written approval from the HSREB except when necessary to eliminate immediate hazards to the subject or when the change(s) involve only logistical or administrative aspects of the study (e.g. change of monitor, telephone number). Expedited review of minor change(s) in ongoing studies will be considered. Subjects must receive a copy of the signed information/consent documentation.

Investigators must promptly also report to the HSREB:

- changes increasing the risk to the participant(s) and/or affecting significantly the conduct of the study;
- all adverse and unexpected experiences or events that are both serious and unexpected;
- new information that may adversely affect the safety of the subjects or the conduct of the study.

If these changes/adverse events require a change to the information/consent documentation, and/or recruitment advertisement, the newly revised information/consent documentation, and/or advertisement, must be submitted to this office for approval.

Members of the HSREB who are named as investigators in research studies, or declare a conflict of interest, do not participate in discussion related to, nor vote on, such studies when they are presented to the HSREB.

Chair of HSREB: Dr. Joseph Gilbert
 FDA Ref. #: IRB 00000940

Ethics Officer to Contact for Further Information

Janice Sutherland Elizabeth Wambolt Grace Kelly

This is an official document. Please retain the original in your files.

cc: ORE File
 LHRI

APPENDIX E – Curriculum Vitae

EDUCATION

- August 2015 - present **Doctor of Medicine (MD) Candidate**
Memorial University of Newfoundland, St. John's
Newfoundland and Labrador, Canada
 Faculty of Medicine, Health Sciences Centre
- August 2012 - present **Doctor of Philosophy (PhD) Candidate**
The University of Western Ontario, London, Ontario, Canada
 Department of Medical Biophysics
Supervisor: Grace Parraga PhD
Supervisory Committee: Daniel Hackam MD, PhD, FRCPC, David McCormack MD, FRCPC, Aaron Fenster PhD, FCCPM
- Sep. 2008 – April 2012 **Bachelor of Science (BSc)**
Memorial University of Newfoundland, St. John's,
Newfoundland and Labrador, Canada
 Department of Biochemistry and Department of Physics and Physical Oceanography
Supervisors: Valerie Booth PhD, Michael Morrow PhD
- ### RESEARCH EXPERIENCE
- June 2012 – present Graduate Student Research Assistant
 Department of Medical Biophysics
 The University of Western Ontario
Project: Hyperpolarized ³He Magnetic Resonance Imaging Phenotypes of Chronic Obstructive Pulmonary Disease
Supervisor: Dr. Grace Parraga
- April 2012 – June 2012 Research Assistant, Summer Research Assistantship
 Department of Biochemistry/Department of Physics and Physical Oceanography
 Memorial University of Newfoundland
Project: Characterizing Antimicrobial Peptide Membrane Interactions Using ³¹P Nuclear Magnetic Resonance
Supervisors: Dr. Valerie Booth and Dr. Michael Morrow

- Sep. 2011 – April 2012 Research Assistant (part time)
 Department of Biochemistry/Department of Physics and Physical Oceanography
 Memorial University of Newfoundland
Project: Differential Scanning Calorimetry of Antimicrobial Peptides
Supervisors: Dr. Valerie Booth and Dr. Michael Morrow
- May 2011 – Sep. 2011 Research Assistant, Summer Student Assistantship
 Department of Biochemistry/Department of Physics and Physical Oceanography
 Memorial University of Newfoundland
Project: Antimicrobial Peptide Structure-Function in Membranes
Supervisors: Dr. Valerie Booth and Dr. Michael Morrow
- Sep. 2010 – April 2011 Research Assistant (part time)
 Department of Biochemistry/Department of Physics and Physical Oceanography
 Memorial University of Newfoundland
Project: Antimicrobial Peptide Membrane Activity in E. Coli using ³¹P Nuclear Magnetic Resonance
Supervisors: Dr. Valerie Booth and Dr. Michael Morrow
- May 2010 – Sep. 2010 Research Assistant, Summer Research Assistantship
 Department of Biochemistry/Department of Physics and Physical Oceanography
 Memorial University of Newfoundland
Project: Structure-Function Relationship of Histidine Rich Antimicrobial Peptides Using Nuclear Magnetic Resonance Imaging
Supervisors: Dr. Valerie Booth and Dr. Michael Morrow

ACADEMIC AWARDS, SCHOLARSHIPS AND DISTINCTIONS

- Apr. 2016 Mach Gaensslen Foundation Research Scholarship
Provincial
Awarded to support the research endeavors of the authors with the highest ranked research proposals to the MGF Research Program
\$5000
- Feb. 2016 Memorial University of Newfoundland Medical Research Forum
 Oral Scientific Presentation and Abstract Award (First Place)
Provincial
Awarded to the author and speaker of the highest ranked scientific abstract and oral presentation
\$3000

- Mar. 2015 Natural Sciences and Engineering Research Council of Canada (NSERC) Doctoral Postgraduate Scholarship (Declined)
National
Awarded to the highest caliber doctoral scholars pursuing research in the natural sciences and engineering based on academic excellence, research ability and potential, scientific communication and leadership abilities
\$42,000
- Feb. 2015 International Society for Magnetic Resonance in Medicine (ISMRM) Abstract Scholarship and Educational Stipend Award
International
Awarded to support the attendance of students, postdoctoral and clinical trainees to present abstracts at the scientific meeting
\$500
- Sep. 2014 Western Graduate Research Scholarship, The University of Western Ontario
Institutional
Awarded to a full time graduate student who has maintained first-class academic average
\$4,500
- Sep. 2014 Canadian Institutes of Health Research (CIHR) Vascular Research Scholar
Provincial
Awarded to CIHR Vascular Research Fellows who have made exceptional scientific progress in the field of vascular research through peer-reviewed publications and presentations
- May 2014 Ontario Graduate Scholarship - Queen Elizabeth II Graduate Scholarship in Science and Technology
Provincial
Awarded to a select number of graduate students enrolled in Ontario universities based on academic merit, research excellence and high impact contributions to their field
\$15,000
- Mar. 2014 American Thoracic Society International Conference Respiratory Structure and Function Scholarship
International
Awarded to the authors of the highest ranked abstracts submitted for presentation at the international ATS conference
\$500

- Feb. 2014 Alan C. Groom Award Nominee
Institutional
Select graduate students who have given exceptional oral presentations at the University of Western Ontario Medical Biophysics Seminar are nominated for the Alan C. Groom Seminar Award
- Oct. 2013 Radiological Society of North America (RSNA) Research Trainee Prize
International
Awarded to honor the most outstanding scientific contribution submitted and accepted to the RSNA international meeting for presentation
\$1000
- Sep. 2013 Western Graduate Research Scholarship, The University of Western Ontario
Institutional
Awarded to a full time graduate student who has maintained first-class academic average
\$4,500
- July 2013 Radiological Society of North America Research Trainee Nominee
International
The highest ranked abstracts submitted to the international meeting are nominated by the RSNA committee for the Trainee Research Prize
- Apr. 2013 University of Western Ontario School of Graduate Studies Out of Province Scholarship
Institutional
Awarded to the highest ranked full time out-of-province graduate students at The University of Western Ontario
\$500
- Jan. 2013 International Society for Magnetic Resonance in Medicine International Conference Abstract Award
International
Awarded to the authors of the highest ranked scientific abstracts submitted to the ISMRM International Conference
\$440

Western Graduate Research Scholarship, The University of Western

- Sep. 2012 Ontario
Institutional
Awarded to a full time graduate student who has maintained first-class academic average
\$4,500
- Sep. 2012 University of Western Ontario School of Graduate Studies Out of Province Scholarship
Institutional
Awarded to the highest ranked full time out-of-province graduate students at The University of Western Ontario
\$500
- Sep. 2012 Canadian Institutes of Health Research (CIHR) Strategic Training Program in Vascular Research
Provincial
Awarded to graduate trainees who show the potential to perform transdisciplinary research and provide high-impact contributions to the understanding, treatment and prevention of vascular diseases
\$24,000
- Apr. 2011 Harlow University Travel Award (Memorial University Biochemistry Research Program)
Institutional
Awarded to undergraduate students who are undertaking a semester of studies at Memorial University Harlow Campus based on academic merit
\$500

PEER-REVIEWED PUBLICATIONS AND PROCEEDINGS

A. Peer Reviewed Journal Manuscripts (16 Published)

Published (16)

1. J Cheng, **D Pike**, T Chow, M Kirby, G Parraga and B Chiu. Three-Dimensional Ultrasound Measurements of Carotid Vessel Wall and Plaque Thickness and their Relationship with Pulmonary Abnormalities in Ex-smokers Without Airflow Limitation. *The International Journal of Cardiovascular Imaging*; DOI: 10.1007/s10554-016-0931-z
2. **D Pike**, M Kirby, R Eddy, F Guo, DPI Capaldi, A Ouriadov, DG McCormack and G Parraga. Regional Heterogeneity of Chronic Obstructive Pulmonary Disease Phenotypes: Pulmonary ³He Magnetic Resonance Imaging and Computed Tomography. *The Journal of Chronic Obstructive Pulmonary Disease*; DOI: 10.3109/15412555.2015.1123682
3. C Davis, K Sheikh, **D Pike**, S Svenningsen, DG McCormack, D O'Donnell, JA Neder and G Parraga. Ventilation Heterogeneity in Never-smokers and COPD: Comparison of Pulmonary Functional Magnetic Resonance Imaging with Poorly Communicating Fraction derived from Plethysmography. *Academic Radiology*; DOI: 10.1016/j.acra.2015.10.022
4. DPI Capaldi, N Zha, F Guo, **D Pike**, DG McCormack, IA Cunningham and G Parraga. Pulmonary Imaging Biomarkers of Gas-trapping and Emphysema in COPD: ³He MRI and CT Parametric Response Maps. *Radiology*; DOI: 10.1148/radiol.2015151484
5. N Zha, **D Pike**, S Svenningsen, DPI Capaldi, DG McCormack and G Parraga. Second-Order Texture Measurements of ³He Ventilation MRI: Proof of Concept Evaluation of Asthma Bronchodilator Response. *Academic Radiology* DOI: 10.1016/j.acra.2015.10.010
6. M Kirby, **D Pike**, DG McCormack, DD Sin, S Lam, HO Coxson and G Parraga. Do Imaging Measurements of Emphysema and Airway Disease Explain Symptoms and Exercise Capacity in Mild-moderate COPD? *Radiology*; DOI: 10.1148/radiol.2015150037
7. **D Pike**, M Kirby, F Guo, DG McCormack and G Parraga. Ventilation Heterogeneity in Ex-smokers without Airflow Limitation. *Academic Radiology*; DOI: 10.1017/j.acra.2015.04.006
8. **D Pike**, S Mohan, W Ma, JF Lewis and G Parraga. Pulmonary Imaging Abnormalities in an Adult Case of Congenital Lobar Emphysema. *The Journal of Radiology Case Reports*; DOI: 10.3941/jrcr.v9i2.2048 2015

9. M McDonald, M Mannion, **D Pike**, K Lewis, A Flynn, M Browne, L Madera, MRP Coombs, D Hoskin, M Rise and V Booth. Structure-Function Relationships in Histidine Rich Antimicrobial Peptides From Cod. *Biochimica et Biophysica Acta (BBA) Biomembranes*; DOI: 10.1016/j.bbamem.2015.03.030
10. M Kirby, **D Pike**, DG McCormack, DD Sin, S Lam, HO Coxson and G Parraga. Thoracic Imaging Network of Canada (TINCan) Study Objectives. *The Journal of Chronic Obstructive Pulmonary Disease Foundation*; DOI: 10.15326/JCOPDF.2014.1.2.0136, 2014
11. W Ma, K Sheikh, S Svenningsen, **D Pike**, F Guo, R Etemad-Rezai, J Leipsic, HO Coxson, DG McCormack and G Parraga. Ultra-short echo-time pulmonary MRI: Evaluation and reproducibility in COPD subjects with and without bronchiectasis. *Journal of Magnetic Resonance Imaging*; DOI: 10.1002/jmri.24680, 2014
12. M Kirby, **D Pike**, HO Coxson, DG McCormack and G Parraga. Hyperpolarized ³He Ventilation Defects Predict Pulmonary Exacerbations in Mild-moderate COPD. *Radiology*; DOI: 10.1148/radiol.14140161, 2014
13. **D Pike**, M Kirby, TJ Lindenmaier, K Sheikh, C Neron, DG Hackam, JD Spence, A Fenster, NAM Paterson, HO Coxson, DG McCormack, DD Sin and G Parraga. Pulmonary Abnormalities and Carotid Atherosclerosis in Ex-smokers without Airflow Limitation. *Journal of Chronic Obstructive Pulmonary Disease*; DOI: 10.3109: 1-0, 2014
14. **D Pike**, TJ Lindenmaier, DD Sin and G Parraga. Imaging Evidence of the Relationship between Atherosclerosis and Chronic Obstructive Pulmonary Disease. *Imaging in Medicine*; DOI: 10.2217/iim. 13.70, 2013
15. TJ Lindenmaier, DN Buchanan, **D Pike**, T Hartley, RD Reid, JD Spence, R Chan, M Sharma, PL Prior, N Suskin and G Parraga. One, two and three-dimensional ultrasound measurements of carotid atherosclerosis before and after cardiac rehabilitation: preliminary results of a randomized controlled trial. *Cardiovascular Ultrasound*; DOI: 11 (1):39, 2013
16. **D Pike** and G Parraga. COPD: More imaging, more phenotypes...better care? *Canadian Respiratory Journal*; DOI: 20 (2):90, 2013

B. Peer Reviewed Presentations and Conference Proceedings (11 Oral (Podium) Presentations, 33 Poster Presentations)

Oral (Podium) Presentations and Conference Proceedings (11)

1. E Lessard, A Ouriadov, **D Pike***, DPI Capaldi, DG McCormack and G Parraga. Novel Biomarkers of Lung Function Destruction and Emphysema Progression in COPD Using Inhaled Gas MRI Morphometry. *The American Thoracic Society Annual Scientific Meeting 2016, San Francisco, CA, USA*
*Speaker
2. RL Eddy, **D Pike**, M Kirby, K Sheikh, GA Paulin, M Kirby, DG McCormack and G Parraga. Testing the Fletcher-Peto Assumptions using Pulmonary Imaging Biomarker Longitudinal Measurements. *The American Thoracic Society Annual Scientific Meeting 2016, San Francisco, CA, USA*
3. **D Pike**, N Zha, DPI Capaldi, F Guo, S Mattonen, A Ward, DG McCormack and G Parraga. Second-order Texture Analysis of Hyperpolarized ^3He MRI: Measuring Ventilation Signal to Treat COPD. The National Student Research Forum 2016. *Galveston, TX, USA*
4. DPI Capaldi, N Zha, **D Pike**, K Sheikh, DG McCormack and G Parraga. Pulmonary Magnetic Resonance Imaging and CT Parametric Response Mapping Phenotypes in Ex-smokers with and without Chronic Obstructive Pulmonary Disease. *Imaging Network Ontario Symposium 2015. London, ON, Canada*
5. N Zha, DPI Capaldi, **D Pike**, DG McCormack, IA Cunningham and G Parraga. Principal component analysis of the CT density histogram to generate parametric response maps of COPD. *Imaging Network Ontario Symposium. London, ON, Canada*
6. N Zha, DPI Capaldi, **D Pike**, DG McCormack, IA Cunningham and G Parraga. Principal Component Analysis of the CT Density Histogram to Generate Parametric Response Maps of COPD. *The International Society for Optical Engineering Annual Scientific Meeting 2015, Orlando, FL, USA*
7. S Svenningsen, G Paulin, **D Pike**, S Mohan, DG McCormack and G Parraga. Pulmonary Functional Imaging of Bronchiectasis: A First Look at Ventilation Abnormalities and their Relationship with Pulmonary Function and Symptoms. *The London Health Research Day Symposium 2014, London, ON, Canada*
8. S Svenningsen, G Paulin, **D Pike**, S Mohan, DG McCormack and G Parraga. Pulmonary Functional Imaging of Bronchiectasis: A First Look at Ventilation Abnormalities and their Relationship with Pulmonary Function and Symptoms. *The American Thoracic Society Annual Scientific Meeting 2014, San Diego, CA, USA*

9. F Guo, **D Pike**, S Svenningsen, HO Coxson, JJ Drozd, J Yuan, A Fenster and G Parraga. Development and Applications of Pulmonary Structure-Function Registration Methods. *The International Society for Optical Engineering Annual Scientific Meeting 2014, San Diego, CA, USA*
10. **D Pike**, M Kirby, F Guo, DD Sin, HO Coxson, DG McCormack and G Parraga. Sex, Airways Disease and Emphysema in Ex-smokers with and without Airflow Limitation. *Imaging Network of Ontario Symposium 2014, Toronto, ON, Canada*
11. **D Pike**, M Kirby, S Svenningsen, HO Coxson, NAM Paterson, DG McCormack and G Parraga. Are Hyperpolarized ^3He Magnetic Resonance Imaging Ventilation Defects Clinically Relevant in Ex-smokers without Airflow Limitation? *Radiological Society of North America Annual Scientific Meeting 2013, Chicago, IL, USA*
Associated Award (International): The Radiological Society of North America Research Trainee Prize, \$1000

Peer Reviewed Poster Presentations and Conference Proceedings (33)

1. E Lessard, A Ouriadov, **D Pike**, DG McCormack and G Parraga. Longitudinal Three-Year Decline in Alpha-1 Antitrypsin Deficiency: Regional Worsening in Emphysema and Ventilation. *The American Thoracic Society Annual Scientific Meeting 2016, San Francisco, CA, USA*
2. **D Pike**, DPI Capaldi, S Mattonen, F Guo, A Ward, DG McCormack and G Parraga. Second-Order Texture Analysis of Hyperpolarized ^3He MRI – Beyond the Ventilation Defect. *The International Society of Magnetic Resonance in Medicine Annual Scientific Meeting 2015, Toronto, ON, Canada*
3. DPI Capaldi, N Zha, **D Pike**, K Sheikh, DG McCormack, G Parraga. ^3He MRI and CT Parametric Response Mapping of Small Airways Disease: The Battle-ground for Ground Truth. *The International Society of Magnetic Resonance in Medicine Annual Scientific Meeting 2015, Toronto, ON, Canada*
4. DPI Capaldi, K Sheikh, S Svenningsen, **D Pike**, DG McCormack, G Parraga. MRI Measurements of Regional Ventilation Heterogeneity: Ventilation Defect Clusters. *The International Society of Magnetic Resonance in Medicine Annual Scientific Meeting 2015, Toronto, ON, Canada*
5. **D Pike**, A Ouridov, S Mohan, DG McCormack and G Parraga. Evaluation of Emphysema in Alpha-1 Antitrypsin Deficiency Patients using ^3He MRI – A Potential Tool for Monitoring Response to Augmentation Therapy. *The American Thoracic Society Annual Scientific Meeting 2015, Denver, CO, USA*

6. **D Pike**, M Kirby, D Capaldi, N Zha, DG McCormack, HO Coxson and G Parraga. Differences in Pulmonary Ventilation in Ex-smokers with and without COPD after Three years: Longitudinal Results of the TINCan Cohort. *The American Thoracic Society Annual Scientific Meeting 2015, Denver, CO, USA*
7. C Davis, **D Pike**, S Svenningsen, DG McCormack, D O'Donnell, JA Neder, G Parraga, Ventilation Heterogeneity in Older Never-Smokers and GOLD stage I-IV COPD: Poorly Communicating Fraction and MRI Ventilation defects in the TINCan Cohort. *The American Thoracic Society Annual Scientific Meeting 2015, Denver, CO, USA*
8. **D Pike**, M Kirby, D Capaldi, N Zha, DG McCormack, HO Coxson and G Parraga. Differences in Pulmonary Ventilation in Ex-smokers with and without COPD after Three years: Longitudinal Results of the TINCan Cohort. *London Health Research Day 2015, London, ON, Canada*
9. **D Pike**, M Kirby, D Capaldi, N Zha, DG McCormack, HO Coxson and G Parraga. Differences in Pulmonary Ventilation in Ex-smokers with and without COPD after Three years: Longitudinal Results of the TINCan Cohort. *Imaging Network Ontario Symposium 2015, London, ON, Canada*
10. C Davis, **D Pike**, S Svenningsen, DG McCormack, D O'Donnell, JA Neder, G Parraga, Ventilation Heterogeneity in Older Never-Smokers and GOLD stage I-IV COPD: Poorly Communicating Fraction and MRI Ventilation defects in the TINCan Cohort. *London Health Research Day 2015, London, ON, Canada*
11. DPI Capaldi, N Zha, **D Pike**, K Sheikh, DG McCormack and G Parraga. Pulmonary Magnetic Resonance Imaging and CT Parametric Response Mapping Phenotypes in Ex-smokers with and without Chronic Obstructive Pulmonary Disease. *Imaging Network Ontario Symposium 2015, London, ON, Canada*
12. N Zha, DPI Capaldi, **D Pike**, DG McCormack, IA Cunningham and G Parraga. Principal component analysis of the CT density histogram to generate parametric response maps of COPD. *London Health Research Day 2015, London, ON, Canada*
13. S Svenningsen, G Paulin, A Wheatley, **D Pike**, J Suggett, DG McCormack and G Parraga. Oscillating Positive Expiratory Pressure (oPEP) Therapy in Chronic Obstructive Pulmonary Disease and Bronchiectasis. *European Respiratory Society Congress 2014, Munich, Germany*
14. **D Pike**, TL Lindenmaier; LM Mielniczuk, DG McCormack and G Parraga. An Airways Disease Phenotype is related to Pulmonary Artery Abnormalities in COPD. *The American Thoracic Society Annual Scientific Meeting 2014. San Diego, CA, USA*

15. **D Pike**, M Kirby, F Guo, DD Sin, HO Coxson, DG McCormack and G Parraga. Sex, Airways Disease and Emphysema in Ex-smokers with and without Airflow Limitation. *The American Thoracic Society Annual Scientific Meeting 2014. San Diego, CA, USA*
16. **D Pike**, M Kirby, S Svenningsen, DD Sin, DG McCormack, HO Coxson and G Parraga. Pulmonary Computed Tomography and ³He Magnetic Resonance Imaging of GOLD Unclassified Ex-smokers: Does Imaging Matter? *The American Thoracic Society Annual Scientific Meeting 2014. San Diego, CA, USA*
17. **D Pike**, M Kirby, DD Sin, DG McCormack, HO Coxson and G Parraga. Pulmonary Imaging of Chronic Obstructive Pulmonary Disease in Ex-smokers: Thoracic Imaging Network of Canada (TINCan) Cross-sectional Evaluation. *The American Thoracic Society Annual Scientific Meeting 2014. San Diego, CA, USA*
Associated Award (International): American Thoracic Society Respiratory Structure and Function Scholarship, \$500
18. W Ma, K Sheikh, **D Pike**, S Svenningsen, HO Coxson, DG McCormack and G Parraga. Conventional Pulmonary MRI and CT of Bronchiectasis and Emphysema: Tissue density measurements and relationship to pulmonary function tests. *The American Thoracic Society Annual Scientific Meeting 2014. San Diego, CA, USA*
19. **D Pike**, M Kirby, DD Sin, DG McCormack, HO Coxson and G Parraga. Thoracic Imaging Network of Canada (TINCan): Answering Clinically Relevant Pulmonary Structure-Function Questions Through Imaging. *Imaging Network of Ontario Symposium 2014, Toronto, ON, Canada*
20. **D Pike**, M Kirby, S Svenningsen, DD Sin, DG McCormack, HO Coxson and G Parraga. Imaging Global Initiative for Chronic Obstructive Pulmonary Disease (GOLD) Unclassified Ex-smokers: A Hyperpolarized ³He MRI and Thoracic CT Investigation. *Imaging Network of Ontario Symposium 2014, Toronto, ON, Canada*
21. F Guo, **D Pike**, S Svenningsen, HO Coxson, JJ Drozd, J Yuan, A Fenster and G Parraga. Deformable Pulmonary Structure-Function Registration Methods: Towards Pulmonary Image-Guidance Methods for Improved Airway Targeted Therapies and Outcomes. *Imaging Network of Ontario Symposium 2014, Toronto, ON, Canada*
22. **D Pike**, M Kirby, DD Sin, DG McCormack, HO Coxson and G Parraga. Pulmonary Imaging of Chronic Obstructive Pulmonary Disease in Ex-smokers: Thoracic Imaging Network of Canada (TINCan) Cross-sectional Evaluation. *The London Health Research Day Symposium 2014, London, ON, Canada*

23. F Guo, **D Pike**, S Svenningsen, HO Coxson, JJ Drozd, J Yuan, A Fenster and G Parraga. Deformable Pulmonary Structure-Function Registration Methods: Towards Pulmonary Image-Guidance Methods for Improved Airway Targeted Therapies and Outcomes. *The London Health Research Day Symposium 2014, London, ON, Canada*
24. S Mohan, **D Pike**, W Ma, JF Lewis and G Parraga. Pulmonary Imaging Abnormalities in an Adult Case of Congenital Lobar Emphysema. *The London Health Research Day Symposium 2014, London, ON, Canada*
25. W Ma, K Sheikh, **D Pike**, S Svenningsen, HO Coxson, DG McCormack and G Parraga. Conventional Pulmonary MRI and CT of Bronchiectasis and Emphysema: Tissue density measurements and relationship to pulmonary function tests. *The London Health Research Day Symposium 2014, London, ON, Canada*
26. **D Pike**, M Kirby, A Wheatley, D. McCormack and G Parraga. Evaluation of Airway Morphology in Chronic Obstructive Pulmonary Disease of Hyperpolarized Helium-3 Magnetic Resonance Imaging and Computed Tomography. *International Society for Magnetic Resonance in Medicine 2013, Salt Lake City, UT, USA*
Associated Award (International): International Society for Magnetic Resonance in Medicine Abstract Scholarship, \$450
27. **D Pike**, M Kirby, K Sheikh, D Buchanan, C Neron, J.D. Spence, N.A. Paterson, H.O. Coxson, D.G. McCormack and G Parraga. Airways Disease in Asymptomatic Ex-smokers without Airflow Limitation: Relationship to Carotid Atherosclerosis. *The American Thoracic Society Annual Scientific Meeting 2013, Philadelphia, PA, USA*
28. **D Pike**, M Kirby, K Sheikh, D Buchanan, C Neron, JD Spence, NAM Paterson, HO Coxson, DG McCormack and G Parraga. On the Relationship Between Carotid Atherosclerosis and Airways Disease in Ex-smokers without Airflow Limitation. *Imaging Network Ontario 2013, Toronto, ON, Canada*
29. **D Pike**, M Kirby, A Wheatley, DG McCormack and G Parraga. Airway Morphology in Chronic Obstructive Pulmonary Disease using Hyperpolarized ³He Magnetic Resonance Imaging and x-ray Computed Tomography. *London Imaging Discovery Day 2013, London, ON, Canada*
30. **D Pike**, M Kirby, A Wheatley, DG McCormack and G Parraga. Evaluation of Airway Morphology in Chronic Obstructive Pulmonary Disease of Hyperpolarized Helium-3 Magnetic Resonance Imaging and Computed Tomography. *London Health Research Day 2013, London, ON, Canada*

31. M Kirby, **D Pike**, A Wheatley, NAM Paterson, D.G. McCormack and G Parraga. Hyperpolarized Helium-3 Magnetic Resonance Imaging Phenotypes of Chronic Obstructive Pulmonary Disease: Relationship to Exacerbations. *American Thoracic Society 2013, Philadelphia, PA, USA*
32. M McDonald, M Mannion, **D Pike**, K Lewis, M Browne, M Rise and V Booth. High Resolution Structures and Structure-Function Relationships in Histidine-Rich Antimicrobial Peptides from Cod. *Biophysical Society Annual Scientific Meeting 2013, Philadelphia, PA, USA*
33. **D Pike**, M Morrow and V Booth. Characterizing Membrane Interactions of Antimicrobial Peptide MSI-78 Using ^{31}P Nuclear Magnetic Resonance. *Memorial University of Newfoundland Research Symposium 2012, St. John's, NL, Canada*

ACADEMIC CONFERENCES WITH PROCEEDINGS FEATURED

- 2016** American Thoracic Society Conference, San Francisco, CA, *International*
 National Student Research Forum, Galveston, TX, *International*
 Memorial University Medical Research Conference, St. John's, NL, *Provincial*
- 2015** International Society of Magnetic Resonance in Medicine (ISMRM) Conference, Toronto, ON, *International*
 American Thoracic Society Conference, Denver, CO, *International*
 Imaging Network of Ontario, Toronto, ON, *National*
 London Health Research Day, London, ON, *Provincial*
- 2014** International Society of Magnetic Resonance in Medicine Conference (ISMRM), Milan, ITA, *International*
 American Thoracic Society Conference, San Diego, CA, *International*
 Imaging Network of Ontario, Toronto, ON, *National*
 London Imaging Discovery Day, London, ON, *Provincial*
 London Health Research Day, London, ON, *Provincial*
- 2013** Radiological Society of North America (RSNA), Chicago, IL, *International*
 International Society of Magnetic Resonance in Medicine (ISMRM) Conference, Salt Lake City, UT, *International*
 American Thoracic Society Conference, Philadelphia, PA, *International*
 Imaging Network of Ontario, Toronto, ON, *National*
 London Imaging Discovery Day, London, ON, *Provincial*
 London Health Research Day, London, ON, *Provincial*

PROFESSIONAL MEMEBERSHIPS

Feb. 2016 – present	Canadian Interventional Radiology Association (CIRA)
Jan. 2016 – present	Clinician Investigator Training Association of Canada (CITAC)
Sep. 2015 - present	Canadian Medical Association (CMA)
Jan. 2013 – present	Radiological Society of North America (RSNA)
Jan. 2013 – present	American Thoracic Society (ATS)
Jan. 2013 – present	Canadian Thoracic Society (CTS)
Jan. 2012 – present	International Society of Magnetic Resonance in Medicine (ISMRM)

RESEARCH EDUCATION DEVELOPMENT

- 2015** **Medical Resident Research Trainee Supervision**
 Resident (PGY-3 Internal Medicine): Michael Mitar, MD
 Project: *Longitudinal Evaluation of Emphysema in Alpha-1 Antitrypsin Deficiency Patients using Diffusion-weighted ³He MRI: Monitoring Response to Augmentation Therapy*
 Abstract: Evaluation of Emphysema in Alpha-1 Antitrypsin Deficiency Patients using ³He MRI – A Potential Tool for Monitoring Response to Augmentation Therapy.
- 2015** **Medical Resident Research Trainee Supervision**
 Resident (PGY-2 Internal Medicine): Chris Davis, MD
 Manuscript: C Davis, K Sheikh, D Pike, S Svenningsen, DG McCormack, D O'Donnell, JA Neder and G Parraga. Ventilation Heterogeneity in Never-smokers and COPD: Comparison of Pulmonary Functional Magnetic Resonance Imaging with Poorly Communicating Fraction derived from Plethysmography. *Academic Radiology*; DOI: 10.1016/j.acra.2015.10.022
- 2014** **Medical Student Research Trainee Supervision**
 Pre-clerkship MD Candidate: Nanxi Zha, BEeng
 Manuscript: N Zha, D Pike, S Svenningsen, DPI Capaldi, DG McCormack and G Parraga. Second-Order Texture Measurements of ³He Ventilation MRI: Proof of Concept Evaluation of Asthma Bronchodilator Response. *Academic Radiology* DOI: 10.1016/j.acra.2015.10.010
- 2013** **Medical Resident Research Trainee Supervision**
 Resident (PGY-2 Internal Medicine): Sindu Mohan, MD
 Manuscript: D Pike, S Mohan, W Ma, JF Lewis and G Parraga. Pulmonary Imaging Abnormalities in an Adult Case of Congenital Lobar Emphysema. *The Journal of Radiology Case Reports*; DOI: 10.3941/jrcr.v9i2.2048 2015
- 2012** **Undergraduate Summer Student Supervision**
 Student: William Alexander, Faculty of Engineering, Memorial University
 6 Week Project: *Differential Scanning Calorimetry of Bacterial Membranes*
- 2011** **Undergraduate Summer Student Supervision**
 Student: Kathleen O'Grady, Faculty of Engineering, Memorial University
 6 Week Project: *³¹P Solid State Nuclear Magnetic Resonance of Dynamic Systems*

RELEVANT GRADUATE COURSEWORK

Conceptual Magnetic Resonance Imaging (Instructor: Charles McKenzie PhD) – 93%

Principles of Medical Imaging (Instructors: David Holdsworth PhD, Maria Drangova PhD, Keith St. Lawrence PhD, Ting Yim-Lee PhD) – 80%

Nuclear Magnetic Resonance (Instructor: Blaine Chronik PhD) – 84%

Vascular Imaging (Instructor: Aaron Fenster PhD, FCCPM) – 99%

Research Ethics and Biostatistics (Instructor: Aaron Fenster PhD, FCCPM) – 94%

Inferencing From Data Analysis (Instructor: Yves Bureau PhD) – 85%

Scientific Communications (Instructor: Terry Thompson PhD) – 94%

Digital Image Processing (Instructor: Hanif Ladak PhD, P. Eng) – 92%

Imaging Principles (Instructor: Ian Cunningham PhD, FCCPM, FAAPM) – 90%

LEADERSHIP, VOLUNTEER AND COMMUNITY ACTIVITIES

2016 **Volunteer**, Memorial University Faculty of Medicine Clinical Research Interest Group – *Co-founder and President*

Volunteer, Memorial University Faculty of Medicine Undergraduate (MD) Research Representative

Volunteer, Memorial University Faculty of Medicine Undergraduate (MD) Radiology Representative

2015 **Volunteer**, Memorial University Faculty of Medicine Medical Doctor (MD) Research Representative

Volunteer, Memorial University Faculty of Medicine Medical Doctor (MD) Radiology Representative

Volunteer, Memorial University Faculty of Medicine Medical Doctor (MD) Research Representative

Volunteer, Camp Delight Oncology Camp Counsellor and Mentor

Volunteer, Memorial University Faculty of Medicine Monte Carlo Fundraiser

Volunteer, Schulich Medicine and Dentistry Society Medical Biophysics Graduate Recruitment Committee

Member, London Ontario Soccer League

Volunteer, Track 3 Ski School Instructor

Volunteer, Schulich Medicine and Dentistry Society Medical Biophysics Graduate Representative

2014 **Volunteer**, Schulich Medicine and Dentistry Society Medical Biophysics Graduate Recruitment Committee

Volunteer, Schulich Medicine and Dentistry Society Medical Biophysics Graduate Representative

Participant/Member, MEC Charity Road Race Series (*London, Ontario*)

Member, London Ontario Soccer League

Volunteer, Track 3 Ski School Instructor

- Member**, Network of Imaging Students (NOISe)
- 2013** **Participant/Member**, Forest City Road Race Series (*London, Ontario*)
Member, London Ontario Soccer League
Volunteer, Track 3 Ski School Instructor
Member, Network of Imaging Students (NOISe)
- 2012** **Participant**, Forest City Road Race Series Half-Marathon (*London, Ontario*)
Participant, MEC Charity Road Race Series (*London, Ontario*)
Member, Network of Imaging Students (NOISe)
Volunteer, Canadian Ski Patrol (Nationwide On-hill Certification), St. John's, NL
Volunteer, Memorial University Campus Foodbank, St. John's Campus
Member, Hockey Newfoundland and Labrador, Provincial Goaltending Development Committee
Member, Memorial University Faculty of Biochemistry Vice President of Athletics
Volunteer, Hockey Newfoundland and Labrador Midget AAA Goaltending Coach
- 2011** **Volunteer**, Canadian Ski Patrol (Nationwide On-hill Certification), St. John's, NL
Volunteer, Memorial University Campus Foodbank, St. John's Campus
Volunteer, Women in Science and Engineering (WISE), Mentor
Member, Hockey Newfoundland and Labrador, Regional Goaltending Development Committee
Volunteer, Hockey Newfoundland and Labrador Midget AAA Goaltending Coach
- 2010** **Volunteer**, Canadian Ski Patrol (Nationwide On-hill Certification), St. John's, NL
Volunteer, Memorial University Campus Foodbank, St. John's Campus
Volunteer, Memorial University Science Matters, Career Development Programme
Member, Hockey Newfoundland and Labrador, Regional Goaltending Development Committee
Volunteer, Hockey Newfoundland and Labrador Midget AAA Goaltending Coach
- 2009** **Volunteer**, Canadian Ski Patrol (Nationwide On-hill Certification), St. John's, NL
Volunteer, Memorial University Campus Foodbank, St. John's Campus
Member, Hockey Newfoundland and Labrador, Regional Goaltending Development Committee